



2809644927



REFERENCE ONLY

UNIVERSITY OF LONDON THESIS

Degree PHD Year 2007 Name of Author GIAMPELLEGRINI, Laurent

**COPYRIGHT**

This is a thesis accepted for a Higher Degree of the University of London. It is an unpublished typescript and the copyright is held by the author. All persons consulting this thesis must read and abide by the Copyright Declaration below.

**COPYRIGHT DECLARATION**

I recognise that the copyright of the above-described thesis rests with the author and that no quotation from it or information derived from it may be published without the prior written consent of the author.

**LOANS**

Theses may not be lent to individuals, but the Senate House Library may lend a copy to approved libraries within the United Kingdom, for consultation solely on the premises of those libraries. Application should be made to: Inter-Library Loans, Senate House Library, Senate House, Malet Street, London WC1E 7HU.

**REPRODUCTION**

University of London theses may not be reproduced without explicit written permission from the Senate House Library. Enquiries should be addressed to the Theses Section of the Library. Regulations concerning reproduction vary according to the date of acceptance of the thesis and are listed below as guidelines.

- A. Before 1962. Permission granted only upon the prior written consent of the author. (The Senate House Library will provide addresses where possible).
- B. 1962-1974. In many cases the author has agreed to permit copying upon completion of a Copyright Declaration.
- C. 1975-1988. Most theses may be copied upon completion of a Copyright Declaration.
- D. 1989 onwards. Most theses may be copied.

***This thesis comes within category D.***

This copy has been deposited in the Library of UCL

This copy has been deposited in the Senate House Library, Senate House, Malet Street, London WC1E 7HU.



Department of Civil & Environmental Engineering  
University College London

**Uncertainty in  
Correlation-Driven Operational  
Modal Parameter Estimation**

by

Laurent Giampellegrini

Supervisors

Paul.D. Greening, Steven. R. Bishop

*Thesis submitted to University of London for Doctorate in Philosophy*

UMI Number: U592836

All rights reserved

INFORMATION TO ALL USERS

The quality of this reproduction is dependent upon the quality of the copy submitted.

In the unlikely event that the author did not send a complete manuscript and there are missing pages, these will be noted. Also, if material had to be removed, a note will indicate the deletion.



UMI U592836

Published by ProQuest LLC 2013. Copyright in the Dissertation held by the Author.  
Microform Edition © ProQuest LLC.

All rights reserved. This work is protected against  
unauthorized copying under Title 17, United States Code.



ProQuest LLC  
789 East Eisenhower Parkway  
P.O. Box 1346  
Ann Arbor, MI 48106-1346



---

# ABSTRACT

---

Due to the practical advantages over traditional input-output testing, operational or output-only modal analysis is receiving increased attention when the modal parameters of large civil engineering structures are of interest. However, as a consequence of the random nature of ambient loading and the unknown relationship between excitation and response, the identified operational modal parameters are inevitably corrupted by errors. Whether the estimated modal data is used to update a finite element model or different sets of modal parameters are used as a damage indicator, it is desirable to know the extent of the error in the modal data for more accurate response predictions or to assess, if changes in the modal data are indicative of damage or just the result of the random error inherent in the identification process. In this thesis, two techniques are investigated to estimate the error in the modal parameters identified from response data only: a perturbation and a bootstrap based method.

The perturbation method, applicable exclusively to the correlation-driven stochastic subspace identification algorithm (SSI/Cov), is a two stage procedure. It operates on correlation functions estimated from a single set of response measurements and, in a first step, the perturbations to these correlation function estimates need to be determined. A robust, data-driven method is developed for this purpose. The next step consists in propagating these perturbations through the algorithm resulting in an estimate of the sensitivities of the modal data to these perturbations. Combining the sensitivities with the perturbations, an estimate of both the random and bias errors in the SSI/Cov-identified modal parameters is found.

The bootstrap technique involves creating pseudo time-series by resampling from the only available set of response measurements. With this additional data at hand, a modal identification is performed for each set of data and the errors in the modal

parameters are determined by sample statistics. However, the bootstrap itself introduces errors in the computed sample statistics. Three bootstrapping schemes are investigated in relation to operational modal analysis and an automated, optimal block length selection is implemented to minimise the error introduced by the bootstrap. As opposed to the perturbation method, the bootstrap technique is more versatile and it is not restricted to correlation-driven operational modal analysis. Its applicability to the data-driven stochastic subspace identification algorithm (SSI/Data) for error prediction of the SSI/data-identified modal data is explored.

The performance of the two techniques is assessed by simulation on simple systems. Monte-Carlo type error estimates are used as a benchmark against which the predicted errors in the modal parameters computed from a single response history from both techniques are validated. Both techniques are assessed in terms of their accuracy and stability in predicting the uncertainty in the operational modal parameters and their computational efficiency is compared. Also, the performance of the bootstrap and the perturbation theoretic method is investigated in hostile ambient excitation conditions such as non-stationarity and the presence of deterministic components and the limitations of both methods are clearly exposed.

*To Mam & Pap*

---

# ACKNOWLEDGEMENTS

---

I wish to express my sincere gratitude to Paul Greening and Steven Bishop for supporting and guiding me patiently towards the completion of this thesis. Also, the assistance on various technical aspects by Richard Chandler, Mike Davies and Gert Van Der Heijden is greatly acknowledged as are the many fruitful discussions with the always helpful David Sinden.

---

# CONTENTS

---

<b>1</b>	<b>Overview of Operational Modal Analysis</b>	<b>1</b>
1.1	Introduction . . . . .	1
1.2	Operational Modal Analysis for Civil Engineering Structures . . . . .	5
1.2.1	Frequency Domain Methods . . . . .	7
1.3	Time Domain Methods . . . . .	12
1.4	Scope of Thesis . . . . .	17
<b>2</b>	<b>Theoretical Basis</b>	<b>21</b>
2.1	Introduction . . . . .	21
2.2	Operational Response Models . . . . .	21
2.2.1	Stochastic Processes, Stationarity and Ergodicity . . . . .	25
2.2.2	Frequency-Domain Operational Response model and NExt . . . . .	29
2.3	Identification Methods . . . . .	34
2.3.1	The Enhanced Frequency Domain Decomposition (EFDD) . . . . .	34
2.3.2	Covariance-Driven Stochastic Subspace Identification (SSI/Cov) . . . . .	38
2.3.3	Data-Driven Stochastic Subspace Identification (SSI/Data) . . . . .	46
2.4	Summary . . . . .	48
<b>3</b>	<b>Estimation Errors in Correlation functions</b>	<b>49</b>
3.1	Introduction . . . . .	49
3.2	Correlation Function Estimators . . . . .	51
3.2.1	Sample Auto- and Cross-Correlation Functions . . . . .	51
3.2.2	Sample Auto- and Cross-Correlation Coefficient Functions . . . . .	54
3.2.3	Auto- and Cross Random Decrement (RD) signatures . . . . .	55
3.3	Bias in Sample Correlation Functions . . . . .	59
3.3.1	Auto- and Cross-Correlation Functions . . . . .	59
3.4	Variance in Sample Correlation Functions . . . . .	64
3.4.1	Single-Degree-of-Freedom Systems . . . . .	65
3.4.2	Auto-covariance function . . . . .	71
3.4.3	Multi-Degree-of-Freedom Systems . . . . .	73

3.5	Plug-in Estimates . . . . .	74
3.5.1	Plug-in Estimates for the Covariance of Correlation functions . . . . .	76
3.5.2	Plug-in Estimates for the Covariance of Correlation Coefficient functions . . . . .	88
3.6	Summary . . . . .	91
<b>4</b>	<b>The Dependent Bootstrap</b>	<b>92</b>
4.1	Introduction . . . . .	92
4.2	Efron's Bootstrap . . . . .	93
4.3	The Dependent Bootstrap . . . . .	99
4.3.1	The Moving Block Bootstrap . . . . .	99
4.3.2	The "Blocks of Blocks" Bootstrap . . . . .	103
4.3.3	The Stationary Bootstrap . . . . .	107
4.4	Performance of the Bootstrap . . . . .	108
4.4.1	Block Length Selection . . . . .	112
4.5	Simulations . . . . .	124
4.6	Summary and Discussion . . . . .	138
<b>5</b>	<b>Perturbation Analysis for Correlation-Driven Identification</b>	<b>141</b>
5.1	Introduction . . . . .	141
5.2	Overview of the Theory . . . . .	143
5.2.1	Variance of $\chi$ , $Var[\chi]$ . . . . .	145
5.2.2	Quadratic Bias of $\chi$ , $b_Q[\chi]$ . . . . .	146
5.2.3	Truncation Bias of $\chi$ , $b_T[\chi]$ . . . . .	146
5.2.4	Variance of the Truncation Bias of $\chi$ , $Var[b_T(\chi)]$ . . . . .	153
5.2.5	Quadratic Bias of Truncation Bias of $\chi$ , $b_{QT}[\chi]$ . . . . .	154
5.3	Derivatives of the Modal Frequencies and Damping Ratios . . . . .	154
5.3.1	Eigenvalue and Eigenvector derivatives . . . . .	158
5.3.2	Derivatives for the Variance and Quadratic Bias . . . . .	161
5.3.3	Derivatives for the Truncation Bias, its Variance and Quadratic Bias . . . . .	163
5.4	Extension to Repeated Eigenvalues . . . . .	168
5.5	Derivatives for Mode shapes . . . . .	175
5.6	Summmary and Discussion . . . . .	176
<b>6</b>	<b>Uncertainty in SSI/Cov-Identified Modal Parameters: A Perturbation Approach</b>	<b>179</b>
6.1	Introduction . . . . .	179



6.2	Perturbations of the Sample Correlation Functions . . . . .	180
6.2.1	Error Sources . . . . .	180
6.2.2	Data-Driven Perturbation Model . . . . .	184
6.2.3	A Noise Model . . . . .	185
6.3	Random Error . . . . .	190
6.3.1	Influence of Instrumentation Noise . . . . .	192
6.3.2	Influence of Estimation Noise . . . . .	199
6.3.3	Robustness of Perturbation Algorithm . . . . .	204
6.4	Bias Error . . . . .	230
6.4.1	Influence of Non-Stationarity on Bias . . . . .	252
6.4.2	Efficiency of Perturbation Algorithm . . . . .	254
6.5	Summary and Discussion . . . . .	255
<b>7</b>	<b>Uncertainty in Identified Modal Parameters: A Bootstrap Approach</b>	
	<b>257</b>	
7.1	Introduction . . . . .	257
7.2	Applicability of the Bootstrap for Operational Modal Parameters . . .	258
7.3	Random Error . . . . .	261
7.3.1	Random Errors in SSI/Cov-identified modal parameters . . . .	261
7.3.2	Random Errors in SSI/Data-identified modal parameters . . .	269
7.4	Non-Stationary, Non-white excitation . . . . .	272
7.5	Bias Error . . . . .	277
7.6	Summary . . . . .	281
<b>8</b>	<b>Conclusion</b>	<b>283</b>
8.1	Rationale . . . . .	283
8.2	Summary of Work . . . . .	284
8.2.1	The Perturbation Method . . . . .	285
8.2.2	The Bootstrap Method . . . . .	290
8.2.3	Future Work . . . . .	292
<b>A</b>	<b>Expressing the Cross-correlation Function of an MDOF system as a</b>	
	<b>sum of Auto-correlation functions of equivalent SDOF systems</b>	<b>296</b>
<b>B</b>	<b>Additional Expressions for the Derivatives of the Modal Frequencies</b>	
	<b>and Damping Ratios</b>	<b>301</b>
B.1	Expression for $\delta_{jk\rho}(\omega_i)$ . . . . .	301
B.2	Expression for $\delta_{jk\rho}(\xi_i)$ . . . . .	302

<b>B.3</b>	<b>Expression for <math>\delta_{jk}(\mathbf{A})</math></b> . . . . .	<b>303</b>
<b>B.4</b>	<b>Expression for <math>\delta_{jk}(\mathbf{U}_1)</math></b> . . . . .	<b>303</b>
<b>B.5</b>	<b>Expression for <math>\delta_j(\Delta\Lambda')</math> and <math>\delta_{jk}(\Delta\Lambda')</math></b> . . . . .	<b>304</b>

---

# CHAPTER 1

## OVERVIEW OF OPERATIONAL MODAL ANALYSIS

---

### 1.1 Introduction

Since the early developments of the Finite Element (FE) method, engineers have been increasingly using this versatile numerical tool for the static and dynamic analysis of structural systems. However, with the desire to develop more complex structural systems, the necessity arose for experimental procedures that enable engineers to verify and validate the numerical models. In the early stages, this was simply achieved by measuring the response of the structure under consideration due to a certain prescribed load and subsequently comparing it to the calculated behaviour. In the case of poor agreement, it was then attempted, mostly by trial-and-error, to carry out some modifications on the model so as to bring the theoretical results closer into line with the experimental outcome. However, a more erudite approach became necessary. In structural dynamics and the study of vibration phenomena, *modal analysis* provided a valuable technique for a more effective reconciliation of the numerical and experimental results as it embraces both analytical/numerical and experimental methods.

*Analytical modal analysis* anchors on a physical model of the structure which, for complex systems, is usually formulated in terms of the mass, stiffness and damping matrices resulting from a spatial discretisation of the system as is done, for instance,

in a finite element model. Modal analysis breaks this spatial model down into its elementary dynamic components called the natural modes of vibration. They are inherent to the system and completely describe its dynamic behaviour. Each mode is described in terms of its modal parameters: the natural frequency, the modal damping factor and characteristic displacement pattern called the mode shape. For linear time-independent systems, any set of displacements can be expressed as a linear combination of the mode shapes weighted by time-dependent coefficients which contain the damping and frequency information and whose amplitudes determine the degree of participation of a particular mode to the general response. This concept is akin to Fourier series and the mode shapes serve the same purpose as the trigonometric functions; they are orthogonal and usually only a few of them are required to describe the response with sufficient accuracy. This modal model thus has a considerable advantage over its spatial counterpart in that it gives a simple physical picture of the dynamic characteristics of the system.

The rapid development over the last two decades of data acquisition and processing capabilities has enabled major advances in the experimental realm of the analysis, known as *experimental modal analysis (EMA)*, *modal testing* or *modal identification*. As is the case for analytical modal analysis, the aim is to derive a modal model of the system, albeit via a different route. The core of this experimental technique is system identification which was originally developed by engineers to study electrical circuits. The similarities between electric circuits and mechanical systems, however, made it possible to apply this theory to mechanical and structural engineering problems. System identification deals with the issue of building mathematical models of dynamical systems based on observed data from the system (Ljung, 1987). In other words, if a system is excited by a known input force and the resulting output is recorded, the objective is to construct a dynamic model of the system using solely the information provided by measured input and output. For linear time-invariant *causal* systems i.e. linear time-invariant systems whose output at a specific time depends on the input up

to that time only, there is a well defined relationship between the input and output in the form of a time-dependent function known as the system's *impulse response function (IRF)*. Its knowledge allows one to compute the response of the system for any known input, for instance using the Duhammel integral (Clough and Penzien, 1993). The IRF is thus a complete characterisation of the system. An equivalent formulation, relating the output to the input, can be expressed in the Laplace domain. In this case, the Laplace transform of the output is related to that of the input via the *transfer function* -the latter being the Laplace transform of the IRF. For a physically realisable and stable system, none of the dynamic characteristics are lost when the transfer function is evaluated only along the imaginary axis i.e in the frequency domain only. This gives rise to the *frequency response function (FRF)* which is now easily seen to be the Fourier transform of the IRF. In general, a model relating the output to the input, such as the IRF, FRF or the transfer function, is called a *response model* of the system. Since the response models completely describe the dynamic behaviour of the system, they admit an expression in terms of its modal parameters. The objective of modal identification is thus to obtain a response model of the test piece from measured input and output data and subsequently to derive a modal model from the response model by ways of curve fitting. Typically, analytical forms of frequency response functions or impulse response functions are matched to measured FRFs or IRFs to determine the modal parameters. There are many techniques available both in the time domain and in the frequency domain to extract the modal model from the response model. An extensive description of these modal parameter identification methods is given in Maia *et al.* (1997) and Ewins (2000). Although most of the principles of modal testing were laid by the end of the first half of the century, renewed practical interest in the subject grew with the invention of the fast Fourier transform (FFT) (Cooley and Tuckey, 1965) and novel instrumentation such as the FFT spectrum analyser, transfer function analysers (TFA) and discrete data acquisition systems together with the increasingly smaller and more powerful digital computers to process the data. In a nutshell, the modal testing procedure consists of three con-

stituent phases: setting up the test specimen which involves the selection of support conditions, the type and the location(s) of the input excitation(s) and the positioning of the response transducer(s) on the structure to measure the output(s). The second step is concerned with determining the response model, either as FRFs or IRFs and finally, in the third phase, the modal parameters are extracted from the response model.

The basic description of the system's dynamics in terms of its natural vibration modes clearly provides a compelling means to verify or validate numerical models using experimental data. Indeed, the past few years have seen increased research efforts directed toward correlating or updating numerical models with the experimentally derived modal data. However, model updating is but one of the broad range of applications covered by experimental modal analysis today. Other applications include troubleshooting which aims to gain a physical understanding of the dynamics of a structure in terms of its modes; identification and evaluation of vibration phenomena; development of experimentally based dynamic models; active vibration control; structural integrity assessment, structural modification and damage detection; establishment of criteria and specifications for design. In short, modal analysis aims to develop reliable dynamic models that may be used with confidence for further analysis. Both the theoretical and analytical aspects of modal analysis are well documented in the technical literature by Maia *et al.* (1997) and Ewins (2000).

The diversity of the applications for modal testing has prompted it to become more strongly interdisciplinary. In particular, modal testing has found increasing acceptance in civil engineering. The need to understand the dynamic behaviour of civil structures under seismic, wind and traffic loading, the verification and updating of finite element models of complex structures such as suspension bridges as well as the continuous ageing and subsequent structural deterioration of a large number of existing structures sparked the interest for using modal testing to address these issues.



## 1.2 Operational Modal Analysis for Civil Engineering Structures

The application of modal identification to civil engineering structures presents some challenges due to the large scale of these structures compared to those in mechanical and aeronautical engineering for which the techniques were initially developed. More precisely, the difficulty resides in the fact that it is a rather intricate matter to excite large civil structures in a controlled manner and with sufficient energy to stimulate the most significant modes, typically  $< 10Hz$ . For small to medium sized structures, the excitation can be induced by instrumented sledge hammers. Although such a device is able to provide wide-band input, the resulting spectral estimates generally have low resolution and further, it may lack the energy to excite some relevant modes (Cunha and Caetano, 2005). In bridge structures, for instance, excitation by impulse is in general not practical to excite lateral modes. An alternative, is the use of large electro-dynamic or *servo-hydraulic shakers*, which can apply a large variety of of input signals controlled in frequency and amplitude by a signal generator. The shakers have the capacity to excite the structure in a lower frequency range and higher low-frequency resolution can be attained. They have been used successfully for modal tests on large infrastructure such as dams (Cantieni, 2001), or bridges (Pietrzko *et al.*, 1996). Other ways for exciting structures, in particular bridges, are the step-relaxation and weight drop methods which can excite a wide range of frequencies. Farrar *et al.* (1999) and Cantieni (2005) present a review of excitation methods for civil engineering structures.

Nevertheless, exciting large structures artificially is often impractical, expensive and can be dangerous when the structure is damaged. The costly equipment needed is seldom available and the disruption caused by the need to close down the structure to be tested is often inconvenient and in many instances not feasible. However, the technological development in the field of transducers over the last years has made it possible to obtain accurate measurements of low levels of structural response in a low frequency range such as that induced by ambient excitations such as wind, traffic or

micro-tremor. Sensitive piezoelectric sensors ( $10V/g$ ) are well suited for structures with a fundamental frequency  $> 1Hz$  (Cantieni, 2005). Accelerometers of the force balance type are particularly appropriate to measure the ambient response of civil engineering structures. Additionally, due to the delays in the feedback loop, these servo-controlled devices have only a limited bandwidth typically in the range from  $0 - 50Hz$  and are virtually insensitive to high frequencies; however in the frequency range in which they are effective, they are optimized for sensitivity without giving up precision and are capable of sensing frequencies below  $1Hz$ . Thus, rather than treating the natural excitation as a source of unwanted noise or disturbances - because the processing procedures in traditional modal testing are based on the assumption that the measured, artificially applied load is the only source of excitation during the test - structural engineers resorted to using the latter as the sole source of excitation. From a practical point of view, this certainly offers a considerable advantage since ambient loading is freely available and the structure can be tested under its usual operating conditions. Ambient forcing, however, cannot be measured so that the traditional *input-output modal testing* techniques had to be adapted to deal with response measurements only without exact knowledge of the input. This is known as *output-only, natural input* or *operational modal analysis (OMA)*.

Operational modal testing typically consists of three stages; the first is to acquire data from the operating structure. This involves deciding on the type and sensitivity of the transducers to be used as well as the number of measurement points and their location along the test piece. The latter choice is conditioned by the spatial resolution required needed to characterise the most relevant modes of vibration. An *a priori* FE model or symmetry considerations of the structure can assist in this choice. The second step is to convert the recorded data into a response model that lends itself to extract the modal parameters of the structure. As for traditional modal analysis, the response model may be formulated in the time or frequency domain but, since the input forces are unknown, it differs from the FRFs or IRFs described previously.

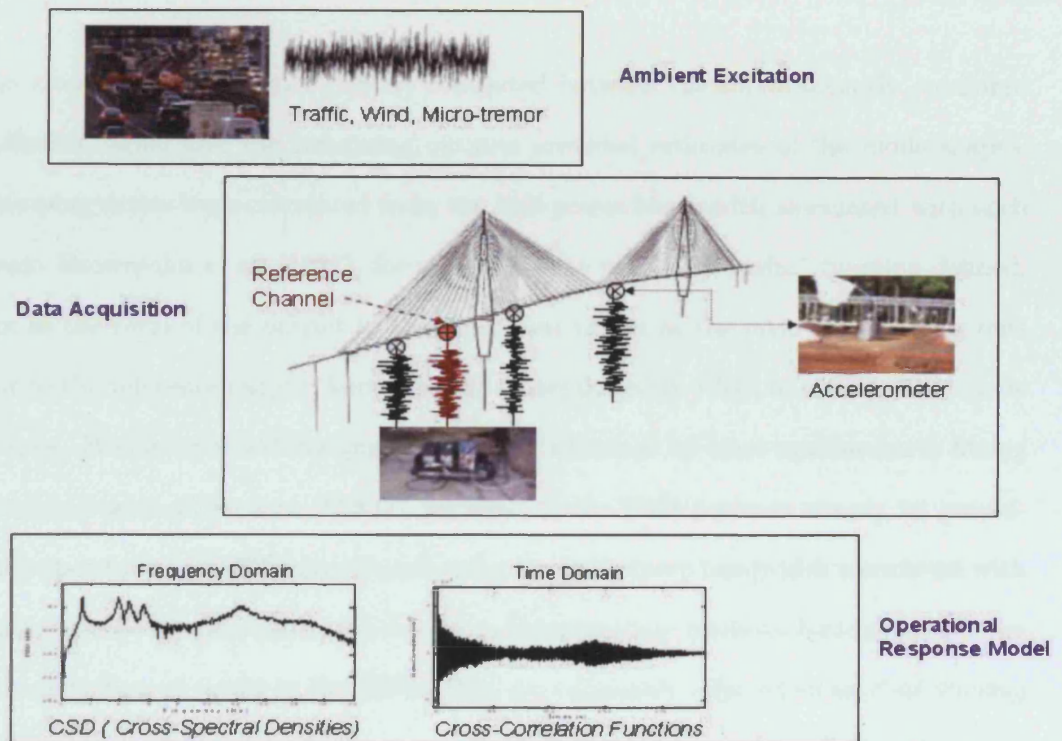


Fig. 1.1: Illustration of the operational modal testing process.

In the final step, the modal parameters are identified from the computed response model. An overview of the various identification techniques, depending on the form of the response model, is presented below.

### 1.2.1 Frequency Domain Methods

One of the earliest applications of ambient vibration testing was carried out by Crawford (1964). Vibrations measured at various locations in a high-rise building were recorded on a magnetic tape recorder and subsequently transformed to power spectral densities (PSDs). The peaks in the PSD of each recorded motion provided estimates of the damped natural frequencies of the building, while a comparison of the PSDs computed from measurements made at different locations and in different directions enabled torsional and lateral modes to be distinguished. This technique was enhanced by McLamore *et al.* (1971) to obtain the modal damping ratios and estimates of the mode shapes in addition to the resonant frequencies. By selecting one of the measurement points as a reference, the amplitude and phase information at a peak in

the cross-spectral densities (CSDs) computed between the simultaneously measured reference signal and the remaining outputs provided estimates of the mode shapes. Damping ratios were calculated from the half-power bandwidth associated with each peak. Brownjohn *et al.* (1987), for instance, have used a “transfer” function defined, not as the ratio of the output to the input, but rather as the ratio of the roving output to the reference output, known as the transmissibility FRF, to estimate the mode shapes. Frequencies and damping ratios were obtained by least squares curve fitting a single-degree-of-freedom (SDOF) response to the PSD peaks or simply by graphical inspection of the PSD graphs and using the half-power bandwidth associated with each peak to estimate the modal damping. Because these methods basically rely upon the inspection of peaks in the PSDs, they are commonly referred to as *Peak-Picking (PP)* or sometimes as *Basic Frequency Domain (BFD)* techniques. Felber (1993) introduced *Averaged Normalized Power Spectral Densities (ANPSD)* and *Modal Ratio Functions (MRF)* which enabled a more efficient and convenient implementation of the PP method. The ANPSD -simply the average of a chosen set of normalized PSDs- serve as a practical tool to capture the peaks of all modes in a single PSD with the byproduct of enhancing the peaks of the power spectra that were computed from time history records taken at or near a node of a particular mode. The *Modal Ratio Function*, which conveniently incorporates the phase, amplitude and coherence information that can be gained from the transmissibility FRFs in a single function, was devised to facilitate the estimation of mode shapes. Although Peak-Picking has been successfully used for ambient vibration testing of civil engineering structures (Abdel-Ghaffar, 1978; Brownjohn *et al.*, 1989; DeSmet *et al.*, 1996; Felber and Ventura, 1996; Felber *et al.*, 1996; Paultre *et al.*, 1995), it has some notable drawbacks. More precisely, the Peak-Picking method treats each peak in the spectral estimates as that of a SDOF system. Ambient excitation, however, has a multiple-input nature and a wide band frequency content stimulating a large number of modes causing spectral overlap of adjacent modes in the spectral estimates which cannot be accounted for by peak-picking.

Thus, unless the peaks are well separated, it is very difficult, if not impossible, to



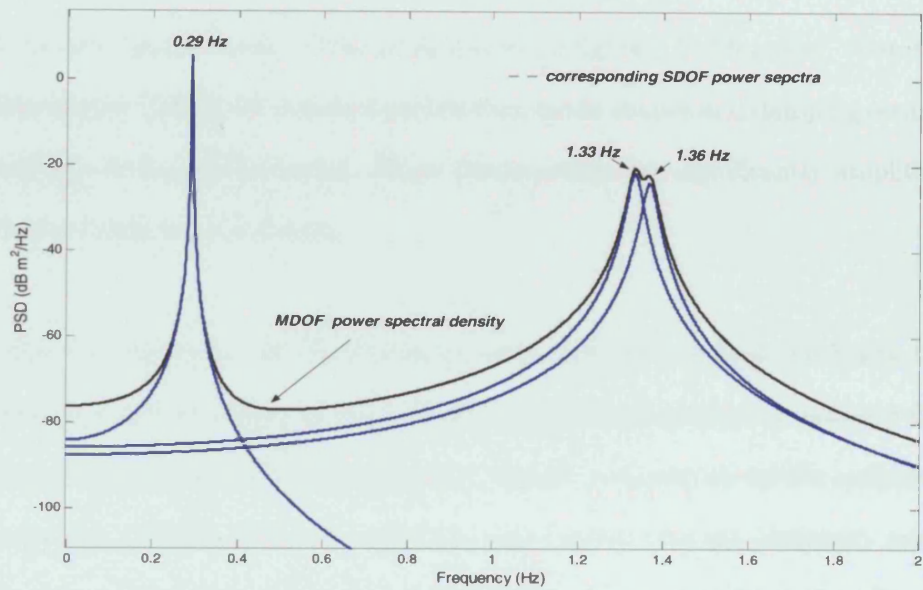


Fig. 1.2: Illustration of the shortcomings of the Peak-Picking. The first peak approximates the corresponding SDOF very well in the vicinity of the peak so that good modal estimates can be obtained. Although frequency estimates can be obtained from the two closely spaced modes, the ODS would yield a poor approximation of the mode shapes and the damping ratios cannot be estimated

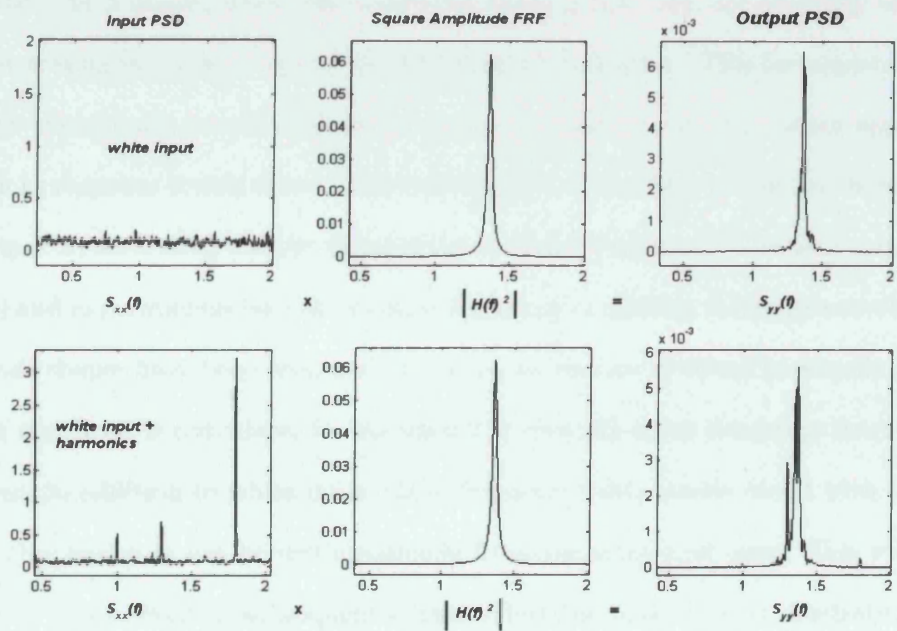


Fig. 1.3: Illustration of the relationship between the input PSD ( $S_{xx}(f)$ ) and the output PSD ( $S_{yy}(f)$ ). For a white noise input, the output PSD is proportional to the square amplitude of the FRF ( $|H(f)|^2$ ) and can be used as a response model for the system. When the input contains harmonics, the output PSD does not only represent system properties but also those of the excitation.

identify closely spaced modes. This is illustrated in figure 1.2. Moreover, operational deflection shapes (ODS) are obtained rather than mode shapes and damping estimates are unreliable or cannot be found. These shortcomings are significantly amplified in case of poor frequency resolution.

Despite its downsides, the Peak-Picking method forms the basis for many OMA techniques as it incorporates the key feature that the cross- and power spectral densities may serve as the fundamental frequency domain response model for output-only modal analysis. Indeed, when the input spectrum is flat over the frequency band of interest, or in other words, when the excitation behaves as band-limited white noise, the power- and cross spectral densities characterize the structure in terms of its modal parameters. However this response model in terms of the output spectra is *incomplete*. Since the ambient forces are not measured, the modal participation factors cannot be determined. As a consequence, the estimated mode shapes are not correctly scaled since their scaling factor will depend on the unknown excitation. This incompleteness, typical for operational modal analysis, somewhat restricts its use in certain applications such as response simulation or structural modification. Also in damage detection procedures, correct scaling may be of importance. Some numerical (Doebbling and Farrar, 1996) and experimental (see for example Parloo *et al.* (2005)) techniques to obtain scaled mode shapes have been proposed. A recent review can be found in Aenelle *et al.* (2005). If the input is not white, for instance if it contains some dominant frequency components in addition to white noise, these frequency components blend with those of the system and may not be distinguishable from the structural ones. This will be discussed in more detail in subsequent chapters but the main idea is illustrated for a SDOF system in figure 1.3. It can be seen that the three harmonics appear in the output PSD which serves as a the operational response model. Although the influence of the harmonics at around 1 and 1.8Hz may be small in this particular case, the influence of the harmonic at around 1.3Hz would certainly be picked up so that a 2-DOF system would be identified instead of the correct SDOF system.



The natural extension of the PP method was to take into account the multiple-input multiple-output (MIMO) nature of the problem. This was achieved by assembling the power and cross spectra into a *power spectral density matrix* which is then decomposed at each frequency line into the individual modes of the system by means of a singular value decomposition (SVD). The singular values thus obtained as a function of frequency signify the power spectrum of the modal coordinates associated with each mode. The natural frequencies appear as local maxima of these power spectra and are then simply obtained by peak-picking. The decomposition of the PSD matrix via the SVD -sometimes referred to as Principal Component Analysis (PCA)- was already employed by Prevosto (1982) to obtain the vibration modes of systems under ambient excitation. Later, the method was applied to decompose the FRF matrix and became known as the Complex Mode Indication Function (CMIF) (Shih *et al.*, 1988). In the context of operational modal analysis for civil engineering structures, this method was adopted by Brincker *et al.* (2000) and called the *Frequency Domain Decomposition (FDD)*. It has subsequently been extended to the *Enhanced Frequency Domain Decomposition (EFDD)* to yield modal damping ratios in addition to frequencies and mode shapes in Brincker *et al.* (2001). Within the classical input-output framework, an application of the CMIF to multiple reference FRF measurements to identify natural frequencies, mode shapes and the corresponding damping ratios appears in Leurs *et al.* (1993). The FDD technique has been widely applied to many civil engineering structures, for example (Brincker and Andersen, 2005; Brincker *et al.*, 2005a; Cunha *et al.*, 2004; Reynolds *et al.*, 2005) owing to its generally good performance and its user friendliness.

The aforementioned modal identification methods are *non-parametric* in nature which means that they do not explicitly make use of a mathematical model to extract the modal parameters from the response model but rather rely on a more direct interpretation of the response model itself. Recently, a parametric frequency domain

identification scheme, known as *PolyMAX*, was introduced by Peeters (2004). This method operates on half-spectra (see section 2.2) and its implementation is based upon a frequency-domain version of the *maximum likelihood method* (Guillaume *et al.*, 1998; Hermans *et al.*, 1998) complemented by a polyreference *least-squares complex frequency-domain (LSCF)* estimation method (Guillaume *et al.*, 2003). The most important advantage of *PolyMAX* lies in the very stable identification of the system poles as a function of the model order which essentially means that it is well suited to distinguish between system modes and so called spurious or computational modes.

### 1.3 Time Domain Methods

Knowing that the output-only frequency response model consists of the spectra of the time history records of a system excited by white noise, the corresponding time-domain response model is easily seen to be given by the correlation functions between the responses since the spectral densities and correlation functions are Fourier transform pairs (Bendat and Piersol, 2000). Thus, just as the spectral densities admit an expression in terms of the modal parameters of the system, the correlation function between any two response measurements can be written as the sum of decaying sinusoids having the same natural frequencies, damping ratios and mode shape coefficients as the modes of the system (see section 2.2). This implies that the correlation functions have the same form as the system's IRF so that time domain algorithms originally developed in traditional modal testing to analyze IRFs can be applied to correlation functions. The conceptual framework for this result was essentially laid by Clarkson and Mercer (1965) but was later applied to ambient data from wind turbines by James *et al.* (1995) and termed the *Natural Excitation Technique (NExT)*. The three time domain classical modal parameter estimation methods that have been widely used in OMA within the NExT framework are the *Polyreference Complex Exponential (PRCE)* method, the *Ibrahim Time Domain (ITD)* method and the *Eigensystem Realisation Algorithm (ERA)*.

The PRCE method (Vold *et al.*, 1982) essentially identifies the modal parameters by curve-fitting the “measured” IRFs (or correlation functions) to a parametric model based on the modal decomposition of the IRFs (or correlation functions). The method was developed as an extension of the single-input multiple-output (SIMO) Least-Squares Complex Exponential (LSCE) method (Brown, 1979) to cope with multiple inputs.

The Ibrahim Time Domain was originally developed by Ibrahim and Mikulcik (1977) as a SIMO method that operates on free decay response measurements and was therefore initially used in conjunction with the random decrement technique (RD). The latter was developed to obtain free responses of a structure from its random responses (Ibrahim, 1977) but was later shown to yield correlation functions (see section 2.2). A MIMO version of the ITD, called the *Multiple-Reference Ibrahim Time Domain (MRITD)* is due to Fukuzono (1986).

The Eigensystem Realization Algorithm (Juang and Pappa, 1984) is a MIMO method whose roots go back to classical *deterministic* minimal system realization theory developed by (Ho and Kalman, 1966). In brief, the ERA is based on a state-space formulation whose constituent system matrices are recovered using the measured IRFs. In operational modal analysis, it is a *stochastic* realization problem that is solved (Akaike, 1974). As a consequence of the natural excitation technique (NExT), the ERA can be employed for this purpose by replacing the IRFs by the correlation functions between the measured outputs. In the context of output-only modal analysis, this procedure is sometimes referred as the NExT/ERA method but a formal treatment of the ERA with data correlations (ERA/DC) is due to Juang *et al.* (1988). An application of this method to ambient response data appears in Desforges and Cooper (1997) and a comparison with the classical ERA operating on impulse data can be found in Cooper and Wright (1992). These NExT-type identification techniques are often called *covariance-driven*<sup>†</sup> or *two-stage* methods referring to the

---

<sup>†</sup>Covariance functions are equal to correlation functions for a zero-mean random process

two steps involved in the process i.e. estimation of the correlation in a first instance and the modal parameter extraction by curve fitting in a second step. The various ways for computing correlation functions (see figure 1.4 and section 2.2) and the different ways of curve fitting thus offer a choice of combinations for implementing the NExT, see for instance (Caicedo *et al.*, 2001; Desforges *et al.*, 1995; Farrar and James, 1997; James *et al.*, 1996; Qin and Qian, 2001). The NExT is sometimes mentioned in conjunction with frequency domain methods due to the Fourier transform relation between correlations and spectral densities (Juang and Suzuki, 1998).

Another method that has been used for operational modal analysis relies on the classical system identification tools based on *Auto-Regressive Moving-Average (ARMA)* models of the vibrating structure. In the case of multiple outputs, the term *Vector-ARMA (ARMAV)* is often used to emphasize their multivariate character. One way to identify the parameters of an ARMAV model is via the *Prediction error method (PEM)* (Ljung, 1987). This technique does not require the computation of a response model (i.e correlation functions) but operates directly on the recorded time histories and is therefore often referred to as a *one-stage* or *data-driven* method. Nevertheless, the application of the PEM method requires the solution of a highly nonlinear least-squares problem which entails a heavy computational load, sensitivity to initial conditions and convergence is not guaranteed. Despite these drawbacks, the *ARMAV-PEM* method has been employed for operational modal analysis of civil engineering structures by Andersen (1997). The identification of the modal parameters of system represented by ARMAV models only requires the coefficients of the Auto-Regressive (AR) part of the model. Nevertheless, a vibrating structure cannot be adequately described by an AR model (see for instance Andersen *et al.* (1996)). It is shown in Peeters and DeRoeck (2001), however, that using an *Instrumental Variable (IV)* method -another classical system identification tool (Ljung, 1987)- enables only the AR coefficients to be identified while the underlying model structure still is an AR-MAV model. Moreover, this is achieved by linear least-squares as the Moving-Average

(MA) coefficients cause the nonlinearity encountered in the PEM method. Although derived in a different way, the final equations of the *ARMAV-IV* are exactly the same as those of the NExT-type Polyreference (PRCE) method and is thus equivalent to the covariance-driven approach described previously (Peeters and DeRoeck, 2001).

The *Stochastic Subspace Identification (SSI)* method, first introduced by (VanOverschee and DeMoor, 1993), provided another way to avoid the solution of the highly nonlinear least-squares problem encountered in the ARMAV-PEM method. A unified description of different subspace algorithms, both deterministic and stochastic, can be found in VanOverschee and DeMoor (1996). Similar to system realizations, subspace methods identify state-space models -which are in fact transformed ARMAV models- from which the modal parameters are subsequently extracted. The SSI can be implemented as a data-driven or covariance-driven method. In the former, the computation of the correlation functions is essentially replaced by a geometric projection of the row space spanned by the future outputs onto the row space of the past outputs. The covariance-driven version (SSI-Cov) is in fact equivalent to the NExT/ERA procedure Peeters and DeRoeck (2001). A detailed description of the SSI and SSI-Cov in relation to output-only modal identification is given by Peeters and DeRoeck (1999). Due to their robust and fast implementation, these methods have been widely applied for operational modal analysis of civil engineering structures (see for example Hermans and der Auweraer (1999); Ren and Zong (2004)).

The ambient vibration identification methods described above together with the required signal processing techniques to obtain the response models are summarized in figure 1.4, which is a variation of the diagram given in (Cunha and Caetano, 2005). Recently, Cunha and Caetano (2005); Zhang *et al.* (2005a) have presented a review of the state of operational modal identification.

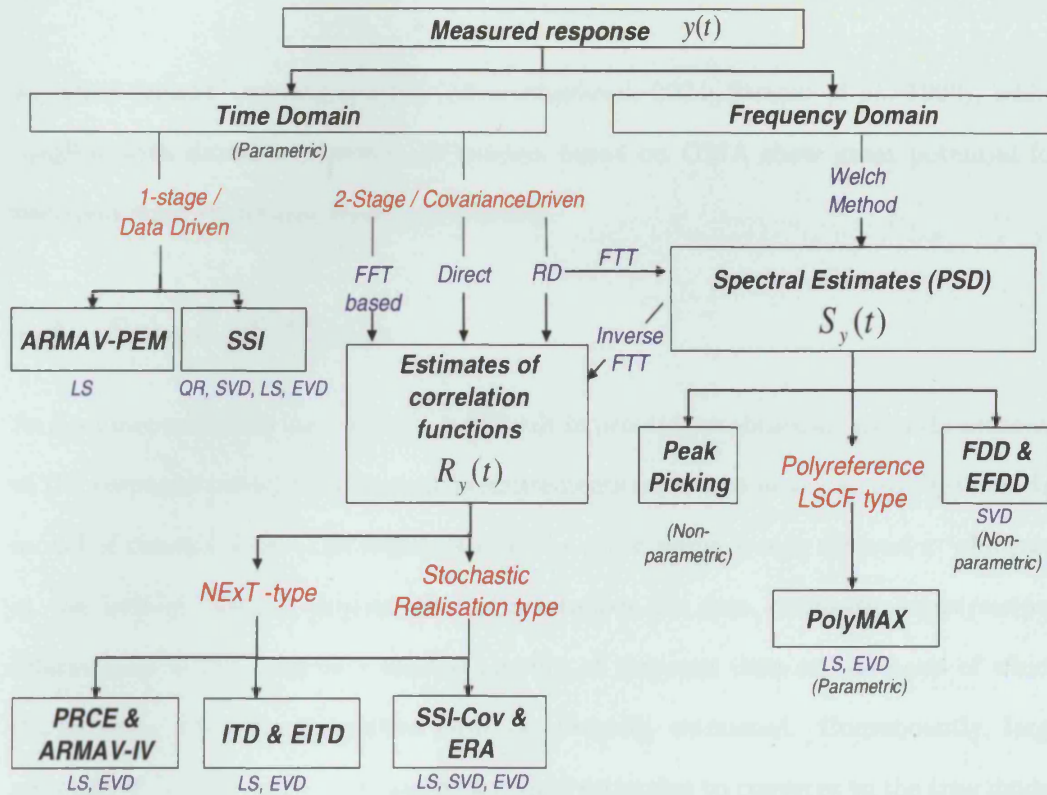


Fig. 1.4: Schematic representation of the various operational identification algorithms and their connections. Legend: (FFT) = Fast Fourier Transform, (RD) = Random Decrement, (LS) = Least Squares, (EVD) = Eigenvalue Decomposition, (SVD) = Singular Value Decomposition, (QR) = Orthogonal Decomposition

The applications of OMA are naturally similar to those described earlier for traditional experimental modal analysis. Two applications, however, are of particular interest in conjunction with OMA: FE Model Updating and damage detection or Structural Health Monitoring (SHM). Ambient testing has the advantage over traditional modal testing that the measured properties describe the dynamics of the structure in its real operating conditions, so that updated models, in principle, reflect better the *in situ* conditions of the system and the as-built structural connectivity. Although classical experimental modal analysis has been used for damage detection of structural systems, this area of research has gained new impetus with the advances made in OMA. The reason is that the non-intrusive testing procedure, for instance using GPS sensors (Brownjohn, 2005), offers the possibility to monitor structures over long time periods so that sudden or progressive damage can be diagnosed in near real time. Therefore, there is a tendency to develop wireless sensing architectures and



so called “smart” sensing systems (Ruiz-Sandoval, 2004; Straser *et al.*, 1998), which coupled with damage detection techniques based on OMA show great potential for near-real time structural health monitoring.

## 1.4 Scope of Thesis

As documented in the literature, it is difficult in practice to obtain an accurate estimate of the response model from output measurements only, and hence an accurate modal model of the structure. The reason is that the practitioner is only allowed a “glimpse” at the infinite random process that characterises the true stochastic input/output relationship in the form of a limited amount of response data on the basis of which the systems’ dynamic properties must be, literally, estimated. Consequently, large amounts of response data are needed for these estimates to converge to the true modal model. Although operational modal analysis is a non-invasive procedure, practical issues often impose limits on the data that can be measured, stored and processed. Not only does the engineer have to estimate the modal parameters from a limited response measurement, but in almost any practical application, the available data is contaminated by unwanted perturbations. In operational modal analysis, these perturbations typically are (also see section 6.1)

- *Non-white, non-stationary ambient excitation* with the consequence that the estimated response model (even if an infinite amount of data were available) will not be representative of the structure’s response only but is mixed with the dynamics of the loading itself
- *Non-linear behaviour* of structure may arise in some cases and -since ambient forcing is typically low- is generally to be attributed to non-linear damping mechanisms. The “classical” techniques used in OMA are applicable to linear behaviour only in both the formulation of the response model and the modal parameter identification therefrom. As a result, using the available linear techniques on non-linear time series will generally introduce significant systematic

errors in the identified modal parameters.

- *Data acquisition errors* refer collectively to disturbances of the data introduced during the measuring process and includes sources such instrumentation noise, discretization/quantization errors or inadequate sensor setup to mention but a few.

With the few exceptions discussed earlier in this introductory chapter, operational modal analysis is a 2-stage procedure. In a first step, the operational response model is estimated -which may be in the time domain (correlation functions) or in the frequency domain (spectral densities)- and from the latter, the modal model is estimated by application of some curve fit algorithm depending on the previously estimated response model (see diagram 1.4). Consequently, the error introduced at each stage during the operational modal analysis will be processed, then propagated to the next stage until it cumulatively affects the final outcome, the modal parameters.

The goal of this thesis is to give a *quantitative* description of the error -both random and systematic (bias)- in the response model and how it propagates through the curve fitting algorithm to affect the identified modal model. The algorithms to extract the modal information out of the response model listed in the diagram 1.4 nearly all give perfect results when the operational response model is exact but distinguish themselves in how they cope with the error present in the response model. Therefore, exactly how the error propagates from the response model to the modal model is specific to the identification algorithm used. In this thesis, the focus is on correlation-driven (or covariance-driven) curve fitting algorithms. Thus, the response model considered consists of a set of auto-and cross-correlation functions computed between simultaneously measured responses histories at different locations on the structural system. As seen from the diagram 1.4, the relevant curve fitting process is the Eigensystem Realisation Algorithm (ERA) or, equivalently, the covariance-driven Stochastic Subspace Identification (SSI/Cov) algorithm. After exposing the necessary theoretical background in Chapter 2, the formulation of the random and bias errors in the correlation-based

response model will be the subject of Chapter 3. In a first instance, an approximate analytic formulation of these errors will be given with the aim to understand in general quantitative terms, the relationship between the estimation errors in the correlation response model and the modal parameters of the system. This will provide the practitioner with a quick tool to assess record length requirements to keep these errors below a desired level, provided a rough estimate of the modal frequencies and damping ratios -for instance from a simple finite element model typically used in pre-test planing- is available. However, this analytical formulation is only able to deal with estimation errors due to finite record lengths and does not incorporate effects due to other error sources such as instrumentation noise for instance. To consider the influence of additional errors in the measured data on the estimated response model, a data-driven method is given. Data-driven in the sense that the errors in the correlation functions are estimated based on the measured response data rather than relying on an analytical model. Such a method will be necessary since the nature of the error introduced into the data during a particular modal test is not known and hence cannot be modeled.

With a description of the errors in the response model at hand, the remainder of the thesis is concerned with the propagation of these errors through the identification algorithm. Two methods are considered: a) a bootstrap approach which is more general and is also applicable to other curve fitting schemes and b) a perturbation theoretic approach which is specific to the the SSI/Cov. A rigorous basis for these two techniques is the subject of Chapters 4 and 5.

In the remaining two chapters, 6 and 7, each of these methods is applied to operational modal identification problems with the intention of studying to what extent the resulting error bounds on the identified modal parameters can be determined. The approach taken uses simulated data where allowing control over the error introduced in the computed time histories and to explore the limits for which the proposed scheme is

applicable. The disturbances considered are estimation errors, external noise sources as well as the effects of nonstationarity and the presence of deterministic components in the ambient loading conditions. The study is restricted to “mild” nonstationary influences and to situations where deterministic components in the ambient loading act as unwanted disturbances rather than the dominant part of the excitation driving the system. This situation is more common in practice than those where the deterministic load is dominant. The effect of nonlinear response characteristics are not considered in this thesis and a linear behaviour of the structural system is assumed. The proposed method will therefore provide the practicing engineer with a tool to obtain approximate error bounds on the identified operational modal parameters and assess the quality of his results. The method is relevant for applications typically associated with operational modal analysis such as damage detection or FE updating and response analysis.

All the algorithms used in thesis were implemented by the author in MATLAB with a few exceptions: 1) Simulated time-response histories and Finite Element models were computed using the freely available Calfem Toolbox by Ristinmaa *et al.* (1999). 2) The implementation of the SSI/Data relies heavily on the implementation in VanOverschee and DeMoor (1996) and some of the files accompanying this book were used<sup>†</sup>. 3) The code for the stationary bootstrap was taken from Kevin Sheppard’s GARCH Toolbox for Matlab\*.

---

<sup>†</sup><http://www.mathworks.com/matlabcentral/fileexchange>  
\*<http://www.kevinsheppard.com/research/>

---

## CHAPTER 2

# THEORETICAL BASIS

---

### 2.1 Introduction

This chapter aims to provide the necessary background theory for operational modal analysis. A formulation of the operational response models used in operational modal analysis is given and various aspects concerning their estimation are presented. The theory behind three identification methods, one in the frequency domain (EFDD), a covariance- and a data-driven time domain algorithm (SSI/Cov and SSI/Data respectively) is briefly presented.

### 2.2 Operational Response Models

Real structures are continuous non-homogeneous systems which have an infinite number of degrees-of-freedom. Therefore, their analysis usually entails an approximation which consists of describing their motion through a finite number of degrees-of-freedom, as many as necessary to ensure enough accuracy. Within this idealization, which includes the lumped mass and the FE type of discretization, the equations of motion of a linear, time-independent  $N$  degree-of-freedom structural system are given in terms of a set of  $N$  second order differential equations of the form

$$\mathbf{M}\ddot{\underline{x}}(t) + \mathbf{C}\dot{\underline{x}}(t) + \mathbf{K}\underline{x}(t) = \underline{f}(t) \quad (2.1)$$

where  $\mathbf{M}$ ,  $\mathbf{K}$ ,  $\mathbf{C} \in \mathbb{R}^{N \times N}$  denote the spatial mass, stiffness and dissipation or damping matrix respectively.  $\underline{x}(t) \in \mathbb{R}^{N \times 1}$  describes the time dependent vector of displacements.

ments at each of the degrees-of-freedom and  $\underline{f}(t) \in \mathbb{R}^{N \times 1}$  is the vector consisting of the external time-varying excitation forces applied at each degrees-of-freedom. The modeling of the damping deserves a few comments. The damping model used in equation 2.1 is the familiar linear viscous damping model but this model does not necessarily imply the actual physical description of the damping mechanism. A combination of different phenomena can be expected to contribute to the damping in structures such as material damping (micro-structure effects), boundary damping (e.g. frictional slipping at joints) and dissipation due to contact between the structure and fluid. For civil engineering structures, boundary damping will generally be responsible for the most significant part of the energy dissipation. The dissipation matrix model used in equation 2.1 does not necessarily offer a physical description of the latter damping mechanism as it cannot be asserted that the dissipation mechanism will only depend on the velocity of the system. However, as far as experimental modal analysis is concerned, it will be possible to obtain equivalent modal damping ratios and the correct associated complex modes as long as the underlying damping mechanism is linear (Woodhouse, 1998). However, the nature of the underlying damping model can, in general, not be determined and if a good physical description of the damping mechanism is needed, a suitable damping model must be chosen and fitted (Adhikari and Woodhouse, 2001*a,b*). Dissipation mechanisms such as boundary damping often exhibit non-linear behaviour and clearly, the form of the non-linear character of the damping will be lost in a linear modal analysis. Nonetheless, if the damping is not too severe, the linearised modal damping ratios obtained via a modal identification procedure may still be good enough to yield reasonably accurate response predictions. More recently, time-frequency identification methods have been employed to determine non-linear damping characteristics (see for instance Staszewski (1998)).

To derive the desired operational response model, consider the case where the excitation  $\underline{f}(t)$  consists of a set of *transient or impulsive* forces i.e. forces that act only for a short time period. Taking the Fourier transform of  $\underline{f}(t)$ , denoted by  $\mathcal{F}$ , on

both sides of equation of motion 2.1 yields

$$\underline{\mathbf{X}}(\omega) = (\mathbf{K} - \omega^2\mathbf{M} + i\omega\mathbf{C})^{-1}\underline{\mathbf{F}}(\omega) = \mathbf{H}(\omega)\underline{\mathbf{F}}(\omega) \quad (2.2)$$

where  $\underline{\mathbf{F}}(\omega) = \mathcal{F}(\mathbf{f}(t)) \in \mathbb{C}^{N \times 1}$ ,  $\underline{\mathbf{X}}(\omega) = \mathcal{F}(\mathbf{x}(t)) \in \mathbb{C}^{N \times 1}$  and  $\mathbf{H}(\omega) \in \mathbb{C}^{N \times N}$ , which relates the input to the output is the receptance FRF matrix. The  $(jk)^{th}$  entry  $H_{jk}(\omega)$  of the receptance FRF matrix corresponds to the individual FRF describing the relation between the response of the system at the  $j^{th}$  coordinate excited by a single force (i.e. all other forces are zero) applied at coordinate  $k$ . In practice, however, if one is interested in the modal parameters only, it is not necessary to obtain the full FRF matrix as given above. Indeed, in classical modal testing the dimension of the FRF matrix is determined by the number of excitations applied to the system, say  $m$ , and the number of outputs measured, say  $l$ . With the interpretation of the entries of the FRF matrix given above, it is easily seen that in this case  $\mathbf{x}(t)$  and  $\underline{\mathbf{X}}(\omega) \in \mathbb{R}^{l \times 1}$ ,  $\mathbf{f}(t)$  and  $\underline{\mathbf{F}}(\omega) \in \mathbb{R}^{m \times 1}$  and  $\mathbf{H}(\omega) \in \mathbb{C}^{l \times m}$  with the frequency-domain input-output relation given by

$$\underline{\mathbf{X}}(\omega) = \mathbf{H}(\omega)\underline{\mathbf{F}}(\omega). \quad (2.3)$$

Henceforth, the latter dimensions will be assumed unless stated otherwise. It is well known that, for general viscous damping,  $\mathbf{H}(\omega)$  can be expressed as (Ewins, 2000)

$$\mathbf{H}(\omega) = \sum_{r=1}^N \left( \frac{\underline{\phi}_r \underline{\varphi}_r^T}{i\omega - \lambda_r} + \frac{\underline{\phi}_r^* \underline{\varphi}_r^H}{i\omega - \lambda_r^*} \right) \quad (2.4)$$

where the poles  $\lambda_r$  are the eigenvalues of the system which occur in complex conjugate pairs. They contain the frequency and modal damping information and are given by  $\lambda_r, \lambda_r^* = -\omega_r \xi_r \pm i\omega_r \sqrt{1 - \xi_r^2}$  where  $\omega_r$  and  $\xi_r$  denote the natural frequency and modal damping ratio respectively. The imaginary part of the pole yields the damped natural frequency  $\omega_{D_r}$ . The residues  $\underline{\phi}_r \underline{\varphi}_r$  consist of the product of the scaled mode shapes  $\underline{\phi}_r \in \mathbb{C}^{l \times 1}$  and the vectors  $\underline{\varphi}_r \in \mathbb{C}^{m \times 1}$ , known as the *modal participation vectors*.  $(\cdot)^*$  denotes the complex conjugate and  $(\cdot)^H$  Hermitian transposition. Equation 2.3 admits a time-domain formulation which can be obtained directly by inverse Fourier

transform leading to the following matrix convolution integral

$$\mathbf{x}(t) = \int_0^{\infty} \mathbf{h}(\tau) \mathbf{f}(t - \tau) d\tau \quad (2.5)$$

where  $\mathbf{h}(t) = \mathcal{F}^{-1}(\mathbf{H}(\omega)) \in \mathbb{R}^{l \times m}$  is the *impulse response function (IRF) matrix*. This relation is often referred to as *Duhammel's integral*. The  $(jk)^{th}$  entry of the IRF matrix,  $h_{jk}(t)$  establishes the relation between the output at the  $j^{th}$  coordinate due to a *single* input at the  $k^{th}$  coordinate. Physically,  $h_{jk}(t)$  is the response of the system at the  $j^{th}$  coordinate due to a unit impulse applied at coordinate  $k$  as may be easily be seen from equation 2.5 by taking the  $k^{th}$  component of  $\mathbf{f}(t)$  to be Dirac delta function  $\delta(t - \tau)$  applied at  $t = 0$ , and all the other inputs are zero. Note that  $\mathbf{h}(t) = 0$  for  $t < 0$ . Like the FRF matrix, the IRF matrix completely characterizes the system in terms of its modal parameters as can be seen by taking the Fourier transform of equation 2.4

$$\mathbf{h}(t) = \sum_{r=1}^N e^{\omega_r \xi_r t} (\underline{\phi}_r \underline{\phi}_r^T e^{i\omega_{D_r} t} + \underline{\phi}_r^* \underline{\phi}_r^H e^{-i\omega_{D_r} t}) \quad (2.6)$$

i.e. each entry is weighted sum of decaying sinusoids which oscillate with the damped natural frequency of the system and the decay is governed by the modal damping ratio.

Ambient excitation, however, is stochastic in nature and since the structural system acts as a linear transformation of the input, the response too will be stochastic. While the time-domain relation (equation 2.5) is still valid for random signals, the frequency-domain input-output relation given above for a transient excitation and response (equation 2.3) is no longer valid. The reason is that the Fourier transforms of the random signals  $x_j(t)$  and  $f_k(t)$  may not be defined at all frequencies  $\omega$ . A sufficient condition for the Fourier integral to exist is that  $x_j(t)$  and  $f_k(t)$  are *absolutely integrable* over the infinite interval  $(-\infty, \infty)$  i.e. that

$$\int_{-\infty}^{\infty} |f_k| dt \quad \text{and} \quad \int_{-\infty}^{\infty} |x_j| dt < \infty \quad (2.7)$$

This requirement for the existence of the Fourier integral is often referred to as the



(weak) Dirichlet condition. Loosely speaking, it requires that  $x_j(t)$  and  $f_k(t)$  will decay as  $t \rightarrow \infty$  and  $t \rightarrow -\infty$ . While this criterion is clearly satisfied for transient inputs, this is not the case when the excitation is stationary so that an alternative approach must be sought.

### 2.2.1 Stochastic Processes, Stationarity and Ergodicity

Suppose that  $x(t)$  is a single record of the response measured from an experiment where a structural system is excited by a stochastic input. If the experiment is repeated under identical conditions, a different response history will be measured due to the random nature of the process. Each observed time history record e.g. the  $p^{\text{th}}$  record, denoted by  $x(t, p)$ , is merely one record of the whole collection or *ensemble* of all possible records that might have occurred and is therefore referred to as a *sample function* or *realization* of the complete stochastic (or random) process denoted by  $\{x(t, p)\}$ . This is illustrated in figure 2.1. For each value of  $t \in (-\infty, \infty)$ ,  $x(t, p)$  represents a random variable over the index  $p$  which admits a range of possible values with an associated *probability distribution* describing the relative likeliness of each possible value.

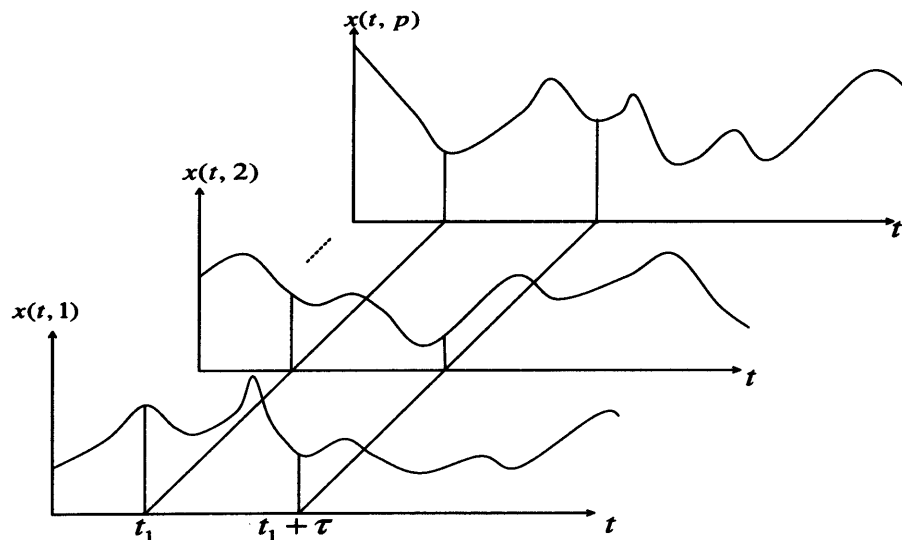


Fig. 2.1: Ensemble of time-history records defining a random process.  $x(t_1, p)$  and  $x(t_1 + \tau, p)$  are two different random variables. (Bendat and Piersol, 2000)

When a physical phenomenon is represented by a stochastic process, it must be characterized by statistical parameters. For most engineering problems involving random data, including operational modal analysis, the most important quantities are often the *statistical moments up to second order* given below (Bendat and Piersol, 2000)

$$\mu_x(t) = E[x(t, p)] \quad (2.8)$$

$$msv_x(t) = E[x^2(t, p)] \quad (2.9)$$

$$C_{xx}(t, t + \tau) = E[(x(t, p) - \mu_x(t))(x(t + \tau, p) - \mu_x(t + \tau))] \quad (2.10)$$

$$C_{xy}(t, t + \tau) = E[(x(t, p) - \mu_x(t))(y(t + \tau, p) - \mu_y(t + \tau))] \quad (2.11)$$

Here,  $E[\cdot]$  denotes the *expectation operator* and represents the average of the random variable across the ensemble (Bendat and Piersol, 2000). The abbreviations (acv.f.) and (xcv.f.) will be used to denote the *auto-covariance*  $C_{xx}(t, t + \tau)$  of the random process  $\{x(t, p)\}$  and *cross-covariance* functions  $C_{xy}(t, t + \tau)$  between the pair of random processes  $\{x(t, p)\}$  and  $\{y(t, p)\}$  respectively.  $\mu_x(t)$  and  $msv_x(t)$  denote the *mean* and *mean square value* at time  $t$  respectively. From the covariance functions, the definition of the *variance* and *auto-and cross-correlation functions* follow immediately as

$$Var[x(t)] = \sigma^2(t) = C_{xx}(t, t) = E[(x(t, p) - \mu_x(t))^2] \quad (2.12)$$

$$R_{xx}(t, t + \tau) = E[x(t, p)x(t + \tau, p)] \quad (2.13)$$

$$R_{xy}(t, t + \tau) = E[x(t, p)y(t + \tau, p)] \quad (2.14)$$

where  $R_{xx}$  denotes the autocorrelation function (ac.f.) and  $R_{xy}$  the cross-correlation function between the pair of stochastic processes  $\{x(t, p)\}$  and  $\{y(t, p)\}$ . It can be seen that correlation and covariance functions agree for a zero-mean processes and that the variance reduces to the mean square value. It might be worth pointing out

that some authors define the correlations as covariance functions normalized to unity at the origin i.e. *as a correlation coefficient function* (see Priestley (2004)) but the definition given in equations 2.13 and 2.14 will be used here.

The statistical parameters described in equations 2.8-2.14 are in general time-dependent. However, for some stochastic processes endowed with a property known as *stationarity*, the statistical moments are constant over time. Such processes arise generally from stable physical systems which have settled to a state of *statistical equilibrium*. More formally, a random process is said to be *stationary* or *completely stationary* if its probabilistic structure is invariant under a shift of the time origin (Priestley, 2004). This means that, for example, the joint probability distribution of the set of random variables  $\{x(t, p), x(t + \tau, p)\}$  for all  $t$  is the same so that the covariance and correlation functions do no longer depend on  $t$  but only on the time separation  $\tau$  (often referred to as the *lag*) between the time points and not on their individual location. Thus, for a stationary stochastic process, equations 2.8-2.14 become

$$\mu_x = E[x(t, p)] \quad (2.15)$$

$$msv_x = E[x^2(t, p)] \quad (2.16)$$

$$\sigma^2 = E[(x(t, p) - \mu_x)^2] \quad (2.17)$$

and

$$C_{xy}(\tau) = E[(x(t, p) - \mu_x)(y(t + \tau, p) - \mu_y)] \quad (2.18)$$

$$R_{xy}(\tau) = E[x(t, p)y(t + \tau, p)] \quad (2.19)$$

The auto-covariance and auto-correlation functions immediately follow from equations 2.18 and 2.19 by letting  $y(t, p) = x(t, p)$ . Complete stationarity is, however, a severe requirement and this concept can be relaxed by introducing the notion of *weak stationarity*. Under this weaker condition, it is not necessary that the complete probability

structure of the process is invariant under time translations but only that its main features are the same i.e. that the statistical moments up to a certain order do not change over time. Typically, weak stationarity is used to describe a process whose *moments up to second order* are invariant under time translations (Bendat and Piersol, 2000) and this convention will be used henceforth. It is worth noting that for a process with a Gaussian probability distribution, weak stationarity implies complete stationarity since a Gaussian process is completely described by its moments up to second order.

In many practical situations it may not be possible to obtain a large ensemble of different realizations of the particular stochastic process so that one is often forced to get the necessary statistical information of the process from a single time history. This is certainly the case in ambient testing. Although it may be possible to increase the length of the observed time series, there will only be a single outcome of the process and a single observation on the random variable at a given time  $t$ . A particular sample function, however, is in general not enough to represent the particular stochastic process to which it belongs. Nonetheless, for a certain class of random processes, called *ergodic processes*, it is possible to obtain statistical information of the entire process from a single realization. More precisely, a process is ergodic if the statistical properties can be computed from *time averages* over individual sample functions of the ensemble and will be the same from one record to the next and will equal the corresponding properties computed from ensemble averages over the records at any time  $t$ . Since the averages are taken over absolute time  $t$ , this implies that the corresponding ensemble averages cannot depend on time so that an ergodic process must be stationary. The converse, however, does not hold. The hierarchy of random processes is illustrated in figure 2.2.1. A sufficient condition for a random process to be ergodic is that it is (a) stationary and that (b) the statistical moments computed from time averages be the same for all sample functions. Additionally, when the process is

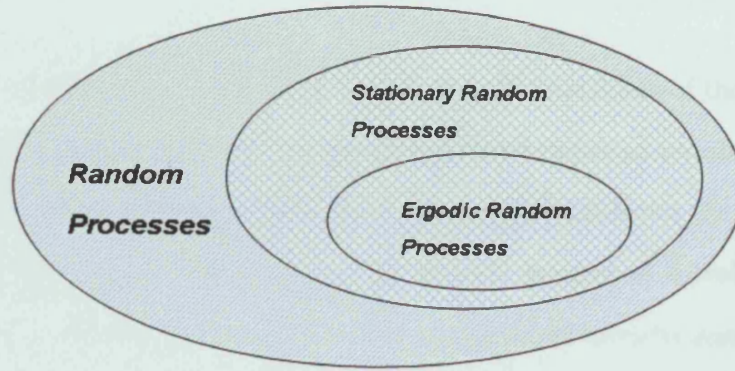


Fig. 2.2: Hierarchy of random processes

Gaussian, condition (b) is equivalent to (Bendat and Piersol, 2000)

$$\frac{1}{T} \int_{-T}^T |C_{xx}(\tau)| d\tau \rightarrow 0 \quad \text{as } T \rightarrow \infty \quad (2.20)$$

When stationarity is replaced by weak stationarity, the above still holds albeit in this case, only the moments up to second order computed from time averages are guaranteed to converge to the corresponding ensemble averages. This is often referred to as *weak ergodicity*.

Much like equation 2.7, the condition in 2.20 requires the auto-covariance function of the process to “decay” to zero as  $t \rightarrow \infty$ . For the response of a linear, time-invariant system such as that described in equation (i.e. a damped system) 2.1, this holds almost certainly (Priestley, 2004). Violations are usually associated with the presence of periodic components in the data. Thus, if the response of a linear, time-invariant system is stationary and Gaussian, this almost certainly implies that the process is ergodic and hence that the statistical properties can be obtained from a single realization of the process.

### 2.2.2 Frequency-Domain Operational Response model and NExT

Having introduced the basic concepts relating to stochastic processes, the frequency-domain input-output relationship can now be derived and be used to formulate the operational response model. Let  $\{x_j(t, p)\}$  and  $\{x_q(t, p)\}$  be the *stationary* random

processes consisting of the response at the  $j^{\text{th}}$  and  $q^{\text{th}}$  coordinate of the system given by equation 2.1, respectively, due to a single stationary input at coordinate  $k$  defined by  $\{f_k(t, p)\}$ . The fact that we have chosen the input -and hence the output- to be stationary does still not guarantee that the Fourier integral of a realization of the processes exists since the very nature of the notion of stationarity suggests that the sample functions will almost certainly not decay at infinity. To overcome this difficulty, a truncated sample function for the response is defined by

$$x_j(t, p, T) = \begin{cases} x_j(t, p), & 0 \leq t \leq T \\ 0, & \text{otherwise} \end{cases} \quad (2.21)$$

and a similar definition applies to the truncated sample functions  $f_k(t, p, T)$  and  $x_q(t, p, T)$ . Since these truncated realizations die away at  $\pm\infty$ , they satisfy the Dirichlet condition and hence their (finite) Fourier transform exists. For the response sample function, it is given by

$$X_j(\omega, p, T) = \int_{-\infty}^{\infty} x_j(t, p, T) e^{-i\omega t} dt = \int_0^T x_j(t, p, T) e^{-i\omega t} dt \quad (2.22)$$

Again, a similar definition applies to the excitation  $F_k(\omega, p, T)$  and the response at the  $q^{\text{th}}$  coordinate  $X_q(\omega, p, T)$ . These quantities can now be used to compute the *auto-spectral or power spectral densities (PSD)* of the response and excitation. Similarly, the *cross-spectral densities (CSD)* between the response and excitation time histories can be computed in this fashion. They are defined as (Bendat and Piersol, 2000)

$$S_{x_j x_j}(\omega) = \lim_{T \rightarrow \infty} E \left[ \frac{X_j^*(\omega, p, T) X_j(\omega, p, T)}{T} \right] \quad (2.23)$$

$$S_{f_k f_k}(\omega) = \lim_{T \rightarrow \infty} E \left[ \frac{F_k^*(\omega, p, T) F_k(\omega, p, T)}{T} \right] \quad (2.24)$$

$$S_{x_q x_j}(\omega) = \lim_{T \rightarrow \infty} E \left[ \frac{X_q^*(\omega, p, T) X_j(\omega, p, T)}{T} \right] \quad (2.25)$$

where  $E[\cdot]$  denotes the expectation operator over the ensemble and  $(\cdot)^*$  the complex conjugate.  $S_{x_j x_j}(\omega)$  and  $S_{f_k f_k}(\omega)$  are the auto-spectral densities between input

and output time-histories respectively and  $S_{x_q x_j}(\omega)$  denotes the cross-spectral density between two outputs measured at different location along the structure. The cross-spectrum between the input and the output can be defined similarly (Bendat and Piersol, 2000). Although the Fourier transform of the truncated time histories  $x_j(t, p, T)$ ,  $x_q(t, p, T)$  and  $f_k(t, p, T)$  is not bounded as  $T \rightarrow \infty$ , the power- and cross-spectral densities defined in equations 2.24-2.25 may, in fact, converge to a finite limit as  $T \rightarrow \infty$ . Indeed, it is a well known result, often called the *Wiener-Khinchine relation* (see for example Bendat and Piersol (2000) or Priestley (2004)), that the PSD of a stationary random process and CSD between any two stationary processes are in fact the Fourier transform of the auto- and cross-correlation functions of these processes i.e.

$$S_{x_j x_j}(\omega) = \mathcal{F}(R_{x_j x_j}(\tau)), \quad (2.26)$$

$$S_{f_k f_k}(\omega) = \mathcal{F}(R_{f_k f_k}(\tau)), \quad (2.27)$$

$$S_{x_q x_j}(\omega) = \mathcal{F}(R_{x_q x_j}(\tau)) \quad (2.28)$$

It can now be seen by comparing equations 2.24-2.25 with 2.28 that a sufficient condition for the limiting operation in equations 2.24-2.25 to converge, or in other words, for the spectral densities to exist for all  $\omega$  is that the auto- and cross-correlation functions in 2.28 possess a Fourier transform. That is, the ac.f. and xc.f. must be absolutely integrable. For the response of a linear, time-invariant damped system, the ac.f. and xc.f. will *decorrelate* with  $\tau$  as long as the process is *zero-mean*, (Clough and Penzien, 1993; Pandit and Wu, 1983; Priestley, 2004) so that the Fourier transform will exist. It is interesting to note that for a zero-mean process, the sufficient condition for the existence of spectral densities is the same as equation 2.20. It thus follows that a zero-mean, (weakly) stationary Gaussian process whose PSD exists at all  $\omega$  is (weakly) ergodic. Since these properties are conserved under a linear, time-invariant transformation (see figure 2.3), it is very often assumed in operational modal analysis

that the ambient excitation is zero-mean stationary and Gaussian. †

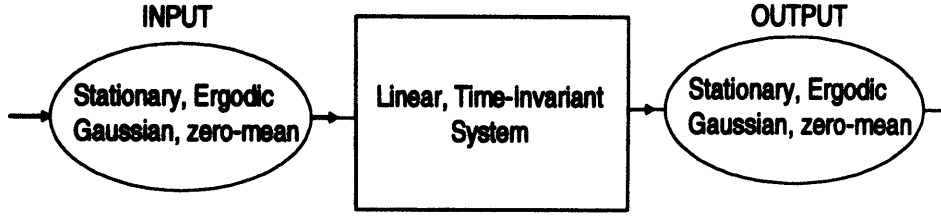


Fig. 2.3: Stationarity, ergodicity, zero-mean and Gaussian distribution is conserved under a linear, time-invariant transformation

The frequency-domain relationship for an  $m$ -input  $l$ -output (MIMO) system in equation 2.1 can now be established for stochastic data, and as a result the operational response model. Making use of equation 2.5 to formulate the product  $\underline{x}(t, p) \underline{x}(t + \tau, p)$  and taking ensemble averages one obtains

$$\mathbf{R}_{\underline{x}\underline{x}}(\tau) = \int_0^\infty \int_0^\infty \mathbf{h}(\alpha) \mathbf{R}_{\underline{f}\underline{f}}(\tau + \beta - \alpha) \mathbf{h}^T(\beta) d\alpha d\beta \quad (2.29)$$

where  $\mathbf{R}_{\underline{x}\underline{x}}(\tau) \in \mathbb{C}^{l \times l}$  and  $\mathbf{R}_{\underline{f}\underline{f}}(\tau) \in \mathbb{C}^{m \times m}$  given by  $E[\underline{x}(t, p) \underline{x}(t + \tau, p)]$  and  $E[\underline{f}(t, p) \underline{f}(t + \tau, p)]$  respectively, denote the input and output *auto-correlation matrices*. The main diagonal of  $\mathbf{R}_{\underline{x}\underline{x}}(\tau)$  contains the auto-correlation functions of the outputs and the off-diagonal terms gives the cross-correlations between different outputs. More specifically, the  $(jq)^{th}$  entry  $R_{x_j x_q}(\tau)$  is given by  $E[x_j(t, p) x_q(t, p)]$ . The same description applies to  $\mathbf{R}_{\underline{f}\underline{f}}(\tau)$ . Taking the Fourier transform on both sides of equation 2.29 then yields the following important relation

$$\mathbf{S}_{\underline{x}\underline{x}}(\omega) = \mathbf{H}^*(\omega) \mathbf{S}_{\underline{f}\underline{f}}(\omega) \mathbf{H}^T(\omega) \quad (2.30)$$

where  $\mathbf{S}_{\underline{x}\underline{x}}(\omega) \in \mathbb{C}^{l \times l}$  and  $\mathbf{S}_{\underline{f}\underline{f}}(\omega) \in \mathbb{C}^{m \times m}$  denote the input and output *power spectral density matrices* given by  $E[\underline{X}^*(\omega, p, T) \underline{X}^T(\omega, p, T)]$  and  $E[\underline{F}^*(\omega, p, T) \underline{F}^T(\omega, p, T)]$  respectively with  $T \rightarrow \infty$ . The main diagonal of  $\mathbf{S}_{\underline{x}\underline{x}}(\omega)$  contains the power spectral densities of the individual outputs and the off-diagonal terms the cross spectral

†Note that the Gaussian distribution is not a necessary condition for ergodicity and nor for the existence of the Fourier integral. Also, the assumption for the input to be a zero-mean process is used for convenience as a non-zero mean value can generally be removed from the signals by detrending operations (Bendat and Piersol, 2000).



densities between different outputs. Again, the same description applies to the input spectral density matrix. Following the same procedure as above, another input-output relation can be obtained, namely  $\mathbf{S}_{\mathbf{f}\mathbf{x}}(\omega) = \mathbf{S}_{\mathbf{f}\mathbf{f}}(\omega) \mathbf{H}^T(\omega)$  (see (Bendat and Piersol, 2000)), where  $\mathbf{S}_{\mathbf{f}\mathbf{x}}(\omega)$  is the cross-spectral density matrix between the input and the output, but for operational modal analysis, this is less useful than equation 2.30. Indeed, under the assumption of a *white noise excitation*, the output power spectral density matrix yields the desired operational response model in the frequency domain. With the assumption of white noise, the input power spectral density is independent of frequency, and assuming further that the input is cross-uncorrelated, all off-diagonal terms become zero so that  $\mathbf{S}_{\mathbf{f}\mathbf{f}}(\omega)$  becomes a constant diagonal matrix denoted by  $\mathbf{S}$ . Indeed, by substituting equation 2.4 into 2.30, multiplying out the factors and writing each in partial fraction form, the output PSD matrix can be written as (Hermans and der Auweraer, 1999)

$$\mathbf{S}_{\mathbf{x}\mathbf{x}}(\omega) = \sum_{r=1}^N \left( \frac{\underline{\mathbf{L}}_r \underline{\phi}_r^T}{i\omega - \lambda_r} + \frac{\underline{\mathbf{L}}_r^* \underline{\phi}_r^H}{i\omega - \lambda_r^*} + \frac{\underline{\phi}_r \underline{\mathbf{L}}_r^T}{-i\omega - \lambda_r} + \frac{\underline{\phi}_r^* \underline{\mathbf{L}}_r^H}{-i\omega - \lambda_r^*} \right) \quad (2.31)$$

with

$$\underline{\mathbf{L}}_r = \sum_{q=1}^N \frac{\underline{\phi}_q^* \underline{\varphi}_q^H \mathbf{S} \underline{\varphi}_r}{-\lambda_r - \lambda_q^*} + \frac{\underline{\phi}_q \underline{\varphi}_q^T \mathbf{S} \underline{\varphi}_r}{-\lambda_r - \lambda_q} \in \mathbb{C}^{l \times 1} \quad (2.32)$$

It can be seen from this equation that the PSD matrix is given in terms of the poles of the system and hence may serve as the operational response model. The residues, however, do not admit the simple form as those of the modally decomposed FRF matrix (equation 2.4). As can be seen from equation 2.32, often referred to as the *operational reference factor* (Peeters, 2004), they contain the contribution of all the other system modes as well as the unknown input spectrum. The fact that the unknown input forms an integral part of the residue inhibits the estimated mode shapes to properly scaled. Although some “tricks” have been devised for the scaling (Aenelle *et al.*, 2005; Doebling and Farrar, 1996; Parloo *et al.*, 2005), this remains a major issue in operational modal analysis. Comparing equation 2.32 with equation 2.4 shows that the operational reference factors replace the modal participation factors in the

input-output frequency domain response model.

The corresponding time-domain operational response model can now easily be obtained from equation 2.31 by inverse Fourier transform i.e.

$$\begin{aligned} \mathbf{R}_{\underline{\mathbf{x}} \underline{\mathbf{x}}}(\tau) = \sum_{\tau=1}^N e^{\omega_r \xi_r \tau} (\underline{\mathbf{L}}_r \underline{\boldsymbol{\phi}}_r^T e^{i\omega_{D_r} \tau} u(\tau) + \underline{\mathbf{L}}_r^* \underline{\boldsymbol{\phi}}_r^H e^{-i\omega_{D_r} \tau} u(\tau) + \\ \underline{\boldsymbol{\phi}}_r \underline{\mathbf{L}}_r^T e^{i\omega_{D_r} \tau} u(-\tau) + \underline{\boldsymbol{\phi}}_r^* \underline{\mathbf{L}}_r^H e^{-i\omega_{D_r} \tau} u(-\tau)) \end{aligned} \quad (2.33)$$

where  $u(t)$  is the Heaviside step function. The first two terms, which are the Fourier transform of the first two terms in equation 2.31, yield the part of the correlation matrix for positive lag times. The PSD matrix defined only by the first two terms of equation 2.31 is often referred to as the *half-spectrum*. The last two terms give the correlations for negative lag times. It can be seen that the positive part of the correlation matrix is of the same form as the IRF matrix in equation 2.6 i.e. a sum of decaying sinusoids governed by the resonant frequencies and damping ratios of the system and thus can be used as the operational response model in the time-domain. In fact, they can serve as the input to classical modal identification algorithms that work on impulse response function. This is generally known as the Natural Excitation Technique (NExT). The original derivation of this result can be found in James *et al.* (1995). In practice, these response model have to be estimated from a single realization of finite sample size from the stochastic process which invariably leads to estimation errors. This will be dealt with in the next chapter.

## 2.3 Identification Methods

### 2.3.1 The Enhanced Frequency Domain Decomposition (EFDD)

The Frequency Domain Decomposition method aims to decouple the individual modes of the system by performing a singular value decomposition (SVD) of the PSD matrix at each discrete frequency line  $\omega = \omega_j$  (Brincker *et al.*, 2000). Let  $\mathbf{S}_{\underline{\mathbf{x}} \underline{\mathbf{x}}}(\omega_j)$  be the

PSD matrix evaluated at frequency  $\omega_j$  consisting of the auto- and cross-spectra taken between the response time-histories measured at *all* transducer locations\*. Then, its SVD can be written as (Brincker *et al.*, 2000; Herlufsen *et al.*, 2005)

$$\mathbf{S}_{\underline{\mathbf{x}} \underline{\mathbf{x}}}(\omega_j) = \mathbf{U}_j \mathbf{S}_j \mathbf{U}_j^H \quad (2.34)$$

where  $\mathbf{S}_j$  is the diagonal matrix of singular values,  $\mathbf{U}_j$  the unitary matrix of associated singular vectors,  $(\cdot)^H$  denotes the Hermitian transpose and the index  $j$  refers to the frequency  $\omega_j$ . The fact that  $\mathbf{U}_j$  is unitary means that  $\mathbf{U}_j^H \mathbf{U}_j = \mathbf{I}$ , i.e. its columns are orthonormal vectors. In the vicinity of a peak, that is, near a modal frequency, say  $\omega_r$ , there is typically a single mode that dominates the response which translates into the fact that the rank of the PSD matrix around this peak approximates to 1. Thus, in the vicinity of a modal frequency, equation 2.34 can be written as

$$\mathbf{S}_{\underline{\mathbf{x}} \underline{\mathbf{x}}}(\omega_j) \approx s_{1j} \underline{\mathbf{u}}_{1j} \underline{\mathbf{u}}_{1j}^H \quad (2.35)$$

for  $\omega_j \rightarrow \omega_r$ .  $s_{1j}$  denotes the first singular value at the  $j^{\text{th}}$  frequency line and  $\underline{\mathbf{u}}_{1j}$  the associated first singular vector. Since the rank of the PSD matrix is close to 1, only the first singular value contains modal information and will reach a maximum. This manifests itself by a peak in the singular value spectrum. In the case, where modes are repeated, the rank of the PSD matrix will equal the multiplicity of the repeated mode.

It is shown in (Brincker *et al.*, 2000) that for a lightly damped structure, in the vicinity of a system mode, say the  $r^{\text{th}}$  mode, the modal reference factor  $L_r$  (c.f. equation 2.32) is dominated by this mode so that it can be approximated by  $L_r \approx d_r \underline{\phi}_r^*$  with  $d_r$  a real scalar given by  $d_r = \underline{\phi}_r^H \mathbf{S} \underline{\phi}_r$ . Also, equation 2.31 then reduces to

$$\mathbf{S}_{\underline{\mathbf{x}} \underline{\mathbf{x}}}(\omega_j) \approx \underline{\phi}_r \text{diag} \left[ 2 \Re \left( \frac{d_r}{i\omega_j - \lambda_r} \right) \right] \underline{\phi}_r^H \quad (2.36)$$

---

\*In practice, the the cross-spectra are often computed only with respect to a few selected reference stations. The principle of the FDD method remains the same (c.f. Gade *et al.* (2005) for instance).

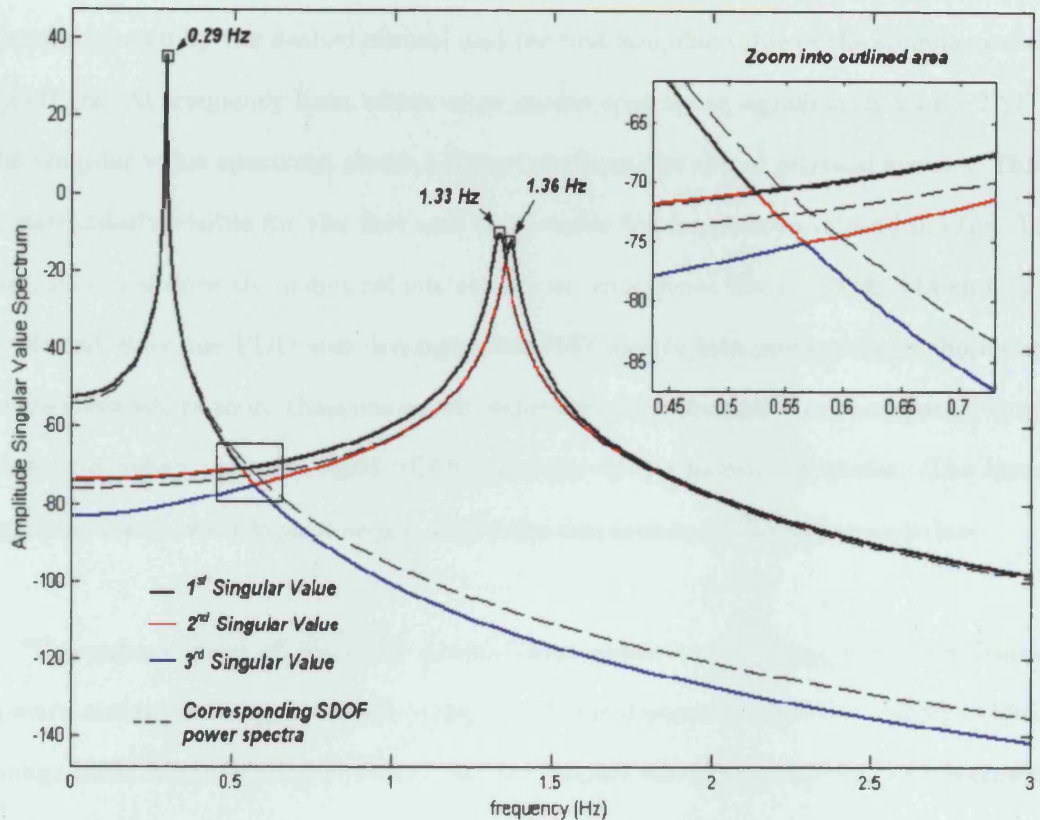


Fig. 2.4: Illustration of the Frequency Domain Decomposition method.

for  $\omega_j \rightarrow \omega_r$ , where  $\Re(\cdot)$  denotes the real part of a complex number and  $\phi_r \in \mathbb{C}^{l \times 1}$  the mode shape of the  $r^{th}$  mode. Comparing equation 2.35 to equation 2.36 it can be seen that at a modal frequency, i.e. at a peak in the singular value spectrum, the singular value decomposed spectrum at the vicinity of this frequency yields the desired modal information: the frequency of the mode is found by the peak in the singular value spectrum and the corresponding singular vector approximates the mode shape.

The FDD is illustrated in figure 2.4 for the same 3DOF, proportionally damped system as used in figure 1.2. The black line represents the first singular value as a function of frequency and the resonant frequencies of the 3 modes of the system are found from its peaks. The second and third singular value are shown in red and blue respectively. At the vicinity of each peak, the SVD decouples the PSD matrix into the equivalent SDOF system auto-spectra as can be seen from the SDOF system auto-

spectra (shown by the dashed curves) and the first singular value of the singular value spectrum. At frequency lines where more modes contribute significantly to the PSD, the singular value spectrum shows a departure from the actual physical system. This is particularly visible for the first and third mode for frequencies around 0.5 Hz. In fact, modes shapes are in general not unitary or orthogonal (Ewins, 2000; Ma and Ng, 2004) but since the FDD also decouples the PSD matrix into unitary mode shapes at frequencies where more than one mode contributes significantly to the response, they no longer reflect the uncoupled SDOF behavior of the individual modes. The inset figure in 2.4 shows a typical region where the dominance of the modes switches.

The enhancement of the FDD method then consists of tracking the SDOF auto-spectra among the singular values using the *Modal Assurance Criterion (MAC)* (Allemang, 2003; Allemang and Brown, 1982) to compare the mode shape at the resonance peak with those obtained at neighbouring frequencies. The singular value spectrum may therefore be taken to correspond to the physical SDOF auto-spectrum up to those frequencies where the MAC coefficient is higher than a certain user specified value. The identified SDOF auto-spectra are then back-transformed to the time-domain via inverse FFT resulting in auto-correlation functions of the individual modes of the system. A SDOF time-domain curve-fitting procedure may then be used to analyse the identified auto-correlation functions. For instance, enhanced estimates of the frequencies of the system can be obtained from the zero-crossing times of the correlation functions as this eliminates the dependence of the frequency bin size of the discrete Fourier transform and the damping ratios can be estimated by logarithmic decrement. It should be noted that in some cases (e.g. noisy spectra due to limited data) only a small portion around the peak of the singular spectrum can be identified as the true SDOF behaviour. The sharp discontinuities at the “cut off” introduce bias into the auto-correlation functions obtained via inverse Fourier transform which affects the quality of the estimated damping ratios (Brincker *et al.*, 2000). An average of the singular vectors weighted by the corresponding singular values computed in the

frequency band defining the SDOF auto-spectra will yield enhanced mode shape estimates (Brincker *et al.*, 2001).

Two recent developments, both based on a better estimation of the PSD matrix, have recently been suggested for use with the EFDD. To reduce noise and avoid leakage in the PSD estimates, Rodrigues *et al.* (2004) have computed the PSD matrix from random decrement signatures via FFT. Using a method very similar to that used in (Shih *et al.*, 1988) for FRFs, Zhang *et al.* (2005b) obtain an enhanced PSD matrix around a peak making use of the singular vector estimated at the resonance. This attenuates the effect of the truncation of the identified SDOF system mentioned previously and hence results in improved damping ratio estimates.

### 2.3.2 Covariance-Driven Stochastic Subspace Identification (SSI/Cov)

As pointed out in the introduction, the covariance-driven stochastic identification algorithm (SSI/Cov) aims to identify the modal model of a particular test structure from output-only measurements and has its roots in the stochastic realization problem originally pioneered by (Akaike, 1974). This algorithm is closely related to the deterministic realisation problem (Ho and Kalman, 1966). Juang and Pappa (1984) applied this concept, in conjunction with the singular value decomposition to deal with noisy data, to classical input-output modal testing and developed the Eigensystem Realisation Algorithm (ERA). The equivalence between impulse response functions (IRF) and correlation functions, shown in the framework of the Natural Excitation Technique (NExT) (James *et al.*, 1993), makes it possible to apply the ERA to output-only modal testing (Juang *et al.*, 1988) by replacing the IRFs by the correlation functions between measured outputs. The latter method is essentially equivalent to the SSI/Cov (Peeters and DeRoeck, 2001). Below, we briefly outline the the SSI/Cov algorithm and introduce the notation and concepts that feature in chapters 5 and 6.

The spatial model of an  $N$  degree of freedom system represented in equation 2.1

can be reformulated as an equivalent  $2N$  dimensional first order system known as the *continuous-time state-space model*. This reformulation of the set of continuous equations of motions in equation 2.1 into the continuous-time state-space model is standard and the reader is referred to Juang (1994), for instance, for its derivation. In practice, the output measurements are typically discretised before the data is processed and consequently a discrete set of equations describing the input-output relations is required. When the excitation of the system, denoted by  $\underline{f}_k = [f_k^1, f_k^2, \dots, f_k^{2N}] \in \mathbb{R}^{2N \times 1}$ , is a stochastic process, generally assumed to be zero-mean, stationary white noise, the *discrete-time state-space model* of the system admits the form (Akaike, 1974)

$$\underline{x}_{k+1} = \mathbf{A}\underline{x}_k + \underline{f}_k, \quad (2.37)$$

$$\underline{y}_k = \mathbf{C}\underline{x}_k + \underline{u}_k \quad (2.38)$$

where  $\underline{x}_{k+1} = [x_k^1, x_k^2, \dots, x_k^{2N}] \in \mathbb{R}^{2N \times 1}$  is an unobserved *state vector* and  $\mathbf{A} \in \mathbb{R}^{2N \times 2N}$  is the *discrete-time state matrix* or *system matrix* whose  $2N$  eigenvalues which occur in complex conjugate pairs completely characterize the dynamics of the discretised system.  $\underline{y}_k = [y_k^1, y_k^2, \dots, y_k^l] \in \mathbb{R}^{l \times 1}$  is the vector of measured, discretised responses at time step  $k \in \mathbb{N}$  measured at  $l$  locations along the structure. Clearly, the continuous-time responses  $\underline{y}_t$  are related to  $\underline{y}_k$  by  $\underline{y}_k \equiv \underline{y}_k \Delta t$ , where  $\Delta t$  is the sampling interval. The second of the above equations is known as the *discrete-time observation equation*. The *output influence matrix*  $\mathbf{C} \in \mathbb{R}^{l \times 2N}$  relates the unobserved state vector  $\underline{x}_k \in \mathbb{R}^{2N \times 1}$  at time step  $k$  to the observed outputs  $\underline{y}_k \in \mathbb{R}^{l \times 1}$  measured at the  $l$  locations at time step  $k$ .  $\underline{u}_k \in \mathbb{R}^{l \times 1}$ , independent of  $\underline{f}_k$ , is a zero -mean random disturbance representing measurement noise. It is noted the latter term is sometimes omitted from the discrete-space state model (Basseville *et al.*, 2001).

The crucial point of the covariance-driven identification is as follows. It can be shown directly from equations 2.37, see for instance Peeters and DeRoeck (1999), that the theoretical  $l \times l$  correlation, or covariance, matrix at lag  $\tau = k\Delta t$  can be written

as<sup>†</sup>

$$\mathbf{R}_k = E[\mathbf{y}_i \mathbf{y}_{i+k}^T] = \begin{pmatrix} E[y_i^1 y_{i+k}^1] & E[y_i^1 y_{i+k}^2] & \dots & E[y_i^1 y_{i+k}^l] \\ E[y_i^2 y_{i+k}^1] & E[y_i^2 y_{i+k}^2] & \dots & E[y_i^2 y_{i+k}^l] \\ \vdots & \vdots & \vdots & \ddots \\ E[y_i^l y_{i+k}^1] & E[y_i^l y_{i+k}^2] & \dots & E[y_i^l y_{i+k}^l] \end{pmatrix} = \mathbf{C} \mathbf{A}^{k-1} \mathbf{G} \quad (2.39)$$

with

$$R_{y^i y^j}(k) = E[y_i^i y_{i+k}^j] \quad (2.40)$$

being the theoretical cross-correlation function between the measured outputs  $y^i$  and  $y^j$ ,  $i, j = 1, 2, \dots, l$  at lag  $k$  (Bendat and Piersol, 2000). The matrices  $\mathbf{A}$  and  $\mathbf{C}$  are recognised as the state-matrix and output-influence matrix of the discrete-time state-space model of the system. The matrix  $\mathbf{G} = E[\mathbf{x}_k \mathbf{y}_{k-1}] \in \mathbb{R}^{2N \times l}$ , for  $k > 0$  is the *next state output correlation matrix*. In practice, the exact correlation matrix is not known and needs to be estimated from the measured data. This is dealt with in detail in the next chapter, and is not needed to continue the exposition of the underlying theory of the SSI/Cov. The stochastic realization problem now consists of recovering the matrix triplet  $\{\mathbf{A}, \mathbf{C}, \mathbf{G}\}$ , up to a similarity transformation, using only the knowledge of the output measurements. To achieve this, the procedure is as follows. Define the  $\alpha l \times 1$  vector of “past” outputs and the  $\beta l \times 1$  vector of “future” outputs by

$$\mathbf{y}_{k|\beta}^+ = [\mathbf{y}_k^T \mathbf{y}_{k+1}^T \dots \mathbf{y}_{k+\beta-1}^T]^T \quad \text{and} \quad (2.41)$$

$$\mathbf{y}_{k|\alpha}^- = [\mathbf{y}_k^T \mathbf{y}_{k-1}^T \dots \mathbf{y}_{k-\alpha+1}^T]^T \quad (2.42)$$

respectively. Consider the matrix

---

<sup>†</sup>It is noted that the definition of ‘correlation function’ and ‘covariance function’ as employed by some authors denotes the same quantity. In this thesis, we adopt the terminology of Bendat and Piersol (2000), where the correlation matrix at lag  $\tau = k\Delta t$  is defined as in equation 2.39.



$$\begin{aligned} \mathcal{H}_s &= E \left[ \mathbf{Y}^-_{k|\alpha} \mathbf{Y}^{+T}_{k+s+1|\beta} \right] \quad (2.43) \\ &= \begin{pmatrix} E[\mathbf{Y}_k \mathbf{Y}_{k+s+1}^T] & E[\mathbf{Y}_k \mathbf{Y}_{k+s+2}^T] & \dots & E[\mathbf{Y}_k \mathbf{Y}_{k+s+\beta}^T] \\ E[\mathbf{Y}_{k-1} \mathbf{Y}_{k+s+1}^T] & E[\mathbf{Y}_{k-1} \mathbf{Y}_{k+s+2}^T] & \dots & E[\mathbf{Y}_{k-1} \mathbf{Y}_{k+s+\beta}^T] \\ \vdots & \vdots & \vdots & \ddots \\ E[\mathbf{Y}_{k-\alpha+1} \mathbf{Y}_{k+s+1}^T] & E[\mathbf{Y}_{k-\alpha+1} \mathbf{Y}_{k+s+2}^T] & \dots & E[\mathbf{Y}_{k-\alpha+1} \mathbf{Y}_{k+s+\beta}^T] \end{pmatrix} \end{aligned}$$

Recognising that each entry of this block matrix is the correlation matrix evaluated at a specific lag (see equation 2.39), equation 2.43 can be rewritten for as (Juang *et al.*, 1988)

$$\mathcal{H}_s = \begin{pmatrix} \mathbf{R}_{s+1} & \mathbf{R}_{s+2} & \dots & \mathbf{R}_{s+\beta} \\ \mathbf{R}_{s+2} & \mathbf{R}_{s+3} & \dots & \mathbf{R}_{s+\beta+1} \\ \vdots & \vdots & \vdots & \ddots \\ \mathbf{R}_{s+\alpha} & \mathbf{R}_{s+\alpha+1} & \dots & \mathbf{R}_{s+\alpha+\beta-1} \end{pmatrix} \quad (2.44)$$

It is seen that this block matrix has its entries, which are the correlation matrices  $\mathbf{R}_k$  arranged in a specific order according to the lag  $k$ . More specifically, the anti-diagonal blocks are constant. Matrices, having this specific structure are known as *Hankel matrices*.

The realisation of the triplet  $\{\mathbf{A}, \mathbf{C}, \mathbf{G}\}$  starts by forming the  $\alpha l \times \beta l$  block Hankel matrix  $\mathcal{H}_0$ , that is

$$\mathcal{H}_0 = \begin{pmatrix} \mathbf{R}_1 & \mathbf{R}_2 & \dots & \mathbf{R}_\beta \\ \mathbf{R}_2 & \mathbf{R}_3 & \dots & \mathbf{R}_{\beta+1} \\ \vdots & \vdots & \vdots & \ddots \\ \mathbf{R}_\alpha & \mathbf{R}_{\alpha+1} & \dots & \mathbf{R}_{\alpha+\beta-1} \end{pmatrix} = \begin{pmatrix} \mathbf{C} \\ \mathbf{CA} \\ \vdots \\ \mathbf{CA}^{\alpha-1} \end{pmatrix} (\mathbf{G}, \mathbf{AG}, \dots, \mathbf{A}^{\beta-1} \mathbf{G}) \quad (2.45)$$

where the last equality in this equation follows directly from equation 2.39. The prod-

uct of the last two block matrices in equation 2.45 is often written as  $\mathcal{P}_\alpha \mathcal{Q}_\beta$  where  $\mathcal{P}_\alpha \in \mathbb{R}^{\alpha \times 2N}$  is known as the *observability* matrix and  $\mathcal{Q}_\beta \in \mathbb{R}^{2N \times \beta}$  as the *controllability* matrix. Since the inner dimensions of the observability and controllability matrices are  $2N$ , choosing both  $\alpha$  and  $\beta \geq 2N$  ensures that the rank of the Hankel matrix cannot exceed  $2N$ , since the rank of any matrix is at most the smallest of its dimensions. If all modes of the system are excited and if the measurement setup is such that they are all captured, the observability and controllability matrices will have rank  $2N$ . In control engineering terminology, this means that the system is both controllable and observable (Juang, 1994). It is well known result in matrix algebra that if the rank of two matrices is equal to their inner dimensions, then this also gives the rank of their product (Golub and Van Loan, 1996). Thus, from the last equality in equation 2.45, the rank of the Hankel matrix is  $2N$  and reveals the model order of the system. In practice, the rank is found by using a singular value decomposition (SVD) of the Hankel matrix and the number of the non-zeros singular values will yield the model order of the system. The Hankel matrix  $\mathcal{H}_0$  can then be expressed in truncated form as

$$\mathcal{H}_0 = \mathbf{U}_{2N} \mathbf{\Sigma}_{2N} \mathbf{V}_{2N}^T \quad (2.46)$$

where  $\mathbf{\Sigma}_{2N} \in \mathbb{R}^{2N \times 2N}$  denotes the diagonal matrix containing only the non-zero singular values. The matrices  $\mathbf{U}_{2N}$  and  $\mathbf{V}_{2N}$  contain the corresponding left and right singular vectors respectively. In practice, where the singular values are never exactly zero, the determination of the correct model order is often difficult. A practical solution to this problem is to look for the largest gap occurring between successive singular values (Hermans and der Auweraer, 1999; Peeters and DeRoeck, 1999) indicating the separation between system modes and noise modes and hence the model order of the system. The matrices obtained via SVD of the Hankel matrix may then be truncated below this gap. Equation 2.46 will only be an approximation to the computed Hankel matrix once the truncation of the noise space (spanned by the truncated singular vectors) has been performed. Nonetheless, this reduced model is desirable since, we do not wish to identify a model that fits the noise in the data as well. Thus, the ben-

eficial consequence of this truncation is that a significant noise reduction is achieved (Juang and Pappa, 1986). On the other hand, however, if the truncated singular values contain system dynamics such as residual modes for instance, the singular value truncation contributes to significant bias error in the identified modal parameters. This issue is dealt with in Chapter 6 in this thesis. Nonetheless, in many practical situations (Hermans and der Auweraer, 1999; Peeters and DeRoeck, 1999), such a gap in the singular values indicating the true model order is not clear and the model order needs to be chosen, based on the singular value diagram at hand and the engineers experience. It often occurs, or it is even desirable (see for instance Peeters and DeRoeck (1999)), to overspecify the model order and as a result, the set of identified modes does not only consist of system modes but also noise or spurious modes. Fortunately, the noise modes tend to vary from model order to model order while system modes tend to be stable. This fact is exploited to distinguish between these two types of modes and this is commonly done by means of a so-called stabilisation diagram (Hermans and der Auweraer, 1999; Peeters and DeRoeck, 1999; Van der Auweraer and Peeters, 2004).

For the next step in the identification of the system matrix  $\mathbf{A}$ , note from equations 2.45 and 2.46 that the observability and controllability matrices may be expressed as

$$\mathcal{P}_\alpha = \mathbf{U}_{2N} \boldsymbol{\Sigma}^{1/2} \quad \text{and} \quad \mathcal{Q}_\beta = \boldsymbol{\Sigma}^{1/2} \mathbf{V}_{2N}^T \quad (2.47)$$

This choice, although not unique, will yield a *balanced* or *unweighted* realization due to fact that equal weight is attributed to the observability and controllability matrices so that the realized system will be as controllable as it is observable. Other weightings include the *Canonical Variate Analysis (CVA)* or the *Principal Component (PC)* method (Arun and Kung, 1990; Hermans and der Auweraer, 1999). However, simulations and practical applications have shown that there is no significant accuracy difference for the different weightings (Herlufsen *et al.*, 2005; Peeters and DeRoeck, 2001). The realization of the system matrices is now straightforward. The output influence matrix  $\mathbf{C}$  and the next state output-covariance matrix  $\mathbf{G}$  can be found from

the first block of  $\mathcal{P}_\alpha$  and  $\mathcal{Q}_\beta$  respectively. The discrete-time state matrix is then found by computing the *shifted Hankel matrix* defined by  $\mathcal{H}_1 = \mathcal{P}_\alpha \mathbf{A} \mathcal{Q}_\beta$  and solving for  $\mathbf{A}$  making use of equations 2.47:

$$\mathbf{A} = \Sigma^{-1/2} \mathbf{U}_{2N}^T \mathcal{H}_1 \mathbf{V}_{2N} \Sigma^{1/2} \quad (2.48)$$

The dynamics of the discretised system is completely characterized by the eigenvalues of  $\mathbf{A}$

$$\mathbf{A} = \Psi \Lambda \Psi^{-1} \quad (2.49)$$

where  $\Psi \in \mathbb{C}^{2N \times 2N}$  is the matrix containing the eigenvectors of  $\mathbf{A}$  and  $\Lambda \in \mathbb{C}^{2N \times 2N}$  is a diagonal matrix containing its discrete-time complex eigenvalues  $\lambda_i$ , for  $i = 1, 2, \dots, 2N$ . However, in order to describe the continuous-time dynamics of the equations of motion in equation 2.1, the discrete-time eigenvalues in  $\Lambda$  need to be transformed to the corresponding continuous-time eigenvalues. The continuous-time eigenvalues are related to the discrete-time eigenvalues by the transformation (Juang, 1994; Peeters and DeRoeck, 1999)

$$\Lambda_c = \frac{\ln(\Lambda)}{\Delta t} \quad (2.50)$$

where  $\ln(\cdot)$  denotes the natural logarithm. The continuous-time eigenvalues occur in complex conjugate pairs and can be written as

$$\lambda_{c_i}, \lambda_{c_i}^* = -\omega_i \xi_i \pm i \omega_i \sqrt{1 - \xi_i^2} \quad (2.51)$$

from which the  $i^{\text{th}}$  modal damping ratio  $\xi_i$  and the  $i^{\text{th}}$  modal frequency  $\omega_i$  (rad/sec) can be found as

$$\omega_i = \left| \frac{\ln(\lambda_i)}{\Delta t} \right| \quad \text{and} \quad \xi_i = -\Re\left(\frac{\ln(\lambda_i)}{\omega_i \Delta t}\right) \quad (2.52)$$

where  $\Re(\cdot)$  denotes the real part. Using the fact that the continuous-time mode shape matrix  $\Psi_c$  is identical to  $\Psi$  (Juang, 1994), the mode shapes at the sensor locations  $\phi$  are obtained using the output influence matrix  $\mathbf{C}$  as (Juang, 1994)

$$\phi = \mathbf{C} \Psi \quad (2.53)$$

Typically, when operational modal analysis is applied to large civil engineering structures, it is not possible to measure all the response at all the desired locations along the test structure simultaneously and therefore, the modal test needs to be done in several setups. This is done by choosing a set of sensors, whose position remains fixed throughout the different setups. This set of sensors serve as a reference against which all other responses, measured with a set of *roving* sensors from one setup to the next, are correlated and are therefore commonly referred to as *reference sensors*. The latter should be chosen at “optimal” locations (Cherng, 2003; Liu, 1995) along the structure which in practice means at locations where the response is strong and has contributions from all the system modes (Peeters and DeRoeck, 1999). When the loading conditions are stationary throughout all the setups, working with multiple setups causes no problems since the factorisation of the correlation matrix in equation 2.39 holds albeit in a slightly different form (Basseville *et al.*, 2001; Peeters and DeRoeck, 1999). From a practical point of view, all that changes is that the correlation matrix in equation 2.39 contains only those correlation functions evaluated between roving and reference sensors. More specifically, assume that the modal test has been performed in  $q$  different setups and denote the measured responses from the designated, say  $r$ , reference sensors in each of the  $q$  setups by  $\underline{y}_k^{(ref, i)} = \{y_k^{ref\ 1, (i)}, y_k^{ref\ 2, (i)}, \dots, y_k^{ref\ r, (i)}\}$  for  $i = 1, 2, \dots, q$ , where  $y_k^{ref\ 1, (i)}$  denotes the measured response at reference sensor 1 at setup  $i$ . Similarly, let the corresponding set of, say  $m$  roving sensors for each setup be given by  $\underline{y}_k^{(rov, i)} = \{y_k^{rov\ 1, (i)}, y_k^{rov\ 2, (i)}, \dots, y_k^{rov\ m, (i)}\}$ , for  $i = 1, 2, \dots, q$ , where  $y_k^{rov\ 1, (i)}$  denotes the measured response at the roving sensor 1 at setup  $i$ . Then, the

reference based correlation matrix at lag  $s$  can be formed as

$$\mathbf{R}_s^{ref} = \begin{pmatrix} E[\mathbf{Y}_k^{(ref,i)} \mathbf{Y}_{k+s}^{(ref,i)T}] \\ E[\mathbf{Y}_k^{(rov,1)} \mathbf{Y}_{k+s}^{(ref,1)T}] \\ E[\mathbf{Y}_k^{(rov,2)} \mathbf{Y}_{k+s}^{(ref,2)T}] \\ \vdots \\ E[\mathbf{Y}_k^{(rov,q)} \mathbf{Y}_{k+s}^{(ref,q)T}] \end{pmatrix} \equiv \begin{pmatrix} \mathbf{R}_s^{ref,ref} \\ \mathbf{R}_s^{(ref,1),(rov,1)} \\ \mathbf{R}_s^{(ref,2),(rov,2)} \\ \vdots \\ \mathbf{R}_s^{(ref,q),(rov,q)} \end{pmatrix} \quad (2.54)$$

The notation  $\mathbf{R}_s^{(ref,i),(rov,i)}$  denotes the correlation matrix at lag  $r$  between the reference and roving sensors at setup  $i$ . Note that no setup is specified for the correlation matrix between the any two set of measured references. This is due to the fact that they are the same for all setups whenever the loading conditions and hence the response data is stationary (Basseville *et al.*, 2001). This block-vector  $\mathbf{R}_s^{ref}$  admits the same factorisation as  $\mathbf{R}_s$  in equation 2.39 so that the system identification is done exactly in the same way as described above, except that the Hankel matrices  $\mathcal{H}_0$  and  $\mathcal{H}_1$  are formed by the reference correlation matrices  $\mathbf{R}_s^{ref}$  rather than  $\mathbf{R}_s$ . When the loading is non-stationary, the merging the data from different setups as above cannot be done, the reason being that the next state output correlation matrix  $\mathbf{G}$  changes from setup to setup which entails that the decomposition, as in 2.39, with constant matrices  $\mathbf{G}$  and  $\mathbf{C}$  is not possible. Mevel *et al.* (2002a,b) circumvented this problem by proposing a normalization correlation matrices from different setups make them appear as if they originate from the same excitation. Simulations in Basseville *et al.* (2001) also seem to indicate that this method smoothes the non-stationary properties in the response data. This method is, however, not considered in thesis but will be further discussed in section 6.3.3, Chapter 6.

### 2.3.3 Data-Driven Stochastic Subspace Identification (SSI/Data)

To conclude this chapter, we present the data-driven version of the stochastic subspace identification algorithm (SSI/Data). However, since this algorithm will be applied in chapter 7 without delving into its technical detail, this presentation will be brief and it

is merely aimed at outlining the main steps involved and pointing out the differences and similarities with its covariance-driven relative.

As for the stochastic realization problem described previously, the aim of the data-driven stochastic subspace method is to identify the discrete-time system matrices of the model described in equation 2.37 using the measured output time histories  $\underline{y}_k \in \mathbb{R}^{l \times 1}$ , assuming the responses are measured at  $l$  different locations along the structure. However, rather than forming a block-Hankel matrix of correlation matrices, the data-driven SSI start by forming large data Hankel matrix comprising the vectors of “past” and “future” outputs as described in the previous section. In a next step, the row space of the of the “future” outputs is projected into the row space of the “past” outputs. This projection effectively takes the role of correlating the measured outputs as in the SSI/Cov (Peeters and DeRoeck, 2001). The rank of this projection yields the model order of the system and is, as in the SSI/Cov, determined by a singular value decomposition and the same practical issue involved in determined the model order described for the SSI/Cov apply to this identification process. At this stage, several different implementations are possible, depending on how the data is weighted before the SVD is applied. These variants include the Canonical Variate Analysis (CVA) or the Principal Components (PC) or, in the simplest form, Unweighted Principal Components (UPC) (Arun and Kung, 1990; VanOverschee and DeMoor, 1996). The latter is equivalent to the balanced realisation used for the SSI/Cov and, since CVA, PC and UPC perform equally well in practice (Herlufsen *et al.*, 2005; Peeters and DeRoeck, 2001), the latter was chosen for simplicity in this thesis. The crucial result enabling the system to be identified via the the SSI/Data, states that this projection can be factorised into the observability matrix of the system (thus containing the information about the output influence matrix  $C$  and the state matrix  $A$ , see previous section) and the Kalman filter state sequence which is effectively an optimal prediction of the state vectors  $\underline{x}_k$  (VanOverschee and DeMoor, 1996). For detail on Kalman filter states, the reader is redirected to Juang (1994); Ljung (1987). The relations

obtained from the latter factorisation and the SVD decomposition of the projection of future onto past outputs, the system matrices can then be identified in a similar manner as for the SSI/Cov; in the latter algorithm, the necessary relation for the identification stemmed from the SVD decomposition of the block Hankel matrix  $\mathcal{H}_0$  and the factorisation of  $\mathcal{H}_0$  into a product of observability and controllability matrices. Once the state matrix  $\mathbf{A}$  and the output influence matrix  $\mathbf{C}$  are at hand, the modal parameters of the system are found in exactly the same way as described in the previous section for the SSI/Cov. The SSI/Data can also be used when the modal test is done in multiple setups and the reference-based version of the algorithm was developed by Peeters and DeRoeck (1999). An efficient implementation of the data driven algorithm is not easy, and the implementation used in this thesis follows closely the one suggested by VanOverschee and DeMoor (1996), but was modified following Peeters and DeRoeck (1999) to account for a reference-based implementation. It is documented by Peeters and DeRoeck (2001), that both the SSI/Data and SSI/Cov perform equally well in practice but a faster execution for the SSI/Cov is reported.

## 2.4 Summary

In this chapter, the basic theory needed in the remainder of this thesis was presented. The concept of stationarity, white noise loading conditions was explained and its important relation to operational modal analysis shown. The operational response model was derived and the use of correlation functions, instead of the classical IRF, was justified. Finally, three operational identification algorithm were given. The exposition of the Enhanced Frequency Domain Decomposition Method (EFDD) and the data-driven Stochastic Subspace (SSI/Data) algorithm was kept a minimum since a more technical description of these algorithms is not needed in this thesis. The SSI/Cov was presented in more detail since in Chapter 5, it will be investigated how errors in the response model propagate through this algorithm to influence the identified modal parameters.



---

## CHAPTER 3

# ESTIMATION ERRORS IN CORRELATION FUNCTIONS

---

### 3.1 Introduction

Correlation-driven operational modal analysis is a 2-stage identification procedure. The measured information about the system consists of simultaneously recorded response histories, most commonly acceleration, recorded at various locations along the structure. In a first stage, this information is processed into a different form, namely correlation functions. The identification algorithm then operates on the latter data to extract the modal parameters of the system. In other words, the measured information about the system is transformed into a different format that is better suited to extract the system's modal parameters. These correlation functions can only be estimated and are therefore corrupted by estimation errors, both bias and random, and are further contaminated by measurement noise. Since these correlation functions are the basic quantities from which the SSI/Cov algorithm identifies the modal parameters, these errors will propagate through the identification algorithm used and affect the identified modal parameters. In order to estimate the error in the identified modal parameters, requires knowledge of the error in the estimated correlation functions, which is the subject of this chapter.

Different techniques to estimate the sample auto- and cross correlation functions

-or equivalent quantities that can be used as input to the SSI/Cov such as the Random Decrement (RD) signatures- are presented and the errors in these estimates are investigated. The techniques considered are

- Direct and indirect estimation of auto-correlation functions (ac.f.) and cross-correlation functions (xc.f.)
- Auto- and cross-correlation coefficient functions
- Random Decrement (RD) signatures

Both bias (systematic) and random errors are considered. It is not aimed at comparing the different estimators as such because, in terms of accuracy, there is no significant advantage of a particular estimator over another. While the random decrement estimator can be computationally more efficient (depending on the record length of the time series, the lag up to which the RD signature is computed and the triggering condition used), a simulation study in Asmussen (1997) for instance, comparing the accuracy of RD signatures with FFT-based correlation function estimates, shows that the two estimators are comparable. Desforges *et al.* (1995) report a favourable performance using correlation functions. In a first instance, it is aimed to give a description of the errors in terms of the the record length of the time-series and the modes of the system to guide the practitioner. The latter analytical formulation is, however, not very practical. Therefore a robust and efficient numerical method, based on the formulation originally given by (Bartlett, 1946), is developed to obtain estimates of these errors in the sample correlation and correlation coefficient functions. The accuracy of the proposed method is assessed, in particular at low lag times, since correlation-driven identification typically operates on this portion of the estimated data (Juang and Pappa, 1984). The various aspects of computation of the random decrement signatures are only briefly discussed for completeness, since this subject is treated extensively by Asmussen (1997).

## 3.2 Correlation Function Estimators

To clarify the terminology, the definition used in this thesis for the auto- and cross-correlation functions is restated (see Chapter 2). For a stationary signal, they are respectively given by Bendat and Piersol (2000)

$$R_{xx}(\tau) = E[x(t)x(t+\tau)] \quad (3.1)$$

$$R_{xy}(\tau) = E[x(t)y(t+\tau)] \quad (3.2)$$

where  $x(t)$  and  $y(t)$  denote two stationary time series. As described in Chapter 2, the above definition of the auto- and cross-correlation function are similar to the definition of the auto- and cross *covariance* function defined in equation 2.18 except that the time-independent mean is not removed. Some authors (Peeters and DeRoeck, 2001) prefer to work with covariance functions but since it is customary to remove the mean from the measured time series by using a detrending operation (Bendat and Piersol, 2000), both quantities are, in general, the same. Various quantities exist that have the same correlation structure as equations 3.1 and 3.2, for instance the RD signatures or correlation coefficient functions described below, and may therefore serve as input to the SSI/Cov algorithm. Zhang *et al.* (2005a) use the generic term Time Response Functions (TRFs) to refer to any of these functions but in this thesis, the term correlation function will be used to refer to these quantities in a general context and it will be clarified when a specific function is meant.

### 3.2.1 Sample Auto- and Cross-Correlation Functions

There exist two common techniques to estimate the ac.f. and xc.f. of simultaneously measured times series: the *direct* method is a direct application of equations 3.1 and 3.2 in which the expectation operator  $E[\cdot]$  is replaced by an integral or a summation for discrete data (Bendat and Piersol, 2000; Priestley, 2004). An alternative estimate can be obtained by making use of the properties of the FFT. This procedure is often referred to as the *indirect* method. Since both methods are explained at length in many

texts, only a brief description is given here and appropriate references are given.

### Direct Method

The biased  $\hat{R}_{xy}^b(\tau)$  and unbiased  $\hat{R}_{xy}(\tau)$  sample cross-correlation function between any two stationary, zero-mean *continuous* time histories  $x(t)$  and  $y(t)$  of length  $T$  can be estimated as (Bendat and Piersol, 2000)

$$\hat{R}_{xy}(\tau) = \frac{1}{T-\tau} \int_0^{T-\tau} x(t)y(t+\tau)dt \quad 0 \leq \tau < T \quad (3.3)$$

$$\hat{R}_{xy}^b(\tau) = \frac{1}{T} \int_0^{T-\tau} x(t)y(t+\tau)dt \quad 0 \leq \tau < T \quad (3.4)$$

where  $\tau$  denotes the time lag at which the the cross-correlation function is evaluated.

For the *discrete* case, the above formulae can be rewritten as (Priestley, 2004)

$$\hat{R}_{xy}(r\Delta t) = \frac{1}{N-r} \sum_{i=0}^{N-r-1} x(i\Delta t)y((i+r)\Delta t) \quad i = 0, 1, 2, \dots \quad (3.5)$$

$$\hat{R}_{xy}^b(r\Delta t) = \frac{1}{N} \sum_{i=0}^{N-r-1} x(i\Delta t)y((i+r)\Delta t) \quad i = 0, 1, 2, \dots \quad (3.6)$$

$N$  denotes the number of sample points in each record such that  $T = N\Delta t$  and  $\Delta t$  is the sampling interval. The estimates are only given for positive time lags as the latter yield the decaying part used in the identification. The sample auto-correlation functions are merely special cases of the above equations when the two records coincide (Bendat and Piersol, 2000). For notational convenience, the sampling interval  $\Delta t$  will be dropped so that for instance  $\hat{R}_{xy}(r)$  is understood to stand for  $\hat{R}_{xy}(r\Delta t)$ .

### Indirect Method

The key to obtaining correlation functions via FFT is to realise that the summand in equations 3.5 and 3.6 is the discrete convolution  $x(r)$  with  $y(-r)$  (Oppenheim and Schaffer, 1988). Computing  $X(k)$  and  $Y(k)$ , which are the discrete Fourier transform (DFT) of  $x(r)$  and  $y(r)$  respectively, it is possible to form the raw cross-spectral es-

estimate  $\frac{X(k)Y^*(k)}{N}$  (Bendat and Piersol, 2000). The raw spectrum estimate  $\frac{X(k)Y^*(k)}{N}$  is often referred to as the cross-periodogram between  $X(k)$  and  $Y(k)$ . Taking the inverse DFT (or FFT) of the raw cross-spectral estimate yields a convolution in the time domain, resulting in equation 3.6. It will be noted, however, that because of the underlying assumption of the periodicity of the DFT and its inverse, one will actually obtain the *circular correlation* between the two signals which appears as though it were calculated from a periodic function. As a consequence, the resulting cross-correlation function at any lag  $r$  ( $r < N$ ) will have components from the periodic extension of the signal. This “wrap-around effect” can easily be avoided by augmenting the signal with zeros (Bendat and Piersol, 2000; Oppenheim and Schaffer, 1988). When the signal is padded with  $N$  zeros, exactly the same linear correlation function, given in equation 3.6, for both +ve and -ve lags is obtained by inverse FFT of the raw spectrum estimate. The above clearly applies to auto-correlation functions when  $x(r)$  and  $y(r)$  coincide.

The advantage of using the indirect method lies in its computational efficiency when the maximum lag value up to which the correlation function is to be computed is sufficiently large (Oppenheim and Schaffer, 1988). In particular, since the maximum lag of interest, say  $m$ , is usually much less than  $N$ , it is computationally advantageous to chop the data into  $n_d$  contiguous blocks of length  $M \geq m$  i.e.  $N = n_d M$ . Augmenting each block by  $M$  data points, the cross-spectral estimate can be computed using Bartlett’s averaged periodogram method. That is  $\hat{S}_{xy}(k) = \frac{1}{n_d M} \sum_{i=1}^{n_d} X_i(k)Y_i^*(k)$ , where  $X_i(k)$  and  $Y_i(k)$  denote the DFT of the  $i^{th}$  block  $x_i(r)$  and  $y_i(r)$  of the time records  $x(r)$  and  $y(r)$ . The inverse FFT of  $\hat{S}_{xy}(k)$  then yields the desired cross-correlation function up to lag  $m$ . This procedure is effectively an application of the Wiener-Khinchine relation (Bendat and Piersol, 2000). For the exact computational effort required by each method, the reader is referred to (Bendat and Piersol, 2000; Oppenheim and Schaffer, 1988).

The FFT procedure described above is statistically equivalent to the direct method (Bendat and Piersol, 2000). In some applications, for instance Farrar and James (1997), the correlation functions have been estimated by inverse FFT of the spectral estimates obtained via Welch's modified periodogram method (Welch, 1967), which is a slight modification of the Bartlett procedure described above. The modification consist of applying a window function  $u(r)$  directly to the individual data blocks  $x_i(r)$  and  $y_i(r)$  before computation of the periodogram. Also, the blocks are often chosen to be overlapping. The motivation for applying Welch's modified periodogram method is to get better spectral estimates, that is reduced leakage due to the windowing operation and reduced variance due to the increased number of blocks made possible by the overlap. The correlation functions obtained via inverse FFT from these spectra have different statistical properties than those obtained from the direct method. These differences will be discussed in subsequent sections.

### 3.2.2 Sample Auto- and Cross-Correlation Coefficient Functions

It may be convenient in some cases to deal with *correlation coefficient functions* rather than with the correlation functions themselves. The latter is defined as (Bendat and Piersol, 2000)

$$\rho_{xx}(r) = \frac{R_{xx}(r)}{\sigma_x^2} = \frac{R_{xx}(r)}{R_{xx}(0)} \quad (3.7)$$

$$\rho_{xy}(r) = \frac{R_{xy}(r)}{\sigma_x \sigma_y} = \frac{R_{xy}(r)}{\sqrt{R_{xx}(0)R_{yy}(0)}} \quad (3.8)$$

where  $\sigma_{(\bullet)}$  denotes the standard deviation of the respective time series<sup>†</sup>. Since, the ac.f. at zero lag is given by  $R_x(0) = E[x^2(r)] = Var[x(r)] = \sigma_x^2$ , it follows that the corresponding auto-correlation coefficient function  $\rho_{xx}(r)$  is unity at  $r = 0$ . The cross-correlation coefficient function satisfies

$$-1 \leq \rho_{xy}(r) \leq 1 \quad (3.9)$$

---

<sup>†</sup>Some authors, (Priestley, 2004) for instance, use this as the definition for auto- and cross-correlation functions.

for all  $r$ . The sample estimates for the correlation coefficient functions can be obtained from equations 3.7 using the *plug-in principle*. In other words, the exact quantities in equations 3.7 are replaced by their estimates i.e.

$$\hat{\rho}_{xx}(r) = \frac{\hat{R}_{xx}(r)}{\hat{\sigma}_x^2} = \frac{\hat{R}_{xx}(r)}{\hat{R}_{xx}(0)} \quad (3.10)$$

$$\hat{\rho}_{xy}(r) = \frac{\hat{R}_{xy}(r)}{\hat{\sigma}_x \hat{\sigma}_y} = \frac{\hat{R}_{xy}(r)}{\sqrt{\hat{R}_{xx}(0) \hat{R}_{yy}(0)}} \quad (3.11)$$

It is clear from its definition, that the correlation coefficient functions are simply correlation functions normalized with respect to the variances of the respective outputs. Therefore, the decay and oscillatory properties are the same as those of the correlation functions and hence the same modal parameters are identified. However, the sample variance of the correlation functions differ from those of the correlation coefficient functions. For instance, it is clear that since the auto-correlation coefficient function computed from each of the  $p$  measured time histories is normalised to unity, the variance of  $\rho_{xx}(0)$  would be zero whereas the variance of  $R_{xx}(0)$  is not.

### 3.2.3 Auto- and Cross Random Decrement (RD) signatures

Random decrement signatures were initially developed by Cole (1973) to estimate damping ratios and natural frequencies and were later extended to cross-RD function by Ibrahim (1977); Ibrahim and Mikulcik (1977). The description given here will be brief and the reader is referred to Asmussen (1997) for a complete and comprehensive treatment of the subject.

The concept of the random decrement signature is based on the fact that the random response of structure at time  $t+t_0$  is composed of two parts: (a) a deterministic part composed of the step response due to the displacement at  $t_0$  and/or the impulse response due to initial velocity at  $t_0$  and (b) a random part due to the random load applied to the system between  $t_0$  and  $t_0 + t$  (Ibrahim, 1977). Let  $x(t)$  and  $y(t)$  be two stationary response histories from a linear system. The RD technique starts by

breaking the time series up into blocks of equal size, say  $M$ . The basic idea behind the RD technique is that, by averaging enough of these blocks, the random part of the response will average out, leaving only the deterministic part. However, to avoid averaging out the deterministic part of the response, the blocks into which the time series are broken need to be chosen under certain conditions. These conditions are commonly referred to as *triggering conditions*. There are a several triggering conditions under which this requirement is fulfilled but they can all be described from the applied general triggering condition (Asmussen, 1997)

$$T_{x(t)}^G = \{a_1 \leq x(t) \leq a_2, \quad b_1 \leq \dot{x}(t) \leq b_2\} \quad (3.12)$$

where  $\dot{x}(t)$  denotes the time derivative of  $x(t)$ . Equation 3.12 means that, in order to avoid averaging out the deterministic part of the response, the blocks of  $x(t)$  need to be chosen starting always at a point of  $x(t)$  lying between the designated levels  $a_1$  and  $a_2$  and having a slope in the interval  $[b_1 \ b_2]$ . The various triggering conditions that can be derived from this general trigger and their consequences are described in great detail in Asmussen (1997). In this thesis, only the *level crossing triggering condition*, denoted  $T_{x(t)}^L$ , is discussed. The latter is obtained from equation 3.12 by letting  $b_1 = -\infty, b_2 = \infty$  and  $a_1 = a$  and  $a_2 = a + \Delta a$  i.e.

$$T_{x(t)}^L = \{x(t) = a, \quad \infty \leq \dot{x}(t) \leq \infty\} \quad (3.13)$$

Denoting the discrete signal obtained from  $x(t)$  by  $x(r)$ , equation 3.13 states that the blocks into which the time series is broken can be chosen to start at any point at time  $r$  for which  $x(r) = a$  irrespective of the slope of  $x(t)$  at that point. Clearly, for discrete signals, it might not happen that  $x(r) = a$  exactly and the triggering condition is never fulfilled. Therefore, in practice, the triggering points are chosen at  $r$  and  $r + 1$  such that  $x(r) \geq x(r + 1)$  for a negative slope and  $x(r) \leq x(r + 1)$  when the slope is positive. It was shown by Brincker *et al.* (1991) that if either the left-hand point  $r$  or the right-hand point  $r + 1$  is chosen, the estimated RD signatures are biased



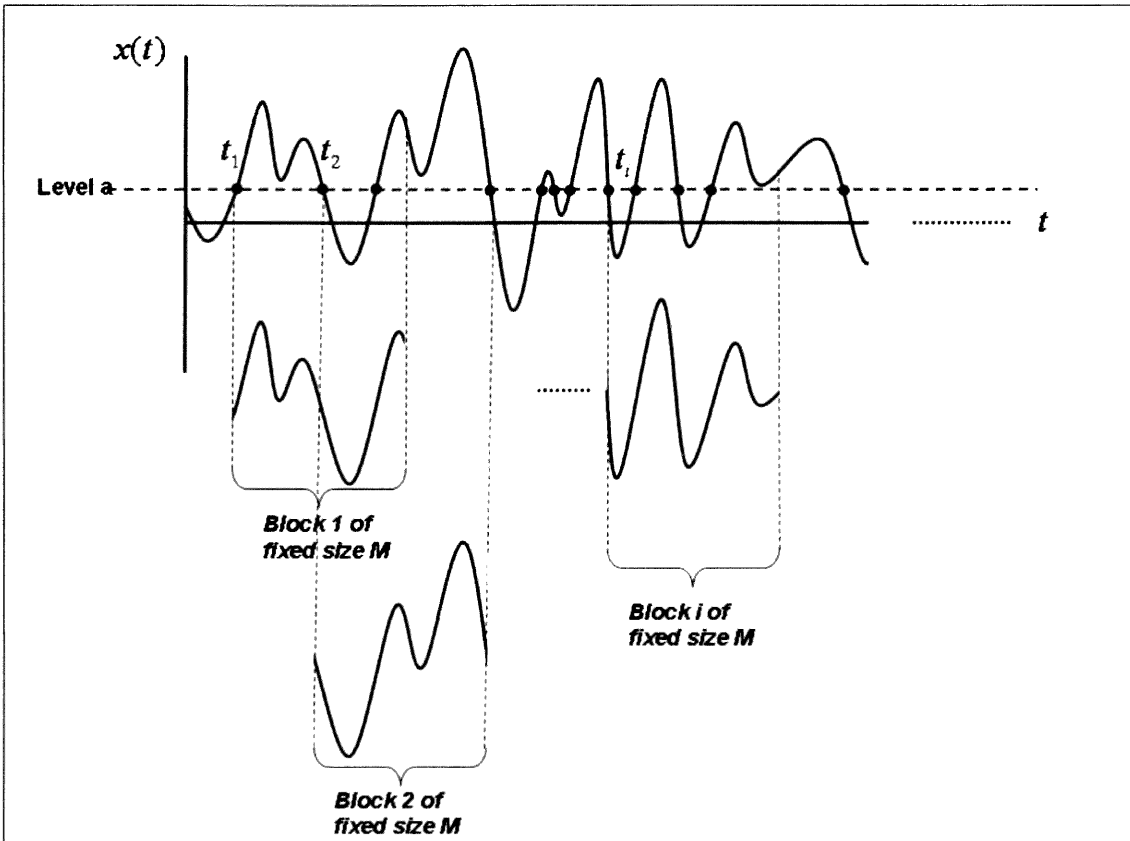


Fig. 3.1: Illustration of the level triggering condition.

and to avoid this bias, both points should be taken to act as triggers. The choice of the level  $a$  determines the number of blocks into which the response is broken. It is evident from the description of the concept of the RD technique that the more blocks we have, the better will be the cancellation of the random part of the response. It is shown in (Asmussen, 1997) that levels between  $\sigma_x$  and  $2\sigma_x$  yield best results, where  $\sigma_x$  denotes the standard deviation of the stationary time-history  $x(t)$ . This process is illustrated in figure 3.1. Suppose that  $N_x$  blocks are obtained from  $x(t)$  and  $N_y$  blocks from  $y(t)$ . The auto-random decrement signatures  $RD_x(\tau)$  and  $RD_y(\tau)$  are then found by taking the average of the  $N_x$  and  $N_y$  blocks respectively. Formally, the sample auto-random decrement signatures are expressed as

$$RD_x(\tau) = \frac{1}{N_x} \sum_{i=1}^{N_x} x(t_i + \tau) \Big|_{T_{x(t_i)}^E} \quad (3.14)$$

$$RD_y(\tau) = \frac{1}{N_y} \sum_{i=1}^{N_y} y(t_i + \tau) \Big|_{T_{y(t_i)}^E} \quad (3.15)$$

The cross random decrement signatures are found by forming the same blocks of  $y(t)$  than was done for  $x(t)$ , i.e. the trigger for  $y(t)$  is taken to be the one for  $x(t)$  (Ibrahim, 1977). Formally,

$$RD_{xy}(\tau) = \frac{1}{N_y} \sum_{i=1}^{N_x} x(t_i + \tau) \Big|_{T_{y(t_i)}^E} \quad (3.16)$$

$$RD_{yx}(\tau) = \frac{1}{N_x} \sum_{i=1}^{N_x} y(t_i + \tau) \Big|_{T_{x(t_i)}^E} \quad (3.17)$$

For the level triggering condition, it was first shown by Vandiver *et al.* (1982) that the auto-RD functions are proportional to auto-correlation functions. This was later extended by (Brincker *et al.*, 1991)\* to include the case for cross-RD functions and it the relation yields

$$RD_{xx}(\tau) = \frac{R_{xx}}{\sigma_x^2} a \quad (3.18)$$

$$RD_{xy}(\tau) = \frac{R_{xy}}{\sigma_y^2} a \quad (3.19)$$

When different triggering conditions are used, the relation between correlation and RD functions changes and the general relation between correlation and RD functions, that is for the general triggering condition in equation 3.12, is given by Asmussen (1997).

---

\*The author could not get hold of the original paper mentioned in this reference but the theory is also given in the appendix of Asmussen (1997).

### 3.3 Bias in Sample Correlation Functions

#### 3.3.1 Auto- and Cross-Correlation Functions

##### Direct Method

It is easily found from equation 3.6 that the bias in the cross-correlation function between  $x(t)$  and  $y(t)$  is (Bendat and Piersol, 2000)

$$b \left[ \hat{R}_{xy}^b(r) \right] = E \left[ \hat{R}_{xy}^b(r) \right] - R_{xy}(r) = -\frac{|r|}{N} R_{xy}(r) \quad (3.20)$$

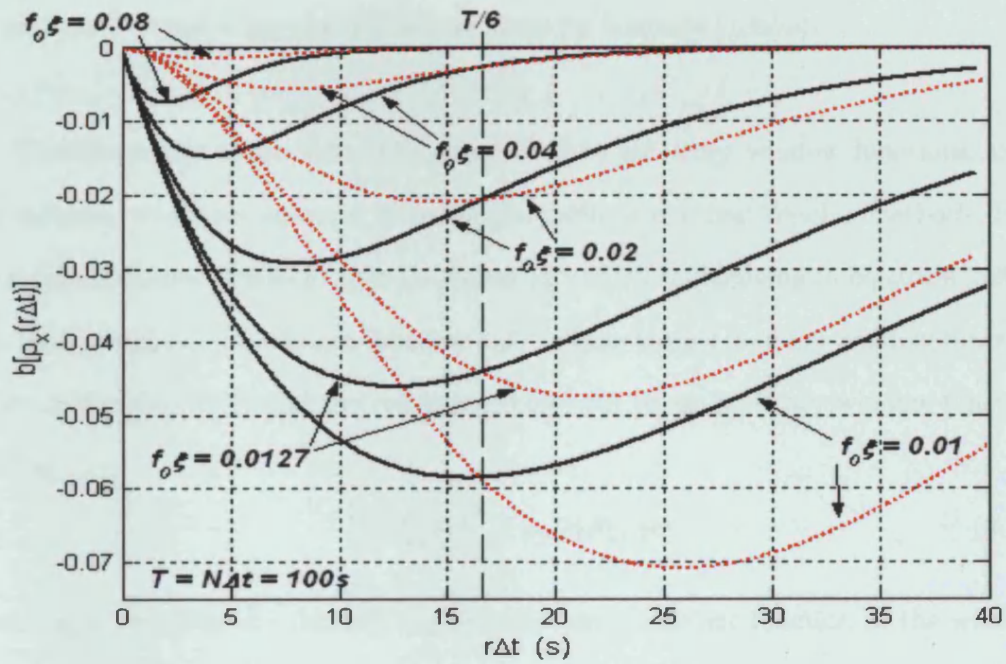
where  $R_{xy}(r)$  is the exact cross-correlation function between  $x(t)$  and  $y(t)$ ,  $E[\cdot]$  denotes the expectation operator and  $b[\cdot]$  the bias error. The magnitude of the bias thus depends on two factors; the ratio of the time lag to the total record length and the value of  $\hat{R}_{xy}(r)$  itself. When  $|r|$  is small compared to  $N$ , the bias will be small but as  $|r|$  approaches  $N$  the bias will effectively be  $R_{xy}(r)$ . There will thus be little difference between the biased and unbiased estimates in the region where  $|r|$  is small compared to  $N$ . On the other hand, however, since the cross-correlation functions between any two response measurements of a damped structural system are decaying functions such that  $R_{xy}(r) \rightarrow 0$  as  $|r| \rightarrow \infty$ , it will be small by the time  $|r|$  approaches  $N$  for large values of  $N$  so that we may expect the bias to remain small. The decay rate of the correlation functions is governed by the product  $\omega_i \xi_i$ , where  $i$  denotes the  $i^{\text{th}}$  mode, as shown in equation (2.33) so that we can expect smaller bias in correlation functions of more heavily damped, higher frequency systems. This behaviour of the bias is shown in figure 3.2(a). A set of SDOF systems were computed using the analytical equations for the ac.f. of a SDOF system excited by white noise given by (3.30),(3.31) and (3.32), for displacement, velocity and acceleration output records respectively. The variance of the noise was assumed to be unity. For presentational convenience, only the envelope of the bias is shown. The dependence of the latter quantity on the modal parameters  $f_0$  and  $\xi$  can be expressed by a single variable  $f_0 \xi$ , so that the results are identical for any combination of natural frequency/damping ratio yielding the same  $f_0 \xi$ .

## Indirect Method

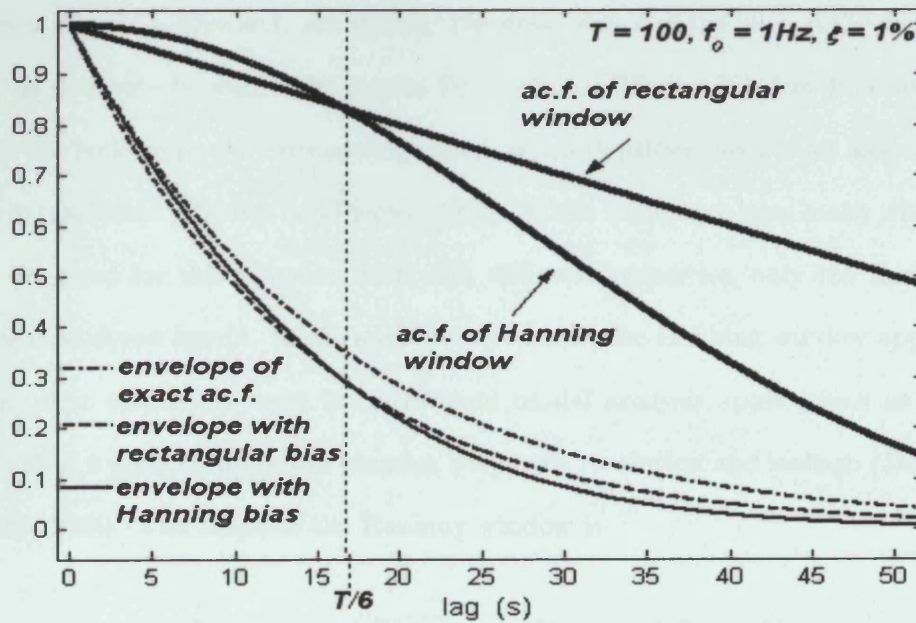
The correlation functions computed by application of the inverse FFT to the raw spectral estimates (or periodogram) are identical to the biased estimates obtained from the direct method. However, when the periodogram is modified using Bartlett's or Welch's method, the bias in the resulting correlation is different. For the Bartlett procedure, this is easily understood by realising that the spectral estimate is just an average of periodograms and that the FFT is linear. More precisely, if the time records  $x(r)$  and  $y(r)$  of length  $N$  are divided into  $n_d$  blocks of length  $M$  such that  $N = n_d M$ , then computing the correlation estimate by inverse FFT from the averaged periodogram  $\hat{S}_{xy}(k) = \frac{1}{n_d M} \sum_{i=1}^{n_d} X_i(k) Y_i^*(k)$ , is the same as averaging the correlation functions obtained by inverse FFT from each periodogram  $\frac{X_i(k) Y_i^*(k)}{M}$ . From the discussion of the direct method and the previous paragraph it follows that bias error in the latter correlation functions is  $b[\hat{R}_{xy}^b(r)] = -\frac{|r|}{M} R_{xy}(r)$ . Since  $M \leq N$ , the bias in the thus estimated correlation functions will be greater than or equal to that in the correlation functions estimated via the direct method, although the random error decreases with with  $n_d$  (Bendat and Piersol, 2000). The origin of this bias error can be attributed to the fact that time-history records have finite length; finite length data records, of length  $N$  say, may be regarded as the product of an infinite record with a finite *Boxcar* or *rectangular* time window defined by

$$u_R(r) = \begin{cases} 1 & \text{for } r = 1, 2, \dots, N \\ 0 & \text{else} \end{cases} \quad (3.21)$$

This behaviour of the bias error in the estimated correlation functions is closely related to the bias error in the corresponding estimated spectral densities, often referred to as *resolution bias*. The reason is that the product of the time history records with a window function in the time domain translates into a convolution of their Fourier transforms in the frequency domain. The Fourier transform of the rectangular window is the well known *sinc* function and the width of its main lobe, determined by the length of the window, serves as a measure of the resolution bandwidth of the spectral



(a)



(b)

Fig. 3.2: (a) Envelope of the bias error in the auto-correlation coefficient function  $\rho_x(r)$  for a set of SDOF systems for both the direct method (rectangular window)[—] and the indirect method using a Hanning window [···]. It is assumed that the total available record length from which the ac.f were computed is  $T = 100$ s. (b) Exact auto-correlation function compared to the envelope of the biased auto-correlation function for the rectangular and Hanning window.

densities (Oppenheim and Schaffer, 1988). A detailed analysis of the resolution bias in relation to windowing operations was given by Schmidt (1985a).

The discussion above is readily generalized to arbitrary window functions, used for instance when the spectral densities are estimated using Welch's method. It is shown in (Schmidt, 1985a,b) that the factor  $(1 - |r|/N)$  multiplying in equation 3.20 is the auto-correlation coefficient function  $\rho_R(r)$  of the the rectangular window function given in equation 3.21 and the result is generalized to an arbitrary window function  $u(r)$  as

$$E \left[ \hat{R}_{xy}^b(r) \right] = \rho_u(r) R_{xy}(r) \quad (3.22)$$

where  $\rho_u(r)$  denotes the (biased) auto-correlation coefficient function of the window function  $u(r)$ . This relation is illustrated below in figure 3.2(b) for the auto-correlation of a SDOF system for the rectangular and Hanning window. For clarity, only the envelopes of the respective ac.f. are shown. The dependence of the bias on the window function used is clearly seen. The reason for applying different window functions is to reduce the leakage in the estimated power spectral densities despite an associated decrease in resolution (Bendat and Piersol, 2000). While there have been many window function designed for this purpose, each with different properties, only the Hanning window is considered herein. In the authors experience, the Hanning window appears to be the most commonly used in operational modal analysis applications as it is known to offer a good compromise between frequency resolution and leakage (Jenkins and Watts, 1968). The shape of the Hanning window is

$$u_H(r) = \begin{cases} \frac{1}{2} \left[ 1 + \cos\left(\frac{2\pi r}{N}\right) \right] u_R(r) & \text{for } r = 1, 2, \dots, N \\ 0 & \text{else} \end{cases} \quad (3.23)$$

and its auto-correlation coefficient function  $\rho_H(r)$  is given by (Schmidt, 1985a,b)

$$\rho_H(r) = \frac{1}{3} \left[ 2 + \cos\left(\frac{2\pi r}{N}\right) \right] \rho_R(r) + \frac{1}{2\pi} \sin\left(\frac{2\pi r}{N}\right) \quad (3.24)$$

As for the direct estimation method -or equivalently for the rectangular window- the dependence on the system's modal parameters of the actual bias error in the correlation functions estimated via the Hanning windowed spectra is shown in figure 3.2(a). While the general behaviour is similar to that for the direct case, it is seen that for  $(f_0\xi) = 0.02, 0.04$  and  $0.08$ , the increase in bias with the lag in the ac.f. is smaller for the Hanning than for the direct method. Also, the maximum bias is smaller for the Hanning window when  $f_0\xi$  is large but tends to increase as  $f_0\xi$  increase. Considering the envelope only, it can be found from equation 3.20 that for the rectangular window, the maximum value of the bias in the envelope occurs at  $r\Delta t = \frac{1}{\omega\xi}$ . For the Hanning window, using equation 3.22 with  $\rho_u = \rho_H$  and expanding the *sin* and *cos* functions as the first two terms of their McLaurin series, the maximum value of the bias can be found to occur approximately at  $r\Delta t = \frac{2}{\omega\xi}$ . Equating the envelopes in both cases for a fixed value of  $\omega\xi$  reveals that the bias error intersects at approximately  $r\Delta t = \frac{T}{6}$  with the bias being smaller for the Hanning window than for the rectangular window for lags  $< \frac{T}{6}$ . This is illustrated in figure 3.2(a). It is noted that the biased correlation functions can easily be unbiased applying equation (3.22) i.e. by multiplying  $\hat{R}_{xy}^b(r)$  by  $\rho_u^{-1}$  (Giampellegrini and Greening, 2005). The biased estimates offers two advantages, (a) it has been asserted that, in general, it has a smaller mean square error than the unbiased estimate and (b) it is a positive semi-definite function implying that its finite Fourier transform or periodogram is a non-negative function at all frequencies. The unbiased correlation estimate, on the other hand, does not have this property (Priestley, 2004).

To conclude this section, a brief discussion of the bias in the correlation coefficient functions and the RD signatures is given. Strictly speaking, the plug-in expressions for the correlation coefficient functions in (3.10) have slightly different bias properties from those of sample correlation functions since the effect of estimating  $\hat{R}_{xx}^b(0)$  and  $\hat{R}_{yy}^b(0)$  has to be taken into account as well. However, it is shown in Priestley (2004) that when the error between the estimate  $\hat{R}_{xx}^b(r)$  and its expectation is small,  $E[\rho_{xx}(r)]$

can be approximated as

$$E[\rho_{xx}(r)] = E\left[\frac{\hat{R}_{xx}^b(r)}{\hat{R}_{xx}^b(0)}\right] \approx \frac{E[\hat{R}_{xx}^b(r)]}{E[\hat{R}_{xx}^b(0)]} = \left(1 - \frac{|r|}{N}\right)\rho_{xx}(r) \quad (3.25)$$

Extending this to cross-correlation coefficients as

$$E[\rho_{xy}(r)] = E\left[\frac{\hat{R}_{xy}^b(r)}{\sqrt{\hat{R}_{xx}^b(0)\hat{R}_{yy}^b(0)}}\right] \approx \frac{E[\hat{R}_{xy}^b(r)]}{\sqrt{E[\hat{R}_{xx}^b(0)]E[\hat{R}_{yy}^b(0)]}} = \left(1 - \frac{|r|}{N}\right)\rho_{xy}(r) \quad (3.26)$$

it is seen that under this approximation, the bias properties of correlation coefficient functions are the same as those of the ordinary sample correlation functions. Since the error is generally small at low lag times, this approximation is valid for all practical purposes.

The bias arising in RD signatures is generally due to implementation problems such as the discretization issue for level triggering discussed in section 3.2.3. By careful implementation, it is generally possible to obtain unbiased estimates. A detailed account of sources of bias in RD signatures can again be found in Asmussen (1997).

### 3.4 Variance in Sample Correlation Functions

While the variance of sample correlation functions for band-limited white noise is described in (Bendat and Piersol, 2000), little work seems to have been devoted to study the random error in sample correlation functions between outputs of linear MDOF systems. A reason might be that the random error can be kept low when the available record length is very large. Long records are, however, not always available and the effect on the sample correlation estimates and hence the effect on the identified modal parameters are severe as is shown in Pridham and Wilson (2003). In this section, it is aimed to expose the behaviour of the variance, and hence the random error, in the estimated sample correlation functions in terms of the system modes and the available record length  $T$ . In a first instance, an analytical formulation of



the variance for SDOF systems are considered and then an approximation for MDOF systems is given. Finally, a numerical plug-in method applicable to MDOF systems is developed to estimate the variance and covariance in practice.

### 3.4.1 Single-Degree-of-Freedom Systems

For a zero-mean, Gaussian time series  $x(t)$ , the variance for the sample correlation  $\hat{R}_{xx}(\tau)$  and  $\hat{R}_{xx}^b(\tau)$  can be calculated as

$$\begin{aligned} Var [\hat{R}_{xx}^b(\tau)] &= \frac{1}{T} \int_{-T+\tau}^{T-\tau} \left(1 - \frac{|t| + \tau}{T}\right) (R_{xx}^2(t) \\ &\quad + R_{xx}(t + \tau)R_{xx}(t - \tau)) dt \end{aligned} \quad (3.27)$$

$$\begin{aligned} Var [\hat{R}_{xx}(\tau)] &= \frac{1}{T - \tau} \int_{-T+\tau}^{T-\tau} \left(1 - \frac{|t|}{T - \tau}\right) (R_{xx}^2(t) \\ &\quad + R_{xx}(t + \tau)R_{xx}(t - \tau)) dt \end{aligned} \quad (3.28)$$

This result was first given in discrete form for the biased estimate by Bartlett (1946), i.e. a summation rather than an integration. It is seen from the above equations that the variance for the unbiased estimate is of the order of  $O(1/T - \tau)$  thus leading to erratic behavior in the tail region of  $\hat{R}_{xy}(\tau)$  while it remains of order  $O(1/T)$  for  $\hat{R}_{xy}^b(\tau)$  for all  $\tau$  (Priestley, 2004). As for the bias, the two estimates differ little at low lags, and since high lags are of no practical interest, only the unbiased estimate will be considered henceforth.

To find the variance of  $\hat{R}_{xx}$ , we can insert the expressions for the auto-correlation function into equations 3.29 and perform the integration. The auto-correlation function of the *displacement* response of a continuous linear SDOF system with natural frequency  $\omega_0$  and damping ratio  $\xi$  excited by stationary white noise with constant spectrum  $S_0$  by  $x(t)$  is given by in Penzien and Clough (1993). Using the relations  $R_{\dot{x}}(\tau) = -d^2 R_x(\tau)/d\tau^2$  and  $R_{\ddot{x}}(\tau) = -d^2 R_{\dot{x}}(\tau)/d\tau^2$  (Penzien and Clough, 1993), where  $\dot{x}(t)$  and  $\ddot{x}(t)$  denote the corresponding velocity and acceleration output respectively,

the velocity auto-correlation can easily be computed. They yield

$$R_x(\tau) = \frac{\omega_0 S_0}{4k^2 \xi} \left[ \cos(\omega_D t) + \frac{\xi}{\sqrt{1-\xi^2}} \sin(\omega_D |t|) \right] e^{-\omega_0 \xi |t|} \quad (3.29)$$

$$R_{\dot{x}}(\tau) = \frac{\omega_0^3 S_0}{4k^2 \xi} \left[ \cos(\omega_D t) - \frac{\xi}{\sqrt{1-\xi^2}} \sin(\omega_D |t|) \right] e^{-\omega_0 \xi |t|} \quad (3.30)$$

$$R_{\ddot{x}}(\tau) = \frac{\omega_0^4 S_0}{k^2} \left\{ \delta(t) + \frac{\omega_0}{4\xi} [(1-4\xi^2) \cos(\omega_D t) - \frac{\xi(3-4\xi^2)}{\sqrt{1-\xi^2}} \sin(\omega_D |t|)] e^{-\omega_0 \xi |t|} \right\} \quad (3.31)$$

where  $\omega_D$  denotes the damped natural frequency of the system and  $-\infty < \tau < \infty$ . The Dirac- $\delta$  function enters the acceleration auto-correlation because of discontinuity of the absolute value at  $\tau = 0$ . This has a physical meaning, however, and is effectively due to the fact that the impulse response function for the velocity is discontinuous at  $t = 0$  (Schmidt, 1985a).

Performing the integration in equation (3.29) is tricky and for a sufficiently large record length  $T$ , equation (3.29) can be approximated as (Bendat and Piersol, 2000)

$$Var [\hat{R}_x(\tau)] \approx \frac{1}{T} \int_{-\infty}^{+\infty} (R_x^2(t) + R_x(t+\tau)R_x(t-\tau)) dt, \quad \tau \geq 0 \quad (3.32)$$

In fact, the requirement on the record length  $T$  for this approximation to be valid is not stringent at all as will be illustrated in the next section. The analytical variance of the ac.f. of the displacement, velocity and acceleration output may now be obtained by substituting equation (3.30), (3.31) and (3.32) into (3.32), respectively, and performing the integration. The exact results are lengthy and hence only an approximation will be given here. More precisely, *time-independent* terms in the nominator involving powers of  $\xi \geq 2$  and *time-dependent* terms involving powers of  $\xi > 2$  have been omitted so that the results will hold for lightly damped systems (roughly  $\xi < 5\%$ ) of critical damping and for  $T$  large compared with the time lag of interest. For displacements

$x(\tau)$ , velocities  $\dot{x}(\tau)$  and acceleration records  $\ddot{x}(\tau)$  one obtains for positive lags  $\tau$

$$\text{Var} [\hat{R}_{x,\dot{x}}(\tau)] \approx \frac{C_{x,\dot{x}}}{(2T\omega_0\xi)} \left\{ 1 + e^{-2\omega_0\xi\tau} [\cos(2\omega_D\tau) (1 + 2\xi\omega_0\tau) \right. \quad (3.33)$$

$$\left. \pm (4\omega_0\tau\xi^2/\sqrt{1-\xi^2}) \sin(2\omega_D\tau)] \right\}$$

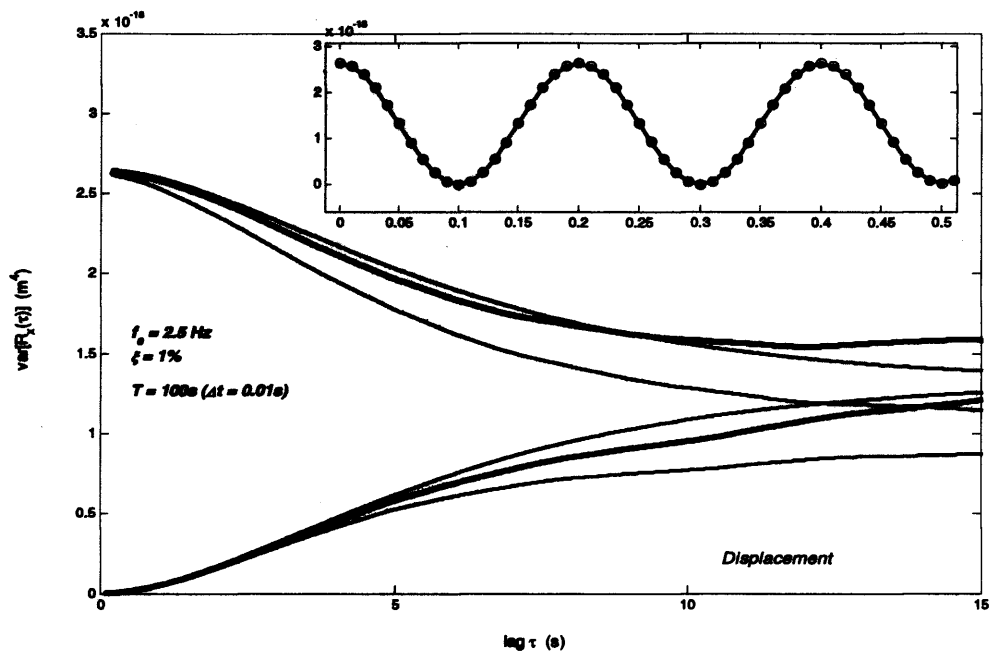
$$\text{Var} [\hat{R}_{\ddot{x}}(\tau)] \approx \frac{S_0^2\omega_0^8}{(32\xi^3k^4T)} \left\{ 1 + e^{-2\omega_0\xi\tau} [\cos^2(2\omega_D\tau) (1 + 2\xi\omega_0\tau) \right. \quad (3.34)$$

$$\left. - (12\omega_0\tau\xi^2/\sqrt{1-\xi^2}) \sin(2\omega_D\tau)] \right\}$$

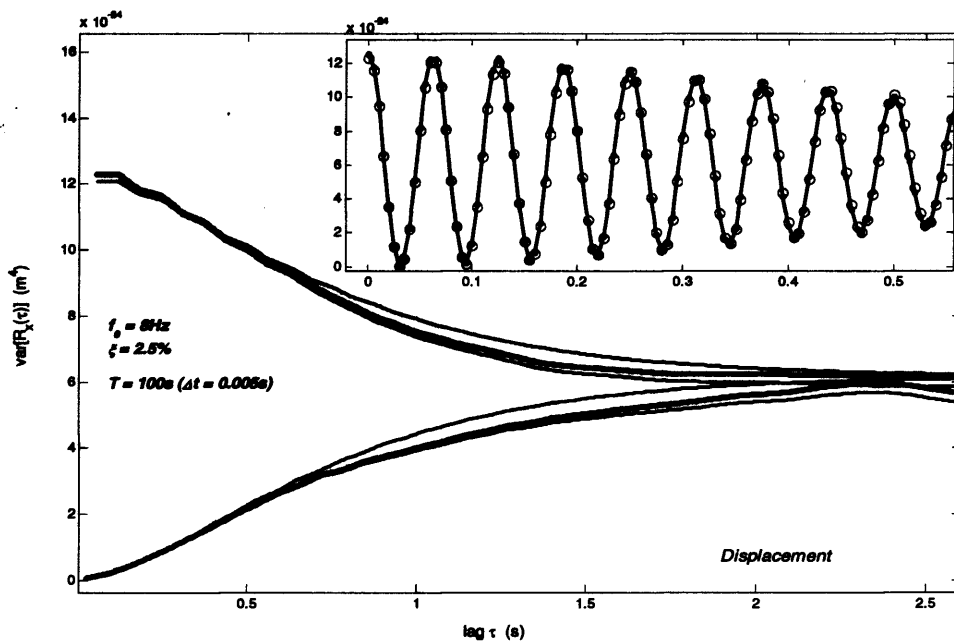
where the expression with  $C_x = \frac{\omega_0^2 S_0^2}{(16k^4\xi^2)}$  and the '+' sign holds for displacements, and the one with  $C_{\dot{x}} = \frac{\omega_0^6 S_0^2}{(16k^4\xi^2)}$  and the '-' gives the variance for velocities. The above equations are verified below by comparing them to the variance of the auto-correlation function computed from an ensemble of 480 realisations of systems 1 and 2 described in table 3.1. The SDOF systems were excited by white Gaussian noise and the response was recorded for a total length of  $T = 100s$ . A time step  $\Delta t = 0.01s$  and  $\Delta t = 0.005s$  was chosen for system 1 and 2 respectively. This is shown for displacement records in figures 3.3. It is seen that equations (3.30) and (3.32) offer a good description of the variance of the auto-correlation function of SDOF systems. Since the integration in (3.32) is from  $-\infty$  to  $\infty$ , these expressions hold for the unbiased estimate. This is illustrated in figure 3.3 by comparison with the envelope of the biased estimate. Since the variance oscillates at twice the frequency of the system's auto-correlation function, the minima (lower envelope of the variance function) gives the variance at zero-crossings while the upper envelope gives the variance of the envelope (upper and lower) of the auto-correlation function. Up to the lag shown, the variance of the maxima (upper envelope) of the variance function decrease with  $\tau$  and the minima (lower envelope) increase. This is illustrated in figure 3.4 and may provide an explanation for why frequencies are generally much better identified than damping ratios. As il-

SDOF systems	Natural Frequency $f_0$	Damping ratio $\xi$
System 1	2.5 Hz	1 %
System 2	8 Hz	2.5 %

Tab. 3.1: The two SDOF systems used for simulation. Their modal parameters were chosen such as to have a representative case for a low frequency/lightly damped and "high" frequency/heavily damped system.



(a)



(b)

Fig. 3.3: Comparison of the analytical approximation of the variance of the displacement ac.f. of SDOF systems with the simulated variance from an ensemble of 480 realizations of systems 1 and 2 in table 3.1. For clarity, only the envelopes of the variances are shown.  $[- -]$  shows the variance of the unbiased ac.f. computed by simulation,  $[-]$  represents the analytical approximation and  $[\dots]$  the simulated variance of the biased ac.f. The inset figures are a zoom at low lags showing the agreement of the oscillatory behaviour. The simulated (unbiased) results are represented by  $[-\bullet-]$  and analytical results by  $[o]$

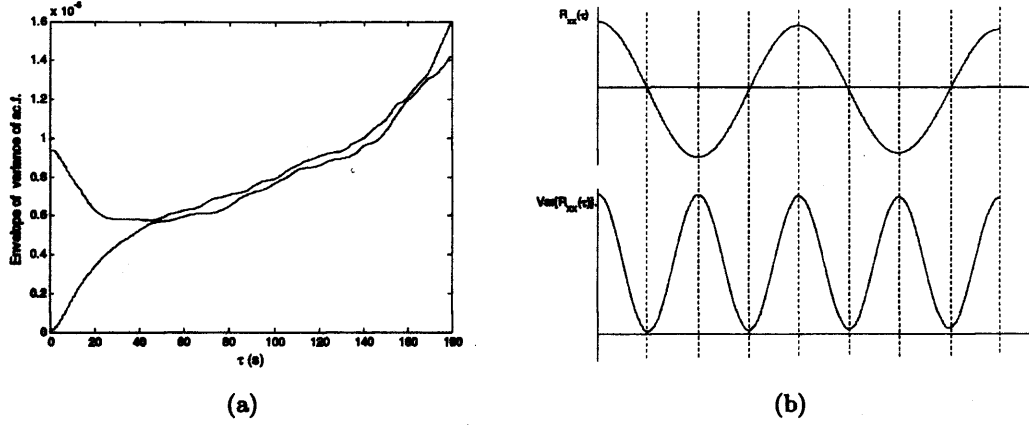


Fig. 3.4: (a) envelope of the sample ac.f. of a 1Hz, 1% damped SDOF system including high lag times  $\tau$ . (b) The minima of the  $Var[R_{xx}(\tau)]$  give the variance at zero crossings of  $R_{xx}(\tau)$  while its maxima give the variance of the the envelope of  $R_{xx}(\tau)$ .

illustrated for a 1Hz, 1% damped SDOF system in figure 3.4, the variance of the ac.f. at zero-crossings and that of its envelope will eventually converge and increase with  $\tau$ . It is noted, however, that the initial decrease in variance of the envelope does not imply that the correlation function is better estimated at these lags. Converting the envelope of the variance function, i.e. at  $\tau = n\frac{\pi}{\omega_D}$ , to the corresponding normalized random error of the ac.f. defined as  $\epsilon_r(\hat{R}_x(\tau)) = \sigma(\hat{R}_x(\tau))/R_x(\tau)$ , where  $\sigma(\cdot)$  denotes the standard deviation, yields

$$\epsilon_r(R_x(\tau = n\pi/\omega_D)) \approx \sqrt{\frac{1}{T} \left( \frac{[1 + e^{2\omega_0\xi\tau}]}{2\omega_0\xi} + \tau \right)} \quad (3.35)$$

and at  $\tau = 0$  one obtains

$$\epsilon_r(R_x(\tau = 0)) \approx \frac{1}{\sqrt{\pi B_H T}} \quad (3.36)$$

where  $B_H = 2\xi f_0$  is the common approximation to the half-power bandwidth of the system's resonance peak (Bendat and Piersol, 2000). It should be noted that, for convenience, equation (3.35) was normalized with respect to the absolute value of the ac.f. so that the normalized random error is always positive. Equation 3.36 may be compared to the expression describing the normalized random error in a white noise signal of bandwidth  $B$  given by  $1/\sqrt{BT}$  in (Bendat and Piersol, 2000). It is noted that within this approximation made in equations (3.30), (3.31) and (3.32), the normalised random error at  $\tau = n\pi/\omega_D$  is the same for displacement, velocity and acceleration

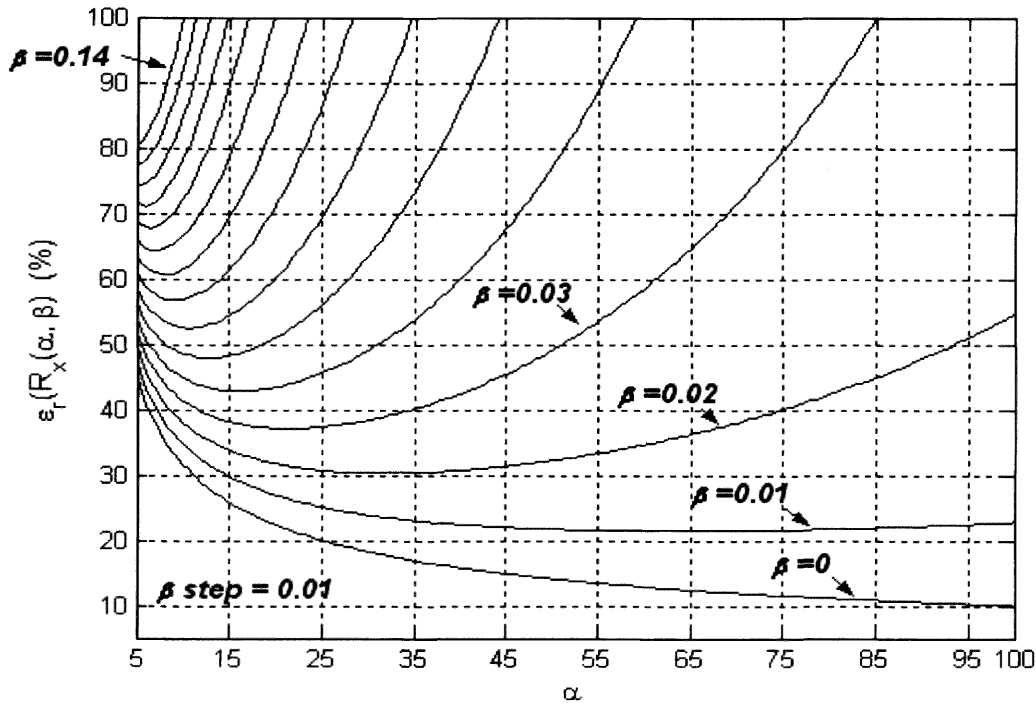


Fig. 3.5: Illustration of the normalized random error at positive and negative peaks of the estimated sample ac.f.  $\alpha = \omega_0 \xi T$  and  $\beta = \frac{\tau}{T}$ .

records and will henceforth be denoted by  $\epsilon_r(R_x(\tau = 2\pi n/\omega_D))$ . The behaviour of  $\epsilon_r(n\pi/\omega_D)$  is illustrated in figure 3.5 below. To plot figure 3.5, equation (3.35) was reformulated in terms of two auxiliary parameters  $\alpha = \omega_0 \xi T$  and  $\beta = \frac{\tau}{T}$  thereby allowing to represent many cases on the same graph. The normalized random error on the ordinate is plotted as a function of  $\alpha$  represented on the abscissa. The various curves are for different values of  $\beta$ . The lowest curve is for  $\beta = 0$  i.e. at zero lag. Moving upwards, successive curves are obtained by incrementing the parameter  $\beta$  by a value of 0.01 up to  $\beta = 0.14$ . Thus, for example, the point at  $\alpha = 25$  may represent the normalized random error in ac.f. of a SDOF system with modal parameters  $f_0 = 2.3\text{Hz}$ ,  $\xi = 1.5\%$  estimated from a total record length of  $T \approx 115\text{s}$ . The different values of  $\beta$  then give the corresponding lag, for example,  $\beta = 0.04$  gives  $\epsilon_r$  at  $\tau = 115 \times 0.04 \approx 4.6\text{s}$  where the normalized random error can then be read from the graph as approximately 45%. For fixed  $T$ , a clear increase in random error can be seen as the  $\tau$  increases and tends towards the 100% error limit relatively quickly, the more so for high frequency and more heavily damped systems. For low frequency and

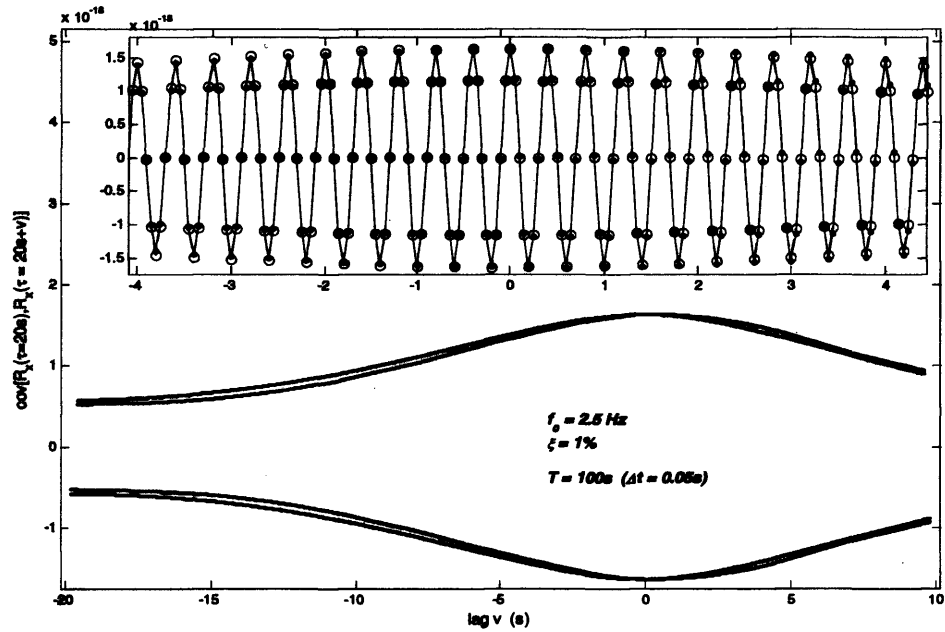
lightly damped systems the error propagates more slowly along the auto-correlation function. At low lag times, however, the level of the error is considerably smaller for high frequency, more heavily damped systems than for low frequency, lightly damped systems. It will be seen in Chapters 6 and 7 that this behaviour is clearly reflected in the random error of the identified modal parameters. Clearly, the random error is seen to decrease with  $T$ . It is remarked that, although equation (3.35) is defined only for  $\tau = n\frac{\pi}{\omega_D}$  for  $n = 0, 1, 2, \dots$ , the results in figure 3.5 are interpolated between these points. Consequently, the normalized random error shown in figure 3.5 should be interpreted as that of the envelope of auto-correlation function.

### 3.4.2 Auto-covariance function

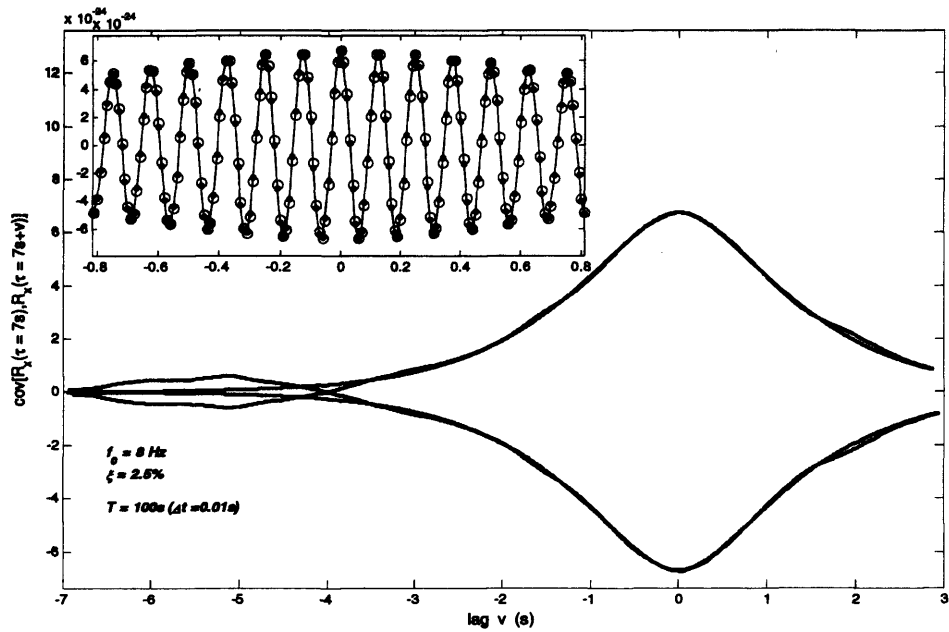
It will be shown in Chapter 5 and 6 that the determination of the random error in the identified modal parameters heavily relies on the covariance structure of the estimated correlation function. An approximate expression for large  $T$  for the covariance of  $\hat{R}_x(\tau)$  can be found to be (Priestley, 2004)

$$\begin{aligned} \text{cov} [\hat{R}_x(\tau), \hat{R}_x(\tau + v)] &\approx \frac{1}{T} \int_{-\infty}^{+\infty} (R_x(t)R_x(t + v) \\ &\quad + R_x(t + \tau + v)R_x(t - \tau)) dt, \\ &\tau \geq 0, \quad \tau + v \geq 0 \end{aligned} \quad (3.37)$$

and it is noted that equation 3.32 follows from the latter expression for  $v = 0$ . An expression for the covariance may then be found as before by carrying out the integration. For convenience, the constant multiplier in the correlation functions was omitted and the covariance function can be found to be



(a)



(b)

Fig. 3.6: The envelope of the covariance function of the estimated sample ac.f. as a function of  $v$ . Figure (a) shows the covariance of the 2.5 Hz SDOF system evaluated at  $\tau = 20s$  and figure (b) depicts the same for the 8 Hz at  $\tau = 7s$ .  $[-]$  denotes the theoretical covariance and  $[-\bullet-]$  the simulated covariance computed from 480 realizations of the system excited by white Gaussian noise. The inset figure shows the oscillatory behaviour of the covariance at lags  $v$  around  $\tau$ . The simulated results are represented by  $[-\bullet-]$  and analytical results by  $[o]$ .



$$\begin{aligned}
\text{cov} [\hat{R}(\tau), \hat{R}(\tau + v)] &\approx e^{-\omega_0 \xi |v|} \left\{ \cos(\omega_D v) [1 + |v| \omega_0 \xi] \right. \\
&\quad \left. + \frac{2\omega_0 |v| \xi^2}{\sqrt{1 - \xi^2}} \sin(\omega_D |v|) \right\} \\
&\quad + e^{-2\omega_0 \xi (2\tau + v)} \left\{ \cos(\omega_D (2\tau + v)) (1 + \xi \omega_0 (2\tau + v)) \right. \\
&\quad \left. + \left( \frac{2\omega_0 (2\tau + v) \xi^2}{\sqrt{1 - \xi^2}} \right) \sin(\omega_D (2\tau + v)) \right\}, \\
\tau &\geq 0, \quad \tau + v \geq 0
\end{aligned} \tag{3.38}$$

It is can be seen that the above equation reduces to the expression for the variance for displacement outputs at  $v = 0$ , (see eq. 3.34), with the constant multiplier set to unity. Figure 3.6 validates equation 3.38 by comparisson with the covariance computed from 480 realizations of each of the two systems in table 3.1. For clarity, only the envelope is shown over 10s of the auto-covariance function and the oscillatory part is depicted only at low lags  $v$  in the inset figure.

### 3.4.3 Multi-Degree-of-Freedom Systems

The equations given above are restricted to a description of the variance and covariance of auto-correlation functions of SDOF systems. In principle, an analytical expression for cross-correlation functions between simultaneously measured responses of MDOF systems could be obtained by integrating the general expression for cross-correlation functions given in the formulation of the natural excitation technique i.e. equation 2.33 (James *et al.*, 1995) according to equation 3.32. As will be argued in the next section and in Chapter 6, such an expression would not be useful in practice and unnecessary for the purpose of giving a general description of the error in xc.f. of MDOF systems. Instead, an approximation is given in this section that uses the known results for SDOF systems. The derivation of the result is rather lengthy and is therefore given in appendix A. It states that under the condition that a) the damping is light and and b) that modes of the system are *sufficiently separated*, the variance of the cross-correlation functions can be approximated as a weighted sum of the ac.f. functions of

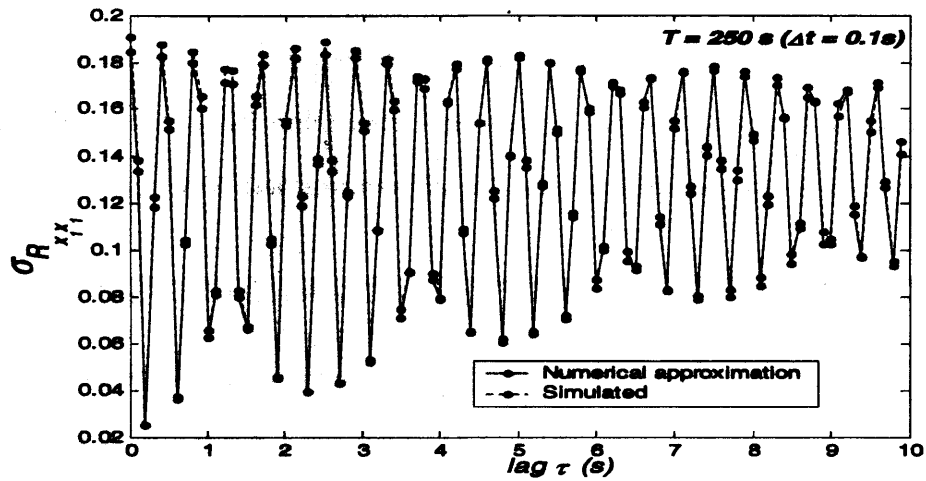
equivalent SDOF systems. More precisely,

$$\text{Var}(R_{x_i x_p}(\tau)) \approx \sum_n \frac{\phi_{pn} \phi_{pn}}{\phi_{in} \phi_{in}} \text{Var}(R_{x_{in} x_{in}}(\tau)) \quad (3.39)$$

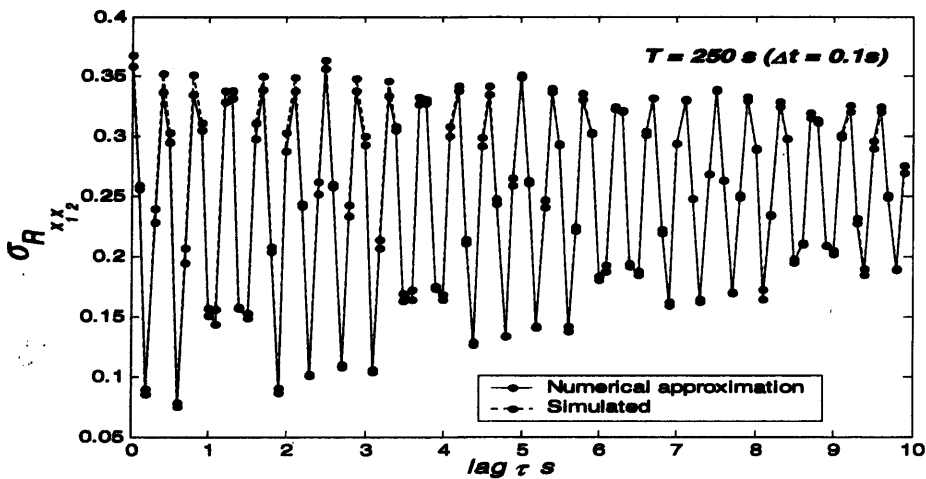
This expression was verified by simulating a proportionally damped 2-DOF system with modal parameters  $f_1 = 1.2Hz$ ,  $f_2 = 2Hz$  and  $\xi_1 = 1.04(\%)$ ,  $\xi_2 = 1.03(\%)$ . The system was excited by Gaussian white noise at each degree-of-freedom and 300 realizations -each consisting of  $250s(\Delta t = 0.1s)$  of displacement response- were recorded. The variance of the cross-and auto-correlation functions of the response was then computed as an ensemble average over the 300 realizations. The square root of the variance thus calculated, normalized by its value at  $\tau = 0$  is shown by the (blue) dotted line in figures 3.7. The solid line is the result obtained by numerically evaluating equation A.23. It can be seen that the results are in good agreement. It appears from this simulation that the requirement of the modal separation for equation 3.39 to yield the variance of auto- and -cross correlation functions of the MDOF systems excited by white noise is  $< 1Hz$ . The limit for the proximity of modes at which equation 3.39 fails was, however, not since the method described in the next section is much more useful in practice and does not suffer from this issue.

### 3.5 Plug-in Estimates

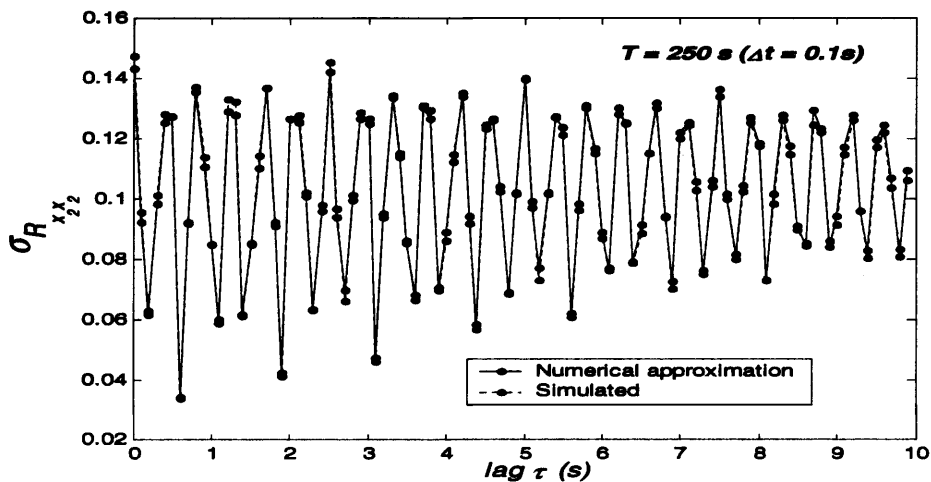
The formulae given in the previous section may be used in practice to calculate the random error in the estimated sample correlation functions, but it transpires that this is not practical and suffers from a few drawbacks: a) a normalization procedure would have to be applied because some of the parameters, for instance  $S_0$  are not known b) the formula for MDOF is not applicable for close modes and b) we require knowledge of the modal parameters of the system in order to implement the formulae. The last point cannot be avoided since the estimation of the variance involves the exact correlation functions which are unknown and an estimate, in this case in terms of the



(a)



(b)



(c)

Fig. 3.7: Normalized standard deviation of the correlation functions of a 2-DOF system excited by white Gaussian noise. Figure (a) and (c) depict the auto-correlation functions at measurement station 1 and 2 respectively; figure (b) depicts the cross-correlation function between the time histories at station 1 and 2. [· · ·] simulated and [—] numerical approximation

modal parameters, needs to be taken instead. However, since the modal identification usually involves model order reduction and spurious modes, a more direct plug-in approach is preferred that involves the estimated correlation functions directly.

### 3.5.1 Plug-in Estimates for the Covariance of Correlation functions

The discrete version of equation 3.28 for cross-correlation functions is given by Priestley (2004) for  $r \geq 0$ ,  $r + v \geq 0$

$$\begin{aligned} \text{Cov} \left[ \hat{R}_{xy}^b(r), \hat{R}_{xy}^b(r+v) \right] &= \frac{1}{N} \sum_{m=(-N+r)+1}^{N-r-v-1} \left( 1 - \frac{\eta(m) + r + v}{N} \right) \times \\ &\quad \times (R_{xx}(m)R_{yy}(m+v) + R_{xy}(m+r+v)R_{yx}(m-r)) \end{aligned} \quad (3.40)$$

with

$$\eta(m) = \begin{cases} m, & m > 0 \\ 0, & -v \leq m \leq 0 \\ -m - v, & -(N-r) + 1 \leq m < v \end{cases}$$

and gives the *exact* estimate for the covariance of  $\hat{R}_{xx}^b(r)$ . The expression for auto-correlation function follows by letting  $y = x$ . As in the previous section, we may again simplify this expression for large  $N$  by letting  $\left( 1 - \frac{\eta(m) + r + v}{N} \right) \rightarrow 0$  and replacing the summation by  $-\infty$  and  $\infty$  so that

$$\begin{aligned} \text{Cov} \left[ \hat{R}_{xy}^b(r), \hat{R}_{xy}^b(r+v) \right] &\approx \frac{1}{N} \sum_{m=-\infty}^{\infty} (R_{xx}(m)R_{yy}(m+v) \\ &\quad + R_{xy}(m+r+v)R_{yx}(m-r)) \end{aligned} \quad (3.41)$$

In practice, the summation is of course bounded by the number of available data. Strictly, equations 3.40 and 3.41 hold for the biased estimate  $\hat{R}_{xx}^b(r)$ . However, the approximation 3.41 may be used to estimate the covariance of the unbiased estimate  $\hat{R}_{xx}(r)$  because a) the dependence on the lag  $r$  in the limits of the summation is relaxed i.e. the summation ranges over more data points than  $2(N-r)$  and b) comparison of the continuous equations for the variance given by 3.28 and 3.29 for the biased and unbiased estimate respectively, reveals that the two expressions converge with

increasing  $T$ . In particular, under the assumption of large  $T$ , or equivalently large  $N$ , the two estimates are very close at low lags. The estimate 3.41 is validated by simulation of a 2DOF system whose modal parameters are given in table 3.2. Only the variance will be displayed here for convenience as it is clear that the effect of this approximation will be the same for the covariance. The system was excited at both degrees of freedom (dofs) with a white noise input and the response was recorded for a total duration of  $5min(\Delta t = 0.04s)$  at both dofs. An ensemble of 500 responses were simulated at each degree-of-freedom. From each one, the ac.f. and xc.f.  $\hat{R}_{11}(r)$  and  $\hat{R}_{12}(r)$  respectively, were computed and used to approximate their variance. The subscripts refer to the dofs at which the response was recorded so that, for instance,  $\hat{R}_{11}(r)$  is the ac.f of the response at dof 1 and  $\hat{R}_{12}(r)$  the xc.f. between the response at dof 1 and 2. This simulated variance is represented in figure 3.8 by  $[\dots \times \dots]$ . The evaluation of equation 3.41 requires knowledge of the true correlation functions  $R_{11}(r)$ ,  $R_{22}(r)$ ,  $R_{12}(r)$  and  $R_{21}(r)$ . The latter were approximated by taking the mean over the ensemble of the 500 estimates of  $\hat{R}_{11}(r)$  and  $\hat{R}_{12}(r)$  and were used as input to equation 3.41. The results are shown up to a lag of  $3s$  in figure 3.8. It is seen that there is good agreement between simulated data and the estimate from equation 3.41. The discrepancies that arise between the simulated data and the estimate 3.41 are due to various sources. Firstly, the sample estimates from the 500 realisations will not have fully converged: i.e. the simulated variance as well as the mean of the correlation functions that was used as input to 3.41 are not exact. Secondly, the estimate 3.41 is an approximation to 3.40. The convergence of equation 3.41 to its exact estimate given by equation 3.40 is illustrated in figures 3.9. These figures depict the variance of  $\hat{R}_{xx}^b(0) = \hat{R}_{xx}(0)$  and is therefore independent of whether the variance of the biased or unbiased correlation is estimated. It is seen that both estimates converge rapidly as  $T$  increases and for record length  $\geq 5min$  the difference is certainly negligible. Also,

Modes	Natural Frequency $f_0$	Damping ratio $\xi$
Mode 1	1.5 Hz	0.97%
Mode 2	2.91 Hz	1.85%

Tab. 3.2: Modal Parameters of the 2DOF system used for simulation.

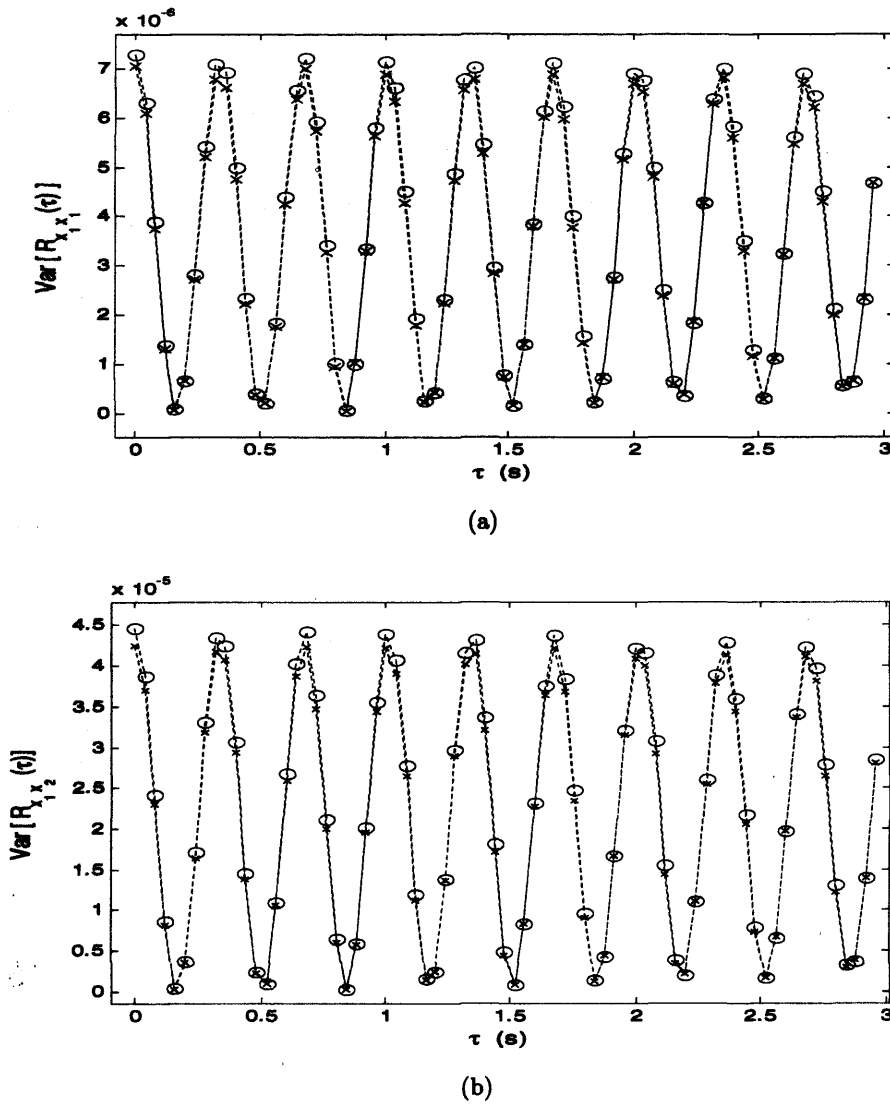


Fig. 3.8: Validating equation 3.41 for unbiased estimates by comparison with simulated data from the 2DOF in table 3.2. An ensemble of 500 realisations was simulated.  $[- \circ -]$  denotes the estimate from 3.41 using  $R_{xy}(r)$  as estimated from the ensemble of 500 response histories and  $[\dots \times \dots]$  the simulated variance. For convenience, only the variance is shown.

figures 3.8 reveal that estimates for  $T \geq 5min$  will also yield a good approximation to the unbiased estimate at low lags.

In practice, the plug-in method presented above has two drawbacks: Firstly, an ensemble of responses that enable to compute the mean of their correlation functions may not be available. Therefore, the covariance needs to be computed using the only

estimate available, that is  $\hat{R}_{xx}(r)$ , by plugging the latter into equation 3.41 as

$$\begin{aligned} Cov [\hat{R}_{xy}(r), \hat{R}_{xy}(r+v)] \approx \frac{1}{N} \sum_{m=-\infty}^{\infty} & \left( \hat{R}_{xx}^b(m) \hat{R}_{yy}^b(m+v) \right. \\ & \left. + \hat{R}_{xy}^b(m+r+v) \hat{R}_{yx}^b(m-r) \right) \end{aligned} \quad (3.42)$$

Due to the estimation errors in  $\hat{R}_{xy}^b(r)$ , the estimate  $Cov [\hat{R}_{xx}^b(r), \hat{R}_{xx}^b(r+v)]$  itself will be in error and its accuracy will depend on how well we can estimate  $\hat{R}_{xx}^b(r)$ . The problem of having to deal with correlation function estimates is even more pronounced in this situation than when they are used as a response model from which the system's modal parameters are extracted. The reason is that in the latter case, a modal identification is possible using only the low lag portion of the correlation functions which has significantly less error than the tail regions. In the present situation, however, the sum needs be computed over the entire two-sided, full length correlation functions and the poorly defined high lag ends must be included. The second difficulty is the computational efficiency. Having to use two-sided, full length correlation functions significantly increases the computational burden. An ideal remedy for both of these drawbacks would be to somehow do without the tail regions, thereby reducing the number of data points used in the computation and, at the same time avoiding the inclusion of the high random errors in high lag estimates. This can indeed be achieved using a suitable taper. Ideally, such a taper would be smooth at low lags to minimize

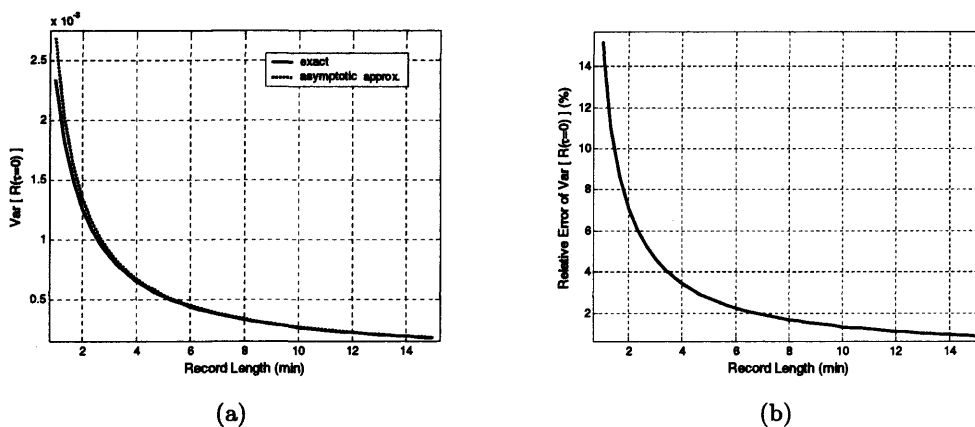


Fig. 3.9: (a) [· · ·] shows the asymptotic approximation in equation 3.41 and [—] the exact value obtained from 3.40 as a function of  $T$  at zero lag. (b) The relative error between 3.41 and 3.40 as a function of  $T$  using a time step  $\Delta t = 0.04s$

bias but then cut off the tail region rather sharply at the point where, in theory, the correlation function has decayed to almost zero. Politis (2003a) used a “flat-top” window to evaluate infinite sums of the type  $\sum_{k=-\infty}^{\infty} |k|^p e^{ik\omega} \hat{R}_{xx}^b(k)$ , where  $i = \sqrt{-1}$  and  $p \geq 0$  and provided an empirical method to choose the optimal length or *bandwidth* of this window adaptive to the auto-correlation function  $R_{xx}^b(k)$  of the problem under consideration. The “flat-top” window, in scaled parameter form, is defined by

$$w_{FT}(t) = w_{FT}(k/M) \begin{cases} 1 & |t| \in [0, 1/2] \\ 2(1 - |t|) & |t| \in [1/2, 1] \\ 0 & \text{otherwise} \end{cases} \quad (3.43)$$

where  $M$  is the length of the window and its bandwidth is defined by  $b = M^{-1}$ . To briefly describe the idea behind their method, we shall start by considering the *biased* auto-correlation functions, denoted  $\hat{R}_{xx}^b(k)$ . It will be seen shortly, that in order for the method to work, a biased estimate of the auto-correlation function must be taken. Firstly, note that for  $p = 0$  and using the flat-top window  $w_{FT}$ , the sum above reads  $\sum_{k=-\infty}^{\infty} e^{ik\omega} w_{FT}(kb) \hat{R}_{xx}^b(k) = 2\pi S_x(\omega)$  with  $\omega = [-\pi, \pi]$  (Priestley, 2004). Thus, the choice of the window length  $M$  amounts to selecting the “optimal” bandwidth of the window to estimate the spectral density  $S_x(\omega)$ ; optimal in the sense that bandwidth is chosen such that the mean-square-error (*mse*) of the spectral density is minimised. In fact, this idea will feature prominently in the selection of the block length for the dependent bootstrap which is treated in the next chapter and, for more clarity, the reader is referred to section 4.4, Chapter 4. Politis (2003a) derived the following *empirical rule* to select  $M = b^{-1}$ .

Construct the the auto-correlation coefficient function  $\hat{\rho}_{xx}^b(k) = \hat{R}_{xx}^b(k)/\hat{R}_{xx}^b(0)$  and let  $\hat{k}_{cut}$  denote the smallest lag such that  $|\hat{\rho}_{xx}^b(\hat{k}_{cut} + k)| < c\sqrt{\log_{10}(n)/n}$ , for  $k = 1, 2, \dots, K$  where  $c > 0$  is a fixed constant and  $K$  and integer of order  $O(\log_{10}(n))$ . Choose  $M = 2\hat{k}_{cut}$ .

The form of this rule essentially arises from an implied hypothesis test (see for



instance (Bendat and Piersol, 2000)). Since an estimate of the correlation coefficient function  $\hat{\rho}_{xx}(k)$  is crude, one can use a hypothesis test to check whether the estimate is consistent with the behaviour of real value  $\rho_{xx}^b(k)$ . For instance, we may compare the estimate of the correlation coefficient function at a specific lag  $k$  to what we would expect to see in the true correlation coefficient at that same lag. In this case, let this lag be  $k_{cut}$ , i.e. the lag where we  $\rho_{xx}^b(k_{cut})$  is not significantly different from zero the reason being that this is where it is desired to cut off the correlation function with the flat-top window. Assume that  $\hat{\rho}_{xx}^b(k_{cut})$  has a normal distribution with mean  $\rho_{xx}^b(k_{cut}) \approx 0$  and variance  $Var[\hat{\rho}_{xx}^b(k_{cut})]$ . The biased estimate of the the ac.f. has a variance of order  $O(n^{-1})$  which means that it will typically have  $\pm 2\sqrt{n^{-1}}$  95% confidence bands around zero at lags  $\geq k_{cut}$  (Politis, 2003a; Priestley, 2004). Therefore, an acceptable estimate of  $\hat{\rho}_{xx}^b(k)$  will fall within these bands where the true correlation coefficient function is approximately zero. Rather than using the  $\pm 2\sqrt{n^{-1}}$  bands, (Politis, 2003a) derives threshold  $c\sqrt{\log_{10}(n)/n}$ . For a rigorous treatment, the reader is referred to the original text but it is seen that both of these values are close. This provides an intuitive explanation for the selection threshold  $c\sqrt{\log_{10}(n)/n}$  for  $\hat{k}_{cut}$ . We emphasise that, for the cutoff selection described above to be applicable, it is important to take the biased estimate of the correlation coefficient for the unbiased estimate will have order  $O((n-k)^{-1})$  at lag  $k$  which means that the 95% confidence bands at around zero given above are not applicable.

The two parameters  $c$  and  $K$  need to be specified by the user. In practice, Politis and White (2004) suggest the empirical values  $c = 2$  and  $K = \max(5, \log_{10}(n))$ . While the choice of  $c = 2$  is followed in this thesis, a slightly different lower bound for  $K$  is imposed. The motivation for this is to avoid selecting a too high bandwidth  $b$  in a situation where the sampling interval  $\Delta t$  is small and the frequencies of the the ac.f are low so that a succession of  $K$  occurs within a period around the zero crossings much before the ac.f. has actually decayed to a level not significantly different from zero. Therefore, it is suggested that  $K$  has to cover at least half a period of the lowest frequency mode in the response so that points near the extrema of the ac.f. are consid-

ered in the selection process. Formally, this means choosing  $K > \lceil (2f_0\Delta t)^{-1} \rceil$ , where  $\lceil \cdot \rceil$  denotes the smallest integer  $\geq x$  and  $f_0$  denotes the lowest frequency component in the response. Only a crude estimate of the latter is necessary and may be obtained by inspection of the correlation functions, an finite element model of the structure or initial modal test data.

Two more issues need to be discussed. Firstly, the problem at hand is not exactly the same as evaluating a sum of the form  $\sum_{k=-\infty}^{\infty} |k|^p e^{ik\omega} \hat{R}_{xx}^b(k)$ , or alternatively, for  $p = 0$ , selecting the bandwidth that minimises the *mse* of spectral estimates. For instance, consider the computation of the variance of the correlation estimate at zero lag. It is easily seen from equation 3.42 that this computation differs from the evaluation of the spectral density at  $\omega = 0$  only in the fact that the correlation estimate is squared. We may therefore think of this estimate as that of computing the spectral density at zero of a process whose ac.f. is  $\hat{R}_{xx}^b{}^2(k)$ . Clearly the latter has an associated correlation coefficient function that decays much faster than that of  $\hat{R}_{xx}^b(k)$  so that the optimal choice of the window bandwidth to compute  $\sum_{k=-\infty}^{\infty} \hat{R}_{xx}^b(k)$  is not the same as that to compute  $\sum_{k=-\infty}^{\infty} \hat{R}_{xx}^b{}^2(k)$ . Since the method in Politis (2003a) does not specify a form for the ac.f., (although different convergence rates apply depending on whether the decay is exponential or polynomial (Carlstein, 1986)) one may apply it directly to the square of the correlation function. This approach was, however, not adopted. Rather, we apply the flat-top window with a bandwidth determined directly from the biased ac.f. according to the empirical rule above to each of the correlation estimates entering equation 3.42 to evaluate its variance and covariances. This implies that the latter estimates may be suboptimal but simulations show that the results thus obtained are satisfactory for all practical purposes (c.f. figure 3.10). It is important to note at this stage, that even to achieve optimality of the bandwidth of the flat-top window for spectral estimates as intended in Politis (2003a), a certain number of conditions on the ac.f. need to hold. Due to the highly technical formulation of these conditions, it was not possible to check them in detail, but the simulations in figures

3.10 strongly support the applicability of this method for the problem at hand.

Secondly, Politis (2003a) considered only auto-correlation functions. However, the empirical rule for selecting the bandwidth of the flat-top window can be applied to cross-correlation functions as well. As explained above, the bandwidth is selected on the basis of an hypothesis test which essentially determines when the estimated auto-correlation coefficient functions are *not* significantly different from zero by looking at the lag  $k_{cut}$  after which  $K$  subsequent values lie within the bands  $\pm c\sqrt{\log_{10}(n)/n}$ . The cross-correlation functions computed between simultaneously measured response histories on a given structure are, according to the Natural Excitation Technique (NExT) sums of decaying sinusoids with frequencies and damping ratios determined by the modes of the system which also applies to the ac.f. computed from these response measurements, although the phase information is lost in the latter. This means that, in general, whenever the auto-correlation coefficient functions have decayed to nearly zero, then the same holds for the cross-correlation functions so that  $k_{cut}$  is more or less the same in both cases. Therefore, since the variance of the estimates of the cross-correlation coefficient functions is also of order  $O(n^{-1})$  the empirical rule for bandwidth selection is applicable to cross-correlation functions. Also, if one is confident that a particular response measurement contains the mode with the slowest decay rate -most commonly the fundamental mode- for all practical purposes, the bandwidth only needs to be computed once and can be applied to all other correlation functions. Finally, to summarise,  $Cov [\hat{R}_{xy}(r), \hat{R}_{xy}(r+v)]$  is computed as follows: a) determine the bandwidth of the flat-top window  $w_{FT}(k)$  according to the selection rule above, b) apply this window to compute weighted correlation estimates  $w_{FT}(m)\hat{R}_{xx}^b(m)$ ,  $w_{FT}(m)\hat{R}_{yy}^b(m)$ ,  $w_{FT}(m)\hat{R}_{xy}^b(m)$  and  $w_{FT}(m)\hat{R}_{yx}^b(m)$  and c) use the latter as input to equation 3.42) to obtain an improved estimate of  $Cov [\hat{R}_{xy}(r), \hat{R}_{xy}(r+v)]$ .

To illustrate the advantage gained by weighting the correlation estimates by the flat-top window as described above, a 2DOF system with modal frequency and modal

damping ratios shown in table 3.3 was simulated. This system was chosen instead of the one in table 3.2 to allow a comparison with results obtained in the next chapter 4, where this system is also employed. A white Gaussian load was applied to each dof of the system. The response was computed using a Newmark- $\beta$  scheme with parameters  $\gamma = 1/2$  and  $\beta = 1/4$ . This choice, often referred to as the constant average acceleration method, makes the time integration unconditionally stable and introduces no numerical damping in the solution (Bathe and Wilson, 1976). The response was recorded at both dofs for a total length of 820s with a sampling interval of  $\Delta t = 0.05s$ . The approximations inherent in the Newmark- $\beta$  method, are known to produce period elongations. The magnitude of these frequency shifts depends both on the sampling interval and the system's frequencies. The shifted frequency can be expressed as (James *et al.*, 1993)

$$\omega_c = \frac{1}{dt} \tan^{-1} \left[ \frac{\omega dt}{1 - \left(\frac{\omega dt}{2}\right)^2} \right] \quad (3.44)$$

where  $\omega$  is the true natural circular frequency of the system and  $\omega_c$  is the circular natural frequency after the integration. In fact, the modes of the original system had natural frequencies of 2.34Hz and 4.52Hz respectively so that the values given in table 3.3 are corrected for the frequency shift introduced due to the time integration. Also, we cut out the non-stationary transients that occur initially in the response when the system is excited from rest. The decay of these transients is governed by the damping ratios and frequencies of the modes of the system; the higher the frequency and damping, the faster steady-state will be reached (Caughey and Stumpf, 1961; Clough, 1960). Following the approach of the latter authors, it was roughly estimated that the mean square response will reach its stationary mean square value after  $\approx 40s$ . Consequently, the first 40s were left out of the response leaving a total of 13min of response. In the remainder of the thesis, unless stated otherwise, this same approach will be adopted to simulate the response of system due to ambient white loading. 500 different realisations of the response were simulated this way.

Modes	Natural Frequency $f_0$	Damping ratio $\xi$
Mode 1	2.24 Hz	1.49%
Mode 2	3.93 Hz	2.85%

Tab. 3.3: Modal Parameters of the 2DOF system used for simulation.

	Lag $r = 0$	Lag $r = 1$
$Var[R_{x_2x_2}(r)]$	$1.65 \cdot 10^{-6}$	$9.61 \cdot 10^{-7}$
$Var[R_{x_1x_2}(r)]$	$2.40 \cdot 10^{-7}$	$1.40 \cdot 10^{-7}$

Tab. 3.4: True values of  $Var[R_{x_1x_2}(r = 0, 1)]$  and  $Var[R_{x_2x_2}(r = 0, 1)]$

To validate the method described above, 100 estimates of  $Var[\hat{R}_{x_1x_2}(r)]$  and  $Var[\hat{R}_{x_2x_2}(r)]$  were computed from the first 100 simulated response histories. Here,  $x_1$  and  $x_2$  denote the responses at degrees-of-freedom 1 and 2 respectively. To simplify the display of the results, only the variance at zero and lag  $r = 1$  were computed without loss of generality. For comparison,  $Var[\hat{R}_{x_1x_2}(r)]$  and  $Var[\hat{R}_{x_2x_2}(r)]$  at lags  $r = 0$  and  $r = 1$  were also computed without weighting the *biased* correlation estimates by the adaptive flat-top window. The true values of  $Var[\hat{R}_{x_1x_2}(r)]$  and  $Var[\hat{R}_{x_2x_2}(0)]$  for  $r = 1, 2$  were approximated by computing the sample variance of the 500 estimates of  $\hat{R}_{x_1x_2}(r = 0, 1)$  and  $\hat{R}_{x_2x_2}(r = 0, 1)$  and are tabulated in 3.4. The results are shown in the histograms in figures 3.10. It is seen from figures 3.10 (b) that the distribution resulting from 100 computations of  $Var[R_{x_1x_2}(r = 0, 1)]$  centres closely around the true values (c.f. table 3.4). The bias in the estimates is considerably low bearing in mind that smoothing generally involves a trade off between variance and bias. The spread of the values described by the standard deviation of  $4.40 \cdot 10^{-7}$  is also acceptable\*. A comparison with 3.10 (a) clearly shows the improvement gained by tapering the correlation functions with the flat-top window. The large bias and random error that occur in the latter case can be attributed to the summation over the ill-defined tail regions of the correlation estimates. The same observations hold for the cross-correlation functions in figures 3.10 (c) and (d). It is noted that to compute the variances for the cross-correlation functions, the same bandwidth for  $w_{FT}$  was used as for the auto-correlation functions. Although not explicitly shown here, the

\*Note that the statistics displayed in figure 3.10 are based on 100 samples only. It was not the aim to get accurate estimates of the mean and standard deviation but only to show the scatter of the variance estimates from different simulated responses.

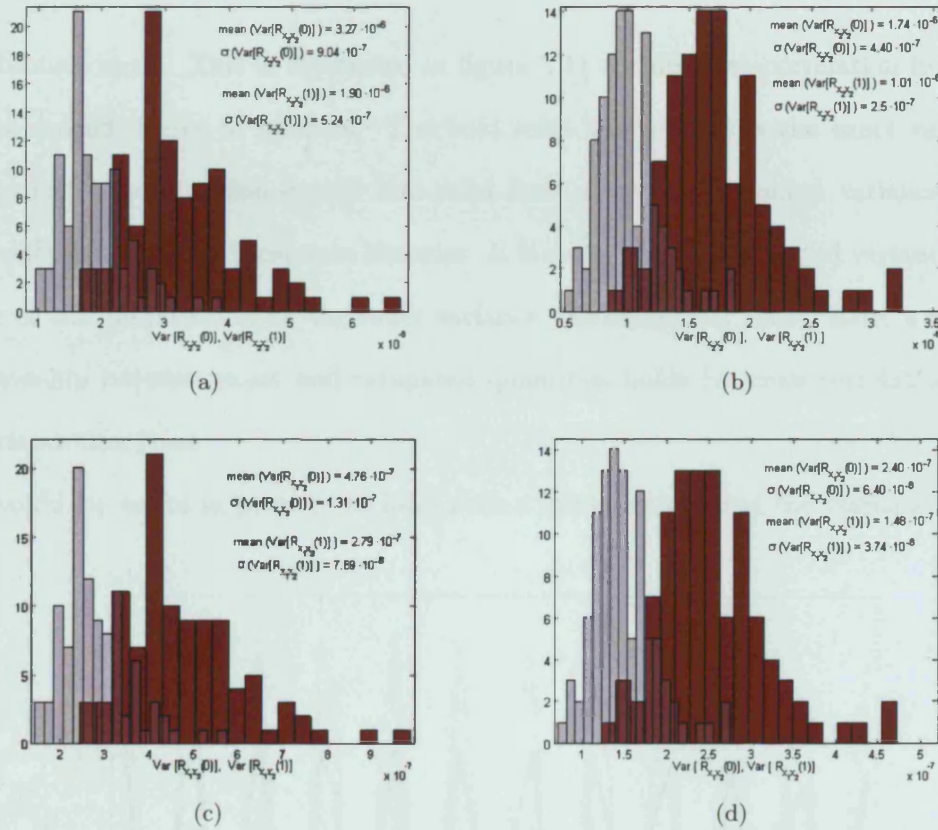


Fig. 3.10: Histogram of  $Var[R_{x_1x_2}(r=0, 1)]$  ((a),(b)) and  $Var[R_{x_2x_2}(r=0, 1)]$  ((c),(d)) from 100 computed simulated responses from the 2DOF system in table 3.3. The narrow (grey) bins represent the results for lag  $r=1$  and the wider bins (red) for lag  $r=0$ . Figures (a) and (c) show the results *without* weighting the biased correlation estimates by the flat-top window and figures (b) and (d) with applied smoothing.

results for the covariances of correlation functions are similar. Therefore, plugging the flat-top tapered auto- and cross correlation functions into equation 3.42 gives good results for estimating the covariances of the sample ac.f and xc.f. from structural response histories. Of course, in practice the covariances have to be estimated from a single measurement only, and it is seen from figures 3.10 (b) and (d) that, although the distributions peak around the true value, an over- or under estimate of the exact covariances is to be expected. Given the estimator, a reduction in variance is only possible by increasing the number of observed data points, i.e. the record length. Also noticeable from figures 3.10 is the similarity of the distribution at the two lags implying that whenever the variance at zero lag is under- or overestimated, then so is the case at lag 1. This appears to hold for all lags so that the relative relation between data points in the estimated variance is preserved but are under- or overestimated in

an absolute sense. This is illustrated in figure 3.11 for the auto-correlation function at the second degree of freedom. The bold solid line represents the exact variance of the ac.f. and the thin dotted and solid lines show the estimated variance from four different computed response histories. It is seen that the estimated variances are more or less proportional to the exact variance. Although not shown here, a similar relationship between exact and estimated quantities holds for cross-correlation and covariance functions.

It would be useful in practice to have even a crude estimate of the variance of the

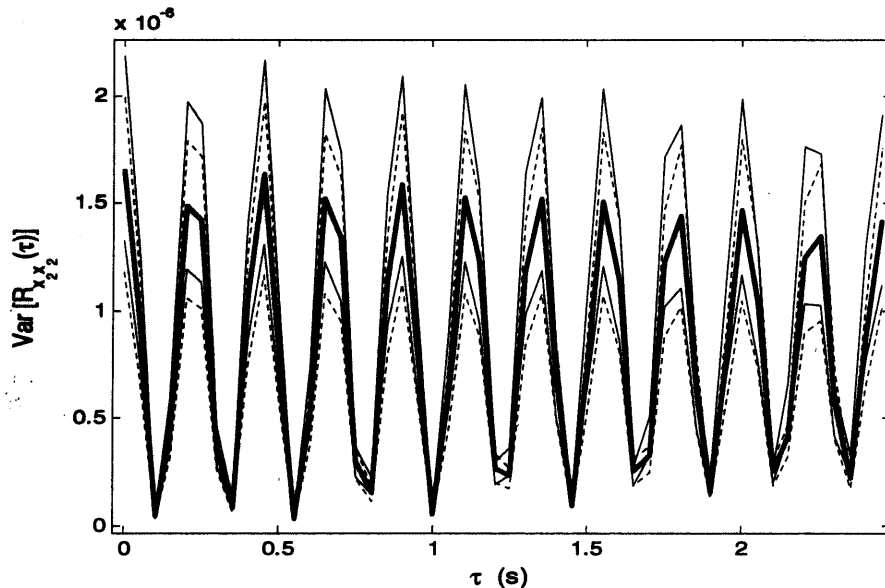


Fig. 3.11: Illustration of how the random error in the variance estimates manifests itself at higher lags.

variance to get a rough idea of the error in the covariance estimate calculated from the available recorded response.

Finally, we note that the cut-off imposed by the flat-top window reduces the number of data points used in the computation significantly. In addition, we used Hankel-type matrices to express the shifted copies of the correlation functions so that the implementation will only depend on  $r$  rather than on  $v$  and  $r$  which makes the implementation of equation 3.42 very efficient.

### 3.5.2 Plug-in Estimates for the Covariance of Correlation Coefficient functions

The variance properties of the the correlation coefficient functions differ from those of the ordinary correlation functions. For instance, it is easily seen that the variance of the auto-correlation coefficient is zero at zero lag because each estimate is normalised to unity at this lag. An asymptotic approximation for the auto-correlation coefficient, equivalent to 3.41, function is given in Bartlett (1946); Priestley (2004) and reads

$$\begin{aligned}
 \text{Cov}[\hat{\rho}_{xx}(r), \hat{\rho}_{xx}(r+v)] &\approx \quad (3.45) \\
 \frac{1}{N} \sum_{m=-\infty}^{\infty} \{ &\rho_{xx}(m)\rho_{xx}(m+v) + \rho_{xx}(m+r+v)\rho_{xx}(m-r) \\
 +2\rho_{xx}(r)\rho_{xx}(r+v)\rho_{xx}^2(m) &- 2\rho_{xx}(r)\rho_{xx}(m)\rho_{xx}(m-r-v) \\
 -2\rho_{xx}(r+v)\rho_{xx}(m)\rho_{xx}(m-r) \} &
 \end{aligned}$$

and is related to the covariance of the ordinary correlation function by

$$\begin{aligned}
 \frac{1}{\hat{R}_{xx}^2(0)} \{ &\text{Cov}[\hat{R}_{xx}(r), \hat{R}_{xx}(r+v)] - \rho_{xx}(r+v) \text{Cov}[\hat{R}_{xx}(0), \hat{R}_{xx}(r)] \quad (3.46) \\
 -\rho_{xx}(r) \text{Cov}[\hat{R}_{xx}(0), \hat{R}_{xx}(r+v)] &+ \rho_{xx}(r)\rho_{xx}(r+v) \text{Var}[\hat{R}_{xx}(0)] \quad r) \\
 -\rho_{xx}(r) \text{Cov}[\hat{R}_{xx}(0), \hat{R}_{xx}(r+v)] &+ \rho_{xx}(r)\rho_{xx}(r+v) \text{Var}[\hat{R}_{xx}(0)] \}
 \end{aligned}$$

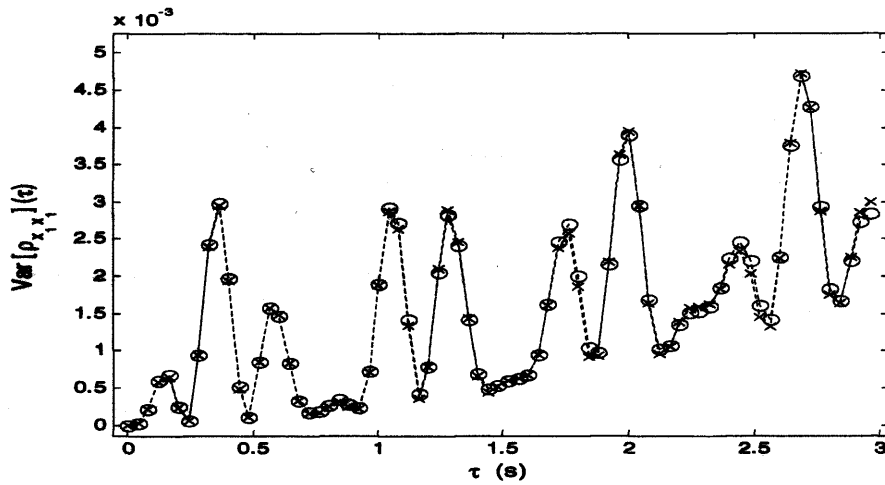
In those texts, this equation is given only for the auto-correlation coefficient  $\hat{\rho}_{xx}^b(r) = \hat{R}_{xx}^b(r)/\hat{R}_{xx}(0)$ . To estimate the covariance of the cross-correlation coefficients, the ap-



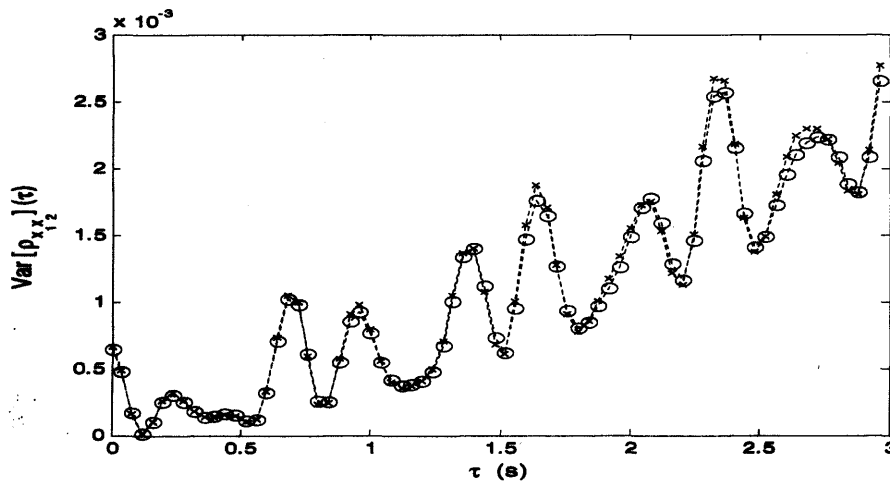
proach in Priestley (2004) is followed. The desired expressions are

$$\begin{aligned}
Cov[\hat{\rho}_{xy}(r), \hat{\rho}_{xy}(r+v)] &\approx \frac{Cov[\hat{R}_{xy}(r), \hat{R}_{xy}(r+v)]}{\hat{R}_{xx}(0)\hat{R}_{yy}(0)} \\
&- \frac{1}{2}\rho_{xy}(r+v) \left[ \frac{Cov[\hat{R}_{xx}(0), \hat{R}_{xy}(r)]}{\hat{R}_{xx}^{3/2}(0)\hat{R}_{yy}^{1/2}(0)} + \frac{Cov[\hat{R}_{yy}(0), \hat{R}_{xy}(r)]}{\hat{R}_{xx}^{1/2}(0)\hat{R}_{yy}^{3/2}(0)} \right] \\
&- \frac{1}{2}\rho_{xy}(r) \left[ \frac{Cov[\hat{R}_{xx}(0), \hat{R}_{xy}(r+v)]}{\hat{R}_{xx}^{1/2}(0)\hat{R}_{yy}^{3/2}(0)} + \frac{Cov[\hat{R}_{yy}(0), \hat{R}_{xy}(r+v)]}{\hat{R}_{xx}^{3/2}(0)\hat{R}_{yy}^{1/2}(0)} \right] \\
&+ \frac{1}{4}\rho_{xy}(r)\rho_{xy}(r+v) \left[ \frac{Var[\hat{R}_{xx}(0)]}{\hat{R}_{xx}^2(0)} + \frac{Var[\hat{R}_{yy}(0)]}{\hat{R}_{yy}^2(0)} + 2\frac{Cov[\hat{R}_{xx}(0), \hat{R}_{yy}(0)]}{\hat{R}_{xx}(0)\hat{R}_{yy}(0)} \right]
\end{aligned} \tag{3.47}$$

It is easily verified by letting  $x = y$  that the above equation reduces to 3.46. As before, setting  $v = 0$  gives the variance of the correlation coefficient estimate. It is certainly possible to transform equation 3.47 into an expression consisting of correlation coefficient functions only as in equation 3.45 but this is not done here. The reason is that the above expression and 3.46 are easy to compute using the same implementation as for the covariance of the ordinary correlation functions without compromising the computational requirement. The covariance of the ordinary correlation functions can be recognised as the nominator of the first terms on the right hand side of equation 3.47. The additional terms are either independent of  $r$  and  $v$  or they can easily be computed as a by-product of the steps used to compute the first term without additional storage requirements or additional “flops” so that the extra computational effort, compared to 3.41 is negligible. Equation 3.47 is verified below by comparison with the the simulated 2DOF system in table 3.2. The exact same parameters were used here as in the previous section for the simulated results shown in figure 3.8. Only the variance is shown here, but it was checked that the expression also predicts the covariances correctly. It can be seen that at low lags the variance estimate of the correlation coefficient function is more accurate than the estimate for the ordinary correlation functions. However, this slight increase in accuracy is negligible in practice when the we must estimate the covariances of the correlation coefficient functions from a single realisation. It is clear that the same practical considerations as discussed



(a)



(b)

Fig. 3.12: Validating equation 3.47 for unbiased estimates by comparison with simulated data from the 2DOF in table 3.2. An ensemble of 500 realisations was simulated.  $[- \circ -]$  denotes the estimate from 3.47 and  $[\dots \times \dots]$  the simulated variance.

above for the ordinary correlation functions are applicable in this case and smoothing with a flat-top window is to be used to get improved estimates.

The estimation of the covariances for random decrement functions will not be considered in detail. The reason being that a complete treatment of this topic is given by Asmussen (1997). An improvement on the original variance estimates given by Vandiver *et al.* (1982) was developed by taking into account the correlation between different time segments. The results in Asmussen (1997) indicate excellent agreement with simulated data. It would be interesting to investigate whether Asmussen's

method couples the RD functions with a more robust variance estimator than the method proposed in this thesis for correlation functions. Since Asmussen's method requires the computation of the correlation functions between different time segments, one may hypothesise that the standard deviation of the variance of the RD functions is likely to be of similar order than that for the plug-in method described above for correlation functions.

### 3.6 Summary

In this chapter, various methods to estimate a correlation based response model were presented, whether this is via ordinary correlation functions, correlation coefficient functions or random decrement signatures. In a first instance, the errors inherent in the estimation of this response model were outlined and for the ordinary correlation functions and a simple analytical formulation was given providing some insight into how this error relates to the modes of the system and the available record length. Because this analytical formulation has only limited applicability, an entirely data-driven estimator for the covariances of the correlation functions was presented. The latter simply consists of the application of the "classical" covariance estimator for correlation functions available in the literature but, to make it robust with respect to estimated correlation functions, the latter are smoothed by an adaptive flat-top window. Moreover, the associated data reduction makes this method computationally efficient for practical application. In the chapters to follow, the errors in the response model, obtained via the techniques in this chapter, will be propagated through the identification algorithm to obtain an error estimate on the identified modal parameters.

---

## CHAPTER 4

---

# THE DEPENDENT BOOTSTRAP

---

### 4.1 Introduction

The bootstrap method, invented by Efron (1979), has been widely applied across various disciplines, such as economics or biology for instance, where an assessment of the estimated statistics is sought on the basis of a limited amount of information. The bootstrap appears to have been applied for the first time to applications related to modal analysis by Paez and Hunter (1998) and Hunter and Paez (1998). Their technique was picked up later by Doebling and Farrar (2001*b*) and applied to classical frequency domain modal testing to estimate confidence intervals on the identified modal parameters. Kijewski and Kareem (2000, 2002) applied a bootstrap scheme to estimate the error on identified damping ratios of SDOF systems from output-only measurements using random decrement signatures.

The bootstrap developed by Efron (1979) relies on the assumption that the observed data is independent. It transpires that, in order to apply the technique to modal testing, where the observed data consists of highly correlated time series, a slight modification of Efron's original bootstrap is necessary. In a nutshell, this modification consists in splitting the time series into independent blocks of data, which then play the same role as the independent individual observations in Efron's original formulation. This is generally referred to as the dependent bootstrap, the idea of which first appeared in Hall (1985) but a rigorous treatment can be attributed to Carlstein (1986); Künsch (1989) and Liu and Singh (1992). It turns out, that the

bootstrapped statistics depend significantly on exactly how the time series is split up into blocks. A poor choice can result in significant bias and/or variance in the desired statistics, and as a result, if applied to determine the error in output-only modal parameters, will yield incorrect bounds. These issues were not considered in Hunter and Paez (1998) or Kijewski and Kareem (2000, 2002) and are the focus of this chapter. It is noted that this does not apply to Doebling and Farrar (2001*b*) as they used a set of *independently* measured FRFs as their starting point. The aim is to establish a firm basis for the application of the bootstrap to the estimation of errors in output-only identified modal parameters.

The rigorous theory behind the dependent bootstrap requires a great deal of mathematical sophistication but it is desired to avoid this in the exposition given below. Rather, the aim is to give a presentation that is geared toward practical application. It is assumed that the reader is not familiar with the bootstrap and therefore, this chapter begins with an outline of Efron's original bootstrap.

## 4.2 Efron's Bootstrap

Suppose the random variable  $x$  is the outcome of some stochastic process with unknown probability distribution  $F$  and that only  $n$  independent measurements, collected in the sample  $X = (x_1, x_2, \dots, x_n)$ , are available to estimate a parameter of interest, say  $\chi$ . Denote the sample estimate of this parameter on the basis of  $X$  by  $\hat{\chi} = s(X)$ . For example, this parameter might be the mean of  $x$ , denoted  $\mu_x$ , and its sample estimate may be computed from the available data in  $X$  according to

$$\hat{\chi} = s(X) = \hat{\mu}_x = \frac{1}{n} \sum_{i=1}^n x_i \quad (4.1)$$

The notation  $(\hat{\cdot})$  is used to denote estimated quantities. Similarly, an unbiased estimate of the the random error of  $\hat{\mu}_x$  can be computed from the sample  $X$  as (Bendat

and Piersol, 2000)<sup>†</sup>

$$\hat{\sigma}_{\hat{\mu}_x} = \hat{\sigma}(\hat{\mu}_x) = \frac{\hat{\sigma}_x}{\sqrt{n}} \quad (4.2)$$

$$\text{with } \hat{\sigma}_x = \left[ \frac{1}{(n-1)} \sum_{i=1}^n (x_i - \hat{\mu}_x)^2 \right]^{1/2} \quad (4.3)$$

The same terminology as in Bendat and Piersol (2000) is used here, where the *random error* or *standard error* denotes the square root of the variance of the estimate i.e  $\hat{\sigma}_{\hat{\mu}_x} = (\text{Var}[\hat{\mu}_x])^{1/2}$ . Thus, without knowledge of the probability distribution  $F$ , these two formulae can be used to estimate the mean of the random variable  $x$  as well as the random error of this estimate using the limited information in  $X$ . However, this is not always feasible:

1. In order for these estimates to converge,  $n$  must be sufficiently large but in many situations, the available data is limited.
2. For most estimators  $\hat{\chi} = s(X)$ , no formulae like equations 4.2 and 4.3 for the mean, are available and it is therefore generally difficult to obtain such an estimate and
3. Expressions such as 4.2 are usually derived on the basis of a certain probability distribution, which may not be known

This is precisely the situation one is faced with when estimating the statistics of identified modal parameters: usually, only a single time-series is available to estimate the modal parameters and no formulae are available to estimate their variance for instance. Moreover, any such formula would have to be specific to the particular identification algorithm used.

The bootstrap technique is well suited to deal with the issues listed above. It was developed by Efron (1979) as a computer-based method to assess the random error on

---

<sup>†</sup>The more commonly used formula for  $\hat{\sigma}_x$  is  $\hat{\sigma}_x = \left[ \frac{1}{n} \sum_{i=1}^n (x_i - \hat{\mu}_x)^2 \right]^{1/2}$  but this estimate is biased (Bendat and Piersol, 2000).

parameter estimates  $\hat{\chi}$  for random variables on the basis of a sample of measured data  $X$  from an unknown probability distribution. It requires no theoretical calculations and is available no matter how complicated the estimator  $s(X) = \hat{\chi}$  may be. This implies for instance that it is applicable to SSI/Cov estimated modal parameters as will be done in Chapter 7.

To illustrate the bootstrap technique, suppose that the situation is the same as above; that is, a collection  $X$  of  $n$  independent measurements  $x_i$  of the random variable  $x$  is available and it is desired to compute the mean  $\hat{\mu}_x$ , and additionally, to find the random error on this estimate. If it were possible to take more independent measurements of  $x$  and form additional collections, say  $X^{(b)} = (x_1^{(b)}, x_2^{(b)}, \dots, x_n^{(b)})$ , for  $b = 1, 2, \dots, B$ , then one could use equation 4.1 to compute  $B$  independent estimates of the mean

$$\hat{\mu}_x^{(b)} = \frac{1}{n} \sum_{i=1}^n x_i^{(b)}, \quad \text{for } b = 1, 2, \dots, B \quad (4.4)$$

For  $B$  is sufficiently large, the  $B$  estimates of the mean  $\hat{\mu}_x^{(b)}$  could be inserted into equation 4.3 to find the standard error of the mean as

$$\hat{\sigma}(\hat{\mu}_x) = \left[ \frac{1}{(B-1)} \sum_{b=1}^B \left( \hat{\mu}_x^{(b)} - \bar{\mu}_x \right)^2 \right]^{1/2} \quad (4.5)$$

where

$$\bar{\mu}_x = \frac{1}{B} \sum_{b=1}^B \hat{\mu}_x^{(b)} \quad (4.6)$$

In many situations, however, it might not be possible to collect further data to form the additional samples  $X^{(b)} = (x_1^{(b)}, x_2^{(b)}, \dots, x_n^{(b)})$ . Such is, for instance, often the case in operational modal analysis when applied to civil engineering structures. Once the measurements have been taken, this will be only data available to the engineer to conduct the modal analysis.

The idea behind the bootstrap method is to create additional collections of data, denoted  $X^{*(b)} = (x_1^{*(b)}, x_2^{*(b)}, \dots, x_n^{*(b)})$ , as a *randomized* or *resampled* version of the original sample  $X = (x_1, x_2, \dots, x_n)$ . The additional samples  $X^{*(b)}$  are called the *bootstrap samples*. Once these additional samples are formed, the usual sample statistics can be applied.

The basic assumptions are that

1. the measured outcomes  $x_i$ , for  $i = 1, 2, \dots, n$  of the random variable  $x$  collected in  $X = \{x_1, x_2, \dots, x_n\}$  must be *independent*
2. the measured outcomes  $x_i$  must be representative of the random source

A probability of  $1/n$  is then assigned to each member of the collection  $X$  and this rule defines the empirical probability distribution  $\hat{F}$  of the the source. The ensemble  $X$  is the empirical source for the bootstrap samples. A bootstrap sample  $X^{*(1)}$  is then generated by drawing  $n$  values *with replacement* from  $X$ , where the chance of drawing a particular sample is  $1/n$ . Sampling with replacement means that one draws  $x_j$  from the collection  $X$  and places a copy of it, labelled  $x_1^{*(1)}$ , into  $X^{(1)*}$  forming the first member of the first bootstrap sample  $X^{(1)*}$ . Then, replace  $x_j$ . Another member  $x_j$  of  $X$  is then drawn at random from  $X$ , relabelled  $x_2^{*(1)}$ , and placed in second position in  $X^{*(1)}$ .  $x_j$  is then replaced in the original collection  $X$ . This process is repeated  $n$  times to complete the first bootstrap sample  $X^{*(1)} = (x_1^{*(1)}, x_2^{*(1)}, \dots, x_n^{*(1)})$ . Because  $X^{*(1)}$  is sampled from  $X$  with replacement, some elements of  $X$  may appear more than once or not at all in  $X^{*(1)}$ . Any number  $B$  of bootstrap samples  $X^{*(b)}$ ,  $b = 1, 2, \dots, B$ , can be sampled from the original data set  $X$  in this manner. Thus, the situation is the same as above, where it was assumed that additional collections  $X^b$  could be measured, except that these additional collections, the bootstrap samples  $X^{*(b)}$ , could be obtained by sampling with replacement from the original measurement set  $X$ . Therefore, it is possible to compute  $B$  bootstrap estimates of the mean  $\hat{\mu}_x^{*(b)}$  -one



estimate from each bootstrap sample- in the same fashion as in equation 4.4 as

$$\hat{\mu}_x^{*(b)} = \frac{1}{n} \sum_{i=1}^n x_i^{*(b)}, \quad \text{for } b = 1, 2, \dots, B \quad (4.7)$$

and the bootstrap estimate of the random error of the mean  $\epsilon_r^{Boot}(\hat{\mu}_x)$  can be computed as in equation 4.5

$$\sigma^*(\hat{\mu}_x) = \left[ \frac{1}{(B-1)} \sum_{b=1}^B \left( \hat{\mu}_x^{*(b)} - \bar{\mu}_x^* \right)^2 \right]^{1/2} \quad (4.8)$$

where

$$\bar{\mu}_x^* = \frac{1}{B} \sum_{b=1}^B \hat{\mu}_x^{*(b)} \quad (4.9)$$

Because the bootstrap is a sampling technique, it is readily applicable to any estimator  $\hat{\chi} = s(X)$  and any of its statistics. The steps of the bootstrap, for an arbitrary estimator  $\hat{\chi} = s(X)$  are shown schematically in figure 4.1. Like every estimator, the bootstrap is not exact and has an inherent error. The performance of the bootstrap is case dependent in the sense that it will depend on the statistic of interest. To illustrate the general qualitative behaviour of the bootstrap, the variance of the standard error of the bootstrap estimate  $s(\chi)$  is considered i.e.  $\hat{\sigma}^*(s(\chi)) = \hat{\sigma}^*$ . It is shown in Efron and Tibshirani (1993) that the variance of the bootstrap standard error takes the general form

$$Var[\hat{\sigma}^*] = \frac{C_1}{n^2} + \frac{C_2}{nB} \quad (4.10)$$

where  $C_1$  and  $C_2$  are constants depending on the underlying distribution  $F$  and on the statistic of interest ( $\hat{\sigma}^*$  in this case) but not on  $B$  and  $n$ . It is seen from this equation that the variance of the estimated bootstrap standard error depends on two factors:  $\frac{C_1}{n^2}$  represents the sample variation and introduces error in the estimate  $\hat{\sigma}^*$  due to the fact that only a sample of size  $n$  is available. The second factor  $\frac{C_2}{nB}$  represents the variation introduced into  $\hat{\sigma}^*$  due to the resampling used to create the bootstrap samples. It is seen that the this estimator is asymptotically consistent since  $Var[\hat{\sigma}^*] \rightarrow 0$ . The bootstrap estimate when  $B \rightarrow \infty$  is often called the *ideal bootstrap*. The important

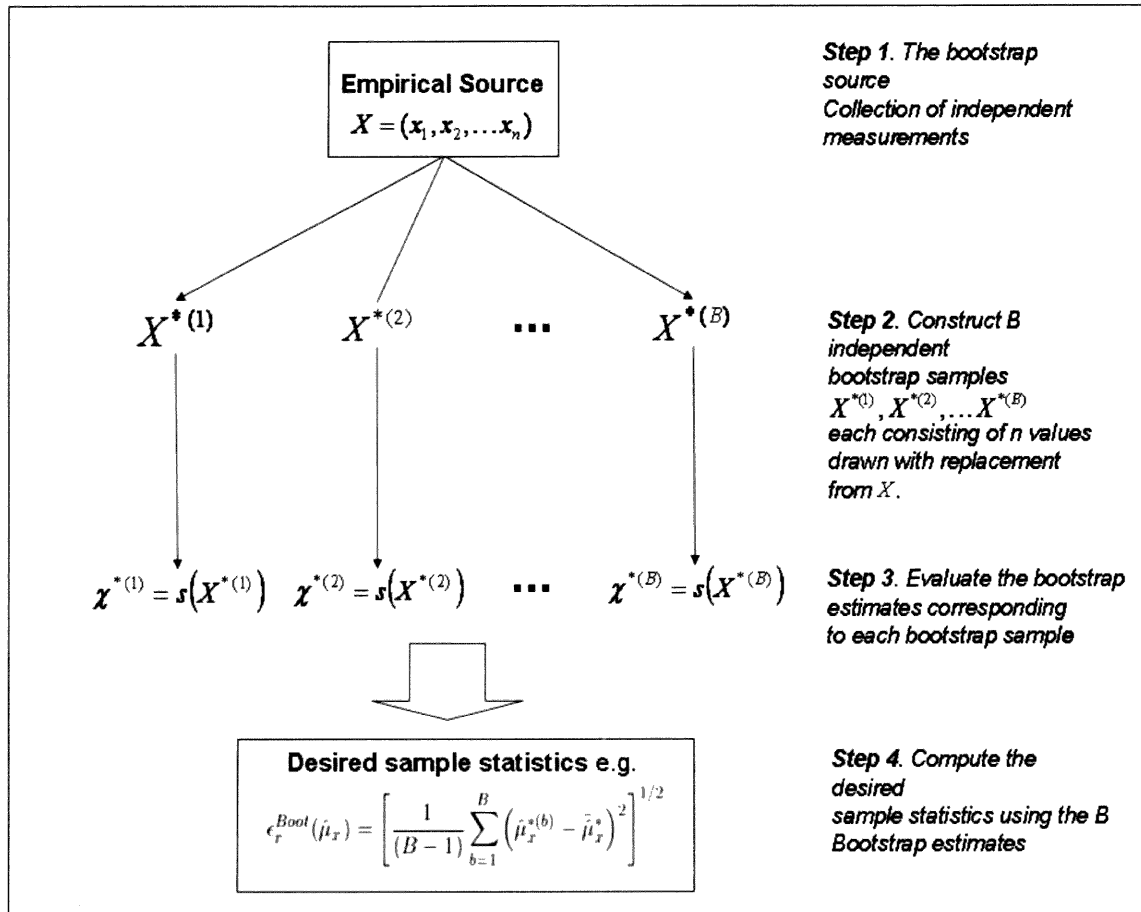


Fig. 4.1: Diagrammatic representation of the bootstrap

message emanating from equation 4.10 is that the generation of additional data does *not* alleviate the dependence on the sample size  $n$  and introduces extra variability due to resampling. This means, for example in the case of the mean, that for  $B$  large enough, the bootstrap estimate  $\hat{\sigma}^*(\hat{\mu})$  approximates the sample estimate  $\sigma(\hat{\mu}_x)$  from equation 4.2. Thus, the bootstrap is effectively a tool to estimate a particular statistic of the parameter of interest that is otherwise not available from standard sample statistics rather than a tool to obtain statistics with improved accuracy. The advantages of the bootstrap over parametric, non-sampling techniques are that the underlying data need not be Gaussian and the method allows for an easy computation of the statistics of any estimator, no matter how complicated (Efron and Tibshirani, 1993).

### 4.3 The Dependent Bootstrap

Application of the bootstrap to time series is different from the situation in the previous section in that the available data, the time series  $X = \{x_1, x_2, \dots, x_n\}$ , is a collection of *serially dependent* measurements. In other words, the elements in  $X = \{x_1, x_2, \dots, x_n\}$  are dependent and the order in which they occur is crucial. Therefore, one cannot simply apply the bootstrap method presented in the previous section as it violates the independence requirement. On a more intuitive note, it is clear that the direct application of the resampling process of the bootstrap will break up the covariance structure of the time series so that any bootstrap time series generated in this fashion is not representative of the source. However, a slight modification will make it possible to extend the bootstrap to time series. In a nutshell, the idea is to resample blocks of data rather than individual observations.

#### 4.3.1 The Moving Block Bootstrap

Let  $X = \{x_1, x_2, \dots, x_n\}$  be a measured time series, which, in our situation, typically consists of the acceleration response measured at some location on a structure. Also, assume that  $X$  is *stationary* and *short-range or weakly dependent*. The latter condition means that the spectral densities are finite at frequency  $\omega = 0$ , that is

$$S_X(\omega = 0) = \sum_{s=-\infty}^{\infty} R_X(s) \cos((\omega = 0)s) = \sum_{s=-\infty}^{\infty} R_X(s) < \infty$$

so that a time series is short range dependent if its ac.f. is summable (Bühlmann, 2002; Heyde and Yang, 1997). Due to the exponential decay of the correlation functions of structural responses, this condition holds. (Politis, 2003b) defines weak dependence as follows:  $X$  is weakly dependent if the subsets of  $X$  of random variables  $X_i = \{x_{i,1}, x_{i,2}, \dots, x_{i,l}\}$  and  $X_{i+k} = \{x_{i+k,1}, x_{i+k,2}, \dots, x_{i+k,l}\}$  are approximately independent for  $k$  sufficiently large (Politis, 2003b). Letting  $s(\cdot)$  denote an estimator, for example the mean, this implies that  $s(X_i)$  and  $s(X_{i+j})$  will be independent.

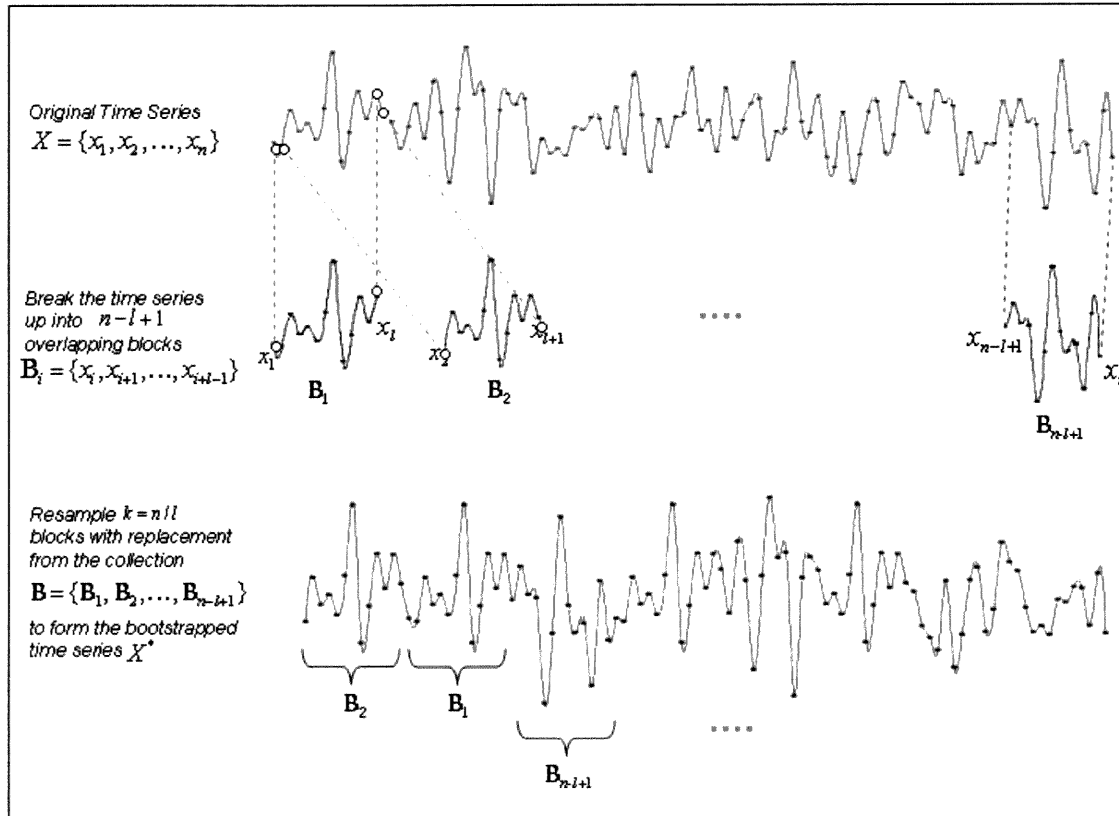


Fig. 4.2: Illustration of the Moving Blocks (MB) Bootstrap.

The idea behind the moving block bootstrap, which shall be abbreviated as the MB bootstrap, follows now easily: by dividing the original time series into more or less independent subsets of *blocks*  $X_i$ , and applying the estimator  $s(\cdot)$  to each, one ends up with a collection  $s(X_i)$  of independent variables and hence, the bootstrap described in the previous section applies. Further, the blocking preserves the correlation structure of the original time series. The time series bootstrapping recipe given by Künsch (1989) can be summarized as follows:

1. Break the time series  $X = \{x_1, x_2, \dots, x_n\}$  into  $n - l + 1$  *overlapping* blocks  $\mathcal{B}_i = \{x_i, x_{i+1}, \dots, x_{i+l-1}\}$  of length  $l$  for  $i = 1, 2, \dots, n - l + 1$ . Form the collection  $\mathcal{B} = \{\mathcal{B}_1, \mathcal{B}_2, \dots, \mathcal{B}_{n-l+1}\}$ .
2. Resample  $k = n/l$  blocks  $\mathcal{B}_i$  with replacement from  $\mathcal{B}$  to form  $B$  bootstrap time series replica by collecting the  $k$  resampled  $\mathcal{B}_i$ . For example, the  $b^{\text{th}}$  bootstrapped

time series may be

$$X^{(b)*} = \underbrace{\{\mathcal{B}_2, \mathcal{B}_4, \dots, \mathcal{B}_{n-l+1}, \dots, \mathcal{B}_4\}}_{k\text{blocks}}$$

3. Compute the bootstrap replica of the statistic of interest,  $s^{(b)*}(X) \equiv s(X^{(b)*})$ .

The estimator  $s^{(b)*}(X)$  could for instance represent the sample correlation estimate of the bootstrapped time series  $X^{(b)*}$  i.e.  $R_{X^{(b)*}}(r) \equiv R_X^{(b)*}(r)$  where  $r$  denotes the lag.

4. Compute the sample statistic of interest over the ensemble of the  $B$  generated bootstrap replica  $s^*(X)$ . For example, the latter estimate could be the covariance  $Cov^*[R_X(r), R_X(v)]$ .

This procedure is illustrated in figure 4.2 and a simple example is given below. Let  $X = \{x_1, x_2, x_3, x_4, x_5, x_6\}$  so that  $n = 6$  and let the block length be  $l = 3$ . Next, form the collection of  $n - l + 1 = 4$  overlapping blocks

$$\mathcal{B} = \{\mathcal{B}_1 = \{x_1, x_2, x_3\}, \mathcal{B}_2 = \{x_2, x_3, x_4\}, \mathcal{B}_3 = \{x_3, x_4, x_5\}, \mathcal{B}_4 = \{x_4, x_5, x_6\}\}$$

Resample  $k = n/l = 2$  blocks from this collection to form the bootstrap replicates  $X^{(b)*}$  of the original time series  $X$ . For instance, the first bootstrap replicate may be  $X^{(1)*} = \{\mathcal{B}_4, \mathcal{B}_2\} = \{x_4, x_5, x_6, x_2, x_3, x_4\}$ . Note that it was assumed that  $l$  divides  $n$  exactly but if this is not the case, simply resample  $k = \lfloor n/l \rfloor + 1$  blocks but use only a portion of the  $k^{\text{th}}$  block so that our bootstrap time series has a total of  $n$  data points. The notation  $\lfloor x \rfloor$  denotes largest integer less than or equal to  $x$ . A similar procedure was proposed by Carlstein (1986). The latter differs from the one described above (Künsch, 1989) in that the times series is broken into contiguous blocks. It was shown by Lahiri (1999) that Künsch's method gives estimates with lower variance than those obtained by Carlstein (1986) using non-overlapping blocks.

The theory for the block bootstrap in Künsch (1989) and Carlstein (1986) are given for univariate time series only. However, the extension to the multivariate case is straightforward. Since the blocking of the time series preserves the auto-correlation structure in a block, the cross-correlation structure between any two time series can be preserved by using the same resampling in all the measured responses. To illustrate this, consider the example given above and assume that an additional time series  $Y = \{y_1, y_2, y_3, y_4, y_5, y_6\}$  is available, which may be the response measured simultaneously with  $X$  but at a different location on the structure. In order to preserve the cross-correlation structure between the measured output  $Y = \{y_1, y_2, y_3, y_4, y_5, y_6\}$  and  $X$  between pairs of bootstrap replicas of each time series, say  $X^{(1)*}$  and  $Y^{(1)*}$ , one needs to apply the same resampling to each of the two time series; that is, if  $X^{(1)*} = \{\mathcal{B}_{x_4}, \mathcal{B}_{x_2}\} = \{x_4, x_5, x_6, x_2, x_3, x_4\}$ , then it is required that  $Y^{(1)*}$  is of the form  $Y^{(1)*} = \{\mathcal{B}_{y_4}, \mathcal{B}_{y_2}\} = \{y_4, y_5, y_6, y_2, y_3, y_4\}$ .

The MB bootstrap presented above has two drawbacks that are effectively due to the fact of joining conditionally independent blocks together to form the bootstrap replicas of the time series: (a) the resampled time series may not be stationary and (b) bias can occur in the estimates. Due to joining conditionally independent blocks, a discontinuity occurs each at every  $l^{\text{th}}$  data point, where  $l$  is the block length. As a result, the observations near this discontinuity will have a different joint distribution from the ones near the centre of a different block. To see how the bias arises, consider again the example given above, in particular the bootstrap replica  $X^{(1)*} = \{x_4, x_5, x_6, x_2, x_3, x_4\}$ . The discontinuity occurs at the joint between  $x_6$  and  $x_2$ . Suppose that the statistic of interest is the auto-correlation function at lag 1, i.e.  $R_X(1)$ . For simplicity, the raw (unweighted) correlation function is considered. The bootstrap replica of  $R_X(1)$  from  $X^{(1)*}$  is then given by  $R_X^{(1)*}(1) = x_4x_5 + x_5x_6 + x_6x_2 + x_2x_3 + x_3x_4$ . Clearly the term  $x_6x_2$  accounts for the correlation of two points much further apart so that the introduction of this term results in an underestimate of the correlation function. As the lag increases, the situation becomes even more

severe, consider for instance  $R_X^{(1)*}(2) = x_4x_6 + x_5x_2 + x_6x_3 + x_2x_4$ . Thus only 2 out of the 4 terms are computed at the correct lag while the terms  $x_5x_2$ ,  $x_6x_3$  belong to the lag 3 estimate resulting therefore again in an underestimate. As the lag increases, the bias introduced due to the discontinuity of contiguous blocks increases. On the other hand, it is seen that the correlation at zero lag does not suffer from this bias. For these reasons, the moving blocks (MB) bootstrap is sometimes referred to as the “naive” bootstrap.

### 4.3.2 The “Blocks of Blocks” Bootstrap

A remedy for this bias has been suggested by Künsch (1989). The method was later picked up by Politis (1992); Politis and Romano (1992) and Liu and Singh (1992) and called the “blocks of blocks” (BB) bootstrap. They mainly considered its application in the context of spectral estimation using Welch’s averaged periodogram method (Welch, 1967). A more general treatment is given by Bühlmann and Künsch (1995). The basic idea relies on the observation made in the example in the previous section, namely that the auto-correlation estimate at *zero lag* is unbiased but correlation estimates for higher lags are not. The reason for this is that the auto-correlation estimate at zero lag is a symmetric function of the observed data. In other words, the sequential order of the observations does not matter. Loosely speaking, the “blocks of blocks” bootstrap therefore involves a block resampling scheme such that the estimator  $s(\chi)$  is symmetric with respect to blocks of data. In general, the BB bootstrap works as follows. Consider the blocks of  $m$  consecutive observations

$$X_i = (x_{i+1}, x_{i+2}, \dots, x_{i+m-1}), \quad \text{for } i = 1, 2, \dots, n - m + 1 \quad (4.11)$$

The block resampling on the basis of these  $m$ -tuples of observations is then achieved by building overlapping blocks of consecutive vectors

$$(X_1, \dots, X_l), (X_2, \dots, X_{l+1}), \dots, (X_{n-m-l+2}, \dots, X_{n-m+1}) \quad (4.12)$$

where  $l$  is the block length parameter. Now, form a resampled time series using these blocks as

$$X^* = X_{S_1}, \dots, X_{S_1+l-1}, X_{S_2}, \dots, X_{S_2+l-1}, \dots, X_{S_k}, \dots, X_{S_{k+l-1}} \quad (4.13)$$

where now  $k = \lfloor n-m+1/l \rfloor$  and the  $S_j$  are the block starting points resampled with replacement from  $\{1, 2, \dots, n-m-l+2\}$ . As for the MB bootstrap, when  $l$  does not divide  $n-m+1$  exactly, choose  $k = \lfloor n-m+1/l \rfloor + 1$  but use only a portion of the  $k^{\text{th}}$  block to get  $n-m+1$  resampled  $m$ -tuples in total. This resampled time series could be referred to as the “blocks of blocks” bootstrap sample but as mentioned in Bühlmann (2002), the notion of bootstrap sample is not so clear in this case, the reason being that the direct application of the ac.f to the block-resampled time series does not give the desired unbiased estimate. To see this, consider the same example used to illustrate the moving blocks bootstrap for the auto-correlation estimate at lag 2 and take  $m = 3$  and  $l = 2$ . The possible  $n-m+1 = 4$   $m$ -tuples are  $X_1 = (x_1, x_2, x_3)$ ,  $X_2 = (x_2, x_3, x_4)$ ,  $X_3 = (x_3, x_4, x_5)$ ,  $X_4 = (x_4, x_5, x_6)$  and the  $n-m-l+2 = 3$  successions of  $l = 2$  overlapping  $m$ -tuples are  $\{X_1, X_2\}, \{X_2, X_3\}, \{X_3, X_4\}$ . Thus, resampling  $k = \lfloor n-m+1/l \rfloor = 2$  out of the 3 possible “blocks of blocks” results, for instance in a bootstrap time series  $X^* = \{\{X_1, X_2\}, \{X_3, X_4\}\} = \{X_1, X_2, X_3, X_4\} = (x_1, x_2, x_3, x_2, x_3, x_4, x_3, x_4, x_5, x_4, x_5, x_6)$ . Clearly, computing the ac.f at lag 2 directly from the block resampled time series will lead to bias in the same way as for the MB bootstrap. Rather, the BB bootstrapped estimator has to be defined on the level of the vectorized observations  $X_i$ . The definition given by Künsch (1989) (also c.f. Bühlmann (2002)) applicable for  $\hat{R}_X^*(r)$  is to be interpreted as follows. If  $s(X) = g(X_1, \dots, X_{n-m+1})$  is a *symmetric function* of  $n-m+1$  vectorised observations (or blocks)  $X_i$ , then  $s^*(X) = g(X_{S_1}, \dots, X_{S_1+l-1}, X_{S_{k+l-1}})$ . For instance, in the case of auto- and cross-correlation functions, the function  $g = g_r$  may be defined as the auto-correlation function between blocks of observations  $X_i$  at lag  $r$  by the composite function  $g_r(X^*) = (n-m+1)^{-1} \sum_i \hat{R}_{X_i}(r)$ , where  $\hat{R}_{X_i}(r)$  is the ordinary auto-correlation estimate at lag  $r$  of the observations  $x_i$  in



the block  $X_i$ . This is again illustrated using the previous example for the bootstrap of the ac.f. from the resampled series  $X^* = \{X_1, X_2, X_3, X_4\}$  and lag  $r = 2$ . Then  $g_r(X^*) = (n - m + 1)^{-1} \sum \left\{ \hat{R}_{X_1}(r), \hat{R}_{X_2}(r), \hat{R}_{X_3}(r), \hat{R}_{X_4}(r) \right\} = (n - m + 1)^{-1} \sum \{x_1x_3, x_2x_4, x_3x_5, x_4x_6\} = 1/4(x_1x_3 + x_2x_4 + x_3x_5 + x_4x_6)$ . This is the desired result. It is seen that the BB bootstrap does not suffer from the bias problem that occurs in the MB bootstrap due to joining conditionally independent blocks. The reason is that the resampling process does not occur between conditionally independent blocks. In general, if the statistic of interest depends on some  $m$ -dimensional marginal distribution, then this statistic will be a symmetric function of blocks of  $m$  consecutive observations. Therefore, the design parameter  $m$  has to be chosen according to the lag  $r$  at which the the auto- and cross-correlation functions are computed and their relation is  $r = (m - 1)$ .

The computation of the BB bootstrap as described above is, however, inefficient when the data is large and the correlation functions need to be specified up to high lags  $r$ . (Politis and Romano, 1992) recognised that when the statistic of interest, say  $s(\cdot)$ , can be expressed as an average of some function say  $\phi(X_i)$  of the vectorized observations  $X_i$ , then the “blocks of blocks” bootstrap is essentially equivalent to resampling blocks of  $l$  consecutive estimates  $\phi(X_i)$ . It should be clear from the example above that this applies to the correlation functions, where the function  $\phi(X_i)$  is simply the correlation function at lag  $r$  of the  $m$ -tuples  $X_i$ . Along the lines of the BB bootstrap applied to spectral estimates in Politis (1992), the following procedure is suggested for correlation functions:

Let  $X = \{x_1, x_2, \dots, x_n\}$  and  $Y = \{y_1, y_2, \dots, y_n\}$  be two simultaneously measured response time histories

1. Determine the maximum lag  $r_{max}$  of interest up to which the bootstrapped correlation functions are computed. This value will determine the length of the

$m$ -tuples  $X_i$  and  $Y_i$  and is  $m = r_{max} + 1$ .

2. Form the possible  $n - m + 1$  overlapping, consecutive  $m$ -tuples  $X_i$  and  $Y_i$  for the measured responses
3. Compute the *unbiased ac.f* and *xc.f.* between the  $n - m + 1$  consecutive  $m$ -tuples  $X_i$  and  $Y_i$  up to lag  $r_{max}$ , denoted by  $\hat{R}_{X_i}$ ,  $\hat{R}_{Y_i}$  and  $\hat{R}_{X_i Y_i}$  respectively.
4. Determine the block length  $l$  and take the arithmetic mean over the  $n - m - l + 2$  possible overlapping sequences of  $l$  consecutive  $\hat{R}_{X_i}$ ,  $\hat{R}_{Y_i}$  and  $\hat{R}_{X_i Y_i}$ . Collect the resulting mean quantities  $B_{i,X} = l^{-1} \sum_i^{i+l-1} \hat{R}_{X_i}$ , for  $i = 1, 2, \dots, n - m - l + 2$ , into the collection

$$B_X = \{B_{1,X}, B_{2,X}, \dots, B_{n-m-l+2,X}\}$$

$$B_{XY} = \{B_{1,XY}, B_{2,XY}, \dots, B_{n-m-l+2,XY}\}$$

where the second of the above equations applies to the cross-correlation functions with  $B_{i,XY} = l^{-1} \sum_i^{i+l-1} \hat{R}_{X_i Y_i}$ .

5. Resample  $k = \lfloor n-m+1/l \rfloor + 1$  values  $S_j$  with replacement from  $\{1, 2, \dots, n - m - l + 2\}$  to determine a sequence of  $k$  functions  $B_{i,X}$ , i.e.  $\{B_{S_1,X}, B_{S_2,X}, \dots, B_{S_k,X}\}$ . The process is the same for the ac.f. of  $Y$  and xc.f. between  $Y$  and  $X$ .
6. Compute the  $b^{th}$  bootstrap estimate  $R_X^{(b)*}(r)$  as  $k^{-1} \sum_{j=1}^k B_{S_j,X}$ . Similarly,  $R_{XY}^{(b)*}(r)$  is given by  $k^{-1} \sum_{j=1}^k B_{S_j,XY}$ . As for the MB bootstrap, the *same resampling* must be used between different time series in order to preserve their cross-correlation structure.

7. Repeat the process to obtain the desired  $B$  bootstrap replica

This process is illustrated in figure 4.3. In a nutshell, the bootstrapped correlation functions computed as described above are effectively the average correlation functions over a resampled set consisting of the arithmetic means of  $l$  consecutive correlation functions. This method is very efficient since (a), the bootstrapped correlation functions can directly be used as input to the SSI/Cov as opposed to computing

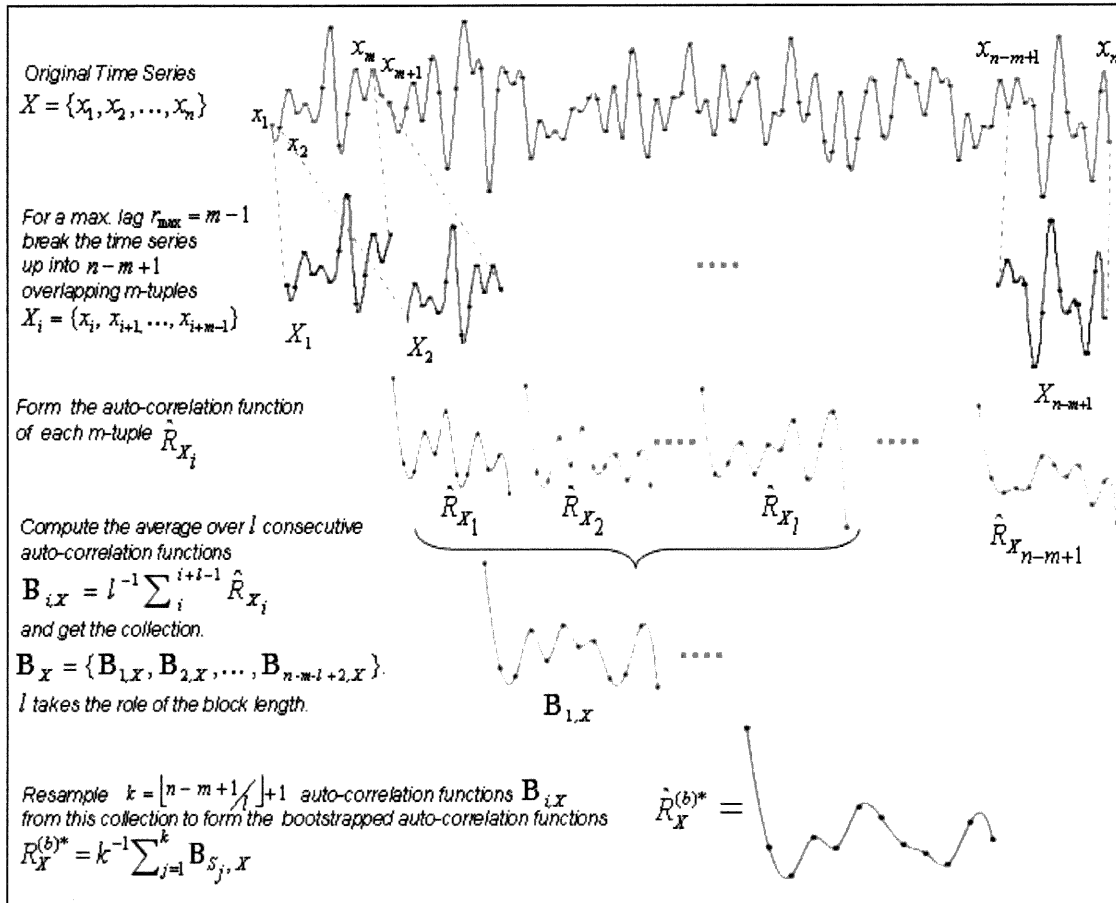


Fig. 4.3: Illustration of the “Blocks of Blocks” (BB) Bootstrap.

a resampled time series and then computing its correlation function and (b) the bootstrapped correlation functions are computed at every desired lag  $r$  in one step.

### 4.3.3 The Stationary Bootstrap

Another bootstrap method was suggested by Politis (1994) to alleviate the effects of joining independent blocks. Joining different blocks of data results in a discontinuities in the pseudo data and introduces a spurious periodicity. Consequently, the data points near the discontinuity will have a different distribution than those at the centre of the block and hence, the resulting pseudo time-series are effectively non-stationary. Politis (1994) introduced the stationary bootstrap to get mitigate these non-stationary effects.

The stationary (SB) bootstrap works in much the same way as the MB block boot-

strap, the difference being that (a) the time series are wrapped around in a circle so that  $x_j = x_i$  when  $j > n$  with  $i = j(\text{mod } n)$  and (b) the length  $l$  of the blocks is not fixed but is chosen randomly. It is precisely this randomization of the block length that mitigates the undesired effects at the edges of contiguous blocks occurring in the MB bootstrap: one may think of the stationary bootstrap as a weighted average of the MB block bootstrap distributions so that the difference between the distributions of points in the vicinity of the edges and near the center of the block is smoothed averaged out and eliminates the non-stationarity. The weights are determined by the distribution used to generate the stochastic block lengths. Politis (1994) use a geometric distribution for the block length  $l_i$  so that the probability that  $l_i$  has length  $d$  is  $(1 - p)^{d-1}p$ , for  $d = 1, 2, \dots$  and  $p$  is a fixed number in the interval  $[0, 1]$ . The average length of the blocks,  $\bar{l}_i = 1/p$  plays the same role as the fixed block length  $l$  in the MB bootstrap. A drawback associated with the SB bootstrap is that it has a higher standard error than the MB bootstrap due to the additional random element introduced by the stochastic block length (Lahiri, 1999).

#### 4.4 Performance of the Bootstrap

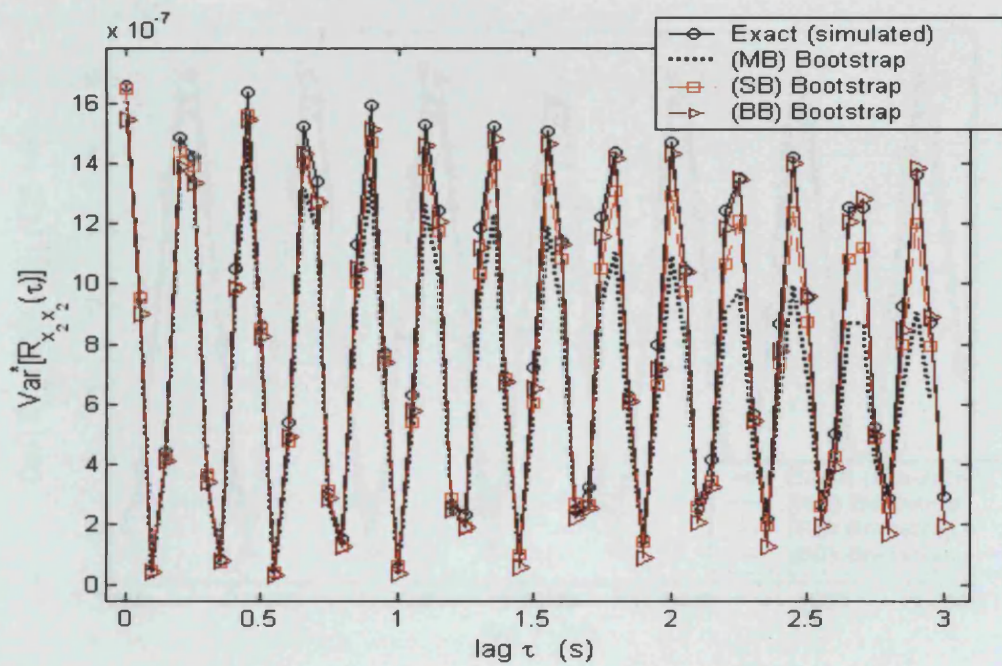
To illustrate the performance of each of these three bootstrap estimators (MB, BB and SB), we use the *exact* same simulation on the 2DOF system with modal frequency and modal damping ratios shown in table 4.1 in the previous chapter, section 3.5.1. For convenience, the table is repeated here as table 4.1. 500 different response time histories were simulated for a duration of 780s ( $\Delta t = 0.05s$ ) at each degree-of-freedom. The three bootstrap methods described above, MB, BB and SB, were applied to a single response measurement to estimate the variance of the ac.f. between of the response at the second degree-of-freedom,  $Var^*[R_{x_2x_2}(\tau)]$  and the variance of the xc.f.  $Var^*[R_{x_1x_2}(\tau)]$  up to  $\tau = 3s$  ( $\Delta t = 0.05s$ ). A block length  $l = 10s$  ( $\Delta t = 0.05s$ ) was chosen in all cases and  $B = 300$  bootstrap correlation replicas were used to compute the bootstrap variances. These estimates are gauged against the “true” variances

$Var[R_{x_2x_2}(\tau)]$  and  $Var[R_{x_1x_2}(\tau)]$  calculated from the 500 simulated responses. The results are depicted in figure 4.4 and 4.5. The behaviour of the different bootstrap estimates described in the previous section is readily recognisable. Bearing in mind that the variability due to having only  $B = 300$  bootstrap replicas, it can be seen from figures 4.4 that at zero lag, the three estimates, MB, BB and SB are comparable. As  $\tau$  increases, however, it is clearly seen that the variance estimated by the MB bootstrap becomes increasingly smaller with  $\tau$  and this is due to the bias that arises due to resampling from different conditionally independent blocks. A similar behaviour, although less pronounced, is seen to occur for the SB bootstrap. It appears, that this bias in the MB and SB bootstrap is less pronounced for the covariance estimate (figure 4.5(a)). This bias is a direct consequence of the bias that occurs in each of the  $B = 300$  bootstrapped correlation functions  $R_{x_1x_2}^{(b)*}(\tau)$  and  $R_{x_2x_2}^{(b)*}(\tau)$ . This is shown for the cross-correlation function only in figure 4.5(b); the mean of the 300 bootstrapped xc.f. estimated from the BB bootstrap matches the simulated results very closely at each lag. When the MB and SB schemes were used, it is seen again that the agreement between the exact xc.f. and bootstrapped mean estimates deteriorates with increasing lag. We can therefore conclude from figure 4.5(b) that the moving blocks and stationary bootstrap add artificial damping to the system with a slight improvement offered by the SB. The “blocks of blocks” bootstrap, on the other, hand gives unbiased estimates as expected. This is important for the applications in Chapter 7 where the bootstrapped correlation functions serve as additional response models for modal identification.

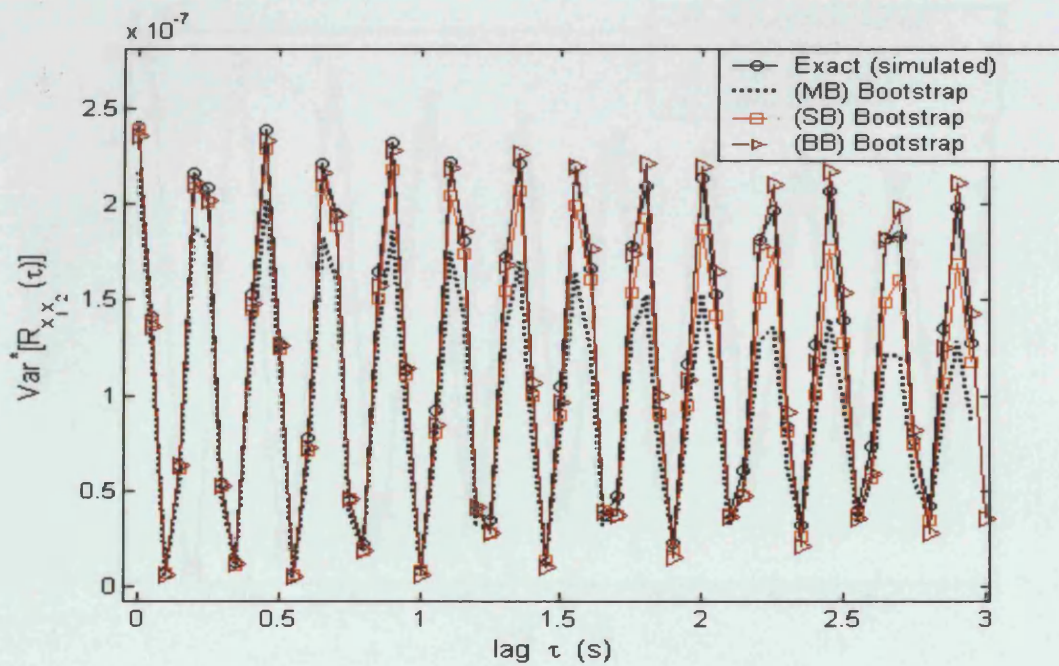
Keeping the block length  $l = 10s$  ( $\Delta t = 0.05s$ ) fixed, no significant increase in accuracy was observed for choices of  $B > 300$ . As mentioned previously, the required number of bootstrap estimates  $B$  to approximate the *ideal bootstrap* is case dependent.

Modes	Natural Frequency $f_0$	Damping ratio $\xi$
Mode 1	2.24 Hz	1.49%
Mode 2	3.93 Hz	2.85%

Tab. 4.1: Modal Parameters of the 2DOF system used for simulation.



(a)



(b)

Fig. 4.4: Comparison of the moving blocks (MB) bootstrap, stationary (SB) and “blocks of blocks” (BB) bootstrap as variance estimators of the sample ac.f and xc.f..  $B = 300$  bootstrapped correlation functions were used in each case with a block length  $l = 10s$  ( $\Delta t = 0.05s$ ).



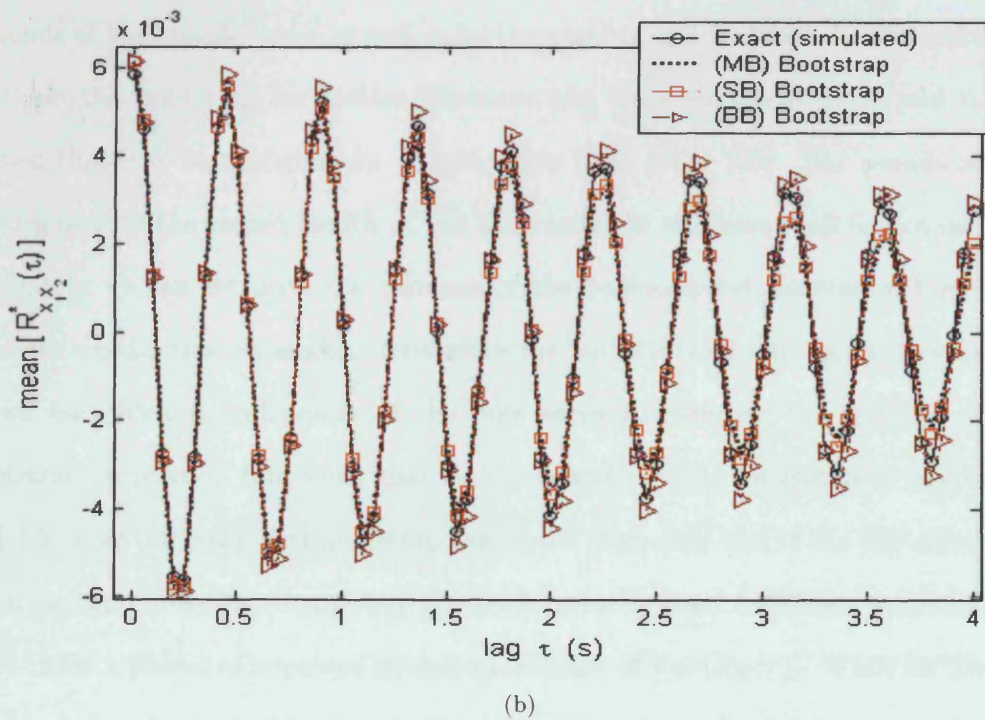
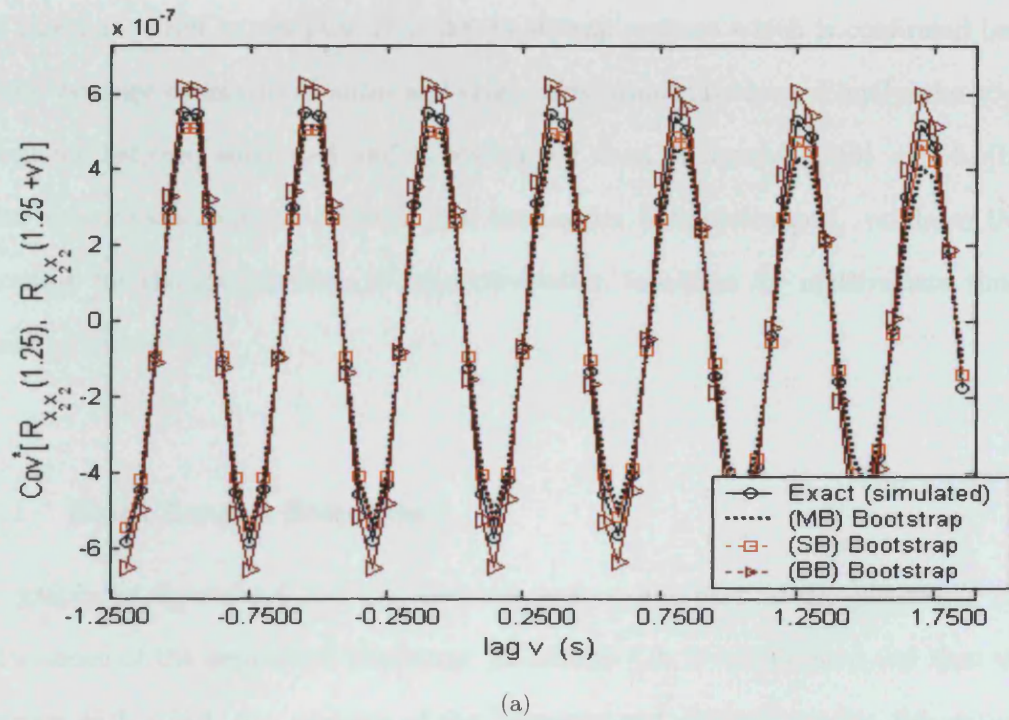


Fig. 4.5: Comparison of the moving blocks (MB) bootstrap, stationary (SB) and “blocks of blocks” (BB) bootstrap estimates of (a) the auto-covariance of the bootstrapped auto-correlation function  $\hat{R}_{x_2 x_2}^*(\tau)$  and (b) the mean of the bootstrapped cross-correlation functions  $\hat{R}_{x_1 x_2}^*(\tau)$  computed from  $B = 300$  bootstrapped correlation functions. A block length  $l = 10s$  ( $\Delta t = 0.05s$ ) was used.

Efron and Tibshirani (1993) indicate that, as a rule of thumb for variance estimates, it is rarely required to compute  $B > 200$  bootstrap replicas which is confirmed here for the variance estimates of auto- and cross correlation functions. Finally, the good agreement between simulated and bootstrapped data in figures 4.4(b) and 4.5(b), where the cross-correlation between two time-series is bootstrapped, validates this procedure for the computation of cross-correlation functions for multivariate times series.

#### 4.4.1 Block Length Selection

The graphs in figures 4.4 and 4.5, however, only paint part of the picture of the performance of the dependent bootstrap. In section 4.2, it was pointed out that the accuracy with which the variance of the bootstrapped statistic can be determined depends of the sample size  $n$  as well as on the number of bootstraps  $B$ . The influence of  $B$  on the bootstrap correlation functions has been discussed above and it was argued that it is negligible for  $B$  sufficiently large ( $B > 300$ ). The sample size  $n$ , determined by the record length of the time series in this case, will determine how accurately we can estimate the variance of the bootstrapped correlation functions. In other words, this parameter determines the variability of our variance estimates as we use different realisations of the time series to compute the variance of the bootstrap correlation functions; that is,  $Var[Var[R_X(\tau)]]$ . For instance, figures 4.4 and 4.5 show the computed bootstrap calculated from only one of the 500 simulated response time histories. Computing the same quantity from a different response will yield either a poorer or improved bootstrap estimate of  $Var[R_X(\tau)]$ . While for Efron's bootstrap (section 4.2), this variance depends only on  $n$  and  $B$ , the situation is further complicated for the dependent bootstrap due to the additional parameter  $l$  that is the block length. It is well know that the choice of block length greatly influences  $Var[Var[s(\chi)]]$  and also controls the bias in  $Var[s(\chi)]$ , denoted by  $bias[Var[s(\chi)]]$ , so that  $l$  must be chosen carefully to get an accurate -although limited by  $n$  and  $B$ -



estimate of  $Var[s(\chi)]$ . This is illustrated in figure 4.6. Using the same response history

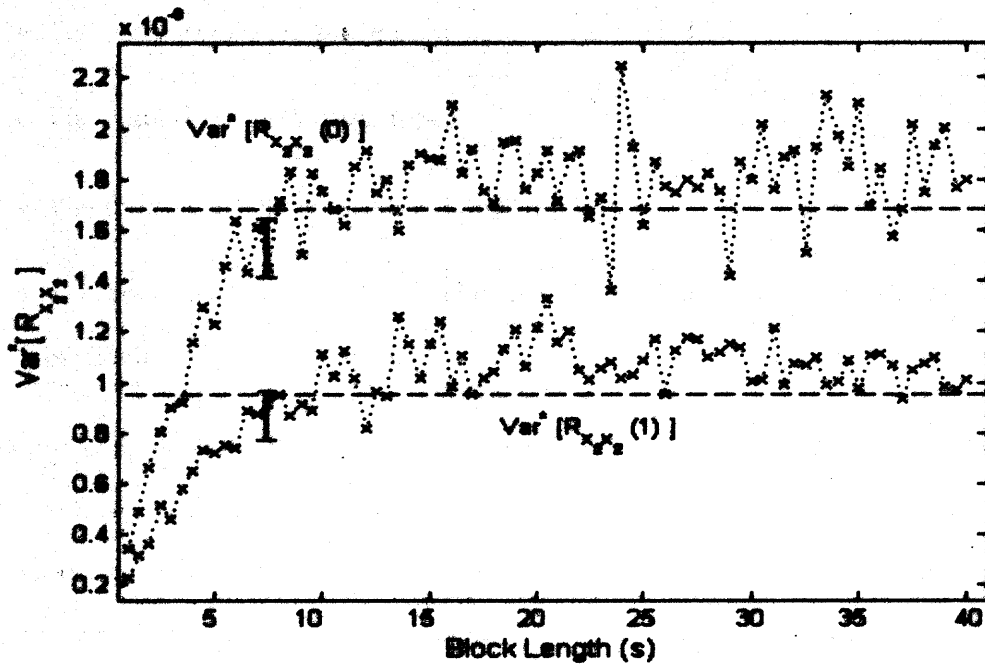


Fig. 4.6: Influence of block length  $l$  (in steps of  $0.5s$ ) on the (MB) bootstrap estimate of the variance of the ac.f of the response  $x_2$  of the system in table 4.1 at lag  $r = 0$  and  $r = 1$ . The two vertical bars indicate the standard error of the results at fixed block length of  $l = 8s$  ( $\Delta t = 0.05s$ ) due to having a finite number of  $B = 300$  bootstrap samples. [—] are the true values of  $Var[R_{x_2x_2}(0)]$  and  $Var[R_{x_2x_2}(1)]$  computed from the 500 simulated responses.

as in figures 4.4 and 4.5, the variance of the ac.f at the second degree-of-freedom is shown at lags 0 and 1 as a function of the block length  $l$ . The vertical lines represent the standard deviation computed at fixed block length of  $8s$  ( $\Delta t = 0.05s$ ) computed from 200 different bootstrap estimates of  $Var[R_{x_2x_2}(0)]$  and  $Var[R_{x_2x_2}(1)]$  using the *same* time series. Thus, this variance is solely due to the resampling and therefore represents the error due to the limited number  $B = 200$  bootstrap replicates in our computations. This does not cause any problems in practice as  $B$  can be increased arbitrarily and is only limited by the computational requirement. It is clearly seen from figure 4.6 that the block length acts as a tuning parameter for the dependent bootstrap and suggests the existence of an *optimal block length*, which in this case, accounting for the error due to finite  $B$ , would roughly lie somewhere between  $7s \leq l \leq 13s$  ( $\Delta t = 0.05s$ ). In practice, where the true value is not known, it is not possible to select the optimal block length from a graph like 4.6 and different approach is needed to assist this selection. The optimal block length depends, in general, on the following factors (Bühlmann, 2002;

Lahiri, 1999):

- The data generating process
- The statistic to be bootstrapped
- The purpose for which the the bootstrap is used
- The bootstrap method that is employed i.e. the stationary, “blocks of blocks” or moving blocks bootstrap.

Due to these different influences on the block length, the treatment given here is tailored toward the application for operational modal analysis. This means that the statistics to be bootstrapped are the auto-and cross-correlation functions between simultaneously measured structural responses and, for now, their variance and covariances are estimated. Later, the bootstrapped correlation functions will be employed to identify the system’s modal parameters but this is postponed to Chapter 7.

Consider the time series  $X = \{x_1, \dots, x_n\}$ , let  $\hat{R}_X$  denote the ac.f estimate of  $X$  and  $\sigma_R^2$  its variance. Let  $\sigma_R^{*2}$  be the corresponding bootstrap estimate. Assume for the moment that latter is obtained using the moving blocks (MB) bootstrap with block length  $l$ . It is shown in Hall *et al.* (1995) that in this case, the asymptotic or ideal ( $B \rightarrow \infty$ ) mean-square-error (*mse*) of  $\sigma_R^{*2}$  defined as  $mse(\sigma_R^{*2}) = Var[\sigma_R^{*2}] + (bias(\sigma_R^{*2}))^2$  has the form

$$mse(\sigma_R^{*2}) = \frac{1}{n^2} \left( \frac{C_1}{l^2} + \frac{l C_2}{n} \right) \quad (4.14)$$

$$\text{with} \quad (4.15)$$

$$bias[\sigma_R^{*2}] = -\frac{\sqrt{C_1}}{nl} \quad (4.16)$$

$$Var[\sigma_R^{*2}] = \frac{l C_2}{n^3} \quad (4.17)$$

where  $C_1$  and  $C_2$  are constants independent of  $n$  and  $l$  (Hall *et al.*, 1995; Lahiri, 1999). The first term in equation 4.14 involving the constant  $C_1$  is the square of the bias and the second term is the variance of  $\sigma_R^{*2}$ . This equation clearly shows the

dependence of the MB bootstrap estimate of  $\sigma_R^{*2}$  on the design parameter  $l$ . The situation is analogous to over - or undersmoothing spectral estimates using Welch's method (Welch, 1967) when periodograms are estimated from short or large blocks of the data and the block length may be thought of as a smoothing parameter. Choosing a large block length  $l$  will reduce the bias in the bootstrap estimate but will increase its variance and vice versa. The optimal choice for the block length is therefore the one that offers the best compromise between these two errors, that is the one that minimises the  $mse(\sigma_R^{*2})$  over  $l$ . Thus, from equation 4.14, the ideal block length  $l_{opt}$  is given by

$$l_{opt} = n^{1/3} \left( \frac{2C_1}{C_2} \right)^{1/3} \quad (4.18)$$

The general form of the equation for  $l_{opt}$  is in fact applicable to all three bootstrap estimators (MB, BB and SB) presented above (Bühlmann and Künsch, 1999; Lahiri, 1999) and holds when the bootstrapped variance and bias are desired for any statistic. When quantities other than the variance and/or the bias are bootstrapped, equation 4.18 is not valid anymore. For instance, when the one-sided or two-sided distributions of the statistic of interest are desired, rather than only their variance or bias, it is shown in Hall *et al.* (1995) that the optimal length is of the order  $O(n^{1/4})$  and  $O(n^{1/5})$  respectively.

To get an estimate for  $l_{opt}$ , the constant  $(2C_1/C_2)$  must be calculated. This constant depends primarily on the correlation structure of the underlying process  $\{X\}$  but is not influenced, for instance, by strength of the dependence of the process (Hall *et al.*, 1995). Other factors that affect this constant are the bootstrap method used (Lahiri, 1999) and the statistic to be bootstrapped (Bühlmann and Künsch, 1999). Therefore, for any chosen bootstrap method applied to a fixed statistic, this factor changes from system to system since the correlation structure of response changes so that it must be estimated empirically. Three methods feature in the literature for this purpose. Hall *et al.* (1995) employed a method which recursively finds the optimal block length by minimizing the  $mse$  computed from bootstrap estimates of subsamples of the original

time series of length  $m \ll n$ . This procedure is not considered in this thesis. Lahiri (1999) derive  $l_{opt}$  from equation 4.18 and give an expression for the constants  $C_1$  and  $C_2$  when the statistic to be bootstrapped is the mean of the underlying process  $X$ . This method is also adopted by Politis and White (2004). Bühlmann and Künsch (1999) approach the problem from a different angle in the sense that they do not determine  $l_{opt}$  by minimising the *mse* of the variance but rather exploit the reciprocal relationship between the block length and the bandwidth in spectral estimates.

The approach of Bühlmann and Künsch's is followed and it will be shown that, when the statistic to be bootstrapped is the mean of  $X$ , it will yield the same theoretical expressions for  $l_{opt}$  as given by Politis and White (2004) and Lahiri (1999). The presentation of the theory is kept practical and technical details are omitted in places but the reader is directed to the original papers if more mathematical rigour is desired. Let the mean of the measured time series  $X = \{x_0, x_1, \dots, x_{n-1}\}$  be  $\hat{\mu}_X = n^{-1} \sum_{i=1}^n x_i$  and let  $\hat{\mu}_X \rightarrow \mu_X$  as  $n \rightarrow \infty$ . It is a well known result that (Bendat and Piersol, 2000)

$$Var[\hat{\mu}_X] = n^{-1} \sum_{k=-n+1}^{n-1} \left(1 - \frac{|k|}{n}\right) C_X(k) \quad (4.19)$$

where  $C_X(k) = R_X(k) - \mu_X^2$  is the auto-covariance function defined in equation 2.11. As argued in Chapter 2, it can generally be assumed that the measured response histories have zero mean. The reason we use the auto-covariance function rather than the ac.f.  $R_X(k)$ , will become clear shortly. Recalling that the two sided spectrum of  $X$  is given by (Bendat and Piersol, 2000)

$$S_X(\omega) = \frac{1}{2\pi} \sum_{k=-\infty}^{\infty} C_X(k) \cos(k\omega), \quad (4.20)$$

it is seen by comparing equation 4.20 to 4.19 that the variance of the mean can be approximated by an estimate of the spectral estimate  $S_X$  at  $\omega = 0$  weighted by the

triangular window  $w_\Delta$  of length  $n$

$$w_\Delta(k) = 1 - \frac{|k|}{n}, \quad (4.21)$$

so that

$$\text{Var}[\hat{\mu}_X] \approx \frac{2\pi}{n} S_X(\omega = 0) \quad (4.22)$$

It was shown by Künsch (1989) (also c.f. Bühlmann and Künsch (1999)) that the variance of the bootstrapped mean  $\hat{\mu}_X^*$  reads

$$\text{Var}[\hat{\mu}_X^*] = n^{-1} \sum_{k=-l+1}^{l-1} \left(1 - \frac{|k|}{l}\right) \hat{C}_X(k), \quad (4.23)$$

where  $\hat{C}_X(k)$  denotes the estimated sample auto-covariance function and  $l$  is the block length. Like equation 4.19, equation 4.23 admits an interpretation in the frequency domain, namely that the variance of the bootstrapped mean is the *empirical* spectral density weighed by a triangular window of length  $l$ . As explained already in Chapter 3 for the flat-top window, the “length” of the window is related to its bandwidth. The latter concept is in fact rather subtle and many definitions have been introduced, see Priestley (2004) for instance. Using a definition due to Brillinger (1975), the bandwidth of the *triangular window* is simply given by the inverse of its “length” in the time domain. Denoting the window length by  $M$ , the definition of its bandwidth  $b_T$  is given by

$$b_T = 1/M \quad (4.24)$$

It is important to note that the definition of the bandwidth of a window as a function of its “length” as in 4.24 applies only to a certain class of window functions, among which is the the triangular window and the flat-top window employed in the previous chapter (Politis and White, 2004; Priestley, 2004). The relation between the decay of the auto-covariance function (or ac.f.) and the spectral bandwidth is well known: the faster the decay, the wider the spectral density, and vice versa. As explained in the previous chapter, applying a window to the ac.f. disturbs its natural decay:

decreasing the bandwidth of the window forces an increased rate of decay resulting in a more poorly resolved spectral density function, thereby introducing resolution bias in the spectral estimates (Schmidt, 1985b). On the other hand, however, the variance in the spectral density decreases. In general,

as  $M \uparrow$ , variance  $\uparrow$ , bias  $\downarrow$

as  $M \downarrow$ , variance  $\downarrow$ , bias  $\uparrow$ .

It is now easily seen that the dependence of the variance estimate on the block length  $l$  (c.f. eq.4.23), is equivalent to choosing the bandwidth of the spectral window, given by  $b_T = 1/l$ . The optimal bandwidth, and hence the block length  $l$ , is therefore the one that gives the best compromise between bias and variance of the spectral estimate  $S_X(\omega)$  at frequency  $\omega = 0$ . Thus, using the well known formulae giving the bias and variance of the spectral density weighed by a triangular window at any frequency  $\omega$  (Priestley, 2004)

$$\text{Var}[\hat{S}_X(\omega)] = \frac{2l}{3n} \hat{S}_X^2(\omega), \quad \omega \neq 0, \pm\pi \quad (4.25)$$

$$\text{Var}[\hat{S}_X(\omega = 0)] = \frac{4l}{3n} \hat{S}_X^2(\omega = 0) \quad (4.26)$$

$$\text{bias}[\hat{S}_X(\omega)] = -\frac{1}{l} \hat{S}_X^{(1)}(\omega), \quad \forall \omega, \quad (4.27)$$

where  $S_X^{(1)}(\omega)$  is the *generalized derivative* (Priestley, 2004) of the spectral density given by

$$S_X^{(1)}(\omega) = \frac{1}{2\pi} \sum_{k=-\infty}^{\infty} |k| C_X(k) \cos(k\omega) \quad (4.28)$$

Thus, the mean-square-error of the spectral density at frequency  $\omega$  is given by

$$\text{mse}[\hat{S}_X(\omega)] = \frac{2l}{3n} \hat{S}_X^2(\omega) + \frac{1}{l^2} (\hat{S}_X^{(1)}(\omega))^2 \equiv \frac{2}{3b_T n} \hat{S}_X^2(\omega) + b_T^2 (\hat{S}_X^{(1)}(\omega))^2 \quad (4.29)$$

Minimizing equation 4.29 over the bandwidth  $b_T$  then yields the optimal bandwidth at frequency  $\omega$ ,  $b_{T_{opt}}(\omega)$ . Thus, at  $\omega = 0$ , we find

$$b_{T_{opt}}(0) = n^{-1/3} \left( \frac{2\hat{S}_X^2(0)}{3(\hat{S}_X^{(1)}(0))^2} \right)^{1/3} \quad (4.30)$$

The optimal block length  $l_{opt}$  may then be taken as the the closest integer to  $b_{T_{opt}}(0)^{-1}$ . Comparing 4.30 to equation 4.18 clearly shows that determining  $l_{opt}$  by minimising  $mse[\sigma_R^{*2}]$  is equivalent to determining  $l_{opt}$  by minimising  $mse[\hat{S}_X(0)]$ . Thus, from equation 4.18 a choice for the constants  $C_1$  and  $C_2$  is

$$C_1 = (\hat{S}_X^{(1)}(0))^2, \quad C_2 = \frac{4}{3}\hat{S}_X^2(0) \quad (4.31)$$

This is precisely the result derived by (Lahiri, 1999; Politis and White, 2004) for the optimal block length  $l_{opt}$  for the *MB* bootstrap, when the statistic to be bootstrapped is the mean  $\hat{\mu}_X$ . The methods in Bühlmann and Künsch (1999) and Politis and White (2004) differ only in the actual computation of these constants which boils down to getting an accurate estimate of  $\hat{S}_X^2(0)$  and  $(\hat{S}_X^{(1)}(0))^2$ . This situation is very similar to that discussed in Chapter 3 when estimating the covariances of the correlation functions using the plug-in formulae in section 3.5.1. In fact, it is easily seen that the computation of  $\hat{S}_X^2(0)$  and  $(\hat{S}_X^{(1)}(0))^2$  are sums of the the type  $\sum_{k=-\infty}^{\infty} |k|^p e^{ik\omega} \hat{R}_{xx}^b(k)$  and thus correspond exactly to the situation for which Politis (2003a) developed their flat-top window (c.f. section 3.5, Chapter 3). For statistics other than the mean, equations 4.19 and 4.23 do no longer hold which implies that the theory presented so far is applicable only to the mean  $\hat{\mu}_X$  and an extension is necessary for the problem under consideration, namely where the statistics to be bootstrapped are correlation functions. We start by considering the latter problem first before dealing with the evaluation of  $\hat{S}_X^2(0)$  and  $(\hat{S}_X^{(1)}(0))^2$ .

To apply the block length selection to other statistics than the mean, we need to introduce the concept of the *influence function* (Hampel *et al.*, 1986). Loosely

speaking, the influence function, denoted here by  $IF(x)$ , describes an infinitesimal change in an estimator  $s(F)$  when the distribution  $F$  of the underlying data  $X$  is changed due to a perturbation  $\epsilon$  on observation  $x$  in  $X$ . Formally, the influence function at point  $x$  is defined as

$$IF(x) = IF(x, F, s) = \lim_{\epsilon \rightarrow 0} \frac{s((1 - \epsilon)F + \epsilon\delta_x) - s(F)}{\epsilon} \quad (4.32)$$

where  $\delta_x$  denotes the degenerate distribution putting mass 1 on  $x$  i.e. it is unity when at  $x$  and zero otherwise. The reason for introducing the influence function is that it allows the following linearisation of a general statistic (Efron and Tibshirani, 1993; Hampel *et al.*, 1986)

$$\hat{s}(X) \approx s_\infty + n^{-1} \sum_{i=1}^n IF(x_i) \quad (4.33)$$

where  $s_\infty$  denotes the exact statistic we are trying to estimate. The variance of  $\hat{s}(X)$  is then simply given by

$$Var[\hat{s}(X)] = Var[n^{-1} \sum_{i=1}^n IF(x_i)] \quad (4.34)$$

Noting that the right hand side of equation 4.34 is the variance of the *mean* of the influence function, it follows directly from equations 4.19 and 4.23 that the theory given for the mean is applicable to the variance of the general bootstrapped statistic  $s^*$  when the original time series  $X$  is replaced by its influence function  $IF(X) = IF(X, F, s)$ . To clarify the notation, we note that the influence function defined in equation 4.32,  $IF(x)$ , applies to a single observation  $x$  of the time series  $X$ . We write  $IF(X)$  to denote the times series  $\{IF(x_1), IF(x_2), \dots, IF(x_n)\}$ . Thus, the equivalent of equation 4.23 is

$$Var[\hat{s}_X^*] = n^{-1} \sum_{k=-l+1}^{l-1} \left(1 - \frac{|k|}{l}\right) \hat{C}_{IF(X)}(k) \quad (4.35)$$



and that of equation 4.30

$$b_{T_{opt}}(0) = n^{-1/3} \left( \frac{2\hat{S}_{IF(X)}^2(0)}{3(\hat{S}_{IF(X)}^{(1)}(0))^2} \right)^{1/3} \quad (4.36)$$

where  $\hat{S}_{IF(X)}(0)$  is the spectral density of the influence function  $IF(X)$ . It is important to recognise that for the linearisation in equation 4.34 to hold, we require the influence function  $IF(X)$  to have zero mean, so that asymptotically  $\hat{s}(X) \rightarrow s_\infty$  as  $n \rightarrow \infty$ . Furthermore, for equation 4.35 to be applicable, we require  $IF(X)$  to be stationary since the definition used for covariance function  $\hat{C}_{IF(X)}(k)$  applies to stationary processes only. When these conditions are met, we can state in general that the selection of the optimal block length  $l_{opt}$  of the MB bootstrap estimator is equivalent to determining the optimal bandwidth of the spectral density weighted by the triangular window; the spectral density being the one corresponding to the influence function of the statistic to be bootstrapped.

Since the influence function relies upon the knowledge of the underlying distribution  $F$ , which is not known, the influence function needs to be determined empirically. Methods to compute  $IF(X)$  from empirical data are given in Efron and Tibshirani (1993) for instance, but in this thesis, the procedure suggested by Bühlmann and Künsch (1999) (also see Campbell (1978)) will be employed. The empirical influence function can be computed as

$$\hat{IF}(x_i) = n [s(x_1, , x_2, \dots, x_n) - s(x_1, , x_2, \dots, x_{i-1}, x_{i+1}, \dots, x_n)] \quad (4.37)$$

where  $s(x_1, , x_2, \dots, x_n)$  denotes the estimator based on  $n$  observations and  $s(x_1, , x_2, \dots, x_{i-1}, x_{i+1}, \dots, x_n)$  is the same estimator but without the  $i^{th}$  observation. This is the jackknife estimate of the influence function.<sup>†</sup> Since the bandwidth selection for spectral density estimation, and hence the block length selection, is independent

---

<sup>†</sup>The jackknife is a method related to the bootstrap (Efron and Tibshirani, 1993) but rather than resampling with replacement, a jackknife estimate is formed from the original sample by leaving out one observation.

of the scale of the data, it is sufficient to compute the influence function only up to a proportionality constant. It is noted that the empirical estimate of the influence function in equation 4.37 does not necessarily have zero mean. However, whenever the influence function is stationary, which is a prerequisite for its application to block length selection, the mean can simply be removed as it is time independent. Alternatively, since only the covariance of the  $IF(X)$  appears in the block length selection procedure, the mean is implicitly removed in the evaluation of  $C_X(k)$ .

The estimation of the spectral densities necessary to compute the optimal block length is considered next. As mentioned already, the method used by Politis and White (2004) for an accurate estimation of  $\hat{S}^2(0)$  and  $(\hat{S}^{(1)}(0))^2$  is to taper the covariance functions by the “flat-top” window of length  $M$  defined by equation 3.43 in the previous chapter, so that, for instance  $\hat{S}_X(0) = (2\pi)^{-1} \sum_{k=-\infty}^{\infty} w_{FT}(k/M) C_X(k)$ . The selection of the length of the window  $M$  follows the same empirical picking method described in chapter 3, section 3.5.1. Bühlmann and Künsch (1999) improve on the direct estimate of equation 4.30 by considering the optimal *global bandwidth*, which, rather than minimising the bandwidth at  $\omega = 0$ , only, minimises the integrated mean-square-error

$$b_{T_{opt}} = n^{-1/3} \left( \frac{\int_{-\pi}^{\pi} \hat{S}_{IF(X)}^2(\omega) d\omega}{3 \int_{-\pi}^{\pi} (\hat{S}_X^{(1)}(\omega))^2 d\omega} \right)^{1/3} \quad (4.38)$$

This is achieved in an iterative manner and once the optimal global bandwidth is found, it is used to estimate the optimal local optimal bandwidth at  $\omega = 0$ . Their algorithm is as follows:

- Start with the “pilot” bandwidth of  $b_0 = n^{-1}$
- Compute an optimized global bandwidth in 4 iterative steps as

$$b_i = n^{-1/3} \left( \frac{\sum_{k=-n+2}^{n-1} \hat{C}_{IF}^2(k)}{6 \sum_{k=-n+2}^{n-1} w_{SC}(kb_{i-1} n^{4/21}) k^2 \hat{C}_{IF}^2(k)} \right), \quad \text{for } i = 1, 2, 3, 4 \quad (4.39)$$

- Compute the optimal local bandwidth at  $\omega = 0$  as

$$b_{opt}(0) = n^{-1/3} \left( \frac{\frac{4}{3} \left( \sum_{k=-n+2}^{n-1} w_{TH}(kb_4 n^{4/21}) \hat{C}_{IF}(k) \right)^2}{2 \left( \sum_{k=-n+2}^{n-1} w_{SC}(kb_4 n^{4/21}) |k| \hat{C}_{IF}(k) \right)^2} \right) \quad (4.40)$$

- Find  $\hat{l}_{opt} =$  closest integer to  $\hat{b}_{opt}(0)$

where

$$w_{SC}(t) = \begin{cases} 1 & |t| \in [0, 0.8] \\ 1 + \cos(5(t-0.8)\pi)/2 & |t| \in [0.8, 1] \\ 0 & \text{otherwise} \end{cases} \quad (4.41)$$

$$w_{TH}(t) = \begin{cases} 1 + \cos(\pi t)/2 & |x| \in [0, 1] \\ 0 & \text{otherwise} \end{cases} \quad (4.42)$$

are the *Split-Cosine (SC)* and *Tukey-Hanning (TH)* windows respectively. It transpires that the methods in Bühlmann and Künsch (1999) and Politis and White (2004) only differ in the way the constants  $C_1$  and  $C_2$  are estimated as it is easily seen that the nominator equation 4.40 corresponds to  $C_2$  and the denominator gives  $2C_1$  in equation 4.14. The inflation factor  $n^{4/21}$  occurring in the window functions in 4.40 are actually the optimal window widths for estimating the generalized derivatives  $S_X^1$ . For improved stability, this factor was also employed in the evaluation of  $S_X$ , see Bühlmann (1996). The latter author also shows that  $i = 4$  is the minimum number of iterations required for the bandwidth  $b_i$  to have the correct asymptotic order  $n^{-1/3}$ . We note that the block size selection methods given so far are, strictly speaking, only applicable to the moving blocks (MB) bootstrap. Bühlmann and Künsch (1999) also give an extension for the “block of blocks” bootstrap but this was not applied in this thesis. The reason is that (as will be argued in a moment) it will be sufficient for all practical purposes to determine the optimal block length based on the correlation functions at zero lag only, for which the “blocks of blocks” and moving blocks bootstrap estimates are equivalent.

For completeness, the optimal block length for the stationary bootstrap is briefly discussed. Since the block lengths are chosen randomly, the mean of the distribution from the block lengths are sampled plays the role of the optimal block length. The latter is easily determined by applying the theory presented so far, namely by changing the constant  $C_2$  in equation 4.18 to (Lahiri, 1999; Politis and White, 2004)

$$C_2 = 4S_{IF(X)}^2(0) + \frac{2}{\pi} \int_{-\pi}^{\pi} (1 + \cos(\omega)) S_{IF(X)}^2(\omega) d\omega \quad (4.43)$$

instead of the value given for the MB in 4.31. The constant  $C_1$  remains the same.

## 4.5 Simulations

This section is concluded by discussing a few practical issues and includes a few simulations validating the theory above for its use in correlation functions from structural responses. Firstly, it is noted that the computation of the influence function, given in 4.37, only allows the estimation of  $IF(X, R_X(k))$  for a particular lag  $k$  at a time i.e. the influence function at lag  $k$ ,  $IF(X, R_X(k))$ , differs from that at lag  $r$ ,  $IF(X, R_X(r))$ , whenever  $k \neq r$ . A more general estimate of the influence function, yielding all desired lags of  $\hat{R}_X(k)$  in a single step is not obvious. Fortunately, it appears that the optimal block length  $l_{opt}$  for bootstrapping the variance of the correlation function at any particular lag, will also be optimal or near-optimal for all other other lags. A rigorous proof to establish the veracity of this statement would involve showing that  $\hat{S}_{IF(X, R_X(k))}^2(0) \approx \alpha \hat{S}_{IF(X, R_X(r))}^2(0)$  and  $(\hat{S}_{IF(X, R_X(k))}^{(1)}(0))^2 \approx \alpha (\hat{S}_{IF(X, R_X(r))}^{(1)}(0))^2$ , for  $k \neq r$  and some constant  $\alpha$ , so that equation 4.30 yields the same result irrespective of the lag of the correlation function for which the influence function is computed. Such a proof was, however, not further pursued. To support this claim, it is argued that due to the strong correlation structure of  $Var[\hat{R}_X(k)]$ , any influences on the estimate of  $Var[\hat{R}_X(k)]$  will be global rather than local in the sense that if  $Var[\hat{R}_X(k)]$  is overestimated (or underestimated), then  $Var[\hat{R}_X(r)]$ ,  $k \neq r$ , will also be overestimated (or

underestimated). This is clearly seen, in figure 4.6 for example where  $Var^*[\hat{R}_X(0)]$  and  $Var^*[\hat{R}_X(1)]$  follow exactly the same trend, and disregarding the random sampling error due to the finite number of bootstrap replicas  $B$ , they seem almost proportional and indicate a very similar block length for both lags. Consequently, it is suggested that the optimal block length  $l_{opt}$  for  $Var^*[\hat{R}_X(k)]$ ,  $\forall k$ , should be determined based on  $IF(X, R_X(0))$ .  $IF(X, R_X(0))$  has same number of data points  $n$  than  $X$ , while the number of data points in  $IF(X, R_X(r))$ , for  $r > 0$  will be  $n - r$  so that an estimate  $C_{IF(X, R_X(r))}(k)$ , for  $r > 0$  would be less accurate than  $C_{IF(X, R_X(r))}(0)$ .

To check the performance of the block length selection methods presented above applied to bootstrapped correlation functions, the same simulated data from the the 2DOF system in table 3.3, section 3.5.1 is used. 100 different response time histories simultaneously measured at each of the two degrees-of-freedom, of length 780s with  $\Delta t = 0.05s$  were used. Politis and White's method as well as Bühlmann and Kuensch's are employed to determine the optimal block length  $l_{opt}$  for the bootstrapped  $Var^*[\hat{R}_{x_2x_2}(0)]$ . Average values are shown in table 4.2 and are complemented by the scatter plot in figure 4.7(a). In cases A1 and A2 in table 4.2, Politis and White's method is employed with the moving blocks (MB) bootstrap for  $c = 2$  and  $K = 5$  (c.f. section 3.5) as suggested by these authors. What distinguishes A1 from A2 is that in the latter case, a lower limit on the bandwidth of the flat-top window is imposed. The bandwidth of the flat-top window is determined as the inverse of  $M = 2k_{cut}$ , where  $k_{cut}$  is the lag of the estimated correlation function after which it is not significantly different from zero. Thus imposing a lower limit on the bandwidth of the flat-top window, implies imposing a maximum for  $M = 2k_{cut}$ . Recall that  $k_{cut}$  is determined in practice as the lag after which the subsequent  $K$  values lie within in the bands  $\pm c\sqrt{\log_{10}(n)/n}$ . However, the values  $c = 2$  and  $K = \max(5, \sqrt{\log_{10}(n)})$ , where  $n$  is the number of data points in the measured time-series, are just recommendations given in (Politis and White, 2004) and not absolute requirements. Consequently, a different choice of these values will result in a different choice for the bandwidth of

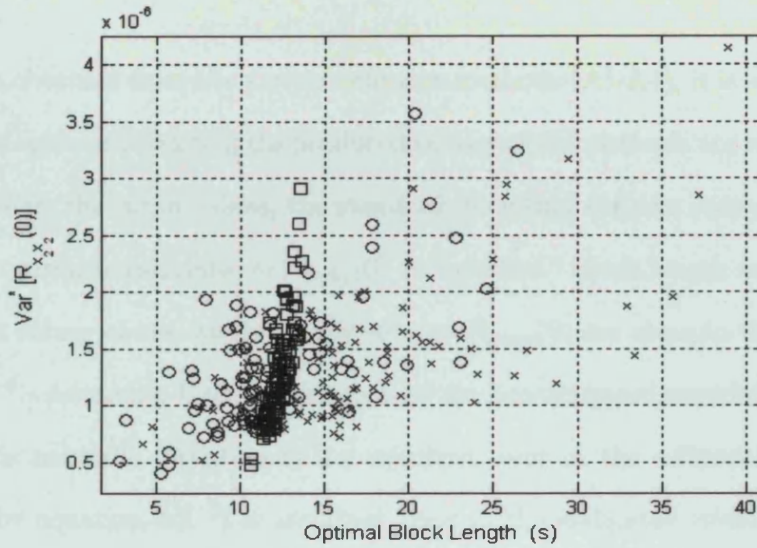
the flat-top window and affect the estimated optimal block length. In section 3.5, a different choice  $K$  was already suggested to avoid selecting a very low value of  $k_{cut}$ , namely by imposing the condition  $K > \lceil (2f_0\Delta t)^{-1} \rceil$ . In this case, where  $n = 15600$ , the lowest frequency mode  $f_0 = 2.24\text{Hz}$  and the time step is  $\Delta t = 0.05$ , this amounts to choosing  $K > 4$ . Similarly, it may occur for instance, due to the higher variance in the tail region of the correlation coefficient function, that the estimated lag  $k_{cut}$  occurs much later than it needs to. It is noted, however, that choosing  $k_{cut}$  according to the method suggested by Politis and White (2004) is adaptive in the sense that, if  $n$  is large and hence the variance smaller, the bands  $\pm c\sqrt{\log_{10}(n)/n}$  will be narrower as well so that a larger width  $M$  will be estimated for the flat-top window, and vice versa. However, the choice of  $c$  and  $K$  still come into play and the values suggested by Politis and White (2004) may not be the best choice in all cases as is pointed out by these authors. The latter authors also give the general guideline that the flat-top lag-window spectral estimators perform best for small values of  $M = 2k_{cut}$ . For this reason, an upper limit for  $M = 2k_{cut}$  is imposed using the fact that the nature of the correlation functions between structural response measurements is known and the same in all cases. Let  $\nu = \min(\xi_i\omega_i)$  be the product of the modal frequency and damping ratio of the system mode  $i$  with the slowest decay, where  $i$  runs over the number modes of the system. When this mode has decayed to a value not significantly different from zero, the same statement then applies to all the other modes of that system. Assuming this happens when the corresponding correlation coefficient function has decayed to  $\alpha\%$  say, it is easily found from the decay envelope of this mode with slowest decay,  $e^{-\nu k\Delta t}$ , that this occurs at lag  $k = -\ln(\alpha)/\Delta t\nu$ . A value for  $\alpha = 1\%$  is suggested and this value of  $k$  is used as an upper limit for  $k_{cut}$ . Clearly, this choice requires to have an initial estimate of the modal parameters of the system but, since the bootstrap will in general be used as a post-processing tool to determine error bounds on the estimated modal parameters, such an estimate is sometimes available either from an initial modal test of a finite element model of the structure.

Lag 0	$mean(\hat{l}_{opt})(s)$	$\sigma(\hat{l}_{opt})(s)$	$mean(Var^*[\hat{R}_{x_2x_2}(0)]) \cdot 10^{-6}$	$\sigma(Var^*[\hat{R}_{x_2x_2}(0)]) \cdot 10^{-7}$	$bias(Var^*[\hat{R}_{x_2x_2}(0)]) \cdot 10^{-7}$	$rmse(Var^*[\hat{R}_{x_2x_2}(0)]) \cdot 10^{-7}$
A1	18.1	9.2	1.43	6.70 (3.16)	-2.24 (-2.78)	7.07 (4.21)
A2	17.9	7.7	1.43	6.30 (3.11)	-2.13 (-2.53)	6.66 (4.01)
A3	12.4	5.7	1.31	5.57 (4.52)	-3.36 (-3.76)	6.51 (5.88)
A4	12.3	0.6	1.27	4.46 (2.08)	-3.73 (-3.04)	5.82 (3.69)

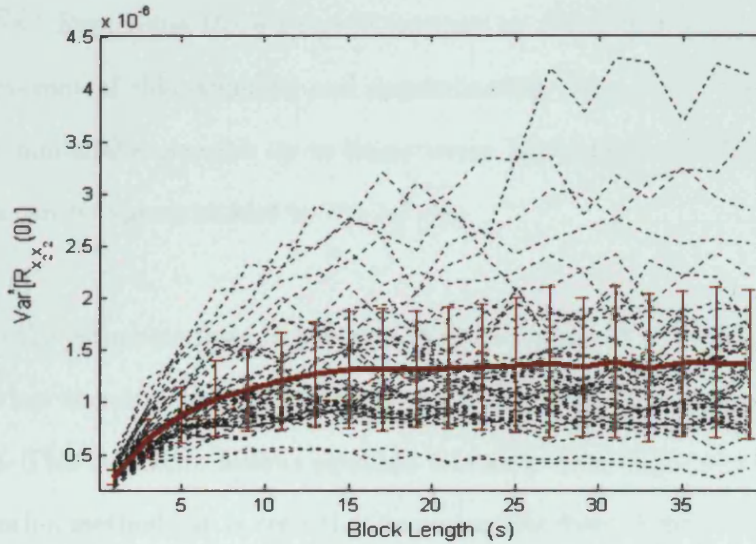
  

Lag 1	$mean(\hat{l}_{opt})(s)$	$\sigma(\hat{l}_{opt})(s)$	$mean(Var^*[\hat{R}_{x_2x_2}(1)]) \cdot 10^{-7}$	$\sigma(Var^*[\hat{R}_{x_2x_2}(1)]) \cdot 10^{-7}$	$bias(Var^*[\hat{R}_{x_2x_2}(1)]) \cdot 10^{-7}$	$rmse(Var^*[\hat{R}_{x_2x_2}(1)]) \cdot 10^{-7}$
A2	/	/	8.34	3.65	-1.27	3.86
A3	/	/	7.59	3.22	-2.01	3.80
A4	/	/	7.41	2.58	-2.19	3.39

Tab. 4.2: Comparison of block length selection methods for the MB, BB and SB bootstrapped auto-correlation functions at lag 0 and 1 from 100 simulated responses of the 2DOF system in table 3.3 for estimating  $Var^*[\hat{R}_{x_2x_2}(0)]$  and  $Var^*[\hat{R}_{x_2x_2}(1)]$ . The cases considered are: (A1) MB/BB bootstrap, method-(Politis and White, 2004) with  $c = 2$ ; (A2) MB/BB bootstrap, method-(Politis and White, 2004) with  $c = 2$  and an upper limit of  $-\ln^{-1}(0.01)(\nu\Delta t)$  imposed on  $k_{cut}$ , with  $\nu = \min(\xi_i\omega_i)$ ; (A3) SB bootstrap, method-(Politis and White, 2004) with  $c = 2$  with the same upper limit on  $k_{cut}$ ; (A4) MB/BB bootstrap, method-(Bühlmann and Künsch, 1999). At each block length, the bootstrap estimates of  $Var^*[\hat{R}_{x_2x_2}(0,1)]$  are computed from 300 bootstrap replicas of  $\hat{R}_{x_2x_2}(0,1)$ .  $\sigma$  denotes the standard deviation,  $rmse$  the root-mean-square-error. The values in the parenthesis denote the the *predicted* estimates from equation 4.14.



(a)



(b)

Fig. 4.7: (a) Scatter diagram depicts the BB bootstrap estimates  $Var^*[R_{x_2 x_2}(0)]$  as a function of the optimal block length  $l_{opt}$  from 100 simulated responses. The block selection schemes used the ones described corresponding to cases A2 [ $\times$ ], A3 [ $\circ$ ] and A4 [ $\square$ ] described above and whose average values are tabulated in 4.2. (b) Bootstrap estimates of  $Var^*[R_{x_2 x_2}(0)]$  computed from 50 simulated responses as a function of the block length. The thick line is their mean and the errorbars indicate the standard deviation. The block length is increased in steps of  $2s$  ( $\Delta t = 0.05s$ ). At each block length, the bootstrap estimates of  $Var^*[\hat{R}_{x_2 x_2}(0)]$  are computed from 300 bootstrap replicas of  $\hat{R}_{x_2 x_2}(0)$ .

Case A3 is the same as A2 but for the stationary (SB) bootstrap. A4 uses Bühlmann and Künsch's method for block length selection. The reader is reminded that the true values  $Var[\hat{R}_{x_2 x_2}(0)]$  and  $Var[R_{x_2 x_2}(1)]$ , tabulated in table 3.4, section 3.5.1, Chapter 3, are  $1.65 \cdot 10^{-6}$  and  $9.61 \cdot 10^{-7}$ . Comparing the mean block lengths



estimates obtained from the various selection methods (A1-A4), it is seen that, on average, the optimal block lengths produced by any of the methods are reasonably close. In particular, the mean values, the standard deviation and the root-mean-square error of the variance estimates of  $\hat{R}_{x_2x_2}(0)$  at “optimal” block length are similar. Also, the mean values of the variance estimates of  $\hat{R}_{x_2x_2}(0)$  are close to the true value of  $1.65 \cdot 10^{-6}$ . Assuming that the variance of the bootstrapped correlation function at zero lag is normally distributed, the standard error in the estimated sample mean is given by equation 4.2. The standard error in the estimated variance is known to be  $\sigma[\hat{\sigma}^2(\chi)] = \sigma^2(\chi)\sqrt{2/N}$  (Rose and Smith, 2002) which can be approximated as  $\hat{\sigma}^2(\chi)\sqrt{2/N}$ . Expressing the estimated variance as  $\hat{\sigma}^2(\chi) \approx \sigma^2(\chi)[1 \pm \sqrt{2/N}]$ , taking the square-root of this equation and approximating  $[1 \pm \sqrt{2/N}]^{1/2}$  as  $1 \pm \sqrt{1/2N}$  by using the binomial expansion up to linear terms, the error in the estimated standard deviation can be approximated by  $\hat{\sigma}(\chi)\sqrt{\frac{1}{2N}}$ .

While the estimates from Politis and White’s method for the MB bootstrap (A1, A2) have less bias compared to Bühlmann and Künsch’s method, they come with larger variances. This behaviour follows equation 4.14 since  $mean(\hat{l}_{opt})$  is lower in Bühlmann and Künsch’s method. It is seen that imposing the lower limit on the flat-top window’s bandwidth (A2) has little effect on the results. Also, on average, Bühlmann and Künsch’s method has the lowest root-mean-square-error (*rmse*). Another striking feature of the latter approach is the high stability of the optimal block length selection as evidenced by  $\sigma(\hat{l}_{opt})$  in the table. This increased stability, compared to the A1, A2, can be attributed to the much narrower widths of the window functions used in equations 4.39-4.40 due to the inclusion of the inflation factor  $n^{4/21}$ . It seems plausible that a slightly higher choice of the constant  $c$  in Politis and White’s method would yield more stable results than for  $c = 2$  but this was not investigated further. Quite interestingly, the results from the stationary bootstrap (case A4) seem to be have a little less scatter than those from the MB bootstrap. Theory predicts that the SB bootstrap will have a higher variance (but similar bias) than MB estimates due to

the additional term in the estimation of the constant  $C_2$  (see eq. 4.43). This is indeed reflected in the predicted variance and *rmse* estimates from of equation 4.14 (these quantities are indicated in the parenthesis in table 4.2). However, the sample variance and *rmse* computed from the 100 estimates of  $Var^*[\hat{R}_{x_2x_2}(0)]$  are lower than those for the MB bootstrap (case A1,A2), indicating a good practical performance of the SB bootstrapping scheme. The same observations hold for the equivalent estimates at lag 1.

Computing the “true” optimal block length is not easy because an analytic expression for  $S_{IF(X,R(0))}^{(1)}$  is not readily available. A numerical estimate of  $S_{IF(X,R(0))}^{(1)} = (2\pi)^{-1} \sum_{k=-\infty}^{\infty} |k| C_{IF(X)}(k)$  by using the mean  $\bar{C}_{IF(X)}(k)$  computed from a many different simulated responses to approximate  $C_{IF(X)}(k)$  can be unreliable too. The reason being that a very large number of simulated responses are required for  $\bar{C}_{IF(X)}(k) \rightarrow C_{IF(X)}(k)$  at high lag. This requirement is very stringent because of the multiplication by  $|k|$  which blows up any error that prevents the convergence toward zero. Thus, a good numerical estimate, even with an improved estimate of  $\bar{C}_{IF(X)}(k)$  as described above, would also require a windowing operation which brings us back to the problem we are trying to solve. However, figure 4.7(b) gives us a very good idea of what the true optimal block length might be. The latter graph displays the bootstrapped variance of  $\hat{R}_{x_2x_2}(0)$  as a function of the block length used. This is shown for estimates computed from 50 different simulated responses. Additionally, the sample mean and the sample variance from these estimates is shown. It is seen that  $mean(Var[\hat{R}_{x_2x_2}(0)])$  does not increase significantly with increasing block length after it has reached a value of approximately  $1.3 \cdot 10^{-6}$  at a block length of about 13s. Thus, the same holds, on average, for the bias. The standard deviation, however, shown by the error bars still increases. Therefore, recalling that the optimal block length is the one that minimizes the *rmse*, it follows from this graph that the true value  $l_{opt}$  lies somewhere between 10s and 20s. We may conclude that both methods -Politis/White and Bühlmann/Künsch- yield, on average, a good estimate of the optimal block length. The negative bias responsi-

ble for the underestimate of  $Var[\hat{R}_{x_2x_2}(0)]$  cannot be avoided as it is intrinsic to the dependent bootstrap estimate and is clearly represented in equation 4.14. Due to the smaller *rmse* in case A4, we may say that Bühlmann and Künsch's method perform slightly better than Politis and White's procedure.

In practice, only one response history is in general available from which the ensemble of bootstrap replicas of the correlation function must be computed. Recall that it is desired to compute this ensemble such that the correlation function replicas yield the true covariance properties. In this particular case, this means that the variance at zero lag estimated from the ensemble of the 300 bootstrap replicas of the correlation function should be  $1.65 \cdot 10^{-6}$ , which is the "true" variance of the original correlation function, which was computed by using additional response histories that are not available in practice. Although, on average, the ensemble of bootstrap replicas estimated at optimal block length yields a good representation of the statistics of the true correlation function as shown in table 4.2, it is seen from figures 4.7, that depending on the particular response used, the corresponding ensemble of bootstrapped correlation functions may have a variance that is significantly lower or higher than that of the true correlation function. Unfortunately, there is not much one can do to eliminate this error apart from taking longer response records, since this variability is mainly due to the fact that we have to estimate the bootstrapped correlation functions from only  $n$  observations of the stochastic process. It is important to recognise, however, that this is *not* due to an inadequate selection of the block length as is clear from figure 4.7(b). Since the record length parameter  $n$  features in equation 4.14, we can get an estimate of the bias, variance and hence root-mean-square error of the bootstrapped estimate  $Var^*[\hat{R}_{x_2x_2}(0)]$  at optimal block length from a single response. The average values of these statistics, over the 100 simulated responses, are shown in table 4.2 in parentheses. It is seen the bias is, on average, very well estimated while the variance is significantly underestimated in all cases which is of course reflected in the corresponding *rms* errors. No definite explanation for this consistent under-

estimate was found. Looking at the *rms* error of the bootstrapped  $Var^*[\hat{R}_{x_2x_2}(0)]$  estimates for each of the 100 simulated responses at optimal block length, shown in figure 4.8(c), it is seen that the predictions from equation 4.14 are far from ideal to say the least. There seems to be a roughly linear correlation between  $Var^*[\hat{R}_{x_2x_2}(0)]$  and  $rmse(Var^*[\hat{R}_{x_2x_2}(0)])$ . This implies that whenever the bootstrap estimate of

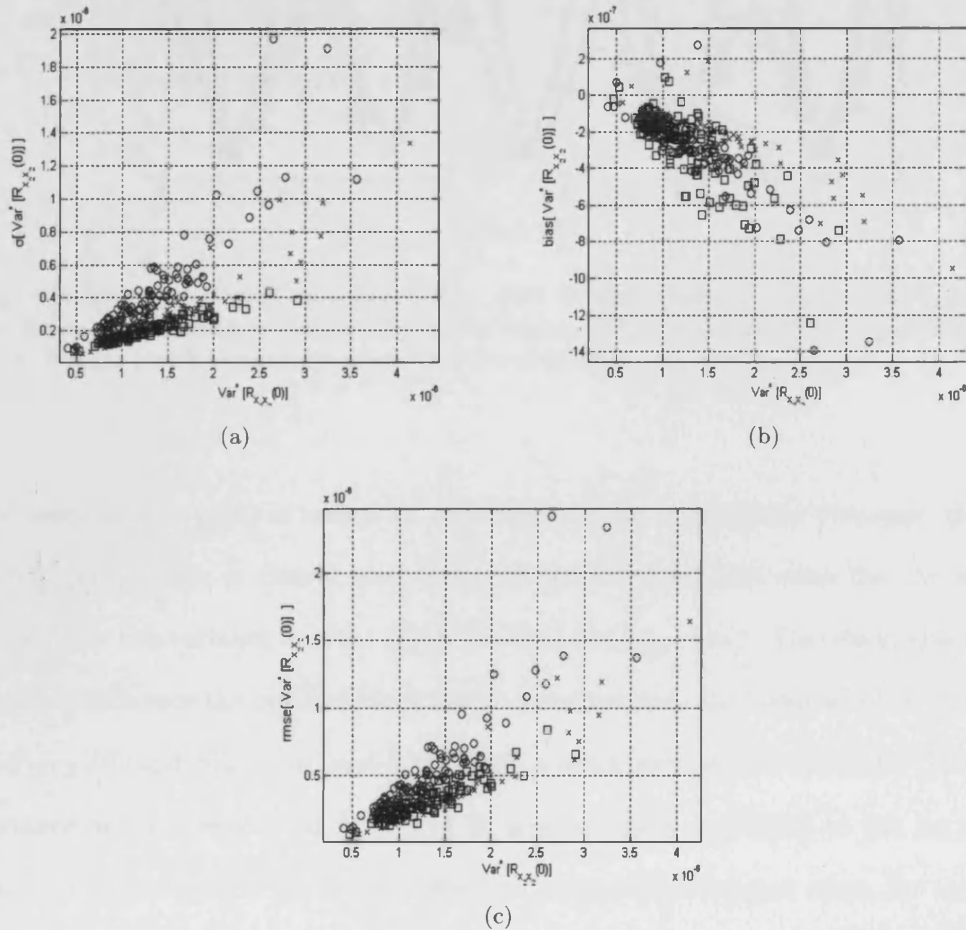


Fig. 4.8: Standard deviation (a), bias (b) and *rmse* (c) of the bootstrapped variance of the correlation function at zero lag,  $Var^*[R_{x_2x_2}(0)]$ , predicted by equation 4.14 at optimal block length for cases A2 [ $\times$ ], A3 [ $o$ ] and A4 [ $\square$ ]. The average values of these quantities are shown in table 4.2 in the parenthesis. As before, the values of  $Var^*[\hat{R}_{x_2x_2}(0)]$  are computed from 300 bootstrap replicas of  $\hat{R}_{x_2x_2}(0, 1)$ .

$Var^*[\hat{R}_{x_2x_2}(0)]$  is near or above the true value, the corresponding estimate of the *rms* error will be representative of the error in the actual estimate but on the other hand, an underestimate of  $Var^*[\hat{R}_{x_2x_2}(0)]$  will come with a *rms* error estimate that bears little relation to the true error. The reason for this behaviour is to be attributed to the different estimates of  $S_{IF(X)}(0)$  and  $S_{IF(X)}^{(1)}(0)$  as different response histories

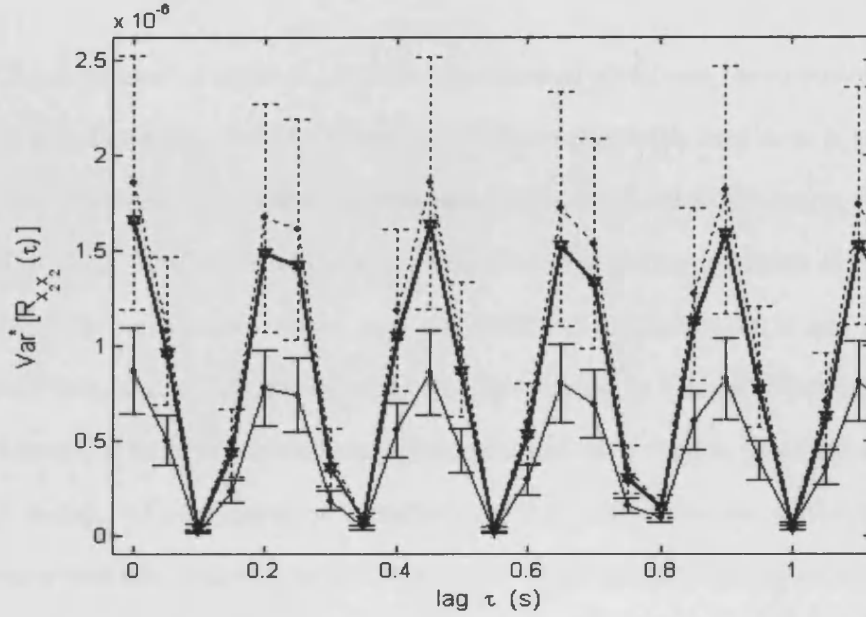


Fig. 4.9: Extrapolation of  $rmse(Var^*[\hat{R}_{x_2 x_2}(0)])$  to higher lags. The thick line represents the exact value and the solid and dotted line represent two different bootstrap estimates of  $Var^*[R_{x_2 x_2}(\tau)]$  with the extrapolated  $rmse$  represented by the errorbars.

are used. If  $S_{IF(X)}(0)$  is under- or overestimated for a particular response, then so is  $S_{IF(X)}^{(1)}(0)$ . This is clearly seen in figures 4.8(a) and 4.8(b) since the former determines the variance and the latter the bias (c.f. eq. 4.14). Therefore, this factor does not influence the optimal block length selection since the latter involves the ratio of  $S_{IF(X)}(0)$  and  $S_{IF(X)}^{(1)}(0)$ , and is therefore a much more robust estimate. The bias, variance or  $rmse$  estimated from 4.14 is, however, only applicable to the lag of the correlation function at which the influence function is computed since, for instance  $S_{IF(X,R(k))}^{(1)}(0) \neq S_{IF(X,R(\tau))}^{(1)}(0)$  for  $k \neq \tau$ . Nonetheless, since this  $rmse$  is representative of the variability due to insufficient observations  $n$  once  $l_{opt}$  is determined, we may assume that this variability is the same for  $Var^*[\hat{R}_{x_2 x_2}(r)]$ , for  $r > 0$  but *relative* to their respective amplitude of  $Var^*[\hat{R}_{x_2 x_2}(r)]$ . In other words, we may write

$$rmse(Var^*[\hat{R}_{x_2 x_2}(k)]) \approx rmse(Var^*[\hat{R}_{x_2 x_2}(0)]) \frac{Var^*[\hat{R}_{x_2 x_2}(0)]}{Var^*[\hat{R}_{x_2 x_2}(k)]} \quad (4.44)$$

This is shown by the errorbars for two different bootstrap estimates of  $Var[\hat{R}_{x_2 x_2}(k)]$  in figure 4.9.

The treatment of optimal block length selection given was based entirely on auto-correlation functions, but the extension to cross-correlation functions is similar since one may linearise the desired multivariate statistic in much the same way than in equation 4.33. The technical difficulty that arises lies in the definition of the influence function for multivariate series, and the definition of the latter is not obvious. It appears that an explicit definition was first formulated by Pires and Branco (2002) but the concept of multivariate influence functions had been used in practical applications much earlier, c.f. for instance Campbell (1978). The definition of the multivariate influence function bears similarity to partial derivatives and for this reason, Pires and Branco (2002) use the terminology “partial” influence function to denote the same quantity. Formally, for a statistic  $s$  depending on the distributions  $F_X$  and  $F_Y$  of  $X$  and  $Y$  respectively, the influence functions are defined as

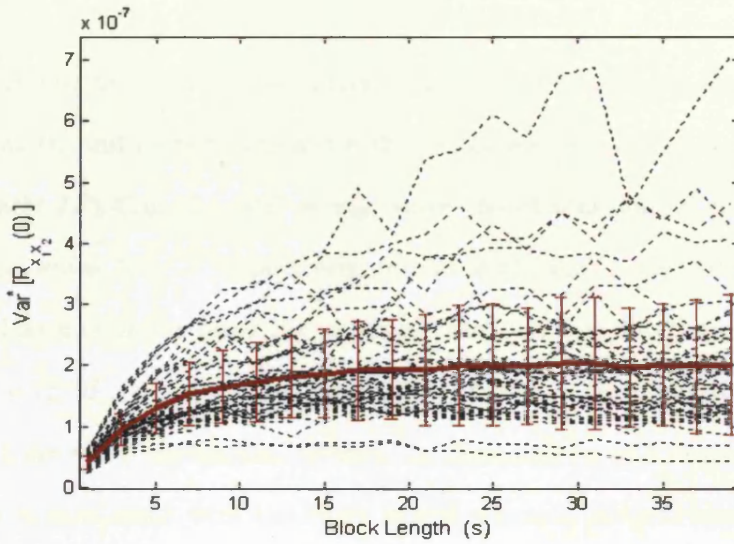
$$IF_X(X, Y) = \lim_{\epsilon \rightarrow 0} \frac{s((1 - \epsilon)F_X + \epsilon \delta_x, F_Y) - s(F_X, F_Y)}{\epsilon} \quad (4.45)$$

$$IF_Y(X, Y) = \lim_{\epsilon \rightarrow 0} \frac{s((1 - \epsilon)F_Y + \epsilon \delta_y, F_X) - s(F_X, F_Y)}{\epsilon} \quad (4.46)$$

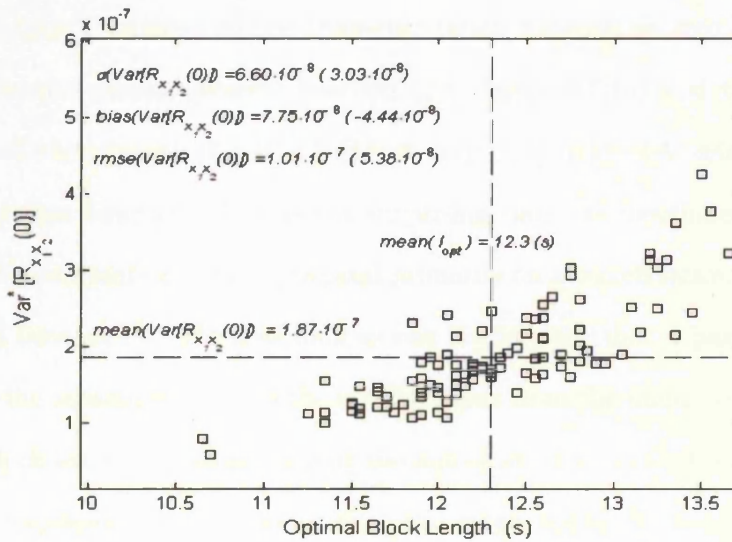
In other words, the theoretical multivariate influence function is then determined by perturbing only one of the distribution functions involved and the others remain unchanged. The definition above is given for the bivariate case since this is all that is needed and is readily generalised to the multivariate case. To evaluate  $IF_X(X, Y)$  and  $IF_Y(X, Y)$  in practice, we adopt again the method suggested in Bühlmann and Künsch (1999) (c.f. equation 4.37), which in the present situation means that an observation from only one of the two time series is eliminated in each case (also see Campbell (1978)). Along the lines of the linearisation in equation 4.33, we linearize the the statistic  $\hat{s}(X, Y)$  as

$$\hat{s}(X, Y) \approx s_\infty + \frac{1}{2} \left[ n^{-1} \sum_{i=1}^n IF(x_i, Y) + n^{-1} \sum_{i=1}^n IF(X, y_i) \right] \quad (4.47)$$

It is seen that the second term on the right-hand-side of equation 4.47 is again just an average over the two influence functions so that the theory developed above is



(a)



(b)

Fig. 4.10: (a) Bootstrap estimates of  $Var^*[R_{x_1 x_2}(0)]$  computed from 50 simulated responses as a function of the block length. The thick line is their mean and the errorbars indicate the standard deviation. The block length is increased in steps of  $2s$  ( $\Delta t = 0.05s$ ). At each block length, the bootstrap estimates of  $Var^*[R_{x_1 x_2}(0)]$  are computed from 300 bootstrap replicas of  $\hat{R}_{x_1 x_2}(0)$  (also c.f. figure 4.7(b)). (b) Scatter diagram depicts the BB bootstrap estimates  $Var^*[R_{x_1 x_2}(0)]$  as a function of the optimal block length  $l_{opt}$  from 100 simulated responses. Only the Buhlmann/Kuensch block selection method is shown. The values in parenthesis are the estimated standard deviation, bias and  $rmse$  from equation 4.14.

again directly applicable to the bivariate case. As for auto-correlation functions, the influence functions is used for the selection of the block length and, if desired, to get an estimate of the mean-square-error of the bootstrapped variance of the statistic of interest, i.e. the cross-correlation function in this case. Again, it is proposed to use

the influence function of the cross-correlation function at zero lag  $\hat{R}_{XY}(0)$ . It is easily seen that the influence functions for this parameter are  $IF(x_i, Y, R_{XY}(0)) = x_i y_i$  and, similarly  $IF(X, y_i, R_{XY}(0)) = x_i y_i$  since the elimination of either  $x_i$  or  $y_i$  in the the time-series  $X$  or  $Y$  respectively, results in the elimination of the term in the cross-correlation estimate involving either of them. This is illustrated in figures 4.10 on the same 2DOF system as used before except that in this case, the bootstrapped variance of the cross-correlation between the first and second degree-of-freedom of the system is considered with the block length selection method applied to the latter cross-correlation function. Figure 4.10(a) clearly shows that the dependence of the bootstrapped variance of the cross-correlation function at zero lag is much the same as for the auto-correlation function (c.f. figure 4.7(b)) and the mean identified optimal block length (figure 4.10(b)) is very close to the one estimated from the auto-correlation function. This is not surprising since -as mentioned earlier in this chapter- the constants  $C_1$  and  $C_2$  depend primarily on the correlation structure of the considered time series. Thus, as long as one is confident that a particular response history of the structure contains the contributions from the main system modes, the optimal block length for bootstrapping the auto-and cross-correlation functions of all measured responses can be obtained from this single response. Since in practice, the reference time-histories against which the other response are cross-correlated are chosen to those that have strong contributions of all the system modes, the latter lend themselves well for the selection of the optimal block length. However, if an estimate of the mean-square-error of the bootstrapped variance of the correlation function is desired too, the corresponding influence function must be chosen (c.f. 4.10(b)) because the response amplitudes measured at different locations on the structure vary. This does not affect the optimal block length due to the ratio involved in its computation.

To conclude this section, the problem of bootstrapping random decrement functions is commented. Bootstrapped RD functions were employed for modal analysis of SDOF systems by Kijewski and Kareem (2000, 2002). These authors formed the



bootstrap replica of the RD signatures by resampling the segments of data corresponding to each identified triggering point. This resampling scheme is, however, not ideal. Firstly, the resampling of segments may introduce bias in the bootstrapped RD functions. The reason -different than for correlation functions- is that reordering of the RD segments introduces artificial trigger conditions and therefore affects the estimate. Asmussen (1997) shows that sorting the segments can lead to bias in the form of apparent increased damping and frequency shifts. Although these effects may be less pronounced when the sorting of the trigger point follows a random resampling process rather than systematic sorting. Secondly, resampling segments of data as described above will not yield the correct covariance structure of the bootstrapped RD functions. To see this, consider the bootstrapped variance of the RD functions at zero lag for instance, which is in fact just the mean of the trigger points. Thus, the bootstrapped RD functions at zero lag computed according to Kijewski and Kareem (2002) effectively treat the trigger points as independent and their method is thus the same as Efron's original bootstrap. Consequently the correlation between the trigger points is lost and the bootstrapped correlation functions will not have the correct covariance structures.\* In fact, they will yield variance properties for instance that agree with the analytical approximate formulae derived by Vandiver *et al.* (1982) which were shown to be incorrect by Asmussen (1997), precisely because the dependence between different observations was neglected. Consequently, resampling blocks of segments corresponding to successive triggering points seems adequate to solve this issue, which in turn raises the question of the optimal block size. Since the RD function at zero lag is just the mean of the trigger points, the block selection methods used above for correlation functions are in principle directly applicable, with the time-series replaced by the trigger points. This procedure was tested by the author. Although the use of blocks of consecutive segments results in bootstrapped variances that reflect their dependence, the agreement with simulated variances was generally poor. Simulations at many different block lengths (similar to figure 4.10(a) and 4.7(b) indicated

---

\*We note that Kijewski and Kareem (2002) resample from non-overlapping segments but that does not change the argument used above.

that this disagreement is not to be attributed to an inadequate choice of block length only and the exact reason for this discrepancy could not be determined and further research is needed.

## 4.6 Summary and Discussion

In this chapter, the theory for bootstrapping time-series was presented with a focus on bootstrapped correlation functions. It was shown that the “blocks of blocks” bootstrap (BB) and the stationary bootstrap (SB) outperform the “naive” or moving blocks bootstrap (MB); more precisely, the MB scheme introduces bias in the bootstrapped correlation functions in much the same way as tapering which introduces an apparent increased damping to the system. While this bias is completely eliminated by the BB method, the stationary bootstrap only offers a slight improvement.

Whichever method is used for bootstrapping time-series, the data is collected into blocks to preserve its correlation structure. It was shown that the size of the blocks chosen significantly influences the covariances of the statistic that is bootstrapped and two methods were presented and compared to select the optimal block size. The applicability of these methods -originally derived for ac.f.- was shown to be applicable to multivariate time-series of MDOF systems. Both methods yielded a reasonably accurate estimate of the optimal block length but the Bühlmann and Künsch’s method was slightly more stable and is therefore preferred. Also, their method is slightly faster and does not require any tuning by user defined parameters as opposed to Politis and White’s method. For clarity, it is desired to put the choice of block length into the practical context initially set out to investigate, namely the uncertainty in operational modal parameters. Referring to figures 4.10(a) and 4.7(b), it transpires that if the response histories are chopped into blocks that are significantly smaller than the optimal block length, the variance of the ensemble of the bootstrapped correlation functions will be much smaller than their true variance dictated by the available record length and the modal parameters of the system as shown in the previous chapter. This

means that the ensemble of bootstrapped response models do not differ significantly from each other, or at least much less so than a set of response models that would be obtained if the modal test were repeated many times. As a result, the modal parameters identified from each of the bootstrapped response models would not differ significantly either and hence, any error bounds established on these grounds would be, in this particular example, grossly underestimated. While it is seen from figures 4.10(a) and 4.7(b) that the variance is, on average, more stable with respect to overestimates of the optimal block length, the choice of a too high block length is associated with a large variance so that the possibility of outliers increases, a situation we wish to avoid in practice. Using the bootstrap to determine the uncertainty in operational modal parameters is the subject of Chapter 7, but this brief example illustrates the significance of adequate block length selection. As a byproduct, a mean-square-error estimate of the variance of the bootstrapped response model is obtained. As, discussed above, however, the information the engineer can obtain from the latter estimate is limited, in particular when the true variance is underestimated.

Finally, a few remarks concerning the theory presented above need to be made. The rigorous theory behind the bootstrap and block length selection requires a great deal of mathematical and statistical sophistication and it was not possible to present it in its full breadth. In particular, many of the theorems used here are stated in the original papers under precise conditions such as the degree of dependence and mixing conditions in the time-series. Again, due to the highly technical nature of these conditions, they could not be verified exactly. This does however not necessarily imply that the bootstrap and block selection schemes presented above are not applicable to the problem at hand -that is structural response histories- but rather that the results may not be optimal. From a practical point of view, this does not pose any serious drawbacks as the practicing engineer has to deal with situation he or she is confronted with, whether the theoretical conditions are verified exactly or not. Moreover, the simulations in this chapter strongly support the practical adequacy

of both the bootstrap as well as the block selection algorithms for the operational response time-histories.

---

## CHAPTER 5

# PERTURBATION ANALYSIS FOR CORRELATION-DRIVEN IDENTIFICATION

---

### 5.1 Introduction

No matter which method is employed to identify the modal parameters of a given structure from output-only measurements, the stochastic nature of the in-operation loading conditions and the noise in the dynamic sensors means that the identified modal parameters are random variables. Thus, even in ideal cases where the structure exhibits purely linear behaviour and the input is band-limited white noise, there will be a certain variability associated with the identified modal parameters due the fact that one has to deal with a finite amount of data which prevents the convergence of the random variables to their true value. In addition to the random error, systematic (bias) errors can occur during the process. The user has to decide upon certain input parameters to “kick off” the estimator used and it is well known that this choice can significantly affect both bias and random error in the identified modal parameters.

The robustness with respect to noise of the classic identification techniques that lend themselves for in-operation modal analysis (see chart 1.4) is well documented in the original papers detailing these algorithms. Several authors have compared the

performance of these algorithms for noisy data on numerical models (Abdelghani *et al.*, 1998; Lew *et al.*, 1993) from input/output measurements and (Desforges *et al.*, 1995; Peeters and DeRoeck, 2001) from output-only data. While these papers expose the qualitative behaviour of the identified modal data and provide user guidelines for improved accuracy, the uncertainty in the modal estimates is not quantified. In recent years, however, the importance of being able to quantify the uncertainty in the identified modal data has been highlighted. For classical input/output modal analysis, Doebling and Farrar (2001a); Paez and Hunter (1998) used a bootstrap techniques to determine confidence intervals for identified modal frequencies and damping ratios from measured FRFs. Systematic errors were not considered.. For output-only identification from ARMA(V) models, much research has been done to estimate the associated variance of the modal parameters. Andersen and Brincker (1999) used the prediction error method (PEM) to obtain the covariance matrix of the identified modal parameters. Moreover, Andersen *et al.* (1995) developed a method to optimize the selection of the predictor and have shown that a proper selection of the initial conditions reduces the variability of the estimates. Also, the selection of the sampling interval has been treated by Ljung (1987), for instance. Other than that, the literature dealing with the uncertainties from other operational modal analysis techniques is, to the authors knowledge, scarce.

In this chapter, the perturbation analysis for covariance-driven stochastic realisations i.e. the SSI/Cov (Peeters and DeRoeck, 1999, 2001; VanOverschee and DeMoor, 1996) or, equivalently, the ERA as applied to operational data (Desforges and Cooper, 1997; Juang *et al.*, 1988) will be presented. This theory was developed in Longman and Juang (1987) and its sequel (Longman *et al.*, 1987). The latter authors, have applied this method to simulated data for classical input/output identification in the case where exact impulse response functions are perturbed by additive white noise. The aim is to extend this method to operational modal analysis and also take the possible bias into consideration. The present chapter provides the theory behind the

perturbation analysis and in the chapter to follow, it will be validated against Monte-Carlo type simulations to determine the accuracy we can expect from this technique in a practical situation. This study was motivated by the generally large variability associated with the estimated modal damping ratios, in particular when the identification has to be performed from short data sequences (Pridham and Wilson, 2003). Cauberghe *et al.* (2004) have presented a FRF-based technique to deal with such cases. This method enables the estimation of the variability due to noise disturbance and can account for using short data sets, using the statistics developed in the previous chapter. Moreover, the bias that arises from sources such as the algorithm itself or from filtering the data can be accurately estimated. As a result, both random and systematic error that one can expect in the identified data can be determined from *a single set of in-operational measurements*. In addition, this method allows the user to determine what choices of input parameters such as the dimension of the Hankel matrix or the sampling interval minimize the error in the estimated modal data.

## 5.2 Overview of the Theory

Suppose the response is measured at  $p$  sensors for a total time  $T$  and  $r$  sensors serve as reference. In order to realise the system using the SSI/Cov, the response time-histories are used to form the one-sided cross-correlation functions between the  $p$  sensors and the  $r$  references resulting in  $p \times r$  cross-correlation functions which are then assembled into the Hankel matrices  $\mathcal{H}_0$  and  $\mathcal{H}_1$  as described in Chapter 2. For notational convenience, these Hankel matrices will henceforth be denoted by  $\mathcal{H}_0(\underline{0})$  and  $\mathcal{H}_1(\underline{0})$  respectively. The meaning of this notation will become clear shortly. Suppose that only the first  $t_c$  seconds of the one-sided cross-correlation functions are included in the analysis i.e. the first  $n_c = t_c/\Delta t$  data points from each of the  $p \times r$  correlation function, where  $\Delta t$  denotes the sampling interval. Thus, there will be a total of  $N = (p \times r \times n_c)$  data points used in the modal parameter extraction. Now suppose that a single data point of any of these sample cross-correlation functions is perturbed - for instance the  $n^{th}$  data point in the cross-correlation function between

the  $p^{th}$  output and the  $r^{th}$  reference sensor. Out of the  $N = (p \times r \times n_c)$  available data points, let this point be indexed as the  $j^{th}$  data point and let the magnitude of its perturbation be expressed by the zero-mean random variable  $\epsilon_j$ . Then, the perturbed Hankel matrices, denoted by  $\mathcal{H}_0(\epsilon_j)$  and  $\mathcal{H}_1(\epsilon_j)$ , may be approximated in terms of the *unperturbed* Hankel matrices  $\mathcal{H}_0(\underline{0})$  and  $\mathcal{H}_1(\underline{0})$  according to the linearisation

$$\mathcal{H}_0(\epsilon_j) = \mathcal{H}_0(\underline{0}) + \epsilon_j \delta_j(\mathcal{H}_0) \quad (5.1)$$

$$\mathcal{H}_1(\epsilon_j) = \mathcal{H}_1(\underline{0}) + \epsilon_j \delta_j(\mathcal{H}_1) \quad (5.2)$$

where the matrices  $\delta_j(\mathcal{H}_0)$  and  $\delta_j(\mathcal{H}_1)$  are matrices consisting entirely of zeros except from being unity in each entry associated with the data point perturbed by  $\epsilon_j$ . In practice, all  $N$  data points in the sample correlation functions will be corrupted so that the Hankel matrices perturbed by  $\epsilon_1, \epsilon_2 \dots \epsilon_N$  are given by

$$\mathcal{H}_0(\underline{\epsilon}) = \mathcal{H}_0(\underline{0}) + \sum_{j=1}^N \epsilon_j \delta_j(\mathcal{H}_0) \quad (5.3)$$

$$\mathcal{H}_1(\underline{\epsilon}) = \mathcal{H}_1(\underline{0}) + \sum_{j=1}^N \epsilon_j \delta_j(\mathcal{H}_1) \quad (5.4)$$

where the vector  $\underline{\epsilon}$  is defined as  $\underline{\epsilon} = [\epsilon_1, \epsilon_2, \dots, \epsilon_N]$ .

**Remark:** *It is important to note that  $\mathcal{H}_0(\underline{0})$  and  $\mathcal{H}_1(\underline{0})$  denote the Hankel matrices formed by the sample correlation functions from the original data. Although the notation may suggest that they are assembled from the true correlation functions. The latter, however, are not known and the estimated cross-correlation functions need to be used instead and thus serve as the “basis” from which the perturbation is applied.*

Let the generic parameter  $\chi$  denote any modal parameter of interest. The change in the SSI/Cov-identified result  $\chi(\underline{0})$  from the original data assembled in  $\mathcal{H}_0(\underline{0})$  and  $\mathcal{H}_1(\underline{0})$ , due to the perturbation  $\underline{\epsilon}$  can then be approximated by a Taylor expansion



about the origin as

$$\chi(\underline{\epsilon}) \approx \chi(\underline{0}) + \sum_{j=1}^N \epsilon_j \delta_j(\chi) + \sum_{k=1}^N \sum_{j=1}^N \epsilon_j \epsilon_k \delta_{jk}(\chi) + \dots \quad (5.5)$$

where, for notational convenience, we have introduced the differential operators defined by

$$\delta_j(\cdot) \equiv \left. \frac{\partial(\cdot)}{\partial \epsilon_j} \right|_{\underline{\epsilon}=\underline{0}} \quad (5.6)$$

$$\delta_{jk}(\cdot) \equiv \left. \frac{1}{2} \frac{\partial^2(\cdot)}{\partial \epsilon_j \partial \epsilon_k} \right|_{\underline{\epsilon}=\underline{0}} \quad (5.7)$$

Equation 5.5 provides the basis to calculate the variance and bias of the identified modal parameters.

### 5.2.1 Variance of $\chi$ , $Var[\chi]$

Using expansion 5.5 through *linear* terms only, the variance of  $\chi(\underline{\epsilon})$  can be estimated as

$$Var[\chi(\underline{\epsilon})] \approx \sum_{j=1}^N Var[\epsilon_j] \delta_j^2(\chi) + 2 \sum_{\substack{j=1 \\ j \neq k}}^N \sum_{k=1}^N Cov[\epsilon_j, \epsilon_k] \delta_j(\chi) \delta_k(\chi) \quad (5.8)$$

This represents how much scatter one would expect to find in the estimated modal parameter due to the stochastic disturbance  $\underline{\epsilon}$  if the identification were performed for many repetitions of the experiment. It is noted that in traditional modal analysis, where the disturbance is due to noise only the second term drops out since  $\epsilon_j$  and  $\epsilon_k$  are uncorrelated (Longman *et al.*, 1987). For operational modal analysis, it will be seen that this term plays a crucial role in determining the error in the identified modal parameters.

### 5.2.2 Quadratic Bias of $\chi$ , $b_Q[\chi]$

Applying the expectation operator to eqn. 5.5 gives

$$E[\chi(\underline{\epsilon})] \approx \chi(\underline{0}) + \sum_{j=1}^N \text{Var}[\epsilon_j] \delta_{jj}(\chi) + \sum_{\substack{j=1 \\ j \neq k}}^N \sum_{k=1}^N \text{Cov}[\epsilon_j, \epsilon_k] \delta_{jk}(\chi) \quad (5.9)$$

It is seen in eqn. 5.9 that the expected value of  $\chi(\underline{\epsilon})$  does not result in  $\chi(\underline{0})$  but instead, a bias error arises due to the quadratic term in the expansion. This bias is therefore referred to as the **quadratic bias** (Longman *et al.*, 1987), denoted by  $b_Q$ , of the estimated parameter  $\chi$ , and is given by

$$b_Q[\chi(\underline{\epsilon})] = E[\chi(\underline{\epsilon})] - \chi(\underline{0}) \approx \sum_{j=1}^N \text{Var}[\epsilon_j] \delta_{jj}(\chi) + \sum_{\substack{j=1 \\ j \neq k}}^N \sum_{k=1}^N \text{Cov}[\epsilon_j, \epsilon_k] \delta_{jk}(\chi) \quad (5.10)$$

The quadratic bias  $b_Q$  expresses how much systematic error we can expect on average due to fact that the random perturbation  $\underline{\epsilon}$  is passed through a quadratic nonlinearity and does not average to zero. To the extent that quadratic terms dominate higher order terms, this yields the full bias due to the nonlinear nature of the algorithm.

### 5.2.3 Truncation Bias of $\chi$ , $b_T[\chi]$

The actual situation, however, is further complicated by the fact that stochastic realizations involve truncation of near zero singular values after choosing an appropriate model order. While it is desirable to truncate near zero singular values that arise due to noise in the data, truncation can however cause significant bias in the estimated modal parameters when the truncated singular values contain system dynamics (Cooper, 1989; Juang and Pappa, 1986). Again, a perturbation analysis can be employed to investigate the effect of truncated singular values on the system modes by formulating an additive perturbation to the eigenvalues of the identified system matrix  $\mathbf{A}$  in terms of the truncated singular values and corresponding singular spaces.

Consider the singular value decomposition (SVD) of the  $n' \times g$  Hankel matrix  $\mathcal{H}_0$  with  $n' \geq g$  (cf. Chapter 2 section 2.3.2)

$$\mathcal{H}_0 = \mathbf{U}\mathbf{\Sigma}\mathbf{V}^T \quad \text{with} \quad \mathbf{\Sigma} = \begin{bmatrix} \mathbf{\Sigma}_1 & \mathbf{0} \\ \mathbf{0} & \mathbf{\Sigma}_2 \\ \mathbf{0} & \mathbf{0} \end{bmatrix} \quad (5.11)$$

where  $\mathbf{\Sigma}_1$  is an  $n \times n$  diagonal matrix containing the first  $n$  singular values of  $\mathbf{\Sigma}$  and the remaining  $(g - n)$  singular values form the diagonal of  $\mathbf{\Sigma}_2$ <sup>‡</sup>. This singular value decomposition of  $\mathcal{H}_0$  can be partitioned as

$$\mathcal{H}_0 = \begin{bmatrix} \mathbf{U}_1 & \mathbf{U}_{21} & \mathbf{U}_{22} \end{bmatrix} \begin{bmatrix} \mathbf{\Sigma}_1 & \mathbf{0} \\ \mathbf{0} & \mathbf{\Sigma}_2 \\ \mathbf{0} & \mathbf{0} \end{bmatrix} \begin{bmatrix} \mathbf{V}_1^T \\ \mathbf{V}_2^T \end{bmatrix} \quad (5.12)$$

Define  $\mathbf{U}_2 = [\mathbf{U}_{21}\mathbf{U}_{22}]$ . Suppose that, for the modal parameters identification, only the first  $n$  singular values in  $\mathbf{\Sigma}$  of the singular value decomposition of  $\mathcal{H}_0$  are retained. In other words, the singular values in  $\mathbf{\Sigma}_2$  are set to zero. Thus, according to eqns. 2.48 and 2.46 in Chapter 2,  $\mathcal{H}_0$  and  $\mathcal{H}_1$  may be expressed as

$$\mathcal{H}_0 = \mathbf{U}_1\mathbf{\Sigma}_1\mathbf{V}_1^T \quad (5.13)$$

$$\mathcal{H}_1 = \mathbf{U}_1\mathbf{\Sigma}_1^{1/2}\mathbf{A}\mathbf{\Sigma}_1^{1/2}\mathbf{V}_1^T \quad (5.14)$$

where  $\mathbf{A}$  is the  $n \times n$  identified system or state matrix. As described in Chapter 2, the eigenvalues  $\lambda_i$  and eigenvectors  $\mathbf{p}_i$ ,  $i = 1, 2, \dots, n$ , of  $\mathbf{A}$  yield the modal damping ratios, frequencies and mode shapes. It should be noted that equations 5.13 and 5.14 are only approximations of  $\mathcal{H}_0$  and  $\mathcal{H}_1$  due to the truncation that has been performed. However, in order not to introduce any confusion about approximations made in the perturbation analysis, the equality sign will be retained because truncation of singu-

---

<sup>‡</sup>The assumption that the number of rows exceeds the number of columns in  $\mathcal{H}_0$  was dictated by the fact that, generally, the total number of sensors exceeds the number of reference sensors. This assumption does, however, not cause any loss of generality and the derivation for the case in which  $n' < g$  is the same.

lar values is common practice and it is understood that any set of identified modal parameters is just an approximation to the true system parameters. To investigate to what extent this truncation affects the SSI/Cov-identified modal parameters, we form a new  $n' \times n'$  matrix, denoted  $\mathbf{A}'$ , as

$$\mathbf{A}' = \mathcal{H}_1 \mathcal{H}_0^\dagger = \mathcal{H}_1 \mathbf{V} \begin{bmatrix} \boldsymbol{\Sigma}_1^{-1} & \mathbf{0} \\ \mathbf{0} & \mathbf{0} \end{bmatrix} \mathbf{U}^T \quad (5.15)$$

where  $(\cdot)^\dagger$  denotes the pseudo-inverse and it is seen that  $\mathcal{H}_0$  has been truncated at the chosen model order  $n$ . The next step consists in establishing that the first  $n$  eigenvalues of  $\mathbf{A}'$  are identical to the eigenvalues of the  $n \times n$  system matrix  $\mathbf{A}$ . To do so, we diagonalize  $\mathbf{A}'$  as follows: consider the eigenvalue equation of  $\mathbf{A}'$

$$\mathbf{A}' \mathbf{p}'_i = \lambda'_i \mathbf{p}'_i \quad \text{for } i = 1, 2, \dots, n' \quad (5.16)$$

where  $\mathbf{p}'_i$  and  $\lambda'_i$  denote the  $i^{\text{th}}$  eigenvector and corresponding eigenvalue of  $\mathbf{A}'$  respectively. Pre-multiplying equation 5.16 by

$$\begin{bmatrix} \boldsymbol{\Sigma}_1^{-\frac{1}{2}} & \mathbf{0} \\ \mathbf{0} & \mathbf{I} \end{bmatrix} \mathbf{U}^T$$

and using equation 5.14, this equation can be rewritten as

$$\begin{bmatrix} \mathbf{A} & \mathbf{0} \\ \mathbf{U}_2^T \mathcal{H}_1 \mathbf{V}_1 \boldsymbol{\Sigma}_1^{-\frac{1}{2}} & \mathbf{0} \end{bmatrix} \bar{\mathbf{p}}_i = \lambda'_i \bar{\mathbf{p}}_i \quad \text{for } i = 1, 2, \dots, n' \quad (5.17)$$

$$\text{with } \bar{\mathbf{p}}_i = \begin{bmatrix} \boldsymbol{\Sigma}_1^{-\frac{1}{2}} & \mathbf{0} \\ \mathbf{0} & \mathbf{I} \end{bmatrix} \mathbf{U}^T \mathbf{p}'_i \Leftrightarrow \mathbf{p}'_i = \mathbf{U} \begin{bmatrix} \boldsymbol{\Sigma}_1^{\frac{1}{2}} & \mathbf{0} \\ \mathbf{0} & \mathbf{I} \end{bmatrix} \bar{\mathbf{p}}_i \quad (5.18)$$

We conclude from the first  $n \times n$  partition of the above equation that  $\lambda'_i = \lambda_i$ ,  $i = 1, 2, \dots, n$ . In other words, the first  $n$  eigenvalues of  $\mathbf{A}'$  are identical to the eigenvalues  $\lambda_i$  of the identified state matrix  $\mathbf{A}$ . Furthermore, we can partition the vectors  $\bar{\mathbf{p}}_i^T$  as  $[\mathbf{p}_i^T \hat{\mathbf{p}}_i^T]$ . As before,  $\mathbf{p}_i$ , for  $i = 1, 2, \dots, n$  denotes the eigenvectors of  $\mathbf{A}$

and the definition of  $\hat{\mathbf{p}}_i^T$  follows from equation 5.18 as

$$\hat{\mathbf{p}}_i = \frac{1}{\lambda_i} \mathbf{U}_2^T \mathcal{H}_1 \mathbf{V}_1 \boldsymbol{\Sigma}_1^{-\frac{1}{2}} \mathbf{p}_i \quad \text{for } i = 1, 2, \dots, n \quad (5.19)$$

Thus, the eigenvectors  $\mathbf{p}'_i$  corresponding to the first  $n$  eigenvalues of  $\mathbf{A}'$ , can be established using the partitioned vectors  $\bar{\mathbf{p}}_i$  in equation 5.18 so that the first  $n$  columns of the eigenvector matrix of  $\mathbf{A}'$  can be written as

$$\mathbf{P}'_{1:n} = \mathbf{U} \begin{bmatrix} \boldsymbol{\Sigma}_1^{\frac{1}{2}} & \mathbf{0} \\ \mathbf{0} & \mathbf{I} \end{bmatrix} \begin{bmatrix} \mathbf{P} \\ \hat{\mathbf{P}} \end{bmatrix} \quad (5.20)$$

where the  $n' \times n$  matrix  $[\mathbf{P}^T \quad \hat{\mathbf{P}}^T]^T$  contains the  $n' \times 1$  vectors  $[\mathbf{p}_i^T \quad \hat{\mathbf{p}}_i^T]^T$  in its columns, for  $i = 1, 2, \dots, n$ . Since the last  $(n' - n)$  columns of the  $n' \times n'$  matrix on the left-hand-side of equation 5.18 are zero, it follows that the last  $(n' - n)$  eigenvalues of  $\mathbf{A}'$  are identically zero and the corresponding  $(n' - n)$  eigenvectors can be chosen to be the  $n' \times 1$  unit vectors  $\mathbf{e}_j$  defined as the  $j^{\text{th}}$  column of the  $n' \times n'$  identity matrix. The matrix  $\mathbf{A}'$  can therefore be diagonalized as

$$\begin{bmatrix} \mathbf{P} & \mathbf{0} \\ \hat{\mathbf{P}} & \mathbf{I} \end{bmatrix}^{-1} \begin{bmatrix} \mathbf{A} & \mathbf{0} \\ \mathbf{U}_2^T \mathcal{H}_1 \mathbf{V}_1 \boldsymbol{\Sigma}_1^{-\frac{1}{2}} & \mathbf{0} \end{bmatrix} \begin{bmatrix} \mathbf{P} & \mathbf{0} \\ \hat{\mathbf{P}} & \mathbf{I} \end{bmatrix} = \begin{bmatrix} \boldsymbol{\Lambda} & \mathbf{0} \\ \mathbf{0} & \mathbf{0} \end{bmatrix} = \boldsymbol{\Lambda}' \quad (5.21)$$

where  $\boldsymbol{\Lambda} = \text{diag} \{ \lambda_1, \lambda_2, \dots, \lambda_n \}$  is the eigenvalue matrix of  $\mathbf{A}$ . The above equation thus establishes that  $\mathbf{A}'$  is a nondefective matrix whose  $n$  nonzero eigenvalues are identical to the eigenvalues of  $\mathbf{A}$ . The  $n'$  eigenvectors of  $\mathbf{A}'$  are given by equation 5.18 as

$$\mathbf{P}' = \mathbf{U} \begin{bmatrix} \boldsymbol{\Sigma}_1^{\frac{1}{2}} & \mathbf{0} \\ \mathbf{0} & \mathbf{I} \end{bmatrix} \begin{bmatrix} \mathbf{P} & \mathbf{0} \\ \hat{\mathbf{P}} & \mathbf{I} \end{bmatrix} \quad (5.22)$$

This fact is now exploited to determine the effect of the truncated singular values on the  $n$  eigenvalues of  $\mathbf{A}$  as an additive perturbation by reinstating  $\boldsymbol{\Sigma}_2$ . To do so, we use the full SVD of the Hankel matrices (eqn. 5.11), i.e. no truncation is performed,

and form the matrix  $\mathbf{A}''$  in the same fashion than  $\mathbf{A}'$ , that is

$$\mathbf{A}'' = \mathcal{H}_1 \mathcal{H}_0^\dagger = \mathcal{H}_1 \begin{bmatrix} \mathbf{V}_1 & \mathbf{V}_2 \end{bmatrix} \begin{pmatrix} \Sigma_1^{-1} & \mathbf{0} & \mathbf{0} \\ \mathbf{0} & \Sigma_2^{-1} & \mathbf{0} \end{pmatrix} \begin{bmatrix} \mathbf{U}_1^T \\ \mathbf{U}_{21}^T \\ \mathbf{U}_{22}^T \end{bmatrix} \quad (5.23)$$

$$= \mathcal{H}_1 \mathbf{V}_1 \Sigma_1^{-1} \mathbf{U}_1^T + \mathcal{H}_1 \mathbf{V}_2 \Sigma_2^{-1} \mathbf{U}_{21}^T \quad (5.24)$$

where the first term in equation 5.24 is recognised to be  $\mathbf{A}'$ , that is

$$\mathbf{A}'' = \mathbf{A}' + \mathcal{H}_1 \mathbf{V}_2 \Sigma_2^{-1} \mathbf{U}_{21}^T \quad (5.25)$$

Pre- and post-multiplying equation 5.25 by  $\mathbf{P}'^{-1}$  and  $\mathbf{P}'$  then yields

$$\mathbf{P}'^{-1} \mathbf{A}'' \mathbf{P}' = \mathbf{P}'^{-1} \mathbf{A}' \mathbf{P}' + \mathbf{P}'^{-1} (\mathcal{H}_1 \mathbf{V}_2 \Sigma_2^{-1} \mathbf{U}_{21}^T) \mathbf{P}' \quad (5.26)$$

Introducing the notation

$$\Lambda'' = \mathbf{P}'^{-1} \mathbf{A}'' \mathbf{P}' \quad (5.27)$$

$$\Lambda' = \mathbf{P}'^{-1} \mathbf{A}' \mathbf{P}' \quad (5.28)$$

$$\Delta \Lambda' = \mathbf{P}'^{-1} (\mathcal{H}_1 \mathbf{V}_2 \Sigma_2^{-1} \mathbf{U}_{21}^T) \mathbf{P}' \quad (5.29)$$

equation 5.26 may then be expressed compactly as

$$\Lambda'' = \Lambda' + \Delta \Lambda' \quad (5.30)$$

Bearing in mind that the first  $n$  eigenvalues of  $\mathbf{A}'$  are identical to the eigenvalues of  $\mathbf{A}$ , that is, the first  $n$  diagonal elements in  $\Lambda'$  are the eigenvalues of  $\mathbf{A}$ , it is clear from the above equation that  $\Delta \Lambda'$  additively affects the identified system eigenvalues. However, since the matrix  $\Delta \Lambda'$  is not diagonal, equation 5.30 does not directly represent the effect on the system eigenvalues. Thus, to take into account the effect of the off-diagonal terms in  $\Delta \Lambda'$  on  $\Lambda'$ , (Longman *et al.*, 1987) introduce the perturbation

parameter  $\rho$  into equation 5.30 as follows

$$\mathbf{\Lambda}'' = \mathbf{\Lambda}' + \rho \mathbf{\Delta} \mathbf{\Lambda}' \quad (5.31)$$

The interpretation of the above equation requires a little care:  $\mathbf{A}$  is the system matrix identified by the SSI/Cov *when small non-zero singular values have been truncated* and its eigenvalues are the first  $n$  diagonal elements in  $\mathbf{\Lambda}'$ . Thus, the first  $n$  eigenvalues in  $\mathbf{\Lambda}'$  already contain the error introduced by the truncation and  $\mathbf{\Delta} \mathbf{\Lambda}'$  in fact cancels this error as the latter term arises due to *reinstating* the truncated singular values in  $\mathbf{\Sigma}_2$  (see eqns. 5.23). It follows that  $\rho = 0$  describes the situation where the singular values in  $\mathbf{\Sigma}_2$  are set to zero, i.e. small non-zero singular values have been truncated while  $\rho = 1$  yields the desired correction to cancel out any error introduced due to truncation of non-zero singular values. In Longman *et al.* (1987), the effect of this truncation on any modal parameter is formulated using a Taylor expansion in  $\rho$

$$\chi(\underline{\epsilon}, \rho) \approx \chi(\underline{\epsilon}, 0) + \rho \left. \frac{\partial \chi(\underline{\epsilon}, \rho)}{\partial \rho} \right|_{\rho=0} + \rho^2 \frac{1}{2} \left. \frac{\partial^2 \chi(\underline{\epsilon}, \rho)}{\partial \rho^2} \right|_{\rho=0} \quad (5.32)$$

which can be re-written as

$$\chi(\underline{\epsilon}, 1) \approx \chi(\underline{\epsilon}) + \delta_\rho [\chi(\underline{\epsilon})] + \delta_{\rho\rho} [\chi(\underline{\epsilon})] \quad (5.33)$$

where  $\rho$  is set to unity in order to give the desired change introduced by the truncation as described above and where we have used the differential operator

$$\delta_\rho (\cdot) = \left. \frac{\partial (\cdot)}{\partial \rho} \right|_{\rho=0} \quad (5.34)$$

$$\delta_{\rho\rho} (\cdot) = \left. \frac{1}{2} \frac{\partial^2 (\cdot)}{\partial \rho^2} \right|_{\rho=0} \quad (5.35)$$

Setting the perturbation  $\underline{\epsilon} = \underline{0}$  in equation 5.33 then gives

$$\chi(\underline{0}, 1) \approx \chi(\underline{0}) + \delta_\rho [\chi(\underline{0})] + \delta_{\rho\rho} [\chi(\underline{0})] \quad (5.36)$$

It follows from the interpretation of equation 5.31 that the first term on the right-hand side in eqn. 5.33,  $\chi(\underline{0})$ , represents the SSI/Cov-identified modal parameters when the chosen set of small singular values has been set to zero. This is exactly the same quantity as the first term on the right-hand side in eqn. 5.5. The linear and quadratic terms in 5.36,  $\delta_\rho[\chi(\underline{0})]$  and  $\delta_{\rho\rho}[\chi(\underline{0})]$  respectively, correct the error due to truncation in the SSI/Cov-identified modal parameters. As will be shown in the next section, the first order term  $\delta_\rho[\chi(\underline{0})]$  accounts for the correction expressed by the diagonal terms of  $\Delta\Lambda'$  while the second order term takes into account the correction due to the off-diagonal terms. The sum of the linear and quadratic terms is therefore the additive inverse of the bias error in  $\chi(\underline{0})$  so that we may define the **truncation bias**,  $b_T$  in the SSI/Cov-identified modal parameters as

$$b_T[\chi(\underline{0})] \equiv -[\delta_\rho[\chi(\underline{0})] + \delta_{\rho\rho}[\chi(\underline{0})]] \quad (5.37)$$

It is noted that the expression for the truncation bias given in Longman *et al.* (1987) is of the opposite sign than the expression given above. However, the explanation provided above leading to equation 5.37 as well as the numerical simulations to follow support the expression given here.

An remark deserves to be made about the above computation. The introduction of the parameter  $\rho$  to linearise the truncation bias appears somewhat artificial. Firstly, the parameter  $\rho$  has only physical meaning when it is treated *discretely*:  $\rho = 0$  describes the situation when small singular values are set to zero and  $\rho = 1$  the case when the identification is performed at full model order. This implies that at 0, the point at which the eigenvalue derivatives are evaluated, the equation is not continuous and therefore, in theory, the eigenvalue derivative should not exist. No concern was raised by Longman *et al.* (1987) and the extent of its effect on the truncation bias, its variance and quadratic bias needs to be established by simulation.



#### 5.2.4 Variance of the Truncation Bias of $\chi$ , $\text{Var} [b_T (\chi)]$

If the estimated modal parameters contain a random error, then so will the estimated truncation bias. This can be concluded from equation 5.33 so that the expression for the truncation bias must be rewritten as a function of the random perturbation  $\underline{\epsilon}$  so that  $b_T [\chi (\underline{\epsilon})] \equiv -[\delta_\rho [\chi (\underline{\epsilon})] + \delta_{\rho\rho} [\chi (\underline{\epsilon})]]$ . As a result, the truncation bias can only be estimated up to a random error. The latter can be evaluated in the same fashion as for the modal parameters themselves.

The variance of  $b_T [\chi (\underline{\epsilon})]$  is found by expanding this expression in a Taylor series as

$$\begin{aligned}
 -[\delta_\rho [\chi (\underline{\epsilon})] + \delta_{\rho\rho} [\chi (\underline{\epsilon})]] &\approx -[\delta_\rho [\chi (\underline{0})] + \delta_{\rho\rho} [\chi (\underline{0})]] & (5.38) \\
 &- \sum_{j=1}^N \epsilon_j (\delta_{j\rho} (\chi) + \delta_{j\rho\rho} (\chi)) \\
 &- \sum_{j=1}^N \sum_{k=1}^N \epsilon_j \epsilon_k (\delta_{jk\rho} (\chi) + \delta_{jk\rho\rho} (\chi))
 \end{aligned}$$

where the differential operators  $\delta_{j\rho} (\cdot)$ ,  $\delta_{j\rho\rho} (\cdot)$ ,  $\delta_{jk\rho} (\cdot)$  and  $\delta_{jk\rho\rho} (\cdot)$  are defined as

$$\delta_{j\rho} (\cdot) = \left. \frac{\partial}{\partial \epsilon_j} \left[ \frac{\partial (\cdot)}{\partial \rho} \right] \right|_{\rho=0} \Bigg|_{\epsilon_j=0} \quad (5.39)$$

$$\delta_{j\rho\rho} (\cdot) = \left. \frac{1}{2} \frac{\partial}{\partial \epsilon_j} \left[ \frac{\partial^2 (\cdot)}{\partial \rho^2} \right] \right|_{\rho=0} \Bigg|_{\epsilon_j=0} \quad (5.40)$$

$$\delta_{jk\rho} (\cdot) = \left. \frac{1}{2} \frac{\partial^2}{\partial \epsilon_j \partial \epsilon_k} \left[ \frac{\partial (\cdot)}{\partial \rho} \right] \right|_{\rho=0} \Bigg|_{\epsilon_j=0} \quad (5.41)$$

$$\delta_{jk\rho\rho} (\cdot) = \left. \frac{1}{4} \frac{\partial^2}{\partial \epsilon_j \partial \epsilon_k} \left[ \frac{\partial^2 (\cdot)}{\partial \rho^2} \right] \right|_{\rho=0} \Bigg|_{\epsilon_j=0} \quad (5.42)$$

Taking equation 5.38 up to linear terms only, we can find the variance of the truncation

bias as

$$\begin{aligned} \text{Var}[b_T(\chi)] &\approx \sum_{j=1}^N \text{Var}[\epsilon_j] \left( \delta_{j\rho}(\chi) + \delta_{j\rho\rho}(\chi) \right) \\ &+ 2 \sum_{\substack{j=1 \\ j \neq k}}^N \sum_{k=1}^N \text{Cov}[\epsilon_j \epsilon_k] \left( \delta_{j\rho}(\chi) + \delta_{j\rho\rho}(\chi) \right) \left( \delta_{k\rho}(\chi) + \delta_{k\rho\rho}(\chi) \right) \end{aligned} \quad (5.43)$$

### 5.2.5 Quadratic Bias of Truncation Bias of $\chi$ , $b_{QT}[\chi]$

Taking the expected value of eqn. 5.38 it can be seen that the truncation bias is itself biased due to the quadratic term. Proceeding in the same way than for the quadratic bias of  $\chi$ , the **quadratic bias of the the truncation bias**,  $b_{TQ}$ , can be found to be

$$b_{QT}[\chi] \approx - \sum_{j=1}^N \text{Var}[\epsilon_j] \left( \delta_{jj\rho}(\chi) + \delta_{jj\rho\rho}(\chi) \right) - \sum_{\substack{j=1 \\ j \neq k}}^N \sum_{k=1}^N \text{Cov}[\epsilon_j, \epsilon_k] \left( \delta_{jk\rho}(\chi) + \delta_{jk\rho\rho}(\chi) \right) \quad (5.44)$$

This finishes the overview of the perturbation analysis. It was shown that its application yields the variance and bias of the SSI/Cov-identified modal parameters. For convenience, the main quantities that are computed are summarised in the diagram shown in figure 5.1. It is seen from the equations summarised in figure 5.1 that the evaluation of the variance and bias of any identified modal parameter  $\chi$  requires knowledge of its derivatives with respect to the perturbation  $\epsilon_j$  and the truncation parameter  $\rho$ . The necessary expressions for the modal frequencies and damping ratios will be derived in the next section. The case for the mode shapes is treated separately thereafter.

## 5.3 Derivatives of the Modal Frequencies and Damping Ratios

The modal frequencies and damping ratios are identified from the *discrete-time eigenvalues*  $\lambda_i$ , for  $i = 1, 2, \dots, n$ , of the realised system matrix  $\mathbf{A}$  according to equations 2.50 and 2.52 given in Chapter 2. Let the system matrix realised from the perturbed

<b>Variance</b>	
	$\text{Var}\{\chi(\underline{\epsilon})\} \approx \sum_{j=1}^N \text{Var}\{\epsilon_j\} \delta_j^2(\chi) + 2 \sum_{\substack{j=1 \\ j \neq k}}^N \sum_{k=1}^N \text{Cov}\{\epsilon_j, \epsilon_k\} \delta_j(\chi) \delta_k(\chi) \quad (4.8)$
<b>Bias</b>	
<b>1. Truncation Bias</b>	$b_T\{\chi(\underline{0})\} \equiv -[\delta_\rho\{\chi(\underline{0})\} + \delta_{\rho\rho}\{\chi(\underline{0})\}]$
Quadratic Bias of Truncation Bias	$b_{QT}\{\chi\} \approx - \sum_{j=1}^N \text{Var}\{\epsilon_j\} (\delta_{j\rho\rho}(\chi) + \delta_{\rho\rho\rho}(\chi)) - \sum_{\substack{j,k \\ j \neq k}}^N \text{Cov}\{\epsilon_j, \epsilon_k\} (\delta_{jk\rho}(\chi) + \delta_{\rho\rho jk}(\chi))$
Variance of Truncation Bias	$\begin{aligned} \text{Var}\{b_T(\chi)\} &\approx \sum_{j=1}^N \text{Var}\{\epsilon_j\} (\delta_{j\rho\rho}(\chi) + \delta_{\rho\rho\rho}(\chi)) \\ &\quad + 2 \sum_{\substack{j=1 \\ j \neq k}}^N \sum_{k=1}^N \text{Cov}\{\epsilon_j, \epsilon_k\} (\delta_{j\rho\rho}(\chi) + \delta_{\rho\rho\rho}(\chi)) (\delta_{k\rho}(\chi) + \delta_{\rho\rho k}(\chi)) \end{aligned}$
<b>2. Quadratic Bias</b>	$b_Q\{\chi(\underline{\epsilon})\} = E\{\chi(\underline{\epsilon})\} - \chi(\underline{0}) \approx \sum_{j=1}^N \text{Var}\{\epsilon_j\} \delta_{jj}(\chi) + \sum_{\substack{j,k \\ j \neq k}}^N \text{Cov}\{\epsilon_j, \epsilon_k\} \delta_{jk}(\chi)$

Fig. 5.1: Summary of the statistics computed from the perturbation analysis.

correlation functions be denoted by  $\mathbf{A}(\underline{\epsilon})$  and its eigenvalues by  $\lambda_i(\underline{\epsilon})$  with  $\mathbf{\Lambda}(\underline{\epsilon})$  the corresponding diagonal eigenvalue matrix. In the same way as described in Chapter 2 by eqns. 2.50 and 2.52, the perturbed modal frequencies  $\omega_i(\underline{\epsilon})$  and damping ratios  $\xi_i(\underline{\epsilon})$  of the system can be obtained from the perturbed *continuous-time eigenvalues*  $\lambda_{c_i}(\underline{\epsilon})$  as

$$\lambda_{c_i}(\underline{\epsilon}) = \frac{\ln(\lambda_i(\underline{\epsilon}))}{\Delta t} \quad (5.45)$$

$$\text{and } \omega_i(\underline{\epsilon}) = |\lambda_{c_i}(\underline{\epsilon})|, \quad \xi_i(\underline{\epsilon}) = \frac{-\Re[\lambda_{c_i}(\underline{\epsilon})]}{\omega_i(\underline{\epsilon})} \quad (5.46)$$

where  $\ln(\cdot)$  denotes the natural logarithm and  $\Re(\cdot)$  the real part of a complex number. Assuming that the modal parameters  $\omega_i(\underline{\epsilon})$ ,  $\xi_i(\underline{\epsilon})$  as well as the the continuous- and discrete-time eigenvalues are differentiable to second order with respect to  $\epsilon_j$  and  $\rho$ , the derivatives of the  $i^{th}$  modal frequency and damping ratio evaluated at  $\underline{\epsilon} = \underline{0}$  (and/or  $\rho = 0$ ) can then be obtained in the form of the differential operators defined

<b>Variance</b>	
	$\text{Var}[\chi(\underline{\epsilon})] \approx \sum_{j=1}^N \text{Var}[\epsilon_j] \delta_j^2(\chi) + 2 \sum_{\substack{j=1 \\ j \neq k}}^N \sum_{k=1}^N \text{Cov}[\epsilon_j, \epsilon_k] \delta_j(\chi) \delta_k(\chi) \quad (4.8)$
<b>Bias</b>	
<b>1. Truncation Bias</b>	$b_T[\chi(\underline{0})] \equiv -[\delta_\rho[\chi(\underline{0})] + \delta_{\rho\rho}[\chi(\underline{0})]]$
Quadratic Bias of Truncation Bias	$b_{QT}[\chi] \approx - \sum_{j=1}^N \text{Var}[\epsilon_j] (\delta_{j\rho\rho}(\chi) + \delta_{j\rho\rho}(\chi)) - \sum_{\substack{j,k \\ j \neq k}}^N \text{Cov}[\epsilon_j, \epsilon_k] (\delta_{jk\rho}(\chi) + \delta_{jk\rho\rho}(\chi))$
Variance of Truncation Bias	$\begin{aligned} \text{Var}[b_T(\chi)] &\approx \sum_{j=1}^N \text{Var}[\epsilon_j] (\delta_{j\rho}(\chi) + \delta_{j\rho\rho}(\chi)) \\ &+ 2 \sum_{\substack{j=1 \\ j \neq k}}^N \sum_{k=1}^N \text{Cov}[\epsilon_j, \epsilon_k] (\delta_{j\rho}(\chi) + \delta_{j\rho\rho}(\chi)) (\delta_{k\rho}(\chi) + \delta_{k\rho\rho}(\chi)) \end{aligned}$
<b>2. Quadratic Bias</b>	$b_Q[\chi(\underline{\epsilon})] = E[\chi(\underline{\epsilon})] - \chi(\underline{0}) \approx \sum_{j=1}^N \text{Var}[\epsilon_j] \delta_{jj}(\chi) + \sum_{\substack{j,k \\ j \neq k}}^N \text{Cov}[\epsilon_j, \epsilon_k] \delta_{jk}(\chi)$

Fig. 5.1: Summary of the statistics computed from the perturbation analysis.

correlation functions be denoted by  $\mathbf{A}(\underline{\epsilon})$  and its eigenvalues by  $\lambda_i(\underline{\epsilon})$  with  $\mathbf{\Lambda}(\underline{\epsilon})$  the corresponding diagonal eigenvalue matrix. In the same way as described in Chapter 2 by eqns. 2.50 and 2.52, the perturbed modal frequencies  $\omega_i(\underline{\epsilon})$  and damping ratios  $\xi_i(\underline{\epsilon})$  of the system can be obtained from the perturbed *continuous-time eigenvalues*  $\lambda_{c_i}(\underline{\epsilon})$  as

$$\lambda_{c_i}(\underline{\epsilon}) = \frac{\ln(\lambda_i(\underline{\epsilon}))}{\Delta t} \quad (5.45)$$

$$\text{and } \omega_i(\underline{\epsilon}) = |\lambda_{c_i}(\underline{\epsilon})|, \quad \xi_i(\underline{\epsilon}) = \frac{-\Re[\lambda_{c_i}(\underline{\epsilon})]}{\omega_i(\underline{\epsilon})} \quad (5.46)$$

where  $\ln(\cdot)$  denotes the natural logarithm and  $\Re(\cdot)$  the real part of a complex number. Assuming that the modal parameters  $\omega_i(\underline{\epsilon})$ ,  $\xi_i(\underline{\epsilon})$  as well as the the continuous- and discrete-time eigenvalues are differentiable to second order with respect to  $\epsilon_j$  and  $\rho$ , the derivatives of the  $i^{\text{th}}$  modal frequency and damping ratio evaluated at  $\underline{\epsilon} = \underline{0}$  (and/or  $\rho = 0$ ) can then be obtained in the form of the differential operators defined

in equations 5.6,5.7, 5.34, 5.35 and 5.39 - 5.42 as

$$\delta_{j, jk, \rho, \rho\rho, j\rho, (\omega_i)} = \delta_{j, jk, \rho, \rho\rho, j\rho, (\lambda_{c_i}(\underline{\epsilon}))} \quad (5.47)$$

$$\delta_{j, jk, \rho, \rho\rho, j\rho, (\xi_i)} = \delta_{j, jk, \rho, \rho\rho, j\rho, (\lambda_{c_i}(\underline{\epsilon}))} \left( \frac{-\Re[\lambda_{c_i}(\underline{\epsilon})]}{\omega_i(\underline{\epsilon})} \right) \quad (5.48)$$

where we have introduced the notation  $\delta_{j, jk, \rho, \rho\rho, j\rho, (\omega_i)}$  to denote any of the derivatives  $\delta_j(\cdot)$ ,  $\delta_{jk}(\cdot)$ ,  $\delta_\rho(\cdot)$ ,  $\delta_{\rho\rho}(\cdot)$ ,  $\delta_{j\rho}(\cdot)$ ,  $\delta_{jk\rho}(\cdot)$  etc.. Thus, to first order, the derivatives of  $\omega_i(\underline{\epsilon})$  and  $\xi_i(\underline{\epsilon})$  in operator form read

$$\delta_{j, \rho}(\omega_i) = \frac{\Re[\lambda_{c_i}(\underline{0})] \Re[\delta_{j, \rho}(\lambda_{c_i})] + \Im[\lambda_{c_i}(\underline{0})] \Im[\delta_{j, \rho}(\lambda_{c_i})]}{|\lambda_{c_i}(\underline{0})|} \quad (5.49)$$

$$\delta_{j, \rho}(\xi_i) = \frac{\Re[\lambda_{c_i}(\underline{0})] \delta_{j, \rho}(\omega_i)}{\omega_i^2(\underline{0})} - \frac{\Re[\delta_{j, \rho}(\lambda_{c_i})]}{\omega_i(\underline{0})} \quad (5.50)$$

where, again, the notation  $\delta_{j, \rho}(\cdot)$  implies that the expression is valid for  $\delta_j(\cdot)$  and  $\delta_\rho(\cdot)$ . The expressions for second order partial derivatives are found in a similar fashion are given by

$$\delta_{jk, \rho\rho}(\omega_i) = \frac{\Re[\lambda_{c_i}(\underline{0})] \Re[\delta_{jk, \rho\rho}(\lambda_{c_i})] + \Im[\lambda_{c_i}(\underline{0})] \Im[\delta_{jk, \rho\rho}(\lambda_{c_i})]}{|\lambda_{c_i}(\underline{0})|} \quad (5.51)$$

$$\begin{aligned} & + \frac{1}{2} \frac{\Re[\delta_{j, \rho}(\lambda_{c_i})] \Re[\delta_{k, \rho}(\lambda_{c_i})] + \Im[\delta_{j, \rho}(\lambda_{c_i})] \Im[\delta_{k, \rho}(\lambda_{c_i})]}{|\lambda_{c_i}(\underline{0})|} \\ & - \frac{1}{2} \frac{\delta_{j, \rho}(\omega_i) \delta_{k, \rho}(\omega_i)}{|\lambda_{c_i}(\underline{0})|} \\ \delta_{j\rho}(\omega_i) & = \frac{\Re[\lambda_{c_i}(\underline{0})] \Re[\delta_{j\rho}(\lambda_{c_i})] + \Im[\lambda_{c_i}(\underline{0})] \Im[\delta_{j\rho}(\lambda_{c_i})]}{|\lambda_{c_i}(\underline{0})|} \quad (5.52) \\ & + \frac{\Re[\delta_j(\lambda_{c_i})] \Re[\delta_\rho(\lambda_{c_i})] + \Im[\delta_j(\lambda_{c_i})] \Im[\delta_\rho(\lambda_{c_i})]}{|\lambda_{c_i}(\underline{0})|} \\ & - \frac{1}{2} \frac{\delta_j(\omega_i) \delta_\rho(\omega_i)}{|\lambda_{c_i}(\underline{0})|} \end{aligned} \quad (5.53)$$

The expressions for  $\delta_{jk\rho}(\omega_i)$  and  $\delta_{jk\rho\rho}(\omega_i)$  are obtained in a similar manner but they are lengthy. The expression for  $\delta_{jk\rho}(\omega_i)$  is given in Appendix B in equation B.1 but the one for  $\delta_{jk\rho\rho}(\omega_i)$  is omitted. For the modal damping ratios, the second order

expressions are

$$\begin{aligned} \delta_{jk, \rho\rho}(\xi_i) &= \frac{\Re[\lambda_{c_i}(\mathbf{0})] \delta_{jk, \rho\rho}(\omega_i)}{\omega_i^2(\mathbf{0})} - \frac{\Re[\delta_{jk, \rho\rho}(\lambda_{c_i})]}{\omega_i(\mathbf{0})} \\ &+ \frac{1}{2} \frac{\Re[\delta_{k, \rho}(\lambda_{c_i})] \delta_{j, \rho}(\omega_i) + \Re[\delta_{j, \rho}(\lambda_{c_i})] \delta_{k, \rho}(\omega_i)}{\omega_i^2(\mathbf{0})} \\ &- \frac{\Re[\lambda_{c_i}(\mathbf{0})] \delta_{j, \rho}(\omega_i) \delta_{k, \rho}(\omega_i)}{\omega_i^3(\mathbf{0})} \end{aligned} \quad (5.54)$$

$$\begin{aligned} \delta_{j\rho}(\xi_i) &= \frac{\Re[\lambda_{c_i}(\mathbf{0})] \delta_{j\rho}(\omega_i)}{\omega_i^2(\mathbf{0})} - \frac{\Re[\delta_{j\rho}(\lambda_{c_i})]}{\omega_i(\mathbf{0})} \\ &+ \frac{\Re[\delta_j(\lambda_{c_i})] \delta_\rho(\omega_i) + \Re[\delta_\rho(\lambda_{c_i})] \delta_j(\omega_i)}{\omega_i^2(\mathbf{0})} \\ &- 2 \frac{\Re[\lambda_{c_i}(\mathbf{0})] \delta_j(\omega_i) \delta_\rho(\omega_i)}{\omega_i^3(\mathbf{0})} \end{aligned} \quad (5.55)$$

Again, the expression for  $\delta_{jk\rho}(\xi_i)$  is given in equation B.2 in Appendix B but the one for  $\delta_{jk\rho\rho}(\xi_i)$  is omitted. To evaluate the above derivatives of  $\omega_i(\underline{\epsilon})$  and  $\xi_i(\underline{\epsilon})$ , it is seen that the corresponding derivatives of the continuous-time eigenvalues  $\lambda_{c_i}(\underline{\epsilon})$  are required.

As is seen from figure 5.1, the computation of  $Var[\chi(\underline{\epsilon})]$ ,  $b_Q[\chi(\underline{\epsilon})]$  and  $b_T[\chi(\underline{\epsilon})]$  involves only the derivatives

$$\delta_j(\cdot), \delta_{jk}(\cdot), \delta_\rho(\cdot) \text{ and } \delta_{\rho\rho}(\cdot)$$

To obtain the latter, differentiate  $\ln(\lambda_i(\underline{\epsilon}))$  with respect to  $\underline{\epsilon}$  to find

$$\delta_{j, \rho}(\lambda_{c_i}) = \frac{1}{\Delta t} \frac{\delta_{j, \rho}(\lambda_i)}{\lambda_i(0)} \quad (5.56)$$

$$\delta_{jk, \rho\rho}(\lambda_{c_i}) = \frac{1}{\Delta t} \left[ \frac{\delta_{jk, \rho\rho}(\lambda_i)}{\lambda_i(0)} - \frac{1}{2} \frac{\delta_{j, \rho}(\lambda_i) \delta_{k, \rho}(\lambda_i)}{\lambda_i^2(0)} \right] \quad (5.57)$$

$$\delta_{j\rho}(\lambda_{c_i}) = \frac{1}{\Delta t} \left[ \frac{\delta_{j\rho}(\lambda_i)}{\lambda_i(0)} - \frac{\delta_j(\lambda_i) \delta_\rho(\lambda_i)}{\lambda_i^2(0)} \right] \quad (5.58)$$

To compute the variance and quadratic bias of the truncation bias, i.e.  $Var[b_T(\chi)]$  and quadratic bias  $b_{QT}[\chi]$ , it is seen from equations 5.43 and 5.44 that the required derivatives are

$$\delta_{j\rho}(\cdot), \delta_{j\rho\rho}(\cdot), \delta_{jk\rho}(\cdot) \text{ and } \delta_{jk\rho\rho}(\cdot)$$

The latter are simply found by differentiating  $\delta_\rho(\lambda_{c_i})$  and  $\delta_{\rho\rho}(\lambda_{c_i})$  given in equations 5.56 and 5.57 respectively with respect to  $\epsilon_j$ . In operator form, these read

$$\delta_{j\rho}(\lambda_{c_i}) = \frac{1}{\Delta t \lambda_i^2(\underline{0})} [\lambda_i(\underline{0}) \delta_{j\rho}(\lambda_i) - \delta_j(\lambda_i) \delta_\rho(\lambda_i(\underline{0}))] \quad (5.59)$$

$$\begin{aligned} \delta_{jk\rho}(\lambda_{c_i}) &= \frac{1}{\Delta t \lambda_i^3(\underline{0})} \{ \lambda_i^2(\underline{0}) \delta_{jk\rho}(\lambda_i) - \lambda_i(\underline{0}) \delta_k(\lambda_i) \delta_{j\rho}(\lambda_i) \\ &+ \delta_\rho(\lambda_i)(\underline{0}) [\delta_j(\lambda_i) \delta_k(\lambda_i) - \lambda_i(\underline{0}) \delta_{jk}(\lambda_i)] \\ &+ \frac{1}{2} \lambda_i(\underline{0}) [\delta_k(\lambda_i) \delta_{j\rho}(\lambda_i) - \delta_j(\lambda_i) \delta_{k\rho}(\lambda_i)] \} \end{aligned} \quad (5.60)$$

$$\begin{aligned} \delta_{j\rho\rho}(\lambda_{c_i}) &= \frac{1}{\Delta t \lambda_i^2(\underline{0})} [\lambda_i(\underline{0}) \delta_{j\rho\rho}(\lambda_i) - \delta_j(\lambda_i) \delta_{\rho\rho}(\lambda_i(\underline{0}))] \\ &- \delta_\rho(\lambda_{c_i}(\underline{0})) \delta_{j\rho}(\lambda_{c_i}) \end{aligned} \quad (5.61)$$

and

$$\begin{aligned} \delta_{jk\rho\rho}(\lambda_{c_i}) &= \frac{1}{\Delta t \lambda_i^3(\underline{0})} \{ \lambda_i^2(\underline{0}) \delta_{jk\rho\rho}(\lambda_i) - \lambda_i(\underline{0}) \delta_k(\lambda_i) \delta_{j\rho\rho}(\lambda_i) \\ &+ \delta_{\rho\rho}(\lambda_i)(\underline{0}) [\delta_j(\lambda_i) \delta_k(\lambda_i) - \lambda_i(\underline{0}) \delta_{jk}(\lambda_i)] \\ &+ \frac{1}{2} \lambda_i(\underline{0}) [\delta_k(\lambda_i) \delta_{j\rho\rho}(\lambda_i) - \delta_j(\lambda_i) \delta_{k\rho\rho}(\lambda_i)] \} \\ &- \frac{1}{2} \delta_{k\rho}(\lambda_{c_i}) \delta_{j\rho}(\lambda_{c_i}) - \delta_\rho(\lambda_{c_i}(\underline{0})) \delta_{jk\rho}(\lambda_{c_i}) \end{aligned} \quad (5.62)$$

The next step then involves the calculation of the first and second order derivatives of the discrete-time eigenvalues  $\lambda_i(\underline{\epsilon})$  of the identified state-space or system matrix  $\mathbf{A}(\underline{\epsilon})$ .

### 5.3.1 Eigenvalue and Eigenvector derivatives

The computation of the eigenvalue and eigenvector derivatives is in general not a trivial task. Many papers document the computation of eigenvalues and eigenvectors for matrices with *distinct* eigenvalues. Expressions for first order derivatives were given by Fox and Kapoor (1968) and second order derivatives are for instance given by Nelson (1976); Plaut and Huseyin (1973). A survey of methods for eigensystem derivatives with distinct eigenvalues can be found in Adelman and Haftka (1986). In Longman and Juang (1987); Longman *et al.* (1987), these results were collected in the

theorem below. For later purposes, the derivatives of the corresponding eigenvectors are given as well.

### THEOREM

Let  $\mathbf{A}(\underline{\epsilon})$  be an  $n \times n$  differentiable function of the parameters  $\underline{\epsilon} = [\epsilon_1, \epsilon_2, \dots, \epsilon_n]$  and assume that its eigenvalues  $\lambda_i$ , for  $i = 1, 2, \dots, n$  are distinct when  $\underline{\epsilon} = \underline{0}$ . Let  $\mathbf{P} = [\mathbf{p}_1, \mathbf{p}_2, \dots, \mathbf{p}_n]$  be the matrix of right eigenvectors of  $\mathbf{A}(\underline{0})$  normalized such that  $\mathbf{p}_i^T \mathbf{p}_i = 1$  for  $i = 1, 2, \dots, n$ . Then  $\mathbf{Q} = \mathbf{P}^{-1T} = [\mathbf{q}_1, \mathbf{q}_2, \dots, \mathbf{q}_n]$  is the matrix of left eigenvectors of  $\mathbf{A}(\underline{0})$ . Then the first and second order derivatives of the eigenvalues  $\lambda_i$  and eigenvectors  $\mathbf{p}_i, \mathbf{q}_i$  for  $i = 1, 2, \dots, n$  evaluated at  $\underline{\epsilon} = \underline{0}$  are given by:

$$\delta_j(\lambda_i) = \mathbf{q}_i^T \delta_j(\mathbf{A}) \mathbf{p}_i \quad (5.64)$$

$$\delta_j(\mathbf{p}_i) = \sum_{m=1}^n \alpha_{im}^j \mathbf{p}_m \quad (5.65)$$

$$\delta_j(\mathbf{q}_i) = \sum_{m=1}^n \gamma_{im}^j \mathbf{q}_m \quad (5.66)$$

and for the second order partial derivatives

$$\begin{aligned} \delta_{jk}(\lambda_i) = & \mathbf{q}_i^T \delta_{jk}(\mathbf{A}) \mathbf{p}_i + \frac{1}{2} \sum_{\substack{m=1, \\ m \neq i}}^n \left\{ \frac{(\mathbf{q}_i^T \delta_j(\mathbf{A}) \mathbf{p}_m)(\mathbf{q}_m^T \delta_k(\mathbf{A}) \mathbf{p}_i)}{\lambda_i - \lambda_m} \right. \\ & \left. + \frac{(\mathbf{q}_i^T \delta_k(\mathbf{A}) \mathbf{p}_m)(\mathbf{q}_m^T \delta_j(\mathbf{A}) \mathbf{p}_i)}{\lambda_i - \lambda_m} \right\} \end{aligned} \quad (5.67)$$

$$\delta_{jk}(\mathbf{p}_i) = \sum_{m=1}^n \beta_{im}^{jk} \mathbf{p}_m \quad (5.68)$$

$$\delta_{jk}(\mathbf{q}_i) = \sum_{m=1}^n \eta_{im}^{jk} \mathbf{q}_m \quad (5.69)$$



where

$$\alpha_{im}^j = \frac{\mathbf{q}_m^T \delta_j(\mathbf{A}) \mathbf{p}_i}{\lambda_i - \lambda_m}, \quad i \neq m \quad \text{and} \quad \alpha_{ii}^j = - \sum_{\substack{m=1 \\ m \neq i}}^n \alpha_{im}^j \mathbf{p}_m^T \mathbf{p}_i \quad (5.70)$$

$$\gamma_{im}^j = -\alpha_{mi}^j, \quad \forall \quad i, k = 1, 2, \dots, n \quad (5.71)$$

$$\beta_{im}^{jk} = \frac{1}{2(\lambda_i - \lambda_m)} \mathbf{q}_m^T \{2\delta_{jk}(\mathbf{A}) \mathbf{p}_i + [\delta_j(\mathbf{A}) - \delta_j(\lambda_i) \mathbf{I}] \delta_k(\mathbf{p}_i) + [\delta_k(\mathbf{A}) - \delta_k(\lambda_i) \mathbf{I}] \delta_j(\mathbf{p}_i)\}, \quad i \neq m \quad (5.72)$$

$$\beta_{ii}^{jk} = - \sum_{\substack{m=1 \\ m \neq i}}^n \beta_{im}^{jk} \mathbf{p}_m^T \mathbf{p}_i - \frac{1}{2} \delta_j(\mathbf{p}_i^T) \delta_k(\mathbf{p}_i) \quad (5.73)$$

$$\eta_{im}^{jk} = \frac{1}{2(\lambda_i - \lambda_m)} \{2\mathbf{q}_i^T \delta_{jk}(\mathbf{A}) + \delta_k(\mathbf{q}_i^T) [\delta_j(\mathbf{A}) - \delta_j(\lambda_i) \mathbf{I}] + \delta_j(\mathbf{q}_i^T) [\delta_k(\mathbf{A}) - \delta_k(\lambda_i) \mathbf{I}]\} \mathbf{p}_m, \quad i \neq m \quad (5.74)$$

$$\eta_{ii}^{jk} = -\eta_{ii}^{jk} - \frac{1}{2} [\delta_j(\mathbf{q}_i^T) \delta_k(\mathbf{p}_i) + \delta_k(\mathbf{q}_i^T) \delta_j(\mathbf{p}_i)] \quad (5.75)$$

The proof can be found in the above mentioned references. The theorem requires that *all* the eigenvalues of the state-matrix  $\mathbf{A}(\underline{\epsilon})$  are distinct. This condition can be relaxed a little by the following corollary.

### COROLLARY

Let  $\mathbf{A}(\underline{\epsilon})$  be an  $n \times n$  differentiable function of the parameters  $\underline{\epsilon} = [\epsilon_1, \epsilon_2, \dots, \epsilon_n]$  and assume that it is nondefective. Define  $\mathbf{P}$  and  $\mathbf{Q} = (\mathbf{P}^{-1})^T$  as above. Then the first and second order derivatives of  $\lambda_i$ ,  $\mathbf{p}_i$  and  $\mathbf{q}_i$  evaluated at  $\underline{\epsilon} = \underline{0}$  for each  $i$  associated with a non-repeated eigenvalue are given by equations 5.65-5.75 as in the theorem above.

In other words, when a matrix has repeated eigenvalues but has a full set of linearly independent eigenvectors (i.e. the repeated eigenvalues are non-defective), we can still use the theorem to find the derivatives of the *non-repeated* eigenvalues and their associated eigenvectors. In typical structures, the occurrence nearly repeated

eigenvalues is relatively common due to slightly imperfect structural symmetry but repeated eigenvalues are rarely encountered.

### 5.3.2 Derivatives for the Variance and Quadratic Bias

To find the variance and the quadratic bias of  $\omega_i$  and  $\xi_i$ , for  $i = 1, 2, \dots, n$ , it is necessary to evaluate  $\delta_{j, jk}(\lambda_i)$ , the computations for which are detailed in the previous section. As mentioned, the latter in turn require  $\delta_{j, jk}(\mathbf{A})$  which can be obtained by differentiating eqn. 5.14

$$\delta_{j, jk}(\mathbf{A}) = \delta_{j, jk} \left( \Sigma_1^{-1/2} \mathbf{U}_1^T \mathcal{H}_1 \mathbf{V}_1 \Sigma_1^{1/2} \right) \quad (5.76)$$

For first order derivatives, we thus obtain in operator form

$$\begin{aligned} \delta_j(\mathbf{A}) = \Sigma_1^{-1/2} \mathbf{U}_1^T \left[ \mathcal{H}_1 \mathbf{V}_1 \delta_j \left( \Sigma_1^{-1/2} \right) + \mathcal{H}_1 \delta_j(\mathbf{V}_1) \Sigma_1^{-1/2} + \delta_j(\mathcal{H}_1) \mathbf{V}_1 \Sigma_1^{-1/2} \right] \\ + \left[ \Sigma_1^{-1/2} \delta_j(\mathbf{U}_1^T) + \delta_j \left( \Sigma_1^{-1/2} \right) \mathbf{U}_1^T \right] \mathcal{H}_1 \mathbf{V}_1 \Sigma_1^{-1/2} \end{aligned} \quad (5.77)$$

The expressions for the second order mixed derivatives  $\delta_{jk}(\mathbf{A})$  are obtained similarly but are lengthy and are therefore given in Appendix B in equation B.3.  $\delta_{j, jk}(\mathbf{A})$  are functions of  $\delta_{j, jk}(\Sigma^{-1/2})$ ,  $\delta_{j, jk}(\mathbf{V}_1)$ ,  $\delta_{j, jk}(\mathbf{U}_1^T)$  and  $\delta_j(\mathcal{H}_1)$ .  $\delta_j(\mathcal{H}_1)$  has been defined in equation 5.1 and since its entries are constant,  $\delta_{jk}(\mathcal{H}_1) = \mathbf{0}$ . To find the derivatives of the singular value matrix  $\Sigma_1^{-1/2}$  and the singular vectors in  $\mathbf{V}_1$ , we can again make use of the above theorem. Indeed, the singular value decomposition of  $\mathcal{H}_0$  (eqn. 5.13) can be obtained from the eigendecomposition of  $\mathcal{H}_0^T \mathcal{H}_0$  since

$$\mathcal{H}_0^T \mathcal{H}_0 = (\mathbf{U}_1 \Sigma_1 \mathbf{V}_1^T)^T (\mathbf{U}_1 \Sigma_1 \mathbf{V}_1^T) = \mathbf{V}_1 \Sigma_1^2 \mathbf{V}_1^T \quad (5.78)$$

Thus, the right singular subspace of  $\mathcal{H}_0$ , spanned by the columns of  $\mathbf{V}_1 = [\underline{v}_1, \underline{v}_2, \dots, \underline{v}_n]$ , where  $\underline{v}_i$  are column vectors, yields both the right and left eigenvectors of  $\mathcal{H}_0^T \mathcal{H}_0$ , and the square of the retained singular values of  $\mathcal{H}_0$  that form  $\Sigma_1$  are the eigenvalues of  $\mathcal{H}_0^T \mathcal{H}_0$ . The derivatives of the left eigenvectors  $\delta_{j, jk}(\mathbf{V}_1)$  as well as  $\delta_{j, jk}(\Sigma_1^2) =$

$diag [\delta_{j,jk} (s_1^2), \delta_{j,jk} (s_2^2), \dots, \delta_{j,jk} (s_n^2)]$  can thus be computed using the results in section 5.3.1 with  $\mathbf{A}(\underline{\epsilon})$  replaced by  $\mathcal{H}_0^T \mathcal{H}_0(\underline{\epsilon})$ ,  $\lambda_i(\underline{\epsilon})$  by  $s_i^2(\underline{\epsilon})$  and  $\mathbf{p}_i(\underline{\epsilon})$  and  $\mathbf{q}_i(\underline{\epsilon})$  replaced by  $\mathbf{v}_i(\underline{\epsilon})$ . Application of the eigenvalue/eigenvector results in section 5.3.1 to  $\mathcal{H}_0^T \mathcal{H}_0(\underline{\epsilon})$  to find the derivatives  $s_i^2(\underline{\epsilon})$  and  $\mathbf{v}_i(\underline{\epsilon})$  requires the derivatives of  $\mathcal{H}_0^T \mathcal{H}_0(\underline{\epsilon})$  itself. The latter can be found by using the definition of  $\mathcal{H}_0(\underline{\epsilon})$  (eqn. 5.1) in  $\mathcal{H}_0^T \mathcal{H}_0$  and applying the differential operators  $\delta_{j,jk}(\cdot)$ . One finds

$$\delta_j (\mathcal{H}_0^T \mathcal{H}_0) = \mathcal{H}_0^T \delta_j (\mathcal{H}_0) + \delta_j (\mathcal{H}_0^T) \mathcal{H}_0 \quad (5.79)$$

$$\delta_{jk} (\mathcal{H}_0^T \mathcal{H}_0) = \frac{1}{2} [\delta_j (\mathcal{H}_0^T) \delta_k (\mathcal{H}_0) + \delta_k (\mathcal{H}_0^T) \delta_j (\mathcal{H}_0)] \quad (5.80)$$

The derivatives of  $\mathbf{U}_1$  are easily obtained by rearranging eqn. 5.13 as  $\mathbf{U}_1 = \mathcal{H}_0 \mathbf{V}_1 \Sigma_1^{-1}$  and differentiating with respect to  $\epsilon_j$ . The first order derivatives in operator form then read

$$\delta_j (\mathbf{U}_1) = \delta_j (\mathcal{H}_0) \mathbf{V}_1 \Sigma_1^{-1} + \mathcal{H}_0 \delta_j (\mathbf{V}_1) \Sigma_1^{-1} + \mathcal{H}_0 \mathbf{V}_1 \delta_j (\Sigma_1^{-1}) \quad (5.81)$$

Evaluation of the second order derivative of  $\mathbf{A}(\underline{\epsilon})$ , that is  $\delta_{jk}(\mathbf{A})$ , requires  $\delta_{jk}(\mathbf{U}_1)$ . This expression can be found analogously and is given in Appendix A in equation B.4.

Finally, it remains to calculate  $\delta_{j,jk}(\Sigma^{-1/2}) = diag [\delta_{j,jk}(s_1^{-1/2}), \delta_{j,jk}(s_2^{-1/2}), \dots, \delta_{j,jk}(s_n^{-1/2})]$  and  $\delta_{j,jk}(\Sigma^{-1}) = diag [\delta_{j,jk}(s_1^{-1}), \delta_{j,jk}(s_2^{-1}), \dots, \delta_{j,jk}(s_n^{-1})]$  to finish the computations of  $\delta_{j,jk}(\mathbf{A})$  and  $\delta_{j,jk}(\mathbf{U}_1)$  respectively. To establish the latter quantities note that  $s_i^a(\underline{\epsilon})$  can be written as  $[s_i^2(\underline{\epsilon})]^{a/2}$  for an arbitrary power  $a$ . A Taylor expansion about the origin of this expression yields the  $\delta_j(s_i^a)$  and  $\delta_{jk}(s_i^a)$  in terms of  $\delta_j(s_i^2)$  as the coefficients of  $\epsilon_j$  and  $\epsilon_j \epsilon_k$  respectively. For  $a = -1$  and  $a = -\frac{1}{2}$

the desired derivatives in operator form read

$$\delta_j (s_i^{-1}) = -\frac{1}{2} \frac{\delta_j (s_i^2)}{s_i^3} \quad (5.82)$$

$$\delta_j (s_i^{-1/2}) = -\frac{1}{4} \frac{\delta_j (s_i^2)}{s_i^{5/2}} \quad (5.83)$$

$$\delta_{jk} (s_i^{-1}) = -\frac{1}{2} \frac{\delta_{jk} (s_i^2)}{s_i^3} + \frac{3}{8} \frac{[\delta_j (s_i^2)]^2}{s_i^5} \quad (5.84)$$

$$\delta_{jk} (s_i^{-1/2}) = -\frac{1}{4} \frac{\delta_{jk} (s_i^2)}{s_i^{5/2}} + \frac{5}{32} \frac{[\delta_j (s_i^2)]^2}{s_i^{9/2}} \quad (5.85)$$

Since  $\delta_{j,jk} (s^2)$  are known from application of the theorem to  $\mathcal{H}_0^T \mathcal{H}_0 (\underline{\epsilon})$ , the above expressions can be evaluated and conclude the necessary computations needed to evaluate the derivatives of the modal frequencies and damping ratios with respect to  $\epsilon_j$  given in equations 5.47 and 5.48. Thus, with  $\delta_{j,jk} (\omega_i)$  and  $\delta_{j,jk} (\xi_i)$  at hand, the variance (eqn. 5.8) and quadratic bias (eqn. 5.10) can now be computed. The final step is to compute the necessary derivatives to establish the truncation bias, its associated variance and quadratic bias.

### 5.3.3 Derivatives for the Truncation Bias, its Variance and Quadratic Bias

The eigenvalue/eigenvector sensitivities given in section 5.3.1 can again be used to find the necessary derivatives to compute the truncation bias, its variance and quadratic bias. However, this time we need to find the derivatives with respect to  $\rho$ , the reason being that the perturbation of the modal parameters due to truncation of small non-zero singular values is not a direct result of the additive disturbance of the correlation functions by  $\underline{\epsilon}$ , (cf. eqn. 5.3). Instead, the perturbation due to truncation was modelled as an additive perturbation that directly affects the eigenvalues  $\Lambda$  of  $\mathbf{A}(\underline{0})$  according to equation 5.31. In other words, the perturbed matrix whose eigenvalue derivatives we wish to find is  $\Lambda' + \rho \Delta \Lambda'$ .

Assume for the moment that the  $n$  first eigenvalues of  $\Lambda'$  are *distinct* and recall that

they are equal to the  $n$  eigenvalues of  $\mathbf{A}(\mathbf{0})$ ,  $\mathbf{\Lambda}' = \text{diag}[\lambda_1, \lambda_2, \dots, \lambda_n]$ . Bearing in mind that, by construction, the  $n' \times n'$  matrix  $\mathbf{\Lambda}' = \text{diag}[\lambda_1, \lambda_2, \dots, \lambda_n, 0, 0, \dots, 0_{n'-n}]$  has  $n' - n$  repeated, identically zero, eigenvalues, the required eigenvalue and corresponding eigenvector sensitivities of the first  $n$  non-zero eigenvalues can be computed by applying the theorem and its corollary from section 5.3.1, with  $\mathbf{\Lambda}' + \rho\Delta\mathbf{\Lambda}'$  taking the role of  $\mathbf{A}(\underline{\epsilon})$  and  $\mathbf{\Lambda}'$  (i.e. at  $\rho = 0$ ) then corresponds to the unperturbed case and takes the role of  $\mathbf{A}(\mathbf{0})$ . Since the columns of the  $n' \times n'$  identity matrix are the eigenvectors of  $\mathbf{\Lambda}'$ , the first and second order eigenvalue derivatives with respect to  $\rho$  follow from the corollary and are found to be

$$\delta_\rho(\lambda_i) = \Delta\Lambda'_{ii} \quad \text{for } i = 1, 2, \dots, n \quad (5.86)$$

$$\delta_{\rho\rho}(\lambda_i) = \sum_{\substack{m=1 \\ m \neq i}}^{n'} \frac{\Delta\Lambda'_{im}\Delta\Lambda'_{mi}}{\lambda_i - \lambda_m} \quad \text{for } i = 1, 2, \dots, n \quad (5.87)$$

where  $\Delta\Lambda'_{im}$  denotes the  $(im)^{\text{th}}$  component of the matrix  $\Delta\mathbf{\Lambda}'$ . Since  $\Delta\mathbf{\Lambda}'$  is known (eqn. 5.29), it transpires from equation 5.37 that the truncation bias  $b_T[\chi]$  in the identified modal parameters  $\omega_i(\mathbf{0})$  and  $\xi_i(\mathbf{0})$ , for  $i = 1, 2, \dots, n$ , can be computed.

It remains to compute the sensitivities required to evaluate the expressions for the variance and the quadratic bias of the truncation bias. Assuming again that the eigenvalues are distinct, the derivatives of  $\delta_{\rho, \rho\rho}(\lambda_i)$  with respect to the perturbation  $\underline{\epsilon}$  are easily evaluated by differentiating equations 5.86 and 5.87 to yield

$$\delta_{j\rho}(\lambda_i) = \delta_j(\Delta\Lambda'_{ii}) \quad (5.88)$$

$$\delta_{jk\rho}(\lambda_i) = \delta_{jk}(\Delta\Lambda'_{ii}) \quad (5.89)$$

and

$$\begin{aligned} \delta_{j\rho\rho}(\lambda_i) = & \sum_{\substack{m=1 \\ m \neq i}}^{n'} \frac{1}{(\lambda_i(\mathbf{0}) - \lambda_m(\mathbf{0}))^2} \left\{ [\lambda_i(\mathbf{0}) - \lambda_m(\mathbf{0})] \delta_j [\Delta\Lambda'_{im}\Delta\Lambda'_{mi}] \right. \\ & \left. - [\delta_j(\lambda_i) - \delta_j(\lambda_m)] [\Delta\Lambda'_{im}\Delta\Lambda'_{mi}] \right\} \quad (5.90) \end{aligned}$$

$$\begin{aligned}
\delta_{jk\rho\rho}(\lambda_i) &= \sum_{\substack{m=1 \\ m \neq i}}^{n'} \frac{1}{(\lambda_i(\mathbf{Q}) - \lambda_m(\mathbf{Q}))^3} \left\{ [\lambda_i(\mathbf{Q}) - \lambda_m(\mathbf{Q})]^2 \delta_{jk} [\Delta\Lambda'_{im} \Delta\Lambda'_{mi}] \right. \\
&+ [\delta_j(\lambda_i) - \delta_j(\lambda_m)] [\delta_k(\lambda_i) - \delta_k(\lambda_m)] \Delta\Lambda'_{im} \Delta\Lambda'_{mi} \\
&- (\lambda_i(\mathbf{Q}) - \lambda_m(\mathbf{Q})) [(\delta_k(\lambda_i) - \delta_k(\lambda_m)) \delta_j (\Delta\Lambda'_{im} \Delta\Lambda'_{mi}) \\
&+ \delta_{jk} (\lambda_i - \lambda_m) \Delta\Lambda'_{im} \Delta\Lambda'_{mi}] \\
&+ \frac{1}{2} (\lambda_i(\mathbf{Q}) - \lambda_m(\mathbf{Q})) [(\delta_k(\lambda_i) - \delta_k(\lambda_m)) \delta_j (\Delta\Lambda'_{im} \Delta\Lambda'_{mi}) \\
&\left. - (\delta_j(\lambda_i) - \delta_j(\lambda_m)) \delta_k (\Delta\Lambda'_{im} \Delta\Lambda'_{mi}) \right\} \quad (5.91)
\end{aligned}$$

with (cf. eqns. 5.30)

$$\delta_j (\Delta\Lambda') = \delta_j [\mathbf{P}'^{-1} (\mathcal{H}_1 \mathbf{V}_2 \Sigma_2^{-1} \mathbf{U}_{21}^T) \mathbf{P}'] \quad (5.92)$$

$$\delta_{jk} (\Delta\Lambda') = \delta_{jk} [\mathbf{P}'^{-1} (\mathcal{H}_1 \mathbf{V}_2 \Sigma_2^{-1} \mathbf{U}_{21}^T) \mathbf{P}'] \quad (5.93)$$

for all  $i = 1, 2, \dots, n$  and where  $\Delta\Lambda'_{mi}$  denotes the  $(mi)^{th}$  component of the matrix  $\Delta\Lambda'$ . To evaluate equations 5.92 and 5.93, the first and second order derivatives with respect to  $\epsilon_j$  of  $\mathcal{H}_1$ ,  $\mathbf{V}_2$ ,  $\Sigma_2^{-1}$ ,  $\mathbf{U}_{21}^T$  and  $\mathbf{P}'$  are required. In principle,  $\delta_{j,jk}(\mathbf{V}_2)$ ,  $\delta_{j,jk}(\Sigma_2^{-1})$  and  $\delta_{j,jk}(\mathbf{U}_{21})$  can be computed from the theorem in section 5.3.1 by reformulating the SVD of  $\mathcal{H}_0$  as the eigenvalue decomposition of  $\mathcal{H}_0^T \mathcal{H}_0$  as was done before to compute the derivatives of  $\delta_{j,jk}(\mathbf{V}_1)$ ,  $\delta_{j,jk}(\Sigma_1^{-1})$  and  $\delta_{j,jk}(\mathbf{U}_1)$ . This time though, near-zero singular values in the SVD of  $\mathcal{H}_0$  are retained i.e.  $\Sigma_2$  is not set to zero. Estimating the sensitivities of singular vectors corresponding to near-zero small singular values can, however, cause some problems (Stewart, 2006). This proved to be indeed the case, in particular for the quadratic bias of the truncation as will be discussed shortly.

The computation of  $\delta_{j,jk}(\mathbf{P}')$  is problematic. In (Longman *et al.*, 1987), it is merely indicated that  $\delta_{j,jk}(\mathbf{P}')$  are to be computed by applying the theorem and its corollary to  $\mathbf{A}'(\underline{\epsilon})$ . A direct application of the theorem to  $\mathbf{A}'(\underline{\epsilon})$ , however, does not yield the  $n'$  derivatives of the  $n'$  eigenvectors  $\underline{p}'_i$  as required by equations 5.92 since, by construction of  $\mathbf{A}'(\underline{\epsilon})$  (c.f. section 5.3.1), the last  $(n' - n)$  eigenvalues of

this matrix are identically zero. Thus, the theorem and its corollary will only yield the eigenvector derivatives of the first  $n$  eigenvectors of  $\mathbf{A}'(\underline{\epsilon})$  but the derivatives of the eigenvectors corresponding to the repeated, identically zero eigenvalues cannot be obtained. Various authors have investigated the problem of finding the derivatives of eigenvectors associated with repeated eigenvalues. A SVD-based approach to this problem, originally developed by Lim and Juang (1989), is presented in the next section to find the derivatives of the repeated eigenvalues and eigenvectors of the system matrix  $\mathbf{A}$  to circumvent the theorem presented earlier, should the system have repeated modes. However, this method does not solve the problem of finding the  $(n' - n)$  eigenvector sensitivities corresponding to the identically zero eigenvalues of  $\mathbf{A}'(\underline{\epsilon})$  because these eigenvalues are zero by construction, and hence their derivatives, for all orders, will be identically zero as well. Similarly, the techniques by Friswell (1996); Juang *et al.* (1989), developed to cope with repeated eigenvalue derivatives, will, also fail to give these eigenvector derivatives. These methods rely on generating additional constraints using higher order derivatives and the eigenvalue derivatives, corresponding to this order, must be distinct to find a unique solution. Since, as explained above, the eigenvalue derivatives of the  $(n' - n)$  zero eigenvalues will be identically zero for all orders, a unique solution cannot be found and therefore, these methods are not applicable.

An approximate solution may nonetheless be found as follows. Let the dimensions of the the Hankel matrix  $\mathcal{H}_0$  be  $\dim(\mathcal{H}_0) = (n' \times g)$  with  $n' \geq g$ , so that its singular value decomposition is given according to equation 5.12. Let the  $n' \times n'$  matrix of left singular vectors  $\mathbf{U} = [\mathbf{U}_1 \mathbf{U}_{21} \mathbf{U}_{22}]$  be re-written as  $\mathbf{U} = [\mathbf{U}_1 \mathbf{U}_2]$  with  $\mathbf{U}_2 = [\mathbf{U}_{21} \mathbf{U}_{22}] \in \mathbb{R}^{n' \times (n'-n)}$ ,  $\mathbf{U}_{21} \in \mathbb{R}^{n' \times (g-n)}$  and  $\mathbf{U}_{22} \in \mathbb{R}^{n' \times (n'-g)}$ . Substituting this expression for  $\mathbf{U}$  in equation 5.22, the eigenvector matrix of  $\mathbf{A}'$  can be reformulated

as

$$\mathbf{P}' = [\mathbf{U}_1 \mathbf{U}_2] \begin{bmatrix} \Sigma_1^{\frac{1}{2}} & \mathbf{0} \\ \mathbf{0} & \mathbf{I} \end{bmatrix} \begin{bmatrix} \mathbf{P} & \mathbf{0} \\ \hat{\mathbf{P}} & \mathbf{I} \end{bmatrix} = \begin{bmatrix} \mathbf{U}_1 \Sigma_1^{\frac{1}{2}} \mathbf{P} + \mathbf{U}_2 \hat{\mathbf{P}} & \mathbf{U}_2 \end{bmatrix} \quad (5.94)$$

where the first partition  $\mathbf{U}_1 \boldsymbol{\Sigma}_1^{\frac{1}{2}} \mathbf{P} + \mathbf{U}_2 \hat{\mathbf{P}} \in \mathbb{R}^{n' \times n}$ . The derivatives, in operator form, of the eigenvector matrix  $\mathbf{P}'$  of  $\mathbf{A}'$  are then reduced to

$$\delta_{j,jk}(\mathbf{P}') = \left[ \delta_{j,jk} \left( \mathbf{U}_1 \boldsymbol{\Sigma}_1^{\frac{1}{2}} \mathbf{P} + \mathbf{U}_2 \hat{\mathbf{P}} \right) \quad \delta_{j,jk}(\mathbf{U}_2) \right] \quad (5.95)$$

The expressions for  $\delta_{j,jk} \left( \mathbf{U}_1 \boldsymbol{\Sigma}_1^{\frac{1}{2}} \mathbf{P} + \mathbf{U}_2 \hat{\mathbf{P}} \right)$ , which consists of the derivatives of the first  $n$  eigenvectors of  $\mathbf{A}'$  corresponding to the  $n$  non-zero eigenvalues of  $\mathbf{A}'$ , or equivalently of  $\mathbf{A}$ , can then be found from the theorem applied to  $\mathbf{A}'$  and it remains to find  $\delta_{j,jk}(\mathbf{U}_2)$  which is obtained by application of the theorem and its corollary to  $\mathcal{H}_0^T \mathcal{H}_0$  with no singular value truncation performed. So far, no approximation has been made but we can actually only obtain the derivatives of the full  $n' \times n'$  matrix  $\mathbf{P}'$  in the case when  $n' \leq g$ , the reason being that the number of singular values resulting from the SVD of  $\mathcal{H}_0$  is equal to its smallest dimension so that when  $n' \geq g$ , the eigenvalue matrix of  $\mathcal{H}_0^T \mathcal{H}_0$  has dimensions  $g \times g$ . Therefore, only the derivatives of the  $g$  first left singular vectors can be found by application of the theorem to  $\mathcal{H}_0^T \mathcal{H}_0$ . Moreover, since this matrix is not square,  $\mathbf{Q}_{1:g}^T \equiv \mathbf{P}'^{-1}_{1:g}$  does not exist but the derivatives of the first  $g$  rows of  $\mathbf{Q}_{1:g}^T \equiv \mathbf{P}'^{-1}_{1:g}$  may be estimated by approximating  $\mathbf{P}'_{1:g}$  as

$$\delta_{j,jk}(\mathbf{P}'_{1:g}) \approx \left[ \delta_{j,jk} \left( \mathbf{U}_1 \boldsymbol{\Sigma}_1^{\frac{1}{2}} \mathbf{P} + \mathbf{U}_{21} \hat{\mathbf{P}}_{1:(g-n)} \right) \quad \delta_{j,jk}(\mathbf{U}_{21}) \right] \quad (5.96)$$

where  $\hat{\mathbf{P}}_{1:(g-n)}$  denotes the first  $(g-n)$  rows of  $\hat{\mathbf{P}}$ . The matrix  $\mathbf{Q}_{1:g}^T$  such that  $\mathbf{Q}_{1:g}^T \mathbf{P}'_{1:g} = \mathbf{I}_{g \times g}$  can be found to be

$$\begin{aligned} \mathbf{Q}_{1:g}^T &= \begin{bmatrix} \mathbf{P}^{-1} & \mathbf{0} \\ \hat{\mathbf{P}}_{1:(g-n)} \mathbf{P}^{-1} & \mathbf{P}^{-1} \end{bmatrix} \begin{bmatrix} \boldsymbol{\Sigma}_1^{-\frac{1}{2}} & \mathbf{0} \\ \mathbf{0} & \mathbf{I} \end{bmatrix} \begin{bmatrix} \mathbf{U}_1^T \\ \mathbf{U}_{21}^T \end{bmatrix} \\ &= \begin{bmatrix} \mathbf{P}^{-1} \boldsymbol{\Sigma}_1^{-\frac{1}{2}} \mathbf{U}_1^T \\ -\hat{\mathbf{P}}_{1:(g-n)} \mathbf{P}^{-1} \boldsymbol{\Sigma}_1^{-\frac{1}{2}} \mathbf{U}_1^T + \mathbf{U}_{21}^T \end{bmatrix} \end{aligned} \quad (5.97)$$

$\hat{\mathbf{P}}$  is given by equation 5.19. The derivatives of all the entries in the matrix  $\mathbf{Q}_{1:g}^T$  are



known so that

$$\delta_{j,jk}(\mathbf{Q}_{1:g}^T) = \begin{bmatrix} \delta_{j,jk} \left( \mathbf{P}^{-1} \boldsymbol{\Sigma}_1^{-\frac{1}{2}} \mathbf{U}_1^T \right) \\ -\delta_{j,jk} \left( \hat{\mathbf{P}} \mathbf{P}^{-1} \boldsymbol{\Sigma}_1^{-\frac{1}{2}} \mathbf{U}_1^T + \mathbf{U}_{21}^T \right) \end{bmatrix} \quad (5.98)$$

can be evaluated using the standard rules of differentiation. These two matrices can then be used to approximate equations 5.88 to 5.92. Some time was devoted to circumvent this problem, since the variance of the truncation bias informs the user of how much confidence he or she can place on these estimates and provides vital information if a bias correction of the identified modal parameters is considered. However, a more adequate solution could not be found and further research is needed. It will be shown in the next chapter, that the approximation above can be considered satisfactory to obtain an indication of the extent of random error in the truncation bias but, clearly, high accuracy cannot be expected. When the same approximation was used on for the quadratic bias of the truncation bias, simulations showed that the results were very unstable. The reason may be attributed to the fact that the singular vectors used in these computations are associated with small singular values and it is known that the singular spaces associated with small singular values are extremely sensitive (Stewart, 1990, 2006) to small perturbations.

## 5.4 Extension to Repeated Eigenvalues

The problem of finding the derivatives of repeated eigenvalues and associated eigenvectors has been studied extensively, in particular in relation to changes in the modal frequencies as a function of the structural design parameters. For instance, Dailey (1989) presents an extension of Nelson's method (Nelson, 1976) to calculate the first order derivatives of eigenvectors associated with repeated eigenvalues but distinct eigenvalues derivatives. Friswell (1996) has extended this approach to account for the situation where both the eigenvalues and their derivatives are repeated. Juang *et al.* (1989) developed a modal expansion approach able to deal with both degenerate

eigenvalues and eigenvalue derivatives. The implementation of any of these methods, that account for repeated eigenvalues, require knowledge of the multiplicity of the degenerate eigenvalue. This is usually clear when one deals with analytical models. In this case, however, in which the model consists of the identified state-matrix  $\mathbf{A}$  from experimentally obtained data, the multiplicity of a particular eigenvalue is not necessarily clear. Using the fact that the singular value decomposition (SVD) is a generally reliable way to calculate the rank, and hence the multiplicity of an eigenvalue, Lim and Juang (1989) have developed an SVD-based method to calculate the first order sensitivities of repeated eigenvalues and corresponding eigenvectors. This method, outlined below and extended to compute second order (mixed) derivatives, is employed in this thesis to assess the degeneracy of repeated eigenvalues and to compute the corresponding eigenvalue and eigenvector sensitivities in a fully automated manner. Assume that the  $n \times n$  identified state-matrix  $\mathbf{A}(\underline{0}) \equiv \mathbf{A}$  is non-defective so that eigenvalue problem for the  $i^{th}$  eigenvalue  $\lambda_i$  of  $\mathbf{A}$  can be written as

$$(\mathbf{A} - \lambda_i \mathbf{I}) \underline{\mathbf{p}}_i \equiv \mathbf{A}_i \underline{\mathbf{p}}_i = \mathbf{0} \quad (5.99)$$

where, as before,  $\underline{\mathbf{p}}_i$  is the  $i^{th}$  right eigenvector of  $\mathbf{A}$  and we have defined  $(\mathbf{A} - \lambda_i \mathbf{I}) \equiv \mathbf{A}_i$ . It follows from equation 5.99 that the  $i^{th}$  eigenvector  $\underline{\mathbf{p}}_i$  belongs to the kernel of  $\mathbf{A}_i$ . If the multiplicity of  $\lambda_i$  is 1, i.e. if it is non-repeated or *simple*, then the kernel of  $\mathbf{A}_i$ , denoted by  $ker(\mathbf{A}_i)$ , is 1-dimensional and  $\underline{\mathbf{p}}_i$  may be chosen as its basis. However, if the multiplicity of  $\lambda_i > 1$ , the dimension of the  $ker(\mathbf{A}_i) > 1$  and -assuming  $\mathbf{A}_i$  to be non-defective- the dimension of the  $ker(\mathbf{A}_i)$  is equal to the multiplicity of the repeated eigenvalue  $\lambda_i$ . As a result, any vector in  $ker(\mathbf{A}_i)$  is an eigenvector of this repeated eigenvalue and hence non-unique. Thus, the rank  $r_i \equiv rank(\mathbf{A}_i)$  of  $\mathbf{A}_i$ , and the dimension of  $ker(\mathbf{A}_i)$ ,  $\nu_i = n - r_i$ , will indicate whether  $\lambda_i$  is degenerate or not. The singular value decomposition of  $\mathbf{A}_i$  then yields

$$\mathbf{A}_i = \begin{bmatrix} \tilde{\mathbf{T}}_i & \mathbf{T}_i \end{bmatrix} \begin{bmatrix} \mathbf{D}_i & \mathbf{0} \\ \mathbf{0} & \mathbf{0} \end{bmatrix} \begin{bmatrix} \tilde{\mathbf{W}}_i^T \\ \mathbf{W}_i^T \end{bmatrix} \quad (5.100)$$

with  $\tilde{\mathbf{T}}_i \in \mathbb{R}^{n \times r_i}$ ,  $\mathbf{T}_i \in \mathbb{R}^{n \times \nu_i}$ ,  $\mathbf{D}_i \in \mathbb{R}^{r_i \times r_i}$ ,  $\tilde{\mathbf{W}}_i \in \mathbb{R}^{n \times r_i}$  and  $\mathbf{W}_i \in \mathbb{R}^{n \times \nu_i}$ . Therefore, the multiplicity of the  $i^{\text{th}}$  eigenvalue is determined by  $\nu_i$  and a basis for the right eigenvector corresponding to the  $i^{\text{th}}$  repeated eigenvalue is given by  $\mathbf{W}_i$ . For  $\nu_i = \ker(\mathbf{A}_i)$  to yield the multiplicity of  $\lambda_i$ , the matrix  $\mathbf{A}_i$  must be non-defective <sup>†</sup>. When the eigenvalue problem is formulated with analytical stiffness and mass matrices as in Dailey (1989); Friswell (1996); Nelson (1976), non-defectiveness is guaranteed since these matrices are real symmetric (Strang, 1998). In the present case, however, where the state-matrix is identified from measured data, which may exhibit non-proportional damping properties, the non-defective property of  $\mathbf{A}_i$  is in general not guaranteed (Luongo, 2006). The eigenvalue and eigenvector sensitivities for defective matrices have been studied, for instance in Luongo (1993); Zhang and Zhang (2001), but this case will not be covered in this thesis because we can generally expect matrices representing physical systems to be non-defective (Pang, 1997) and we shall use this assumption henceforth. Assume that the algebraic multiplicity of the  $i^{\text{th}}$  eigenvalue  $\lambda_i$  is  $\nu_i$ . Thus,  $\lambda_i = \lambda_i^{(1)} = \lambda_i^{(2)} = \dots = \lambda_i^{(\nu_i)}$  and let  $\{\mathbf{p}_i^{(1)}, \mathbf{p}_i^{(2)}, \dots, \mathbf{p}_i^{(\nu_i)}\}$  be some choice of right eigenvectors corresponding to  $\lambda_i$ . Since  $\mathbf{W}_i$  forms a basis for the right eigenvectors of  $\lambda_i$ , the  $l^{\text{th}}$  eigenvector corresponding to  $\lambda_i$  can be written as

$$\mathbf{p}_i^{(l)} = \mathbf{W}_i \mathbf{a}_i^{(l)} \quad (5.101)$$

where  $\mathbf{a}_i \in \mathbb{R}^{\nu_i \times 1}$  is the vector of coordinates for  $\mathbf{p}_i$  in the basis  $\mathbf{W}_i$ . Similarly, the left singular vectors in  $\mathbf{T}_i^*$  form a basis for the corresponding left eigenvectors  $\mathbf{q}_i^{(l)}$  where  $(\cdot)^*$  denotes the complex conjugate. The matrix of left eigenvectors corresponding to the  $\lambda_i$  may then be written as  $\mathbf{Q}_i = \mathbf{T}_i^* \mathbf{b}_i$  with  $\mathbf{b}_i = [\mathbf{b}_i^{(1)}, \mathbf{b}_i^{(2)}, \dots, \mathbf{b}_i^{(\nu_i)}]$  being the matrix containing the vectors of coefficients  $\mathbf{b}_i^{(l)}$  in the basis  $\mathbf{T}_i^*$ . Imposing the same normalisation as in the theorem above, namely  $\mathbf{Q}_i^T \mathbf{P}_i = \mathbf{I}_{\nu_i \times \nu_i}$ , the matrix of left eigenvector coefficients  $\mathbf{b}_i$  satisfying this condition is  $\mathbf{b}_i^T = \mathbf{a}_i^{-1} (\mathbf{T}_i^H \mathbf{W}_i)^{-1}$ ,

<sup>†</sup>To clarify the terminology used here, it is noted that by the multiplicity of  $\lambda_i$ , we refer to the multiplicity of the root  $\lambda_i$  to the polynomial  $\det(\mathbf{A}_i) = 0$ . This is also known as the *algebraic* multiplicity of  $\lambda_i$ . The dimension of  $\ker(\mathbf{A}_i)$ ,  $\nu_i = n - r_i$  is known as the *geometric* multiplicity of  $\lambda_i$ . For defective matrices the geometric multiplicity is strictly smaller than the algebraic multiplicity.

with  $\mathbf{a}_i = [\mathbf{a}_i^{(1)}, \mathbf{a}_i^{(2)}, \dots, \mathbf{a}_i^{(\nu_i)}]$  and  $\mathbf{P}_i$  the matrix of the right eigenvectors. Unlike the expressions for the non-repeated eigenvalue/eigenvector derivatives given in the theorem, no closed-form solutions for the sensitivities of repeated eigenvalues and corresponding eigenvectors are found using this approach. Differentiating equation 5.99 with respect to  $\epsilon_j$ , premultiplying by the result by the Hermitian of the left singular vectors  $[\tilde{\mathbf{T}}_i \ \mathbf{T}_i]$ , it can be shown that (Lim and Juang, 1989) the first order derivative of the repeated eigenvalue  $\lambda_i$  with corresponding eigenvector  $\mathbf{p}_i^{(l)} = \mathbf{W}_i \mathbf{a}_i^{(l)}$  satisfies the generalized eigenvalue problem of order  $\nu_i$

$$[\mathbf{T}_i^H \delta_j^{(l)}(\mathbf{A}) \mathbf{W}_i] \mathbf{a}_{i,j}^{(l)} = \delta_j^{(l)}(\lambda_i) \mathbf{T}_i^H \mathbf{W}_i \mathbf{a}_{i,j}^{(l)} \quad (5.102)$$

It is seen the the solution to this eigenvalue equation has eigenvalues yielding the eigenvalue derivative of the  $l^{\text{th}}$  repeated eigenvalue with respect to  $\epsilon_j$ ,  $\delta_j^{(l)}(\lambda_i)$ , and eigenvectors giving the coefficient vector  $\mathbf{a}_{i,j}$ , and hence the corresponding eigenvector  $\mathbf{p}_i^{(l)} = \mathbf{W}_i \mathbf{a}_{i,j}^{(l)}$ . Note that we have introduced the notation  $\mathbf{a}_{i,j}$  instead of simply  $\mathbf{a}_i$  as in equation 5.101 above to signify that  $\mathbf{a}_{i,j}$  is the eigenvector corresponding to  $\delta_j^{(l)}(\lambda_i)$ , i.e. when derivative is taken with respect to  $\epsilon_j$ . It is important to note that, in order to determine  $\mathbf{a}_{i,j}$  uniquely, it is required that the eigenvalue derivatives  $\delta_j^{(l)}(\lambda_i)$ , for  $l = 1, 2, \dots, \nu_i$  are distinct. It is also noted that if  $\lambda_i$  is simple, the above equation reduces to the exact same equation as in the theorem. To find the corresponding first order eigenvector derivative, we expand  $\delta_j^{(l)}(\mathbf{p}_i)$  in the basis formed by the right singular vectors as

$$\delta_j^{(l)}(\mathbf{p}_i) = \tilde{\mathbf{W}}_i \tilde{\gamma}_{i,j}^{(l)} + \mathbf{W}_i \gamma_{i,j}^{(l)} \quad (5.103)$$

where  $\tilde{\gamma}_{i,j}^{(l)} \in \mathbb{R}^{r_i \times 1}$  and  $\gamma_{i,j}^{(l)} \in \mathbb{R}^{\nu_i \times 1}$  are the coefficients of the eigenvector derivative in the range and kernel of  $\mathbf{A}_i$  respectively that need to be determined. This is similar to the expansion in the theorem above except that it is done in the orthonormal basis found through the SVD of  $\mathbf{A}_i$  since the eigenvectors are not linearly independent in this case and hence do not form a basis. The computation of  $\tilde{\gamma}_{i,j}^{(l)}$  is straightforward

and can be found from the first order derivative of the eigenvalue equation 5.99 to be

$$\tilde{\gamma}_{i,j}^{(l)} = -\mathbf{D}_i^{-1} \mathbf{T}_i^H \delta_j^{(l)}(\mathbf{A}_i) \mathbf{W}_i \underline{\mathbf{a}}_{i,j}^{(l)} \quad (5.104)$$

with  $\delta_j^{(l)}(\mathbf{A}_i) = \delta_j^{(l)}(\mathbf{A}) - \delta_j^{(l)}(\lambda_i) \mathbf{I}$ . The first order derivative of the eigenvalue equation 5.99, that is  $\delta_j^{(l)}(\mathbf{A}_i) \underline{\mathbf{p}}_i^{(l)} = -\mathbf{A}_i \delta_j^{(l)}(\underline{\mathbf{p}}_i)$ , does not contain any information about  $\gamma_{i,j}^{(l)}$  since, by definition, it expresses the coefficients of  $\delta_j^{(l)}(\underline{\mathbf{p}}_i)$  that lie in the kernel of  $\mathbf{A}_i$  and therefore vanishes from  $\delta_j^{(l)}(\mathbf{A}_i) \underline{\mathbf{p}}_i^{(l)} = -\mathbf{A}_i \delta_j^{(l)}(\underline{\mathbf{p}}_i)$ . On the other hand, however,  $\mathbf{W}_i \gamma_{i,j}^{(l)}$  is not in the kernel of  $\delta_j^{(l)}(\mathbf{A}_i)$  so that an equation for  $\gamma_{i,j}^{(l)}$  can be found from the second order derivative of the eigenvalue equation 5.99 and reads (Lim and Juang, 1989)

$$\left[ \mathbf{T}_i^H \delta_j^{(l)}(\mathbf{A}_i) \mathbf{W}_i \right] \gamma_{i,j}^{(l)} = -\mathbf{T}_i^H \left[ \delta_{jj}^{(l)}(\mathbf{A}_i) - \delta_j^{(l)}(\mathbf{A}_i) \bar{\mathbf{W}}_i \mathbf{D}_i^{-1} \bar{\mathbf{T}}_i^H \delta_j^{(l)}(\mathbf{A}_i) \right] \mathbf{W}_i \underline{\mathbf{a}}_{i,j}^{(l)} \quad (5.105)$$

This yields  $\nu_i$  equations to solve for the  $\nu_i$  coefficients in  $\gamma_{i,j}^{(l)}$ . However, these equations are not linearly independent. Assuming that  $\delta_i^{(l)}(\lambda_i)$ , for  $l = 1, 2, \dots, \nu_i$ , are distinct, it follows from the eigenvalue equation 5.102 that the pencil  $(\mathbf{T}_i^H \delta_j^{(l)}(\mathbf{A}) \mathbf{W}_i - \mathbf{T}_i^H \mathbf{W}_i)$  has rank  $\nu_i - 1$  and so does the matrix  $[\mathbf{T}_i^H \delta_j^{(l)}(\mathbf{A}_i) \mathbf{W}_i]$  so that the system of equations in 5.105 is underdetermined. The remaining constraint may be found from the consistent normalisation of the eigenvectors, namely that  $\underline{\mathbf{p}}_i^{(l)T} \underline{\mathbf{p}}_i^{(l)} = 1$ . Differentiating the latter expression with respect to  $\epsilon_j$  and using equations 5.101 and 5.103 then yields the additional condition as

$$\underline{\mathbf{p}}_i^{(l)T} \delta_j^{(l)}(\underline{\mathbf{p}}_i) = \underline{\mathbf{a}}_{i,j}^{(l)T} \gamma_{i,j}^{(l)} = 0 \quad (5.106)$$

Inspection of equation 5.105 reveals that the second order derivative of  $\lambda_i$  is needed to evaluate  $\delta_{jj}^{(l)}(\mathbf{A}_i) = \delta_{jj}^{(l)}(\mathbf{A}) - \delta_{jj}^{(l)}(\lambda_i) \mathbf{I}$ . Differentiating the first order derivative of the eigenvalue equation with respect to  $\epsilon_k$  and premultiplying the result with the transpose of left eigenvector  $\underline{\mathbf{q}}_i^{(l)}$ , the expression for the mixed second order eigenvector

derivative reads

$$\delta_{jk}^{(l)}(\lambda_i) = \mathbf{q}_i^{(l)T} \delta_{jk}(\mathbf{A}) \mathbf{W}_i \mathbf{p}_{i,j}^{(l)} + \frac{1}{2} \mathbf{q}_i^{(l)T} \left[ \delta_j^{(l)}(\mathbf{A}_i) \tilde{\mathbf{W}}_i \tilde{\gamma}_{i,k}^{(l)} + \delta_k^{(l)}(\mathbf{A}_i) \tilde{\mathbf{W}}_i \tilde{\gamma}_{i,j}^{(l)} \right] \quad (5.107)$$

and the expression for  $\delta_{jj}^{(l)}(\lambda_i)$  follows by replacing  $k$  with  $j$ . In equation 5.107, we made use of the fact that  $\mathbf{q}_i^{(l)T} \delta_j^{(l)}(\mathbf{A}_i) \mathbf{W}_i = \mathbf{0}$  (Lim and Juang, 1989). It now remains to find the second order derivatives of the eigenvectors  $\mathbf{p}_i^{(l)}$ . As for the first order derivative, we start by expanding  $\delta_{jk}^{(l)}(\mathbf{p}_i)$  as

$$\delta_{jk}^{(l)}(\mathbf{p}_i) = \tilde{\mathbf{W}}_i \tilde{\theta}_{i,jk}^{(l)} + \mathbf{W}_i \theta_{i,jk}^{(l)} \quad (5.108)$$

$$\delta_{jj}^{(l)}(\mathbf{p}_i) = \tilde{\mathbf{W}}_i \tilde{\theta}_{i,jj}^{(l)} + \mathbf{W}_i \theta_{i,jj}^{(l)} \quad (5.109)$$

Since the expressions for the second order derivatives of  $\mathbf{p}_i^{(l)}$  are not given in Lim and Juang (1989), the derivations to follow are a little more detailed. The second order mixed derivative of the eigenvalue equation 5.99 yields

$$\delta_{jk}^{(l)}(\mathbf{A}_i) \mathbf{p}_i^{(l)} + \frac{1}{2} \left[ \delta_j^{(l)}(\mathbf{A}_i) \delta_k^{(l)}(\mathbf{p}_i) + \delta_k^{(l)}(\mathbf{A}_i) \delta_j^{(l)}(\mathbf{p}_i) \right] = -\tilde{\mathbf{T}}_i \mathbf{D}_i \tilde{\mathbf{W}}_i \delta_{jk}^{(l)}(\mathbf{p}_i) \quad (5.110)$$

Premultiplying 5.110 by  $[\tilde{\mathbf{T}}_i \quad \mathbf{T}_i]^H$ , and using 5.108, the first partition reads

$$\tilde{\mathbf{T}}_i^H \delta_{jk}^{(l)}(\mathbf{A}_i) \mathbf{p}_i^{(l)} + \frac{1}{2} \tilde{\mathbf{T}}_i^H \left[ \delta_j^{(l)}(\mathbf{A}_i) \delta_k^{(l)}(\mathbf{p}_i) + \delta_k^{(l)}(\mathbf{A}_i) \delta_j^{(l)}(\mathbf{p}_i) \right] = -\mathbf{D}_i \tilde{\theta}_{i,jk}^{(l)} \quad (5.111)$$

so that

$$\tilde{\theta}_{i,jk}^{(l)} = -\mathbf{D}_i^{-1} \tilde{\mathbf{T}}_i^H \delta_{jk}^{(l)}(\mathbf{A}_i) \mathbf{p}_i^{(l)} + \frac{1}{2} \tilde{\mathbf{T}}_i^H \left[ \delta_j^{(l)}(\mathbf{A}_i) \delta_k^{(l)}(\mathbf{p}_i) + \delta_k^{(l)}(\mathbf{A}_i) \delta_j^{(l)}(\mathbf{p}_i) \right] \quad (5.112)$$

The expression for  $\tilde{\theta}_{i,jj}^{(l)}$  follows directly from 5.112 by replacing  $k$  with  $j$ . In the same fashion as the second order derivative was needed to compute  $\gamma_{i,j}^{(l)}$ , the third order derivatives are needed to find  $\theta_{i,jk}^{(l)}$ . Define  $\delta_{jkk}(\cdot) = \frac{\partial}{\partial \epsilon_k} [\delta_{jk}(\cdot)]$ . Differentiating equation 5.110 with respect to  $\epsilon_k$ , premultiplying by  $[\tilde{\mathbf{T}}_i \quad \mathbf{T}_i]^H$ , the equation for  $\theta_{i,jk}^{(l)}$

then follows from the second partition as

$$\begin{aligned} \left[ \mathbf{T}_i^H \delta_k^{(l)}(\mathbf{A}_i) \mathbf{W}_i \right] \underline{\varrho}_{i,jk}^{(l)} &= -\frac{1}{2} \mathbf{T}_i^H \left[ \delta_{jkk}^{(l)}(\mathbf{A}_i) \mathbf{p}_i^{(l)} + 2\delta_{jk}^{(l)}(\mathbf{A}_i) \delta_k^{(l)}(\mathbf{p}_i) \right. \\ &\quad \left. + \delta_j^{(l)}(\mathbf{A}_i) \delta_{kk}^{(l)}(\mathbf{p}_i) + \delta_{kk}^{(l)}(\mathbf{A}_i) \delta_j^{(l)}(\mathbf{p}_i) \right] - \mathbf{T}_i^H \delta_k^{(l)}(\mathbf{A}_i) \tilde{\mathbf{W}}_i \tilde{\underline{\varrho}}_{i,jk}^{(l)} \end{aligned} \quad (5.113)$$

and the expression for  $\underline{\varrho}_{i,jj}^{(l)}$  follows from the above equation by replacing  $k$  by  $j$ . It is noted that  $\delta_{kk}^{(l)}(\mathbf{p}_i)$  features in the expression of  $\delta_{jk}^{(l)}(\mathbf{p}_i)$ . Thus equation 5.113 needs to be evaluated first for  $\delta_{kk}^{(l)}(\mathbf{p}_i)$  and which can then be used to evaluate  $\delta_{jk}^{(l)}(\mathbf{p}_i)$ . Also,  $\delta_{jkk}^{(l)}(\lambda_i)$  is required in equation 5.113. Differentiating equation 5.110 with respect to  $\epsilon_k$ , premultiplying this derivative by  $\mathbf{q}_i^{(l)T}$  and using  $\mathbf{q}_i^{(l)T} \delta_j^{(l)}(\mathbf{A}_i) \mathbf{W}_i = \mathbf{0}$ , gives the desired result

$$\begin{aligned} \delta_{jkk}^{(l)}(\lambda_i) &= \mathbf{q}_i^{(l)T} \delta_{jkk}^{(l)}(\mathbf{A}_i) \mathbf{p}_i^{(l)} + 2 \mathbf{q}_i^{(l)T} \left[ \delta_{jk}^{(l)}(\mathbf{A}_i) \delta_k^{(l)}(\mathbf{p}_i) + \delta_k^{(l)}(\mathbf{A}_i) \tilde{\mathbf{W}}_i \tilde{\underline{\varrho}}_{i,jk}^{(l)} \right] \\ &\quad + \mathbf{q}_i^{(l)T} \left[ \delta_{kk}^{(l)}(\mathbf{A}_i) \delta_j^{(l)}(\mathbf{p}_i) + \delta_j^{(l)}(\mathbf{A}_i) \tilde{\mathbf{W}}_i \tilde{\underline{\varrho}}_{i,kk}^{(l)} \right] \end{aligned} \quad (5.114)$$

Following the same argument as for the first order case, this system of  $\nu_i$  equations is rank deficient by 1. Again, the extra constraint can be found from the consistent normalisation of eigenvectors. Taking the mixed second order derivative of  $\mathbf{p}_i^{(l)T} \mathbf{p}_i^{(l)} = 1$ , and using equations 5.101 and 5.108, gives the expression for the remaining constraint can be found to be

$$\mathbf{a}_{i,j}^{(l)T} \underline{\varrho}_{i,jk}^{(l)} = \frac{1}{2} \delta_k^{(l)}(\mathbf{p}_i^T) \delta_j^{(l)}(\mathbf{p}_i) \quad (5.115)$$

To solve the the underdetermined systems in equations 5.105 and 5.113, a particular solution is first computed by taking the pseudo-inverse of  $\left[ \mathbf{T}_i^H \delta_k^{(l)}(\mathbf{A}_i) \mathbf{W}_i \right]$ . of For equation 5.105, the particular solution  $\underline{\gamma}_{i,j}^{(l,Part.)}$  then yields

$$\underline{\gamma}_{i,j}^{(l,Part.)} = - \left[ \mathbf{T}_i^H \delta_j^{(l)}(\mathbf{A}_i) \mathbf{W}_i \right]^\dagger \mathbf{T}_i^H \left[ \delta_{jj}^{(l)}(\mathbf{A}_i) - \delta_j^{(l)}(\mathbf{A}_i) \tilde{\mathbf{W}}_i \mathbf{D}_i^{-1} \tilde{\mathbf{T}}_i^H \delta_j^{(l)}(\mathbf{A}_i) \right] \mathbf{W}_i \underline{\mathbf{a}}_{i,j}^l \quad (5.116)$$

$\underline{\gamma}_{i,j}^{(l,Part.)}$  is the unique solution to 5.105 in the  $(\nu_i - 1)$ -dimensional subspace in  $\mathbb{R}^{\nu_i}$  orthogonal to the kernel of  $\left[ \mathbf{T}_i^H \delta_j^{(l)}(\mathbf{A}_i) \mathbf{W}_i \right]$  and has minimal Euclidean norm (Penrose, 1956). The general solution of  $\underline{\gamma}_{i,j}^{(l)}$  in  $\mathbb{R}^{\nu_i}$  therefore requires the additional compo-

ment in the kernel of  $[\mathbf{T}_i^H \delta_j^{(l)} (\mathbf{A}_i) \mathbf{W}_i]$ . Since this kernel is 1-dimensional (by the assumption of non-repeated eigenvalue derivatives) and  $\underline{\mathbf{a}}_{i,j}^{(l)}$ , by equation 5.102, is in the kernel, the general solution can be written as

$$\gamma_{i,j}^{(l)} = \gamma_{i,j}^{(l,Part.)} + g_{i,j}^{(l)} \underline{\mathbf{a}}_{i,j}^{(l)} \quad (5.117)$$

The scalar  $g_{i,j}^{(l)}$  can then be determined from the additional constraint imposed by the consistent normalisation 5.106, i.e.

$$g_{i,j}^{(l)} = \frac{\underline{\mathbf{a}}_{i,j}^{(l)T} \gamma_{i,j}^{(l,Part.)}}{\underline{\mathbf{a}}_{i,j}^{(l)T} \underline{\mathbf{a}}_{i,j}^{(l)}} \quad (5.118)$$

Exactly the same process applies to solve for  $\theta_{i,jk}^{(l)}$  from equation 5.113 except that the constraint imposed by the consistent normalisation is given by equation 5.115. This finishes the exposition of the computation of the first and (mixed) second order eigenvalue/eigenvector derivatives. This method was not extended to allow the computation of the truncation bias and its associated variance and quadratic bias.

## 5.5 Derivatives for Mode shapes

To establish the error in the complete identified modal model, it remains to find the random and bias error in the SSI/Cov-identified mode shapes  $\phi$ . The latter are computed in the SSI/Cov according to equation 2.53

$$\phi = \mathbf{C} \mathbf{P} \quad (5.119)$$

where  $\mathbf{P}$ , in the notation used in this chapter, denotes the matrix of left eigenvectors of the identified state-matrix  $\mathbf{A}$  and  $\mathbf{C}$  is the identified output-influence matrix described in Chapter 2, section 2.3.2. Like the state-matrix, the identified output-influence matrix  $\mathbf{C}$  can be factorized into the factors obtained through the SVD of the Hankel matrix  $\mathcal{H}_0$ , i.e.  $\mathbf{U}_1, \Sigma_1$  and  $\mathbf{V}_1$ . More precisely, the factorization is (Juang and Pappa,



1984)

$$\mathbf{C} = \mathbf{E}^T \mathbf{U}_1 \boldsymbol{\Sigma}_1^{\frac{1}{2}} \quad (5.120)$$

where  $\mathbf{E}$  is a  $(n' \times p)$  matrix consisting of zeros ( $p$  being the number of sensors) and the first  $p$  rows replaced by the  $p \times p$  identity matrix. This matrix is constant so that its derivative is zero. Since the sensitivities of  $\mathbf{U}_1$  and  $\boldsymbol{\Sigma}_1^{\frac{1}{2}}$  are known (see section 5.3.2), the derivatives of  $\mathbf{C}$  can be computed. In operator form, they yield

$$\delta_j(\mathbf{C}) = \mathbf{E}^T \delta_j(\mathbf{U}_1) \boldsymbol{\Sigma}_1^{\frac{1}{2}} + \mathbf{E}^T \mathbf{U}_1 \delta_j \left( \boldsymbol{\Sigma}_1^{\frac{1}{2}} \right) \quad (5.121)$$

$$\begin{aligned} \delta_{jk}(\mathbf{C}) &= \mathbf{E}^T \delta_{jk}(\mathbf{U}_1) \boldsymbol{\Sigma}_1^{\frac{1}{2}} + \mathbf{E}^T \mathbf{U}_1 \delta_{jk} \left( \boldsymbol{\Sigma}_1^{\frac{1}{2}} \right) \\ &+ \frac{1}{2} \mathbf{E}^T \left[ \delta_j(\mathbf{U}_1) \delta_k \left( \boldsymbol{\Sigma}_1^{\frac{1}{2}} \right) + \delta_k(\mathbf{U}_1) \delta_j \left( \boldsymbol{\Sigma}_1^{\frac{1}{2}} \right) \right] \end{aligned} \quad (5.122)$$

Since the derivatives of the eigenvectors are known from section 5.3.1, the derivatives of the mode shapes at the sensor locations yield

$$\delta_j(\boldsymbol{\phi}) = \delta_j(\mathbf{C}) \mathbf{P} + \mathbf{C} \delta_j(\mathbf{P}) \quad (5.123)$$

$$\begin{aligned} \delta_{jk}(\boldsymbol{\phi}) &= \delta_{jk}(\mathbf{C}) \mathbf{P} + \mathbf{C} \delta_{jk}(\mathbf{P}) \\ &+ \frac{1}{2} [\delta_j(\mathbf{C}) \delta_k(\mathbf{P}) + \delta_k(\mathbf{C}) \delta_j(\mathbf{P})] \end{aligned} \quad (5.124)$$

with  $\delta_{j,jk}(\mathbf{C})$  as given by equations 5.121 and 5.123 respectively.

With  $\delta_{j,jk}(\boldsymbol{\phi})$  at hand, the variance and the quadratic bias of the mode shapes at the sensor locations can be computed. For the computation of the truncation bias, together with its variance and quadratic bias, similar to the approach given here for modal damping ratios and frequencies can be found in Longman *et al.* (1987).

## 5.6 Summary and Discussion

In this chapter, a perturbation theoretic method to compute the variance and the bias, and hence the random and systematic error of the SSI/Cov-identified natural frequen-

cies, modal damping ratios and mode shapes was presented. Although not obvious at this stage, the inclusion of the covariances of the sample correlation functions in the general error formulation, makes it possible to apply this theory -initially developed by Longman and Juang (1987); Longman *et al.* (1987) for the same purpose in classical input/output modal analysis- to output-only modal analysis. Additionally, the method was extended to estimate the random error of repeated modes. Not only does this perturbation method allow to estimate the random and bias error in practical applications, but also provides us with a causal representation (up to second order) of how the errors in the response model are propagated through the correlation-driven identification algorithm and results in random and bias errors in the estimated system modal parameter. This was summarised in diagram 5.1. To use the perturbation theory in practice, it is seen from the latter diagram that an estimate of the covariances of the perturbations  $\epsilon_j$  at each data point  $j$  of the sample correlation functions is required. As will be shown formally in the next chapter, the latter are in fact the same as the covariances of the sample correlation functions themselves expressions for which were given in chapter 3. In particular, the robust plug-in method developed in section 3.5, chapter 3 will allow to get a good estimate of the perturbations  $\epsilon_j$  directly from the measured responses. This allows to take into account many different perturbations -such as instrumentation noise and correlation estimation errors- into the statistics of  $\epsilon_j$  without having to make any assumptions about the errors that might be present in the estimated response model so that the method is fully automated.

This chapter has been entirely theoretical and, with the exception of the approximation made in equations 5.96-5.98 involved in the computation of the variance and quadratic bias of the truncation bias, it should in principle be possible to get an accurate estimate of both bias and random error in the identified modal model. Due to the fact that the covariances of  $\epsilon_j$  are only estimates and , as already pointed out, the algorithm can be ill-conditioned when eigenvalue/eigenvector sensitivities of near zero singular values are involved in the computations, the accuracy and reliability of the

predicted errors needs to be assessed by simulation which is the subject of the next chapter.

---

## CHAPTER 6

### UNCERTAINTY IN

### SSI/COV-IDENTIFIED MODAL

### PARAMETERS: A PERTURBATION

### APPROACH

---

#### 6.1 Introduction

In this chapter, the perturbation analysis presented in chapter 5 is applied to estimate the errors, random and bias, in the SSI/Cov-identified modal parameters. The aim is to establish the performance of the perturbation theoretic method in chapter 6. In Longman and Juang (1987); Longman *et al.* (1987), where the perturbation method was first developed for application to input/output modal analysis, the effect of white noise perturbations on exact impulse response functions was considered. These authors did not compare the estimated error with the “true”, error, which can, for instance, be computed from Monte-Carlo type simulations. Effectively, in the latter work, the perturbation approach was employed to assist the choice of the parameters the user has to specify in order to implement the ERA (or SSI/Cov). In (Bergman *et al.*, 1989), the same authors use the information obtained from the calculated errors in a *relative* manner to determine which set of parameters resulted in the lowest error in the modal estimates. In this chapter, it is investigated how well

the errors are predicted in an *absolute* sense by direct comparison with the error from Monte-Carlo type simulations. The theory developed by Longman and Juang (1987) was employed by Peterson *et al.* (1996) to assess the variance of the modal damping ratios and frequencies of a pyramidal truss from input/output measurements. In the latter paper, the only stochastic component considered was noise. Bias errors as well as the accuracy of the estimated random error were not investigated.

To assess the perturbation analysis presented in Chapter 5, SDOF systems are employed although the theory presented in the previous chapter covers the MDOF case. If the perturbation analysis fails to give consistent results for such simple systems, then this will almost certainly be the case for more complex systems.

## 6.2 Perturbations of the Sample Correlation Functions

### 6.2.1 Error Sources

The variance and bias in the estimated modal damping ratios and frequencies obtained from the perturbation analysis presented in the previous chapter are functions of the statistics of  $\epsilon$ , the perturbation of the sample correlation functions computed between the measured time-histories of a chosen set of reference and roving sensors along the structural system. Consequently, the degree of accuracy with which the uncertainty in the identified results can be predicted will depend on the exactness with which the perturbation  $\epsilon$  can be modelled. This is not a trivial task since there are, in general, many sources that contribute to the random and bias error in the estimated sample correlation functions and hence to the error in the identified modal parameters. The various sources that may introduce error into the estimated sample correlation functions will be briefly discussed below and are shown schematically in figure 6.1.

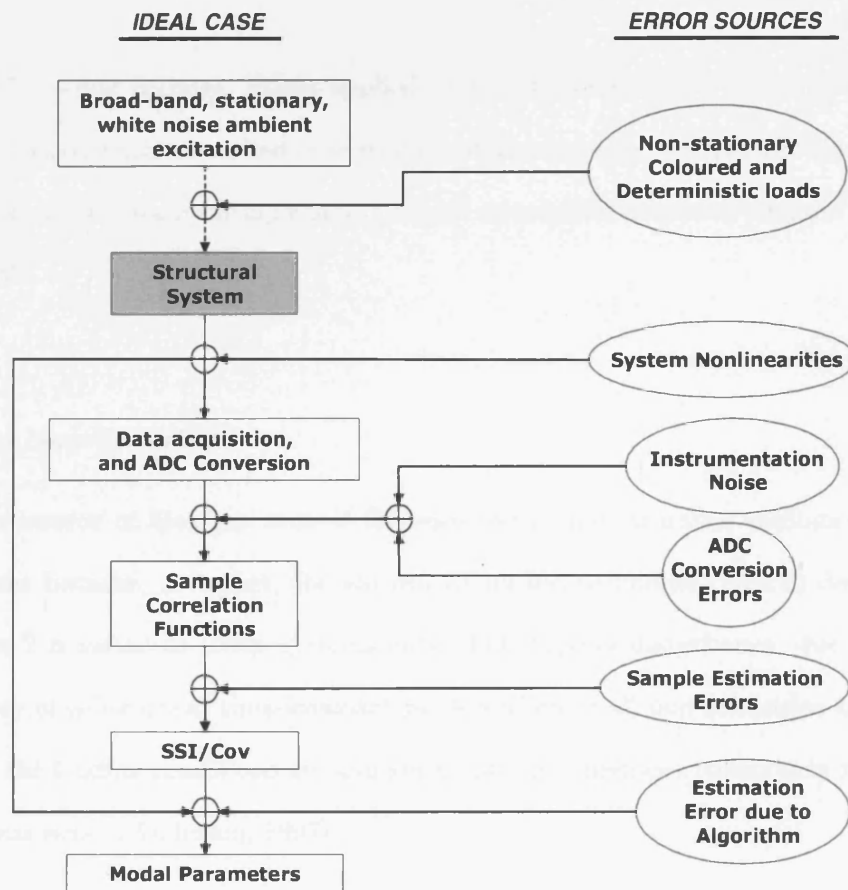


Fig. 6.1: Error sources affecting the SSI/Cov-identified modal parameters.

### Non-stationary, Coloured and Deterministic loads

As described in detail in section 2.2.1 in Chapter 2, operational modal analysis relies on the assumption that the excitation of the structural system can be approximated by stationary white noise. When this condition is violated, for instance, if the spectrum of the ambient loading is coloured and/or of a non-stationary nature, the “free response” behaviour of the sample correlation functions can be significantly corrupted. Coloured inputs occur when the random excitation of the structural system is correlated in some fashion, and this correlation will ultimately be reflected in the estimated sample correlation functions causing a systematic deviation from the free response characteristics and thereby introducing bias in the identified modal parameters. The methods described in Chapter 3 to compute the sample correlation functions are not suited to deal with non-stationary data. Neither is the random decrement method in theory although Jeary (1992, 1996) presents this method as particularly useful under

“hostile” loading regimes. When applied to non-stationary data, the computation of the correlation function suited to stationary data, averages through the time-varying structure of the data resulting again in biased correlation estimates (Bendat and Piersol, 2000).

### **System Non-linearities**

Another source of bias can arise if the response of the structure exhibits nonlinear behaviour because, as before, the natural excitation technique (NExT) described in Chapter 2 is suited to linear systems only. This type of disturbance, due to the inadequacy of using linear time-invariant models when small non-linearities are present and/or the loading conditions are non-stationary, is sometimes collectively referred to as *process noise* (Andersen, 1997).

### **Instrumentation Noise**

During the data acquisition process, the response data is polluted by the noise floor from the instrumentation due primarily to the electronic noise of analogue instruments and/or the quantization noise (round-off error) of digital equipment occurring in the analogue-to-digital conversion (ADC). The ADC error is nevertheless usually unimportant compared to the other instrumentation noise when a sufficiently high bit-rate is used for the conversion.

### **Sample Estimation Errors**

Since the sample correlation functions are estimated from finite random time-histories, these estimates do not converge and hence contain a certain amount of random error controlled by length  $T$  of the data that is available. The latter error has been discussed in detail in Chapter 3. Additionally, depending on which method is used to compute the sample correlation functions (cf. Chapter 3) these estimates are biased.

As described in (Giampellegrini and Greening, 2005), this situation is analogous to leakage and resolution bias when frequency domain methods are used to perform the system identification.

### **Errors induced by the Identification Algorithm**

For completeness, the last step in the diagram 6.1 shows that additional errors may be conveyed to the modal parameters as the error in the sample correlation functions is passed through the algorithm. This was shown theoretically in Chapter 5 where, it can be seen how quadratic bias may arise due to the perturbation  $\underline{\epsilon}$  being passed through the nonlinear algorithm or how bias is introduced due to truncation of small non-zero singular values. It should be clear, however, that the errors introduced by the algorithm are not to be modeled in  $\underline{\epsilon}$  but are the result of the perturbation equations formulated in the previous chapter.

As already mentioned, the confidence one can place on the variance and bias obtained from the perturbation analysis in Chapter 5 will ultimately depend on how well we can approximate the statistics of  $\underline{\epsilon}$  and how close this model is to the true disturbance in the measured data. Due to the many error sources that can arise in operational modal testing, it is a difficult task to take into account all these sources. Moreover, since the loading conditions are not measured, a rigorous analysis of the response data would be required to detect whether the data has been perturbed due to correlated and/or nonstationary inputs Bendat and Piersol (2000) or whether the response exhibits a certain degree of nonlinearity (Kantz and Schreiber, 1997). This is further complicated by the fact that, if the presence of nonlinear or nonstationary behaviour can be established, this is generally a negative statement in the sense that it only specifies a lack of linear or stationary properties rather than defining the precise nature of nonlinearity or nonstationarity involved. Consequently modelling these disturbances into the perturbation parameter  $\underline{\epsilon}$  is extremely challenging. While it will



always be assumed in this thesis that the response is linear, the influence of a nonstationary characteristics in the response will be briefly considered. It is noted, however, that within the classical input-output framework, the subspace identification methods have been used to identify simple nonlinear systems, see for instance Horta and Juang (1986). It follows from this discussion, that, in order to capture the statistics of the perturbation  $\epsilon_j$  in the response model from all the contributing sources, a data-driven method is required. That is, a method that does not rely on specific models for each of the possible sources but rather estimates the statistics  $\epsilon_j$  numerically directly from the measured data.

### 6.2.2 Data-Driven Perturbation Model

This data-driven estimate of the statistics of  $\epsilon_j$  can, when the statistics of interest is  $Cov[\epsilon_\tau, \epsilon_s]$ , be directly obtained from the data-driven or plug-in estimate of  $Cov[\hat{R}_x(\tau), \hat{R}_x(s)]$  developed in section 3.5, Chapter 3. Let  $\hat{R}_x(\tau) = R_x(\tau) + \epsilon_\tau$  where  $\epsilon_\tau$  denotes the perturbation of the exact auto-correlation function  $E[\hat{R}_x(\tau)] = R_x(\tau)$  at lag  $\tau$  as in chapter 5. Also, let this perturbation have zero mean so that  $E[R_x(\tau) + \epsilon_\tau] = R_x(\tau)$  as expected for an unbiased estimate of the auto-correlation function. Then, by definition

$$\begin{aligned} Cov[\hat{R}_x(\tau), \hat{R}_x(s)] &= E\left[\left(\hat{R}_x(\tau) - E[\hat{R}_x(\tau)]\right)\left(\hat{R}_x(s) - E[\hat{R}_x(s)]\right)\right] \quad (6.1) \\ &= E\left[\hat{R}_x(\tau)\hat{R}_x(s)\right] - E[\hat{R}_x(\tau)]E[\hat{R}_x(s)] \end{aligned}$$

Using  $\hat{R}_x(\tau) = R_x(\tau) + \epsilon_\tau$  and  $\hat{R}_x(s) = R_x(s) + \epsilon_s$  in equation 6.1, it is then easily shown that

$$Cov[\hat{R}_x(\tau), \hat{R}_x(s)] = E[\epsilon_\tau\epsilon_s] - E[\epsilon_\tau]E[\epsilon_s] = Cov[\epsilon_\tau, \epsilon_s] \quad (6.2)$$

Thus, the perturbations of the auto-correlation function are the same as those of the auto-correlation function itself. The result for the variance follows immediately by letting  $\tau = s$ .

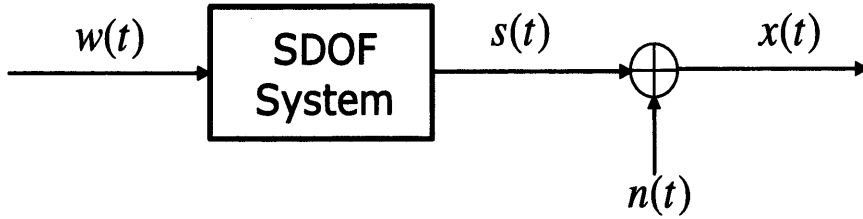


Fig. 6.2: Illustration of noise corrupted signal.

### 6.2.3 A Noise Model

As mentioned in the introduction, to assess the accuracy of the errors predicted by the perturbation analysis, we start by considering simple systems and we wish to eradicate any sources of uncertainty that can influence the error estimate other than those set out to investigate. For this reason, and also to have a theoretical description of how measurement noise affects the estimated sample correlation functions, having a theoretical expression describing the perturbation of the auto-correlation function due to noise in the measurement records is useful. It is noted, however, that this model is mainly of theoretical interest.

As documented in Bendat and Piersol (2000), instrumentation noise has a near-uniform spectral density so that we may simulate the noise floor as a broadband white noise signal  $n(t)$  with a frequency bandwidth  $B$ . Letting  $s(t)$  be the uncorrupted response of the SDOF system subject to white noise excitation, the corrupted response can then be written as

$$x(t) = s(t) + n(t) \quad (6.3)$$

This is illustrated schematically in figure 6.2. Assuming that  $n(t)$  is independent of  $s(t)$ , the ac.f of the system can be written as (Bendat and Piersol, 2000)

$$\hat{R}_{xx}(\tau) = \hat{R}_{ss}(\tau) + \hat{R}_{nn}(\tau) \quad (6.4)$$

where  $\hat{R}_{xx}(\tau)$ ,  $\hat{R}_{ss}$  and  $\hat{R}_{nn}$  denote the estimated sample auto-correlation functions of the  $x(t)$ ,  $s(t)$  and  $n(t)$  respectively. Since we wish to avoid the influence of the sample

estimation errors, we simply replace  $\hat{R}_{ss}$  by the exact ac.f of the system, denoted by  $R_{ss}$ , in equation 6.4

$$\hat{R}_{xx}(\tau) = R_{ss}(\tau) + \hat{R}_{nn}(\tau) \quad (6.5)$$

or in discretized form

$$\hat{R}_{xx}(r\Delta t) = R_{ss}(r\Delta t) + \hat{R}_{nn}(r\Delta t) \quad (6.6)$$

If  $\hat{R}_{xx}(r\Delta t)$ , as described by equation 6.6, is fed into the SSI/Cov algorithm, the error in the identified modal parameters is solely due to the additive noise perturbation  $\hat{R}_{nn}(r\Delta t)$  to  $R_{ss}(r\Delta t)$ . Thus,  $\hat{R}_{nn}(r\Delta t)$  is the desired perturbation, or in terms of the notation used in Chapter 5

$$\epsilon_j = \hat{R}_{nn}(j\Delta t), \quad \text{for } j = 1, 2, \dots, N \quad (6.7)$$

where, as before,  $N$  denotes the number data points included in the analysis. In order to obtain statistical information about the error in the identified modal parameters from the perturbation theory, we require a model for  $\hat{R}_{nn}(r\Delta t)$  so that its variance and covariance can be established and hence the perturbation equations 5.8, 5.10, 5.37, 5.43 and 5.44 can be evaluated.

The auto-correlation function of a band-limited white noise signal  $n(t)$  of bandwidth  $B$ ,  $R_{nn}(\tau)$  is given theoretically by Bendat and Piersol (2000) as

$$R_{nn}(\tau) = \sigma_n^2 \frac{\sin(2\pi B\tau)}{2\pi B\tau} \quad (6.8)$$

where  $\sigma_n^2$  is the variance of the noise signal  $n(\tau)$ . It is common practice in operational modal analysis to low-pass filter the measured data in order to avoid aliasing. Typically, one uses analogue infinite impulse response (IIR) or digital finite impulse response (FIR) filters for this operation, the most common of which are the Butterworth and Chebyshev filters. These filters are linear (Williams and Taylor, 1995) and

thus preserve the additive form of equation 6.3. Hence, if the bandwidth of the applied filter is  $B$ , then so will be the bandwidth of the additive noise term  $n(t)$ . Noise levels in signals are commonly expressed as a percentage, but it seems, that there is no clear consensus on exactly how this percentage is defined. In this thesis, therefore, the noise level in the measured signal  $x(t)$  will be defined by

$$\text{noise level} = \frac{\text{rms}[n]}{\text{rms}[s]} \quad (6.9)$$

where  $\text{rms}[\cdot]$  denotes the *root-mean-square value* defined as  $\text{rms}[\cdot] = \sqrt{E[(\cdot)^2]}$ . Note that, when the time series has zero mean, then the  $\text{rms}$  value is the same as the standard deviation of the process, i.e.  $\text{rms}[\cdot] = \sqrt{\sigma^2(\cdot)}$ , where  $\sigma^2(\cdot)$  denotes the variance. This definition, also used by Desforges *et al.* (1995), is analogous to the the signal-to-noise (SNR) ratio traditionally used to assess the dynamic range of the data acquisition system (Bendat and Piersol, 2000). Equation 6.8 is illustrated in

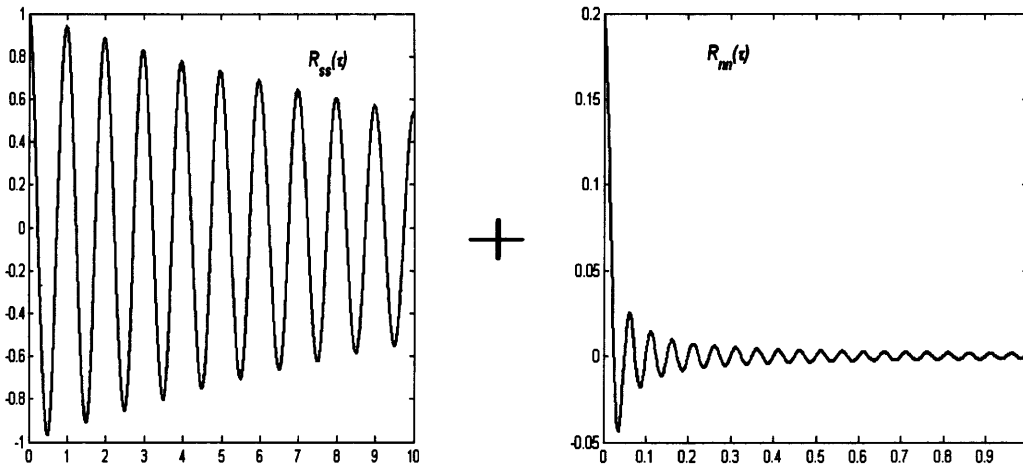


Fig. 6.3: Illustration of equation 6.8 for a  $B = 20 \text{ Hz}$  bandwidth-limited white signal with variance  $\sigma_n^2 = 0.2$ . This represents the theoretical noise ac.f. that is added to the exact ac.f.  $E[\hat{R}_{ss}(\tau)] = R_{ss}(\tau)$  estimated from the uncorrupted signal  $s(t)$  with  $\sigma_s^2 = 1$ . This represents a noise level of approximately 45% in  $x(t) = s(t) + n(t)$ .

figure 6.3 for a white noise signal  $n(t)$  of bandwidth  $B = 20 \text{ Hz}$  and with variance  $\sigma_n^2 = 0.2$ . Also shown is the exact ac.f.  $E[\hat{R}_{ss}(\tau)]$  of the uncorrupted signal  $s(t)$  of a SDOF system with natural frequency  $1 \text{ Hz}$  and 1% modal damping and with variance  $\sigma_s^2 = 1$ . It is seen from equation 6.8 and its display in figure 6.3 that the resulting

additive perturbation on the ac.f due to the noise term  $n(t)$  is substantially mitigated at lags  $> 0$  due to the fast decorrelation of the band-limited white signal. Qin and Qian (2001) have exploited this fact to reduce the noise in the random decrement (RD) signatures by correlating the RD functions with themselves. This technique is known as correlation filtering. However, a certain degree of correlation exists between the data sequence of the bandwidth-limited white signal  $n(t)$ , which manifests itself by the decaying oscillation with frequency  $2B\pi$  as can be seen from equation 6.8 and figure 6.4. The latter will appear as a noise mode in the identification process and can, as will be shown later in this chapter, introduce significant bias into the identified modal parameters. Asmussen *et al.* (1998), for instance, has taken into account correlation effects due to noise effects by assuming that they behave as the free decays of the structure.

The variance and covariance of the noise ac.f.  $\hat{R}_n(\tau)$  can be estimated from equations 3.32 and 3.38 respectively in Chapter 3. Bendat and Piersol (2000) computed the variance of  $\hat{R}_n(\tau)$  as

$$Var[R_{nn}(\tau)] \approx \frac{1}{2BT} \left[ \sigma_n^4 + \sigma_n^4 \frac{\sin^2(2\pi B\tau)}{(2\pi B\tau)^2} \right] \quad (6.10)$$

where the second term in the square brackets is recognised as the square of the ac.f. of  $n(t)$  as given in equation 6.8. However, adopting exactly the same approach as Bendat and Piersol (2000), the variance is found to be

$$Var[R_{nn}(\tau)] \approx \frac{1}{2BT} \left[ \sigma_n^4 + \sigma_n^4 \frac{\sin(4\pi B\tau)}{(4\pi B\tau)} \right] \quad (6.11)$$

Equations 6.10 and 6.11 are compared with the mean of the auto-correlation functions simulated from 2000 realizations of a 20 Hz bandwidth limited white noise signal  $n(t)$  of length  $T = 100s$  sampled at 15 Hz. This is shown in figure 6.4 where it can be seen that equation 6.11 is in better agreement with the simulated data. The 20 Hz stopband was achieved using a digital Butterworth filter. This choice of filter was

motivated by the fact that the frequency response of the Butterworth filter is flat in the pass-band, and rolls off toward zero in the stop-band. It maintains this same shape for higher orders but with a steeper decline in the stop-band (Williams and Taylor, 1995) so that a high order filter gives a relatively sharp cutoff without compromising the “whitness” of the signal in pass-band too much. A small part of the disagreement

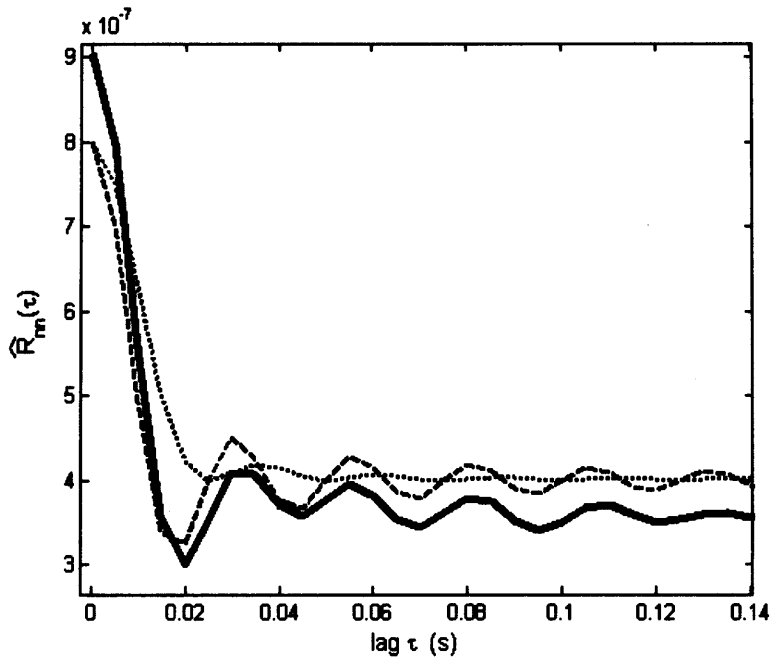


Fig. 6.4: Comparison of equations 6.10 (*dotted line*) and 6.11 (*dashed line*) with the mean sample ac.f of a 1 Hz, 1% damped SDOF estimated from 2000 realizations of a 20 Hz band-limited white noise signal of record length  $T = 100s$  sampled at 15 Hz (*thick, solid line*). The 20 Hz band-pass was achieved with a 10<sup>th</sup> order Butterworth filter.

between equation 6.11 and the simulated data may be attributed to the fact that the simulated data has not entirely converged to its true value. However, we suspect that the principal cause is that it is very difficult to model the correlation function of the filtered response exactly by, for instance, taking into account the fact, that the cutoff of the filter is not as sharp as assumed in the analytical equations so that the bandwidth is slightly higher than the desired 20 Hz. Similarly, we obtain from equation 3.38

$$Cov[R_{nn}(\tau), R_{nn}(\tau + v)] \approx \frac{\sigma_n^4}{2BT} \left[ \frac{\sin(2\pi Bv)}{(2\pi Bv)} + \frac{\sin(2\pi B [2\tau + v])}{(2\pi B [2\tau + v])} \right] \quad (6.12)$$

Since  $\hat{R}_{nn}(r\Delta t)$  also yields the desired perturbation to the exact auto-correlation func-

tion  $R_{ss}(\tau)$  (cf. eqn. 6.7), equations 6.11 and 6.12 provide the necessary statistics to evaluate the perturbation equations given in the previous chapter.

### 6.3 Random Error

The aim of this section is to assess how accurately and reliably we can expect the perturbation theory presented in chapter 5 to predict the random errors in operational modal parameters. To do so, we proceed by simulation. Two SDOF systems, system A and B whose modal parameters are shown in table 6.3, are employed for this purpose. To avoid ambiguity in the notation used in this chapter, recall that the *random error* in an estimated statistic, say  $\hat{\chi}$ , is commonly defined (Bendat and Piersol, 2000) as the square-root of the variance of this statistic. Thus, the random error in  $\hat{\chi}$  is the same as its standard deviation and the term *standard error* is often used to describe the same quantity (Bendat and Piersol, 2000). The standard or random error of  $\hat{\chi}$  will be denoted by  $\sigma[\hat{\chi}]$ . It is often convenient to work with the *normalised standard error* which expresses the random error as a fractional portion of the quantity being estimated, that is

$$\epsilon_r(\hat{\chi}) = \sigma[\hat{\chi}]/\chi \quad (6.13)$$

A slight variation if this definition will be used in this section, namely, that the error is normalised with respect to sample mean of  $\hat{\chi}$  rather than the true value  $\chi$ . The reason for this will become clear shortly. The normalised random error is also sometimes referred to as the coefficient of variation of  $\hat{\chi}$ .

The variance of the SSI/Cov-identified modal parameter predicted by the perturbation analysis is given by equation 5.8 in Chapter 5 and, for convenience, is displayed

	Natural Frequency $f_0$	Damping ratio $\xi$
SDOF System A	1 Hz	1%
SDOF System B	4 Hz	1.5%

Tab. 6.1: Modal parameters of the two SDOF systems used in the simulations.

again below

$$\text{Var} [\chi (\underline{\epsilon})] \approx \sum_{j=1}^N \text{Var} [\epsilon_j] \delta_j^2 (\chi) + 2 \sum_{\substack{j=1 \\ j \neq k}}^N \sum_{k=1}^N \text{Cov} [\epsilon_j \epsilon_k] \delta_j (\chi) \delta_k (\chi). \quad (6.14)$$

Note that the notation used to denote the estimated parameter in the perturbation analysis,  $\chi (\underline{\epsilon})$ , means the same as  $\hat{\chi}$ . It is seen from this equation that  $\text{Var} [\chi (\underline{\epsilon})]$ , and hence the random error in  $\hat{\chi}$ , depends on the two parameters; (a) the sensitivities  $\delta_j (\chi)$  of the modal parameters due to a perturbation at the  $j^{\text{th}}$  data point in the correlation function and (b) the variance and covariance between the perturbations  $\epsilon_j$ . Any error in the estimated sensitivities  $\delta_j (\chi)$  and/or estimated variance and covariances will therefore compromise the accuracy of the predicted random error. In practice, this is to be expected; the variances and covariances from the data driven or plug-in method described in section 3.5, Chapter 3 are only estimates and are contaminated by random and possibly bias errors, although using a flat-top window with ‘optimal’ band-width considerably mitigates these errors as was shown in section 3.5. Similarly, the sensitivities  $\delta_j (\chi)$ , which result from the eigenvalue sensitivities of the *identified* state matrix  $\mathbf{A}$ , will be in error since the identified state matrix  $\mathbf{A}$  itself is an estimate as it is identified from the only available measured response data. In Chapter 5, the sensitivities were treated as deterministic quantities in the sense that the Hankel matrices  $\mathcal{H}_0(\underline{0})$  and  $\mathcal{H}_1(\underline{0})$ , computed from the only available response data, play the role of the exact Hankel matrices (c.f. the remark in section 5.2). Nonetheless, it is important to recognise that, if a different set of response data is used,  $\mathcal{H}_0(\underline{0})$  and  $\mathcal{H}_1(\underline{0})$  will change and so will the computed sensitivities  $\delta_j (\chi)$ . In other words, the estimated variance, covariance and sensitivities are random variables and so is the predicted random error.

In a first step, it is desired to investigate the performance of the perturbation algorithm when the variance, covariance and the system sensitivities are exact. After all, the equation yielding the variance of the identified modal parameter is derived from a first order Taylor expansion in the perturbation  $\underline{\epsilon}$  and there is no obvious argument



to suggest that the random error in the identified modal data does indeed change linearly with this perturbation. As perturbations, we will consider the influence of measurement noise, which affect the sample correlation functions as described in section 6.2.3, and the errors inherent in estimating the sample correlation function from finite response data. For convenience, we shall refer to the latter errors as estimation “noise”. It is seen from the figure 6.1 that, if the basic assumptions of the measured output time-histories for operational modal analysis hold, namely that the response is the result of white, stationary loading conditions and the structure behaves linearly, then instrumentation and estimation noise are the only two perturbations affecting the estimated correlation-driven response model. The propagation of these error to the identified modal data is captured by the computed sensitivities  $\delta_j(\chi)$ . It is instructive to consider the influence of these two perturbations -that is measurement and estimation noise- on the the identified modal parameters separately and we shall start by investigating the influence of instrumentation noise. We note that our treatment differs from the studies in Bergman *et al.* (1989); Longman *et al.* (1987) and Peterson *et al.* (1996) in that the correlation of the band-limited noise is taken into consideration, while the latter authors considered the effect of adding uncorrelated noise (which is the true definition of noise) to measured or simulated impulse response functions.

### 6.3.1 Influence of Instrumentation Noise

To consider the influence of instrumentation noise only on the SSI/Cov-identified modal parameters, we eradicate the perturbation caused by estimation noise. To do so, the auto-correlation functions of the two SDOF systems tabulated in 6.3 were directly obtained from the exact expressions in equations 3.29 given in Chapter 3, section 3.4.1. These auto-correlation functions were computed with a sampling interval  $\Delta t = 0.05s$  and  $0.08s$  for system *A*, and  $\Delta t = 0.04s$  and  $0.07s$  for system *B*. Without loss of generality, they were normalised to unity at zero lag and we chose to work with displacement responses. White noise signals, denoted collectively by  $n(\tau)$ , of total

record length  $T = 900s$  sampled at  $\Delta t = 0.05s, 0.04s, 0.07s$  and  $0.08s$  respectively were then generated to correspond to each of the four cases of auto-correlation functions. Two sets of noise signals were generated, one with standard deviation  $\sigma = 0.15$  and one with  $\sigma = 0.30$ . Having normalised the exact auto-correlation functions of the two systems to unity at zero lag is equivalent to assuming that the hypothetical, infinite length responses of these systems have unit variance and hence unit standard deviation. Thus, the noise signals generated correspond, according to equation 6.9, to noise levels of 15% and 30% respectively. Since it is common practice to apply an anti-aliasing filter to the measured response histories, the computed noise signals were filtered with a low-pass Butterworth filter with a band-pass of  $0 - 6Hz$ . 500 such noise signals, were generated for each of the two noise levels and sampling intervals considered above and their auto-correlation functions  $\hat{R}_{nn}(\tau)$  were estimated. The perturbation due to noise was then added according to equation 6.6 resulting in 500 noise perturbed auto-correlation functions for each of the two SDOF systems in table 6.3 with sampling intervals  $\Delta t = 0.05s, 0.08s$  for system  $A$  and  $\Delta t = 0.04s, 0.07s$  for system  $B$  and noise levels of 15% and 30%. This gives eight different cases with 500 simulated responses each but only six of them, shown in table 6.2, were used.

For each of these six cases, the SSI/Cov was applied to each of the 500 simulated responses. Since it is known that the dimensions chosen to construct the Hankel matrices affect the identified parameters, 3 different sizes of Hankel matrices,  $dim(\mathcal{H}_0) = (7 \times 4), (13 \times 8)$  and  $(22 \times 14)$  were considered. Recall from Chapter 2 that the shifted Hankel matrix  $dim(\mathcal{H}_1)$  has the same dimensions as  $dim(\mathcal{H}_0)$  and that this dimension determines the portion of the auto-correlation function used in the identification. Proceeding in this fashion, 500 estimated sets of modal parameters are obtained for each of the six cases and for each of the three Hankel matrix dimensions chosen from which, the sample variance of the identified damping ratios and frequencies, and hence their normalised random errors, are estimated. The random error thus computed and shown in table 6.2 for the six cases described above, serve as

a benchmark against which the random error predicted by the perturbation analysis is validated.

To get an idea of the accuracy of the random error in the modal damping ratios and frequencies, computed from a population of 500 samples, it was assumed that the identified modal parameters are normally distributed. In this case, it is known (see for instance Rose and Smith (2002)) that the expected value of the standard deviation of the estimated variance is  $\sigma[\hat{\sigma}^2(\hat{\chi})] = \sigma^2(\hat{\chi})\sqrt{2/N}$  which can be approximated as  $\hat{\sigma}^2(\chi)\sqrt{2/N}$  since the exact variance is unknown. To convert this into the error in the estimated normalised random error  $\hat{\epsilon}_r(\hat{\chi})$ , one may express the estimated variance as  $\hat{\sigma}^2(\chi) \approx \sigma^2(\chi)[1 \pm \sqrt{2/N}]$ . Taking the square-root of this equation, approximating  $[1 \pm \sqrt{2/N}]^{1/2}$  as  $1 \pm \sqrt{1/2N}$  by using the binomial expansion up to linear terms and normalising with respect to  $\chi$ , the estimated normalised random error can then be written as

$$\hat{\epsilon}_r(\hat{\chi}) \approx \epsilon_r(\hat{\chi}) \pm \hat{\epsilon}_r(\hat{\chi})\sqrt{\frac{1}{2N}} \quad (6.15)$$

It is noted that the assumption that the identified modal parameters are distributed normally is not guaranteed and the above equation is only used to get an idea of the error  $\epsilon_r(\chi)$  computed from a finite sample population. The errors in the estimated  $\epsilon_r(\cdot)$ , computed according to equation 6.15, are shown in brackets in table 6.2. When no error is indicated means that the error was not significant relative to the accuracy of the random error shown.

The normalised error, estimated by the perturbation theory is shown next to the simulated errors in table 6.2. As mentioned, these predicted errors are computed by using the exact auto-correlation functions as input to the perturbation analysis so that the sensitivities  $\delta_j(\chi)$  are exact too.

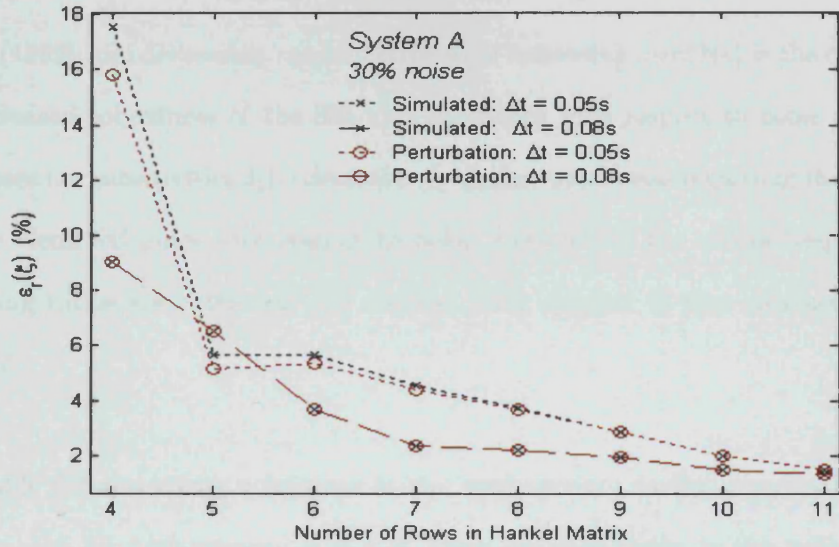
Influence of Instrumentation Noise

		$dim(\mathcal{H}_0) = 7 \times 4$		$dim(\mathcal{H}_0) = 13 \times 8$		$dim(\mathcal{H}_0) = 22 \times 14$	
		True	Perturbation	True	Perturbation	True	Perturbation
SODF System A							
Case 1 30% noise, $\Delta t = 0.05s$	$\epsilon_r(\xi)$ (%)	5.37 ( $\pm 0.17$ )	5.01	1.42 ( $\pm 0.05$ )	1.42	0.74	0.74 ( $\pm 0.02$ )
	$\epsilon_r(f_0)$ (%)	0.10	0.10	0.016	0.016	0.0067	0.0067
Case 2 30% noise, $\Delta t = 0.08s$	$\epsilon_r(\xi)$ (%)	3.65 ( $\pm 0.12$ )	3.65	1.23 ( $\pm 0.04$ )	1.23	0.55 ( $\pm 0.02$ )	0.55
	$\epsilon_r(f_0)$ (%)	0.030	0.030	0.013	0.013	0.0056	0.0056
Case 3 15% noise, $\Delta t = 0.05s$	$\epsilon_r(\xi)$ (%)	1.23 ( $\pm 0.04$ )	1.21	0.33 ( $\pm 0.02$ )	0.33	0.19 ( $\pm 0.01$ )	0.19
	$\epsilon_r(f_0)$ (%)	0.026	0.026	0.042	0.042	0.0016	0.0016
SODF System B							
Case 4 30% noise, $\Delta t = 0.04s$	$\epsilon_r(\xi)$ (%)	1.09 ( $\pm 0.04$ )	1.08	0.38 ( $\pm 0.02$ )	0.38	0.19 ( $\pm 0.01$ )	0.19
	$\epsilon_r(f_0)$ (%)	0.012	0.012	0.048	0.049	0.0023	0.0023
Case 5 30% noise, $\Delta t = 0.07s$	$\epsilon_r(\xi)$ (%)	0.60 ( $\pm 0.02$ )	0.60	0.28 ( $\pm 0.01$ )	0.28	0.14	0.14
	$\epsilon_r(f_0)$ (%)	0.008	0.008	0.0038	0.0038	0.0021	0.0021
Case 6 15% noise, $\Delta t = 0.04s$	$\epsilon_r(\xi)$ (%)	0.27 ( $\pm 0.01$ )	0.27	0.09	0.09	0.042	0.042
	$\epsilon_r(f_0)$ (%)	0.0027	0.0027	0.0012	0.0012	$6 \cdot 10^{-4}$	$6 \cdot 10^{-4}$

Tab. 6.2: Comparison of the normalized random error in the SSI/Cov-identified modal damping ratios ( $\epsilon_r(\xi)$ ) and frequencies ( $\epsilon_r(f_0)$ ) due to measurement noise estimated from Monte-Carlo simulation (500 response histories) and perturbation analysis. The error in ( $\epsilon_r(\cdot)$ ) is indicated in brackets. When no error is given means that the error was not significant relative to the accuracy of ( $\epsilon_r(\cdot)$ ) shown.

Also, the exact variance and covariance of the noise perturbations were used to compute these random errors. Although, the exact variance and covariance could have been computed from equation 6.11 and 6.12 respectively, it was opted to compute these statistics by simulation from the 500 perturbed correlation functions available for each case. The reason for doing so is that this gives a more accurate representation than is offered by the approximate equations 6.11 and 6.12. The discrepancies between the simulated and analytical auto-correlation function was illustrated in figure 6.4 and this disagreement was attributed to the fact that it is very difficult to account for all the influences of the filter in the modelled the auto-correlation function of the noise signal.

It is seen from table 6.2 that the random error predicted by the perturbation analysis agrees overall very well with the simulated error. On one hand, this near perfect agreement should not come as too much of a surprise since, after all, the two parameters entering equation 6.14, that is, the statistics of the perturbation and the sensitivities, were determined “exactly”. On the other hand, this result indicates that a linear approximation of the identified modal parameters in terms of the perturbations  $\epsilon_j$  (see equations 5.5-5.8, Chapter 5) is sufficient to describe the random error in the modal parameters accurately, at least when the correlation functions are perturbed by noise only. Up to the accuracy shown, the perturbation theory predicts the random error exactly for all cases except for the damping ratio in case 1, where the random error is underestimated. This discrepancy may be attributed to the fact that the portion of the auto-correlation function included in the analysis barely covers half a period. Recall from section 2.3.2 in chapter 2, that the maximum lag of the correlation function included in the analysis occurs in the shifted Hankel matrix  $\mathcal{H}_1$  and is given by  $\tau_{max} = (\alpha + \beta)\Delta t$ , where  $\Delta t$  is the sampling interval and  $\alpha$  and  $\beta$  are the block row and column dimensions of  $\mathcal{H}_0$  (and  $\mathcal{H}_1$ ). For Case 1, system A, the maximum lag is  $\tau_{max} = (\alpha + \beta)\Delta t = 11 \times 0.05 = 0.55s$  and as mentioned, barely covers half an oscillation of the auto-correlation function. When  $\Delta t = 0.08s$ , i.e.  $\tau_{max} = 0.88$ , it is seen from Case 2 in the table that this discrepancy disappears.



(a)

Fig. 6.5: Comparison of the normalised random error  $\epsilon_r(\xi)$  of modal damping ratios identified with small Hankel matrix dimensions. The abscissa gives the rows in  $\mathcal{H}_0$  and  $\mathcal{H}_1$ . The number of columns is one less in each case than the number of rows.

The convergence of the predicted random error to the true value as the portion of the correlation function included in the analysis increases is illustrated in figure 6.5. As the noise level in the signal decreases, so will the discrepancy between predicted and true error even for low dimensional Hankel matrices since, in theory, the dimensions of the Hankel matrix need not be bigger than the model order of the system, for instance  $2 \times 2$  in this case. This is indicated by comparing Case 1 and Case 3 in the table.

However, it is very clear from the results presented that, in practice, it is of advantage to work with large Hankel matrices: the sharp drop in random error with increasing dimension of the Hankel matrices is clearly visible from table 6.2. This is very similar to behaviour of the random error as a function of the size of the Hankel matrix described in Bergman *et al.* (1989). In the latter work, white noise was added directly to simulated impulse response functions so that the covariances of the perturbations  $\epsilon_j$  is zero and  $Var[\epsilon_j]$  is the same at each data point of the IRF. These observations suggest that the influence of the covariance of the band-limited noise on the random error of the modal parameters is small. As was already shown in Bergman

*et al.* (1989), the decreasing random error with increasing  $\dim(\mathcal{H}_0)$  is the consequence of increased robustness of the SSI/Cov algorithm with respect to noise as  $\dim(\mathcal{H}_0)$  increases i.e. sensitivities  $\delta_j(\cdot)$  decrease. A similar conclusion regarding the sensitivity of the identified poles with respect to noise, from which the modal frequencies and damping ratios are extracted (c.f. section 2.3.2, chapter 2) was obtained by Bazan (2004).

Table 6.2 also shows a decrease in the random error as the sampling interval  $\Delta t$  is increased, for both systems *A* and *B*. From the data shown in this table, it cannot be concluded that this trend holds in general. In fact, the explanation for the drop in random error with increased sampling interval is as follows; recalling that the noise was low-pass filtered with a band-width of  $B = 6 \text{ Hz}$ , it is seen from equation 6.6, that the perturbation of the auto-correlation function oscillates with a frequency of  $6 \text{ Hz}$  and thus has a period of approximately  $0.166\text{s}$ . Thus, a discretisation in steps of  $\Delta t = 0.08\text{s}$  and  $0.07\text{s}$  picks out those perturbations that are, on average, nearer to the zero crossings and hence smaller in magnitude than when a sampling interval of  $\Delta t = 0.05\text{s}$  and  $0.04\text{s}$  is considered. Since the same holds for the variances and covariances of the perturbations (c.f. equations 6.11 and 6.12), it is clear that the choice of  $\Delta t = 0.08\text{s}$  and  $0.07\text{s}$  in this particular case results in a smaller random error. General guidelines on how to choose the sampling interval to minimise the random error were not further investigated. As can be seen from the table 6.2, the perturbation analysis accounts for different sampling intervals, so that in practice, the “best” choice for  $\Delta t$  can be obtained by comparing the random errors of the modal parameters from different runs using the same data but with a different  $\Delta t$ . The best choice of sample interval among the different runs considered being the one yielding the lowest error in the modal parameters. We finally note that, as expected, the random error drops as the level of the perturbation is decreased.

### 6.3.2 Influence of Estimation Noise

In the previous section, the behaviour of the random error in the estimated modal parameters due to noise in the measured data was described. In this section, the same is done for perturbations of the correlation functions due to the sample estimation errors described in Chapter 3. For this purpose, the same two SDOF systems -system A and B in table 6.3- were employed and the same six cases as in the previous sections were considered. In each case, the particular system was excited by a normally distributed, white noise input and the response was computed for a total duration of  $T = 900s$  using a Newmark- $\beta$  time integration scheme. As for the simulations in Chapter 3, section 3.5, the 900s of response data consists only of the stationary part of the response; that is, care was taken to remove the initial, non-stationary portion of the response that occurs when the system is excited from rest. 500 response histories were generated in this fashion in each case and the sample auto-correlation function was computed from each output and the modal frequency and damping ratio estimated. From the 500 sets of modal parameters thus obtained for each case, the "true" normalised error was approximated according to equation 6.13 and the error in this approximation is given by equation 6.15. We note that the random error was normalised with respect to the mean of the identified modal parameters, rather than with respect to the true value. This was done to enable a more direct comparison with the errors predicted by the perturbation analysis, because in the latter, the errors were normalised with respect to the identified modal parameters for each realisation. These values are tabulated in table 6.3.

To compute the errors predicted by the perturbation method, the same approach was adopted as in the previous section: the sensitivities were computed from the exact auto-correlation functions which were approximated as the mean of the 500 auto-correlation functions available for each case. The exact perturbations were approximated similarly from the variance and covariances from the 500 response histories. The resulting normalised random error is shown in table 6.3.



Influence of Estimation Noise

		$dim(\mathcal{H}_0) = 7 \times 4$		$dim(\mathcal{H}_0) = 13 \times 8$		$dim(\mathcal{H}_0) = 22 \times 14$	
		True	Perturbation	True	Perturbation	True	Perturbation
<b>SODF System A</b>							
Case 1 $T = 15 \text{ min}, \Delta t = 0.05s$	$\epsilon_r(\xi)$ (%)	13.59 ( $\pm 0.43$ )	13.62	13.71 ( $\pm 0.43$ )	13.76	14.11 ( $\pm 0.45$ )	14.15
	$\epsilon_r(f_0)$ (%)	0.14	0.14	0.14	0.14	0.14	0.14
Case 2 $T = 15 \text{ min}, \Delta t = 0.08s$	$\epsilon_r(\xi)$ (%)	13.27 ( $\pm 0.42$ )	13.61	13.67 ( $\pm 0.43$ )	14.00	14.07 ( $\pm 0.44$ )	14.45
	$\epsilon_r(f_0)$ (%)	0.22	0.14	0.22	0.14	0.22	0.14
Case 3 $T = 10 \text{ min}, \Delta t = 0.05s$	$\epsilon_r(\xi)$ (%)	17.17 ( $\pm 0.54$ )	17.24	17.32 ( $\pm 0.55$ )	17.50	17.74 ( $\pm 0.56$ )	17.93
	$\epsilon_r(f_0)$ (%)	0.17	0.17	0.17	0.17	0.17	0.17
<b>SODF System B</b>							
Case 4 $T = 15 \text{ min}, \Delta t = 0.04s$	$\epsilon_r(\xi)$ (%)	6.43 ( $\pm 0.20$ )	6.42	6.65 ( $\pm 0.21$ )	6.64	7.12 ( $\pm 0.22$ )	7.71
	$\epsilon_r(f_0)$ (%)	0.08	0.08	0.09	0.09	0.10	0.10
Case 5 $T = 15 \text{ min}, \Delta t = 0.07s$	$\epsilon_r(\xi)$ (%)	8.42 ( $\pm 0.26$ )	8.38	8.68 ( $\pm 0.27$ )	8.66	9.17 ( $\pm 0.29$ )	9.16
	$\epsilon_r(f_0)$ (%)	0.08	0.08	0.08	0.08	0.09	0.09
Case 6 $T = 10 \text{ min}, \Delta t = 0.04s$	$\epsilon_r(\xi)$ (%)	7.79 ( $\pm 0.25$ )	8.03	6.96 ( $\pm 0.25$ )	8.00	8.57 ( $\pm 0.27$ )	8.52
	$\epsilon_r(f_0)$ (%)	0.10	0.10	0.11	0.11	0.12	0.11

Tab. 6.3: Comparison of the normalized random error in the SSI/Cov-identified modal damping ratios ( $\epsilon_r(\xi)$ ) and frequencies ( $\epsilon_r(f_0)$ ) due to estimation noise estimated from Monte-Carlo simulation (500 response histories) and perturbation analysis. The round brackets give the error in  $\epsilon_r(\cdot)$  as computed by equation 6.15

The analytical expressions given in Chapter 3 for the auto-correlation functions and corresponding covariances could also have been employed but for a direct comparison with the simulated errors, the frequency shift due to the Newmark time integrations needs to be accounted for. It is seen in table 6.3 that, apart from a few negligible discrepancies, the normalised random errors predicted by the perturbation method agree well with the true errors. It can therefore be concluded that, like for perturbation by noise only, a linear approximation in term of the perturbations due to sample estimation errors is sufficient to describe the errors in the SSI/Cov-identified modal parameters and that the perturbation analysis presented is suitable for output-only modal analysis problems.

It is worth pointing out some of the differences in the random error in the identified modal parameters when the perturbation is due to noise and sample estimation errors. Comparing tables 6.3 and 6.2, it is seen that a substantially higher error is caused by estimation noise, even compared to the conservative case in which a 30% noise level was chosen. Since the auto-correlation function of the measurement noise, which yields the effective perturbation of the Hankel matrix, was computed with the same record lengths as in each of the cases in table 6.3, the influence of measurement and estimation noise is directly comparable. Also different, is the behaviour of the error as a function of the dimension of the Hankel matrix: while the error due to measurement noise drops sharply as the dimensions of  $\mathcal{H}_0$  increases, the error due to the perturbation by estimation errors in the sample correlation functions increases slowly with  $\dim(\mathcal{H}_0)$ . This is to be attributed to the strong covariances in the perturbations causes by the sample estimation errors and is illustrated in figures 6.6. For convenience, only system  $B$  is used for illustration. When the perturbation is due to noise only (figure 6.6(a)), the effect of the covariances on the random error is slight due to the fast decorrelation of the noise with increasing lag. On the other hand, when the perturbation is due to sample estimation errors, the behaviour of the random error is largely governed by the covariance term in equation 6.14. When this term is ignored,

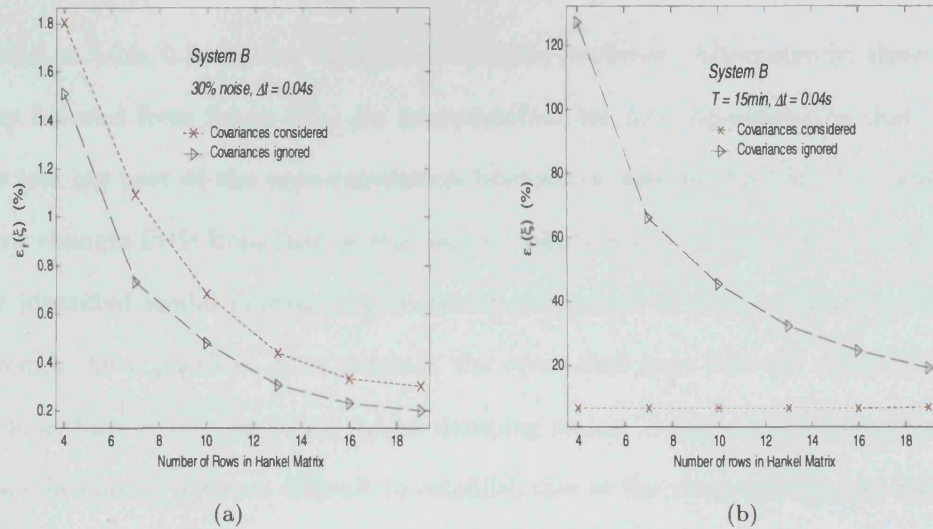


Fig. 6.6: Comparison of the influence of the covariance of the perturbation due to (a) noise and (b) sample estimation errors. The number of columns in the Hankel matrices used is one less than the number of rows.

the behaviour of the random error is similar to that caused by noise perturbations. It may be concluded that as a rule of thumb, “larger” Hankel matrices are favourable since the error due to noise will be significantly mitigated compared to the slight increase in error due to estimation noise.

Also interesting to note from table 6.3 is the rate of increase in the error of the modal damping ratios with increasing record length  $T$ . More precisely, as  $T$  is increased from 600 s to 900 s, that is by a factor of 1.5, the normalised error in the damping ratios decreases roughly by the square root of the inverse of this factor. This is observed for both systems  $A$  and  $B$ . Precisely the same behaviour as a function of the record length  $T$  was shown in Chapter 3 to hold for the normalised random error at zero lag in the estimated auto-correlation functions, see equation 3.35 and figure 3.5. In fact, it is observed that the normalised random error at zero lag in the auto-correlation function closely matches the normalised random error in the SSI/Cov-identified modal damping ratios. For system  $A$  and  $B$ , equation 3.35 predicts a normalised random error in their correlation functions of 13.3% and 5.43% respectively, which is indeed very close to the errors in the modal damping ratios tab-

ulated in table 6.3, for low dimensional Hankel matrices. Alternatively, these values may be read from figure 3.5. An interpretation for this observation is that, if only the low lag part of the auto-correlation function is used in the SSI/Cov, where the error changes little from that at zero lag, no additional random error is introduced in the identified modal damping ratios as the perturbed correlation function is passed through the algorithm. In a nutshell, the error that goes into the algorithm is the same as that in the computed modal damping ratios. A more precise formulation of this relationship appears difficult to establish due to the many parameters that enter the SSI/Cov and was not further pursued. However, this observation may be used as a rule of thumb to get an initial idea of the order of magnitude of the relative error in the identified modal damping ratios, or, in the pre-test stage, be used to determine the record length necessary to identify the modal damping with a particular accuracy. For example, if it is assumed, based on experience with similar structures, that the modal parameters are of the order of  $1Hz$ ,  $1\%$  damping, and it is desired to estimate the modal damping ratios with an accuracy of less than  $10\%$ , equation 3.35 yields a required record length of  $26.5min$ . The record length  $T$  obtained in this fashion should be considered as a minimum requirement to encompass the influence of other error sources on the identified modal damping ratios and also to cover the case when larger Hankel matrices are used. A rough estimate of the order of the error of the frequency can also be obtained since, as shown in Peterson *et al.* (1996), the absolute error in the modal damping ratio, that is  $\xi - \hat{\xi}$ , approximately yields the normalised error in the modal frequency. For instance, if the modal parameters of the structure are assumed to be of the order of  $1Hz$ ,  $1\%$  damping as above, and  $T$  is chosen such as to estimate the damping ratio within  $10\%$ , then the frequency is identified with an accuracy of roughly  $0.1\%$ .

It was shown, that the perturbation analysis yields very accurate predictions of the random error in the SSI/Cov-identified modal parameters when the perturbations are caused by noisy data and sample estimation errors. However, so far, the sensitivi-

ties and perturbations were modelled exactly, which is not possible in practice, where both these quantities can only be approximated. It needs to be established whether the predicted random errors are robust with respect to deviations in the sensitivities and estimated perturbations.

### 6.3.3 Robustness of Perturbation Algorithm

When the perturbation method is applied in practice, the system sensitivities and the perturbations of the correlation functions are only estimates: the sensitivities are obtained directly from the estimated (as opposed to exact) sample correlation functions and the perturbations follow from the estimated sample variance and covariance from the single set of available response data. Due to the random errors in both the sample correlation functions and its variance and covariance estimates, the random error predicted by the perturbation method is a random variable itself.

#### Influence of Errors in the Estimated Perturbations

Four situations are considered:

- (a) *Perturbation is due to measurement noise only.* The effect on the predicted random errors in the modal damping ratios is considered when the noise level in the data is under- or overestimated up to 15%. The sensitivities were computed exactly.
- (b) *Perturbation is due to estimation noise only.* The effect on predicted random errors in the modal damping ratios is considered when the variances and covariances of the auto-correlation functions are under- or overestimated up to 15%. More precisely, if  $Var[\hat{R}(\tau)]$  and  $Cov[\hat{R}(\tau), \hat{R}(\tau+v)]$  denote the exact variances and covariances of the sample auto-correlation function  $\hat{R}(\tau)$  at all lags  $\tau$  included in the SSI/Cov algorithm (and hence the perturbation analysis), then the estimated quantities were modelled as  $\alpha(Var[\hat{R}(\tau)])$  and  $\alpha(Cov[\hat{R}(\tau), \hat{R}(\tau+v)])$ ,

with the factor  $\alpha$  covering the range of values such that  $\alpha(\text{Var}[\hat{R}(0)])$  represents a  $\pm 15\%$  error in  $\text{Var}[\hat{R}(0)]$ . This situation arises when the data-driven or plug-in method is employed to estimate the variance and covariances of the sample correlation functions. As argued in section 3.5.1, the estimated variance and covariances manifest themselves as stretched or compressed versions of the exact quantities (also c.f. figure 3.11) and the idealisation to model these estimates as proportional to the exact variance and covariance functions is appropriate. The sensitivities were computed exactly.

- (c) *Over and -underestimated frequency content.* The effect on the predicted random errors in the modal damping ratios is considered when the frequency content of the system is under- or overestimated up to 15%. In other words, if the natural frequency of the system is  $1\text{Hz}$  for instance, it is assumed that the system is identified with frequencies ranging from  $0.85 - 1.15\text{Hz}$ . The auto-correlation functions and the corresponding covariances are computed at the identified frequencies. Such frequency shifts can occur in practice when the response data has a non-stationary frequency content. It is well known that (Bendat and Piersol, 2000) the stationary correlation estimates obtained by applying the usual estimators to non-stationary data are effectively time-averaged non-stationary correlation functions. This time-averaging process can cause deviations from the true system frequency and, if the plug-in method is used, this shift is clearly transmitted to the estimated perturbations.
- (d) *Mismatch between the frequency content of the data and estimated perturbations.* In this case, the auto-correlation functions used to estimate the perturbations are shifted in frequency by 15% either side of the correct system frequency. The sensitivities, on the other hand, are computed at the correct natural frequency.

To illustrate the 4 situations above, system  $A$  is employed, but the normalisation to be used makes the results valid for arbitrary systems. Using the perturbation method

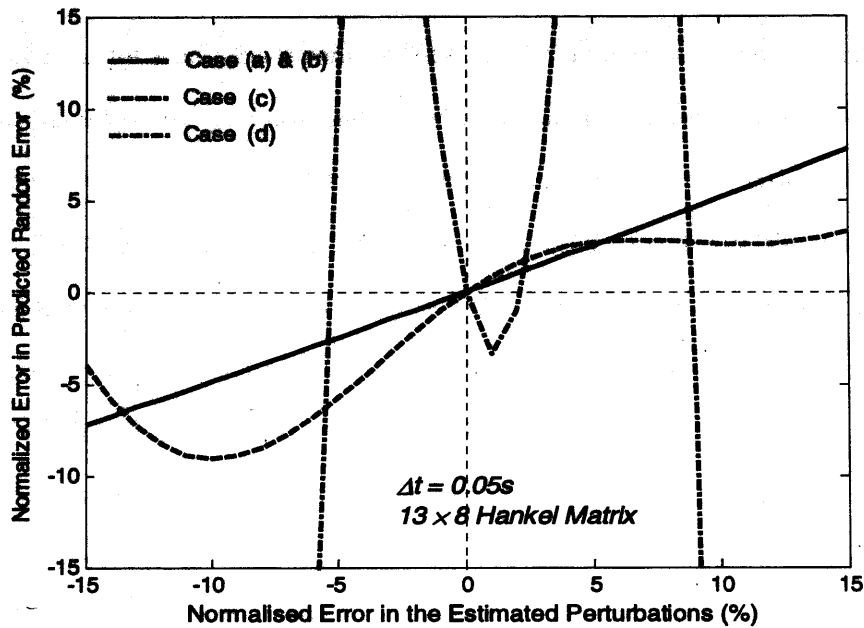


Fig. 6.7: Illustration of the robustness of the perturbation method with respect to errors in the computed perturbations.

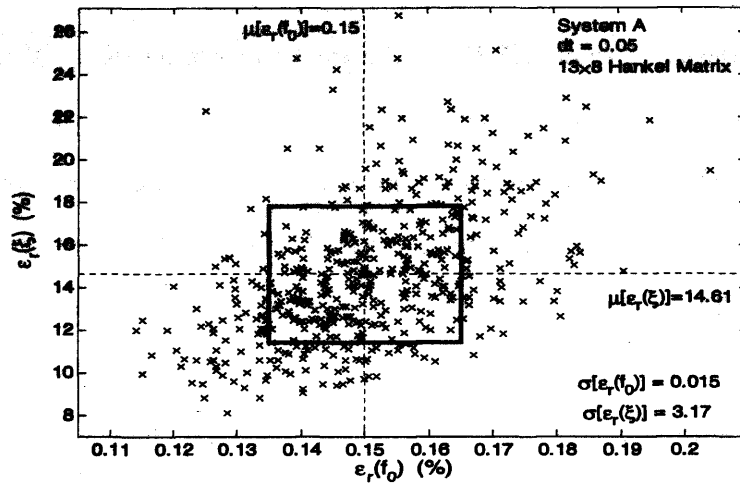
with the exact auto-correlation function and covariances, the normalised random error in the identified damping ratio was computed for the same parameters as in case 1 in tables 6.2 and 6.3, depending on whether the influence of noise or estimation errors is considered. The thus computed normalised random error was then normalised with respect to the true normalised error. As mentioned, this implies that the results shown are not only valid for system *A* but also, proceeding in this fashion shows the deviation from the true error due solely to inaccuracies in the modelled perturbations as described in cases (a), (b), (c) and (d) above. Since the error in the natural frequency is small, only the damping ratios are considered and the results are shown in figure 6.7.

It is seen from figure 6.7 that the random error is well behaved in cases (a), (b) and (c) in the sense that the over- or underestimation in the perturbation causes a deviation from the true normalised random error that is lower than the error in the perturbation itself. It is also seen from cases (a) and (b) that the effect of under- or over estimating the perturbations results in the same relative deviation from the true error. For case (d), however, the perturbation method is not well behaved and it is

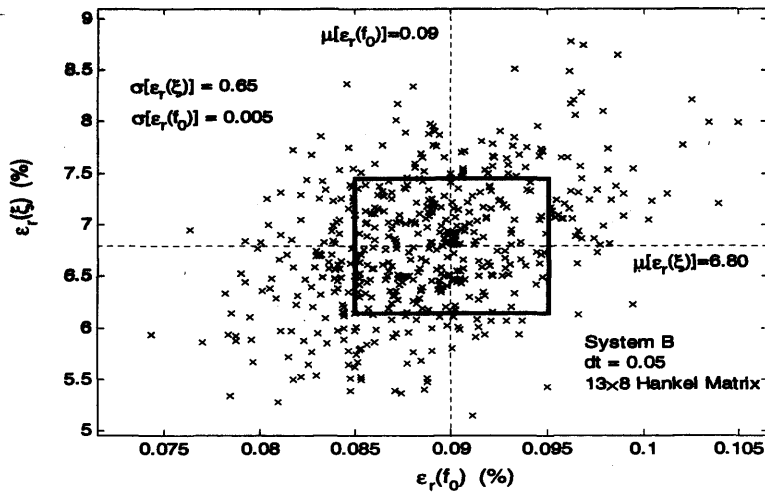
seen that even for small discrepancies between the frequency in the correlation function and the estimated variance and covariances, the normalised random error is very poorly predicted by the perturbation method. However, such a situation is unlikely to occur in practice provided the plug-in method is used to compute the perturbations since, as illustrated in chapter 3, section 3.5.1, the variance and covariance estimators of the sample correlation functions described in equation 3.42 combined with the flat-top window does not affect the oscillatory character of the true covariances but only over-or underestimates the amplitudes. Case (d) was chosen with the aim to emphasize the importance of estimating the perturbations using the plug-in method, rather than relying on a model computed independently from the sample correlations.

Due to the idealised modelling assumptions made above, it is worth checking the results depicted in figure 6.7 by simulation. To do this, 500 response histories with the same parameters as in cases 1 and 4, for systems *A* and *B* respectively, are computed and the variance and covariances, and hence the perturbations, are obtained using the plug-in method described in chapter 3 and the system identification was performed using a  $13 \times 8$  Hankel matrix. In this fashion, 500 error estimates were obtained for each of the modal parameters for each of the two systems. A scatter plot of the latter are shown in figures 6.8. The mean normalised error,  $\mu[\epsilon_r(\cdot)]$ , of both modal parameters as well as their standard error  $\sigma[\epsilon_r(\cdot)]$  are given and represented on the figures. The width and height of the rectangles represent the standard error of the modal damping ratios and frequencies respectively. In a first instance, it is seen from the standard error that the perturbation algorithm is very stable in the sense that, on average, we can expect a 3.17% and 0.65% deviation from the mean damping ratios for system *A* and *B* respectively as a result of the estimation errors in the perturbations. It remains to illustrate the linear behaviour of this deviation with respect to under- and overestimation of the perturbations as shown in figure 6.7: since the variance and covariances were computed from each of the 500 responses for each system, it is possible to estimate the normalised random error of the thus computed variances and covariances. As before, the random error at zero lag is chosen as representative. A





(a)



(b)

Fig. 6.8: Illustration of robustness of perturbation method with respect to errors in the estimated perturbation due to sample estimation errors.

normalised random error of 45.39% and 18.97% of the variance at zero lag was found for system A and B respectively. This means that, on average, the variance is an over- and underestimation by this amount and represents the error in the abscissa in figure 6.7. Since the behaviour of the normalised random error in the modal parameters as a function of the the normalised error in the estimated perturbations is linear, we can extrapolate this error for the estimated damping ratios from the figure. For a 15% error in the perturbation estimates, it is seen from figure 6.7 that, roughly a 7.2% error in the predicted normalised error for the modal damping ratios is to be expected.

Thus, for 45.39%, the extrapolated error yields 21.79% in case of system *A*. Similarly for system *B*, an extrapolated value of 9.11% can be found. From the scatter plots 6.8 and the computed standard deviation of the normalised random error, we can compute the normalised error (with respect to the computed mean, taken to be the true error) in this normalised error to find  $3.17/14.61 = 21.70\%$  and  $0.65/6.80 = 9.56\%$ . These values are very close to the extrapolated values above thereby supporting the idealised simulation in figure 6.7, and the robustness of the perturbation algorithm with respect to errors in the computed perturbations obtained via the plug-in method from chapter 3.

### **Influence of Errors in the Computed Sensitivities**

To illustrate the effect on the predicted random error due to inaccuracies in the computed sensitivities, again system *A* is considered and the parameters used in the perturbations analysis are the same as in tables 6.2 and 6.3, depending on whether the influence of noise or estimation errors is considered. A  $13 \times 8$  Hankel matrix was used. However, instead of using the true auto-correlation functions as input to the perturbation algorithm, the estimated sample correlation functions from each of the 500 simulated response histories were used and the perturbation analysis was run for each of the 500 simulations. This results in an ensemble of 500 estimates of the normalised random error in the modal parameters. Since the perturbations were modelled exactly as in tables 6.2 and 6.3, the scatter of the normalised random error is entirely due to the inaccuracies in the computed sensitivities. The results are depicted in figures 6.9. It is seen from figures 6.9(a) and 6.9(b), showing the results where the sample correlation functions were corrupted by 15 and 30% noise respectively, that the system sensitivities are robust with respect to noise disturbance since the scatter in the predicted normalised random errors is small and clusters closely around the true error as can be seen by comparison with case 1 in table 6.2. The standard deviation of the normalised random error in the natural frequency and damping ratio is indicated in these figures and represented by width and height of the rectangle respectively.

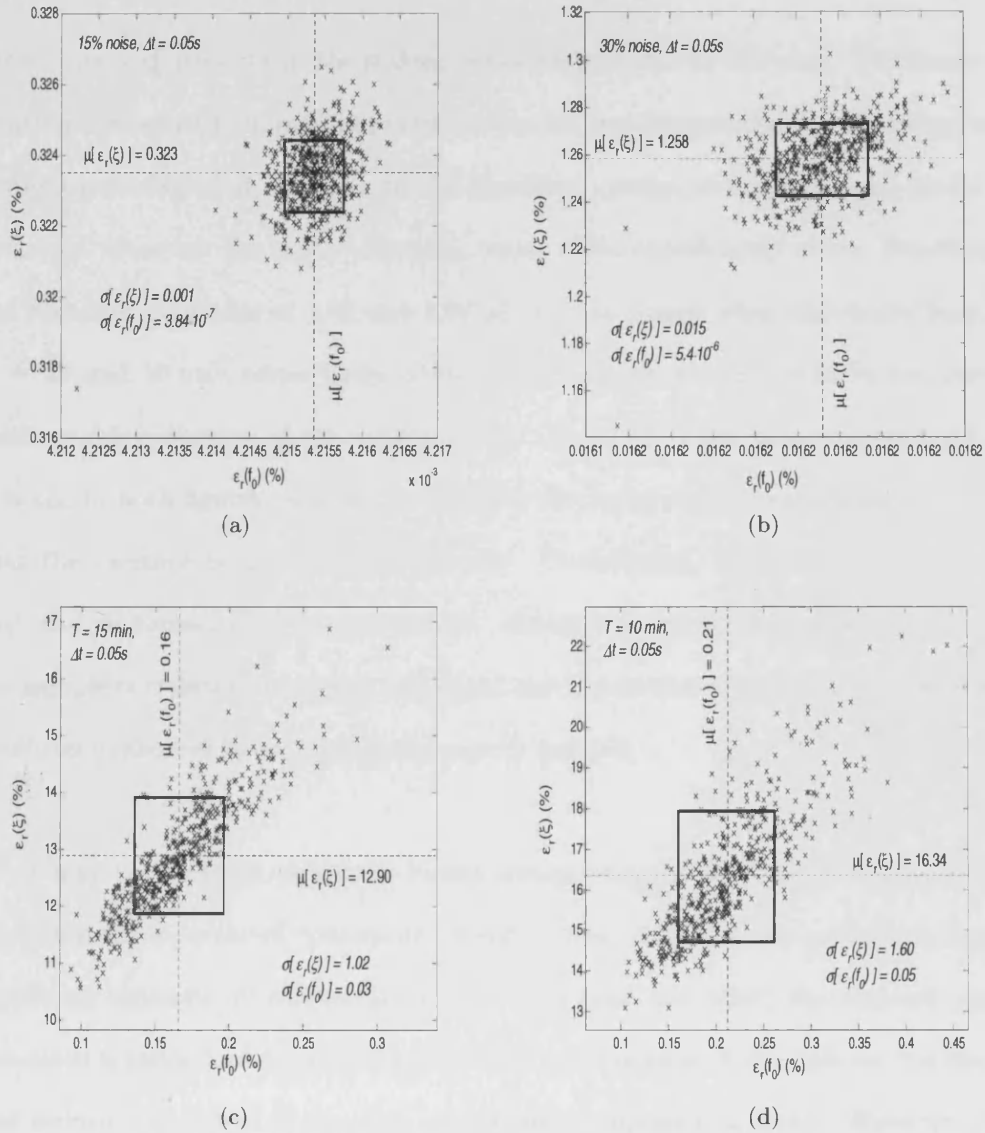


Fig. 6.9: Illustration of robustness of perturbation method with respect to errors in the estimated system sensitivities. The simulations are performed on system *A*. Figures(a) and (b) show the scatter due to 15% and 30% measurement and figures (c) and (d) due to estimation noise due to record length of duration  $T = 900$  and  $600s$  respectively.

Although a slight bias is observed in the 30% noise case, the scatter in the modal damping ratios is roughly within 1% of the true error as can be seen from the 0.015% standard deviation. The scatter in the frequencies is negligible.

Figures 6.9(c) and 6.9(d) depict the scatter of the normalised errors predicted by the perturbation method when the computation of the sensitivities are corrupted by the estimation errors in the sample auto-correlation function. It is seen that, as for

the normalised error itself, the scatter is more significant in this case. The linear correlation between the normalised error in the natural frequencies and damping ratios is due to the fact that the error in the identified system pole affects both modal parameters, although the modal damping ratios suffer significantly more. Nonetheless, the standard deviation of 1.02 and 1.60 percentage points when the record length is  $T = 15$  and  $10 \text{ min}$  respectively, shows that, on average, the perturbation method yields stable estimates of the random error. As for the noise case, a downward bias is noted in both figures. A possible cause for the latter may be attributed to the fact that the variance is not corrected for bias. Nonetheless, figures 6.9(a)-6.9(d) show that the perturbation method is robust. Clearly as the record length is increased, the sample correlation are better estimated and the perturbation results become more stable as evidenced by comparing figures (c) and (d).

It may be worth at this stage briefly commenting on the record length. Due to the noninvasive nature of operational modal testing, it is generally possible to acquire significant amounts of response data. The total time over which the response can be measured is influenced by a few factors. In a first instance, it depends on the bit-rate and storage capability of the data acquisition equipment at hand. However, since the modal frequencies of civil engineering structures are typically low, and hence a low sampling rate can be chosen, long response records are possible. Record lengths ranging from 30 – 60 mins can be considered typical, see for instance Cantieni (2005); DeSmet *et al.* (1996); Farrar and James (1997); Felber *et al.* (1996), but longer response histories are becoming commonplace (Qin and Qian, 2001). But the size of the structure, the number of channels available and the coarseness of the desired measurement grid also play a role. When the measurement grid is smooth and the size of the structure large, many setups may be required if the number of available channels is low. Performing such a test takes time and the length of the response histories is often compromised. Such a situation is, for instance, described for a dam in Cantieni (2005), where the response histories were limited to 6 mins. If only frequencies are

desired, short record lengths are often sufficient to obtain a reasonably accurate estimate Cunha *et al.* (2001) or in other cases, for instance, when the response due to earthquake loading is sought, which have a duration of about 60 – 120 s short records must be used. In most ambient testing applications to civil engineering structures, one can expect to collect data for  $\geq 15$  min which means that our choice of using 10 – 15 min can be considered conservative.

### **Influence of Combined Instrumentation and Estimation Noise**

Having investigated the influence of measurement noise and estimation errors in the sample correlation functions on the identified modal parameters, as well as the robustness of the perturbation method with respect to errors in the estimated perturbations, the behaviour of the predicted normalised random error is investigated when both error sources contribute to the perturbation. Again, we proceed by simulation on the two systems *A* and *B*. For each system, 500 response histories were simulated by adding a 30% broad-band white noise signal to the computed response time-histories. The response and noise signal were computed using the same parameters as in cases 1 and 4, for the two systems respectively, given in tables 6.3 and 6.2. The variance and covariances, and hence the perturbations, were obtained using the plug-in method described in Chapter 3. The system identification was performed using a  $7 \times 4$  Hankel matrix for system *A* and a  $22 \times 14$  Hankel matrix for system *B*. In this fashion, 500 error estimates were obtained for each of the modal parameters for each of the two systems. A scatter plot of the latter are shown in figures 6.10. As before, the mean normalised error,  $\mu[\epsilon_r(\cdot)]$ , of both modal parameters as well as their standard error  $\sigma[\epsilon_r(\cdot)]$  are given and represented on the figures. The width and height of the rectangles represent the standard error of the modal damping ratios and frequencies respectively. For comparison, the true normalised errors are given in table 6.4. As expected, it is seen by comparing table 6.4 to tables 6.2 and 6.3 that most of the error stems from the estimation noise. However, the contribution from the measure-

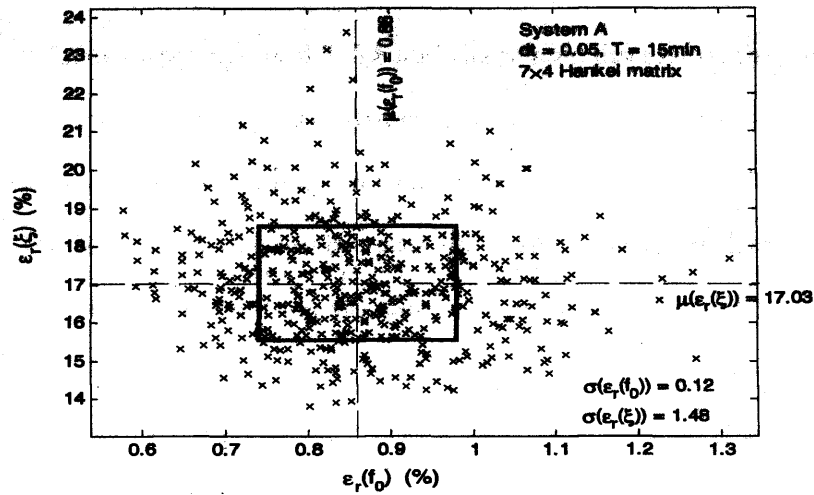
ment noise is clearly visible for system A (compare with tables 6.2 and 6.3) and it appears that the contribution of both sources add up to yield the total error. Quite surprisingly, however, this does not appear to be the case for the random error in the frequencies, for which a much higher error is observed. It is not clear why this is the case but, importantly, the perturbation method predicts the correct error.

Due to the fact that noise is so significantly mitigated when a higher dimensional Hankel matrix is employed, the addition of both errors is less obvious for the simulation on system B, although a slight increase in random error is picked up. Since the random error in the estimated modal parameters due to noise decreases sharply as more correlation lag values are used (c.f. table 6.2 and figures 6.6) but, on the other hand, increases gently due to estimation errors (c.f. table 6.3), one can expect the random error to reach a minimum when the influence of the noise starts to fade and starts to be dominated by the estimation errors only. Such a behaviour of the scatter of the modal damping ratios identified via the correlation fit method was already reported by Cooper (1989). Comparing the true errors in table 6.4 with the mean predicted error in figures 6.10 it transpires that the latter are slightly overestimated. The precise reason for this discrepancy is not known but the slight errors that ensue due to the windowing and approximations in the plug-in method are plausible candidates. These simulations show that the plug-in method is capable of accounting for both disturbances in the data with good accuracy and in fact, due to the nature of the method, any random disturbance will be picked up in this fashion as long as it is stationary.

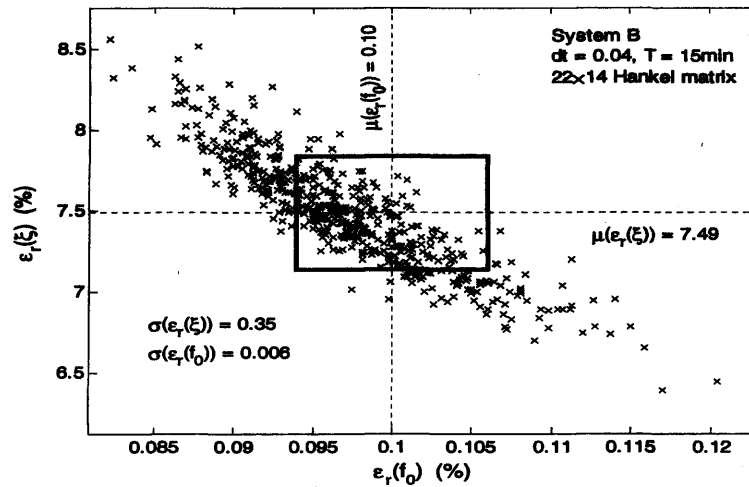
It is seen from figure 6.10 that the standard deviation in both cases is small so that

	$\epsilon_r(f_0)(\%)$	$\epsilon_r(\xi)(\%)$
System A	0.82	16.01
System B	0.10	7.36

Tab. 6.4: True normalised error of the estimated natural frequencies and damping ratios due to the combined influence of measurement noise and sample estimation errors.



(a)



(b)

Fig. 6.10: Illustration of the perturbation method in the presence of combined measurement noise (30%) and sample estimation errors.

the true error is on average predicted with good accuracy. It appears from figures 6.10 that the linear correlation between the error in the identified modal damping ratios and frequencies is negative i.e. as the accuracy in the frequencies increases, its drops for the damping ratios and vice versa. However, the frequencies are identified accurately and the outliers do not deviate excessively from the mean with a maximum absolute error of 6% occurring for system A. When only a single response record is available from which the error in the SSI/Cov-identified modal parameters is predicted, it is very difficult to tell how accurately the error prediction approximates the

true error. It follows from figures 6.7, 6.8 and the related discussion, that an estimate of how well the true error is approximated could be obtained if the random error in the sample variance of the auto-correlation function at zero lag were available. However, due to the gentle slope of the line in figure 6.7 relating the normalised error in the perturbations to the deviation from the true error in the identified modal parameters, a rough estimate of the the random error in the sample variance of the auto-correlation function at zero lag may be sufficient to get a good idea of the accuracy of the single error predicted by the perturbation method. Although this knoweldge would be desirable to place confidence in the predicted error, this issue was not pursued further and should be the subject of further research. Due to the stable nature of the perturbation method as well as the plug-in method to estimate the perturbations, the simulations so far have shown that, on average, one can expect to predict the random error in the modal parameters with good accuracy for all practical purposes. It is worth pointing out that, as shown in Chapter 4, the variance and covariances, and hence the perturbations may alternatively be computed using the bootstrap method. In this case, an estimate of the root-mean-square error of the resulting estimates is obtained as a by-product, although the latter has the undesirable porperty that it is accurate only if the estimate of the variance and/or covariance is accurate too. Nonetheless, this may be used to get a crude idea of the accuracy of the actual error prediction. The performance of the bootstrap in conjunction with the perturbation method is not investigated in this thesis and the use of the bootstrap as a separate tool to determine the errors in identified modal parameters is investigated in the next chapter.

For completeness, it is shown that the perturbation method also takes into account the random error introduced due to model order selection. As described in Chapter 2, the SSI/Cov requires the model order to be specified by the user with the aim to separate the noise modes from system modes. For a more detailed explanation, the reader is referred to Chapter 5. In practice, the model order is determined by inspection of the singular value diagram, and the largest gap in the singular values



indicates the model order. However, this gap is not always obvious and consequently, the model order is often under- or over specified. In the latter situation, part of the noise space is retained in the curve fit and clearly, this affects the random error of the identified modal parameters. This is shown in table 6.5. The simulation is performed using system A and B and the record length and sample interval are the same as in the previous section. The identification is performed with a  $22 \times 14$  Hankel matrix. The first case shown (that is for the true model order 2) is the same as in the previous section, but is repeated here for a better comparison. It is seen that when the system is identified with a higher model order, the random error in the modal parameters increases and this behaviour is correctly predicted by the perturbation method. The increasing random error with model order reflects the fact that part of the noise space is retained in the identification of the system matrices. It is noted that not only does the random error in the modal parameters increase but also the scatter in the predicted errors. This can be seen from the standard deviations shown in the table. In practice, the distinction between the identified system modes and noise modes is made using stabilisation diagrams. However, as pointed out by Bergman *et al.* (1989), the random errors of the spurious modes predicted by the perturbation analysis tends to be significantly larger compared to those of the system modes and this information may be used to separate noise from system modes. It is shown in Peterson *et al.* (1996), however, that it is possible for spurious modes to be identified with a random

	System A			System B		
Model Order	2	4	6	2	4	6
True Error (%)						
$\epsilon_r(f_0)$	14.42	14.64	14.91	7.36	7.50	7.78
$\epsilon_r(\xi)$	0.15	0.15	0.15	0.10	0.10	0.10
Predicted Error (%)						
$\mu[\epsilon_r(f_0)]$	15.37	15.58	15.88	7.49	7.62	7.98
$\sigma[\epsilon_r(f_0)]$	0.016	0.016	0.016	0.006	0.007	0.011
$\mu[\epsilon_r(\xi)]$	0.16	0.16	0.16	0.10	0.10	0.11
$\sigma[\epsilon_r(\xi)]$	1.50	1.50	1.51	0.35	0.38	0.92

Tab. 6.5: Influence of model order selection on the predicted random errors.

error comparable to that of the system modes so that a mode selection, based solely on the associated predicted random errors is not always reliable and therefore should be used only as a tool to assist the stabilisation diagram interpretation. In the simulation above, due to the cumbersome task of analysing a stabilisation diagram for each 500 realisations, the system modes were picked based on their significantly lower predicted random errors. This is acceptable in this case, because the true modal parameters as well as the true system order is known which allows checking whether the true system mode has been picked in each case.

### **Influence of Non-white, Non-stationarity Loading**

It has been shown so far that the perturbation method yields accurate and robust estimates of the random error in the SSI/Cov-identified modal parameters when the excitation of the system is broad-band white noise and the response is corrupted by measurement noise. The data-driven method developed in chapter 3 to estimate the perturbations to the sample correlation functions takes into account the combined influence of the estimation and measurement noise and in fact, since this plug-in method is designed to estimate the variance and covariance of sample correlation functions computed from random stationary data, any disturbance of the response other than estimation and measurement noise is accounted for by this method, as long as it is stationary. Although it is common practice in operational modal analysis to assume that ambient loading conditions and hence the response of the structure is stationary, examination of full-scale real response data has shown that this is not always the case. In this section, it is investigated whether the perturbation method also yields acceptable random error predictions in the SSI/Cov-identified modal parameters when the loading conditions exhibit non-stationary characteristics. Also, the departure from white loading conditions is considered.

- For the vast majority of applications of operational modal analysis to civil en-

gineering structures, the assumption of white and stationary loading conditions is applicable, at least in a relaxed form: for instance, Turner and Pretlove (1988) have shown by simulation -which is validated against measured data- that traffic, with its random weight of vehicles, their random arrival times and the randomly distributed road irregularities has a broad enough spectrum to excite the fundamental modes of bridge structures. Although the spectrum of traffic induced excitation may not be "flat", their findings suggest that the spectrum is slowly varying and that a white noise approximation may be appropriate, at least over the low frequency range covering the fundamental modes of bridges. Also, as reported by Holmes (1998); Kareem (1987), the spectra of wind loads on structures falls within a  $10Hz$  frequency band and are relatively slowly varying so that the above argument applies and a white noise excitation can generally be taken as a valid assumption. However, exceptions occur for instance in structures where periodic forces mix with random ambient loads. Such situations occur commonly in structures associated with harmonically moving components arising most commonly from unbalanced rotating parts such as blades in wind turbines (James *et al.*, 1993) or floor slabs supporting plant for instance. Mohanty (2005) has developed an extension to the SSI/Cov (or the ERA) to deal with such cases and Brincker *et al.* (2005b) developed an indicator to distinguish between structural modes and modes caused by harmonic excitation.

Deviations from stationary loading regimes are much more common in practice. For instance, in traffic induced bridge vibration, the passing of vehicles over bridge deck causes transients in the response, and also, as shown by Calcada *et al.* (2005a,b) that the interaction force between vehicle and bridge deck has harmonic components. A typical response of the vibration of bridge deck induced by traffic is shown in figure 6.11, clearly showing the transients due to a vehicles crossing the deck. This measurement was taken by the author in collaboration with the University of Luxembourg on a four-span bridge over the river Alzette in Luxembourg in 2004. Non-stationary responses of bridge decks to aerodynamic loading, resulting in clear frequency changes

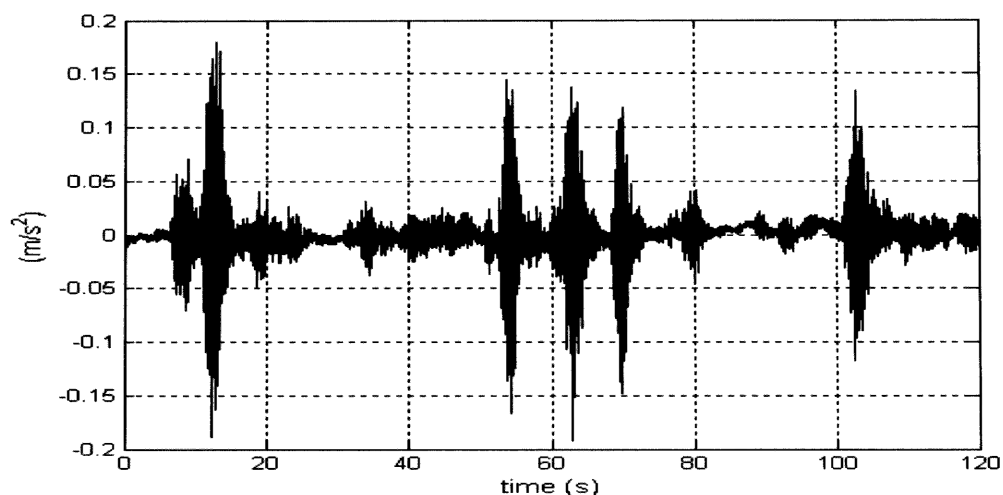


Fig. 6.11: A typical response acceleration record of traffic induced bridge deck vibration.

in the response with time, have also been reported, see for instance Zhang *et al.* (2006).

Studying the influence of non-stationary, non-white ambient loading conditions on modal parameters in a *general* framework is very challenging. The reason is that non-stationarity as well as non-whiteness are negative statements in the sense that they describe a lack of properties rather than specifying the exact nature of the non-stationarity or the precise spectrum of the frequency content of the data respectively. The situation is further complicated by the fact that the specific nature of the non-stationary characteristics and non-white ambient loading conditions will inevitably vary from case to case and to the authors knowledge, there is no clear consensus on the form of non-stationary, coloured loading typically occurring in operational modal testing of civil engineering structures. Even in particular cases, where the sources of ambient excitation forces are known, realistic simulations of the resulting loading is extremely challenging on its own, in particular for wind excitation which generally depends on the geometric properties of the structure as well as on its urban or sub-urban condition. Therefore, to achieve our aim, we content ourselves by modelling a generally hostile loading regime departing from the common assumptions of stationary, broad-band white noise excitation.

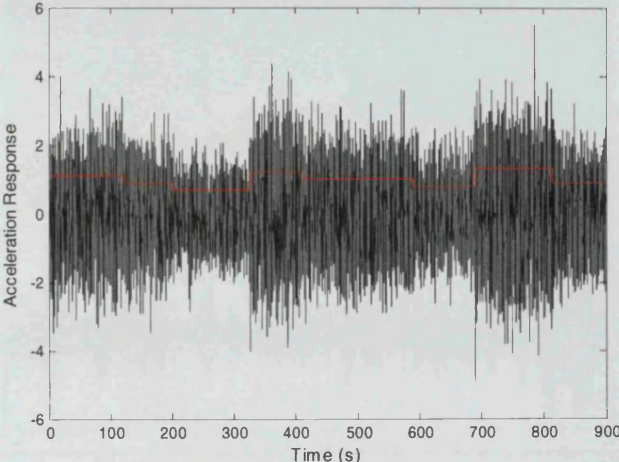
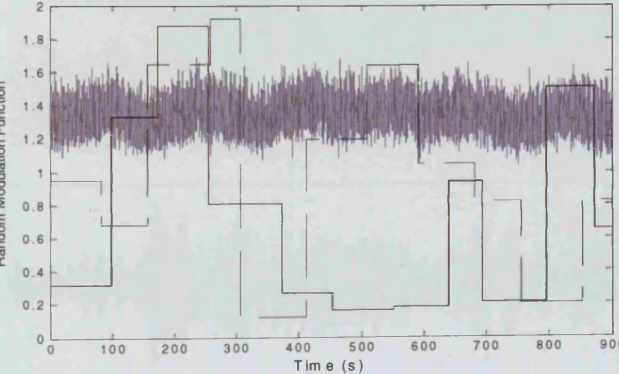
Load case	Description	Illustration
1	<ul style="list-style-type: none"> <li>• Normally distributed, white noise signal with <i>unit mean-square value</i> (<math>msv = 1</math>) is modulated by a stepped modulation function. The latter is shown in the figure on the right (red) superposed on the modulated signal.</li> <li>• This yields an excitation that is non-stationary in the mean. The maximum and minimum <math>msv</math> of the modulated signal are 1.3 and 0.7 respectively.</li> <li>• Additionally, a <math>2\text{Hz}</math> harmonic is superposed with a peak amplitude of <math>0.6</math>.</li> <li>• The modulation function remains the same for all simulated load cases so that the only random factor stems from the underlying white noise signal.</li> </ul>	
2	<ul style="list-style-type: none"> <li>• Normally distributed, white noise signal with <i>unit mean-square value</i> (<math>msv = 1</math>) is modulated by a stepped modulation function.</li> <li>• Unlike load case 1 above, the stepped modulation function changes for each simulated load case. Two such modulation functions are depicted on the right. These changes are random and the plateaus have duration drawn uniformly on the interval <math>40\text{-}120\text{s}</math>. The respective amplitudes are sampled from a uniform distribution with a <math>msv</math> of <math>1.3</math>.</li> <li>• The mean square value over an ensemble of 500 simulated load cases is shown in grey.</li> </ul>	

Fig. 6.12: Description of load cases 1 and 2.



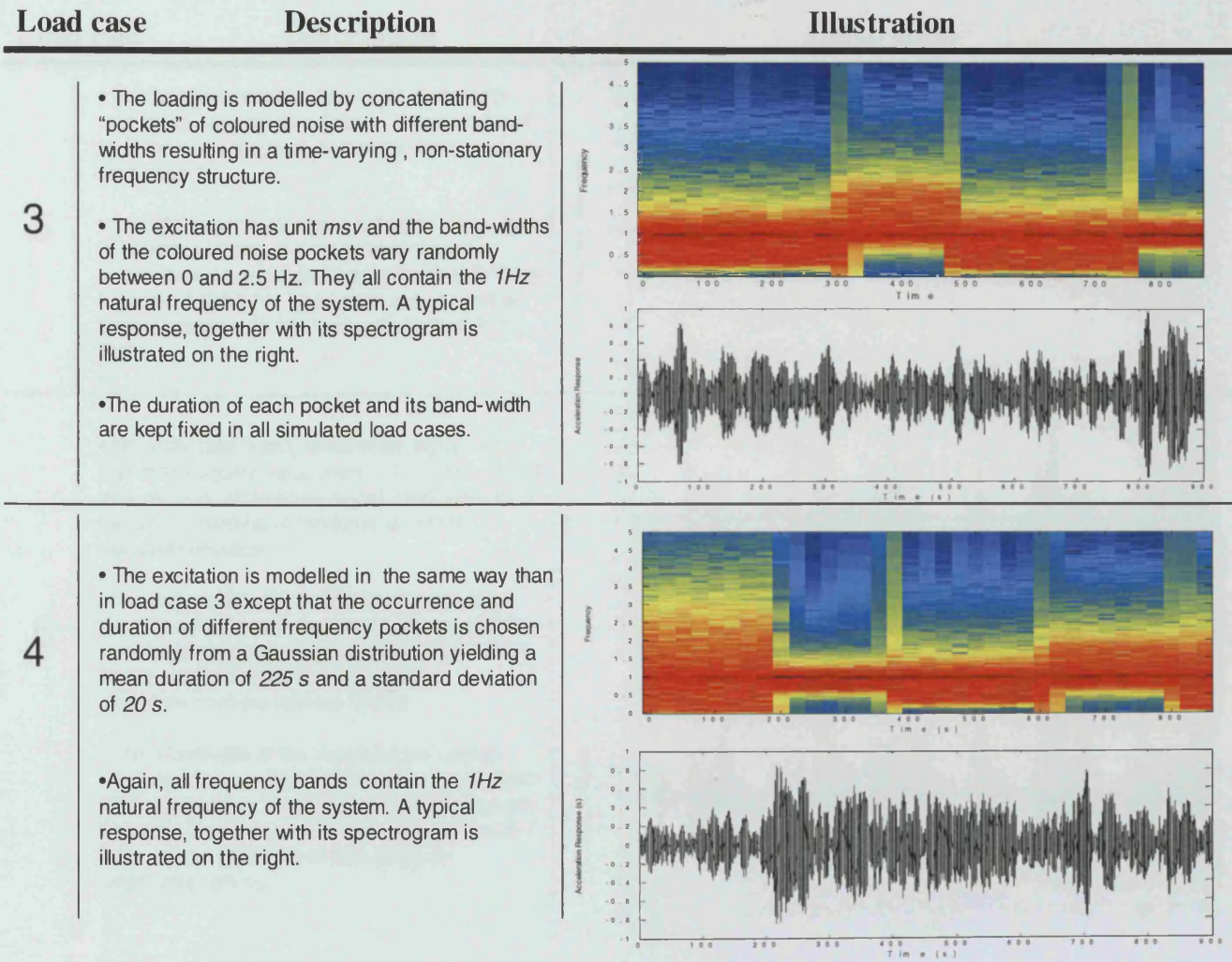


Fig. 6.13: Description of load cases 3 and 4.

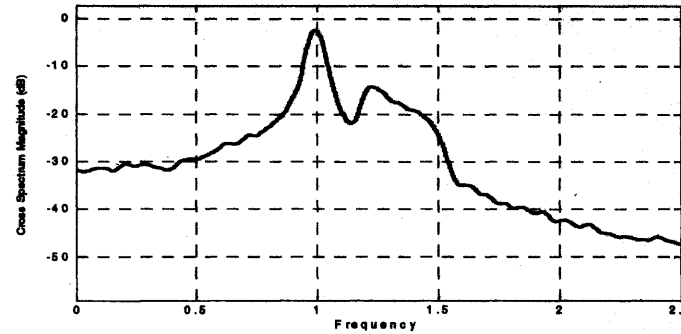
**Load case**

**Description**

**Illustration**

5

- Normally distributed, white noise signal with unit mean-square value ( $msv = 1$ ) is modulated by a the same stepped modulation function as in load case 1.
- In addition, a narrow-band coloured noise signal is superposed onto the modulated signal. The coloured noise signal has a band-width lying between 1.2-1.5 Hz. The power spectrum of a typical response to this load is illustrated on the right.



6

- Normally distributed, white noise signal with unit mean-square value ( $msv = 1$ ) is superposed with another white noise signal modulated by a function consisting of randomly occurring Gaussian impulses.
- It is assumed that, on average, an impulsive force occurs 3 times per minute. These events are drawn randomly from a uniform distribution. The duration of each impulse is drawn uniformly from the interval 10-20s.
- The amplitudes of the impulses are random samples from a uniform distribution ranging from 0-25. Since the arrival times of the impulses are Random, it may occur that two impulses occur more or less at the same time and their amplitudes add up.

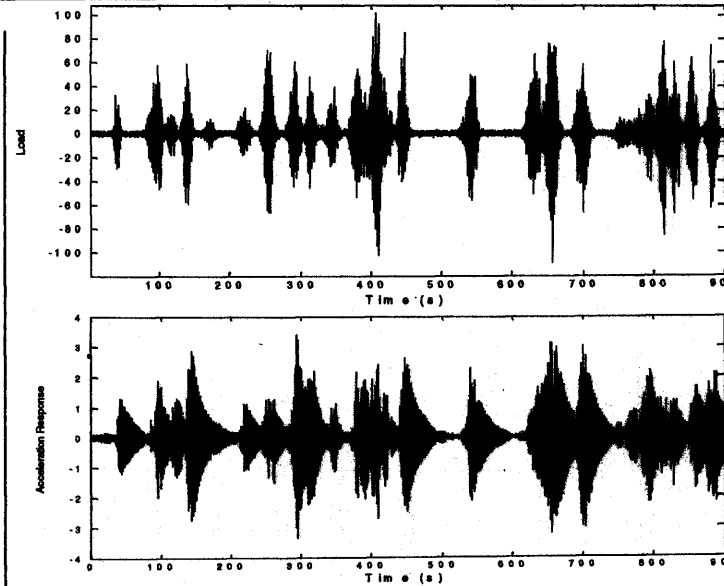


Fig. 6.14: Description of load cases 5 and 6.

As described in Bendat and Piersol (2000), non-stationary time-series can be build by combining three elementary models:

- (a) a stationary, stochastic signal  $w(t)$  to which a deterministic function  $M(t)$  is added, resulting in non-stationary mean value,
- (b) modulation of a stationary, stochastic signal  $w(t)$  by a deterministic envelope function  $M(t)$  and
- (c) signal in which the instantaneous frequency changes with time.

Combinations of such elementary non-stationary models have been used, for instance, by Gasparini (1979); Sun and Kareem (1989) to describe excitation due to ground vibration and by Giuffre and Pinto (1974) to simulate the response of bridges to non-stationary excitation loading. In this section, these models are used to build 6 different load cases described in figures 6.12, 6.13 and 6.14. Simulations are performed on system *A* and the results are shown in table 6.6. 900s ( $\Delta t = 0.05s$ ) of data are used and a  $22 \times 14$  Hankel matrix is used in the identification process. 500 records are simulated for each load case.

The first load case (c.f. figure 6.12 ) consists of a combination of the elementary models (a) and (b). Both the 2Hz harmonic and the deterministic modulation function are repeated exactly for each record which results in a time-varying mean and mean-square value, the latter being equal to the modulation function since the stationary white noise signal has unit mean-square value. The different amplitudes imparted by the modulation function on the load time-history may, for instance, represent varying wind pressures acting on a structure during the test time. The harmonic, on the other hand, may be representative of a driving force caused, for instance, by rotating components in/on the structure (e.g. wind turbines, plant excitation on floor slabs). While it is reasonable to assume that the harmonic driving force does not change for a particular test case, it is in general unlikely that the modulation remains the same for repeated tests on the same structure. Exceptions occur, for example, in



earthquake induced ground motion, where the build up and decay follows a similar trend for different load cases. Load case 2, therefore, is a variation on load case 1 where the modulation profile changes randomly from record to record. It is important to note, however, that the thus modelled excitation is not necessarily non-stationary. To see this, consider the instantaneous mean-square value at a specific time  $t_i$  of the load computed over the ensemble of all load cases generated by this stochastic process. Since the amplitudes of modulation function are random, the mean-square value over the ensemble of excitations at any time  $t_i$  will tend to the mean-square value of the uniform stochastic process used to generate the random amplitudes of the modulation function. This is clearly seen in figure . Nonetheless, this case is still of interest since the mean-square value is clearly time-dependent in a single record as would easily be established numerically using short-time averaging procedure (Bendat and Piersol, 2000) and the SSI/Cov cannot account for this time dependence. Before discussing the results of the simulations in table 6.6, it is worth reviewing briefly how the SSI/Cov deals with non-stationary data. The SSI/Cov identifies the system modal parameters from correlation functions of stationary data i.e. the correlation functions depend on a single time variable describing the separation of two points in the response record. Non-stationary correlation functions depend additionally on the time at which this lag is measured, and hence are functions of two time variables. The SSI/Cov, however, is unable to deal deal with non-stationary correlation functions and hence ordinary stationary correlation functions need to be used. Clearly, when stationary correlation functions are estimated from non-stationary response records, the non-stationary characteristics of the data is lost. Effectively, the time-varying statistics are averaged out (Bendat and Piersol, 2000). When the non-stationarity follows model (b) described above, a more precise description is available. Essentially, modulating a stationary noise signal by a deterministic function is the same than applying a window, and the effects of the latter on sample correlation functions was briefly described in Chapter 3. In a nutshell, the modulation (or the window) function applied to the response record appears in the sample correlation function estimate as its own correlation func-

tion and affects the unmodulated correlation function multiplicatively (see. eqn. 3.22 in chapter 3, page 62 or Schmidt (1985a) for more detail). For convenience, this is illustrated on a simple example below. Figure 6.15(a) shows the time-history -chosen

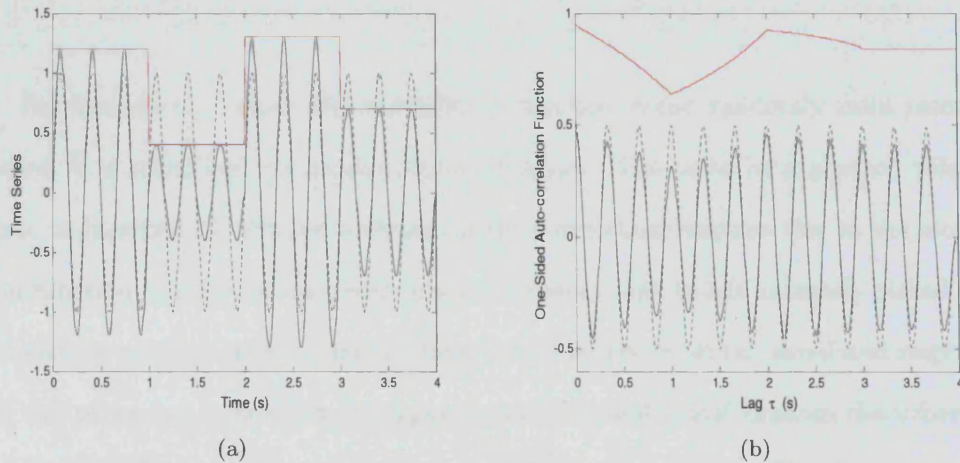


Fig. 6.15: Illustration of the effect of a modulating function on the sample auto-correlation functions. The unmodulated time history and its correlation function are represented by the dotted back line, the modulation function and its correlation function by the solid red line and the modulated signal with its correlation function by the solid black line.

here to be a  $3Hz$  harmonic in order not to include any random errors in the sample correlation function- modulated by the stepped function and the resulting modulated signal. Figure 6.15(a) shows the corresponding correlation functions and it is clearly seen that auto-correlation function of the modulated signal takes on the profile of the correlation function of the modulation function. It is precisely this additional disturbance we wish to account for.

The results of the simulations involving load cases 1 and 2 are shown in table 6.6. For a better appreciation of the influence of the non-stationarity that was introduced, the random error due to the underlying white noise signal only is also given in table 6.6. As in the previous section, the  $\approx 1\%$  discrepancy between the true and predicted random error may again be attributed to small bias errors in the sample estimates of the perturbations via the plug-in method. It is seen that for load case 1, the random error in both the true and perturbation estimate is practically identical to the one due to white noise only. The explanation for this is simply that the harmonic and the

modulation function are repeated exactly for each signal and no additional randomness is introduced. On the other hand, however, it can be seen from the illustration of the problem in figures 6.15 that a bias error is introduced. This issue is dealt with in the next section.

For load case 2, where the modulation function varies randomly from record to record, it is seen that the random error increases. This is to be expected: referring again to figures 6.15, the perturbation of the correlation function due to the modulation function changes for each response time-history and, this is naturally picked up in the sample random error computed from the ensemble of all the simulated responses. On the other hand, however, it appears that this additional random disturbance is not accounted for by the perturbation method. It was anticipated by the author that, at least to some degree, the extra disturbance caused by the modulation would be reflected in the random error as predicted by the perturbation analysis. The reason being that the plug-in method estimates the perturbations from the full length, flat-top windowed, sample correlation functions and since the latter are affected by the perturbation of the non-stationarity as illustrated in figures 6.15, it was expected that the estimated perturbations, and hence the random error predicted by the perturbation analysis would be affected likewise. However, this does seem to be the case. Comparing the variance of the true correlation function at zero lag in table 6.6, the influence of the additional disturbance due to the modulation function is clearly noticeable. When the plug-in method is used to estimate the perturbations, the influence of the random, slowly varying modulation functions is almost entirely eradicated, evidenced by the almost identical random errors in both the modal parameters and the correlation function at zero lag. A plausible reason for this is that the variations due to the modulation function are too slow compared to the system frequency to be picked up. To support this, one can imagine the scenario of what would happen if the duration in the changes of the modulation function were increasingly reduced until the changes occur on average at intervals of the same order than the sampling interval. In this

case, we would have a very good approximation of white noise signal, the influence of which would clearly be picked up the plug-in method as previously shown. To make sure that the cause of this discrepancy is due mainly to the estimated perturbations, it was checked that, if the true perturbations, estimated from the sample population of the 500 simulated response histories, are used in the perturbation analysis, then the predicted random error in the modal parameters agrees with the true values. This does not mean, however, that the system sensitivities are unaffected, but rather that they incorporate the influence of the modulation function adequately.

Next, the influence of a non-stationary, non-white frequency content is investigated. Load case 3, described and illustrated in figures 6.13, is composed of piecewise stationary coloured noise signals with a narrow band-width encompassing the 1Hz natural frequency of the system. The mean-square value of each noise "pocket" is unity and the duration of each is kept fixed for each simulated load record. This means that the only time-varying quantity is the instantaneous frequency content. The disturbance introduced to each stationary sample correlation function due to the averaging over the time-varying frequency content inherent in the computational process (Bendat and Piersol, 2000) results again is an increased random error as can be seen from the true error in table 6.6. As for load case 2, the perturbation method seems unable to account for the additional random error due to the non-stationarity and, as before, the reason can again be attributed to the inability of the plug-in method to account for the extra perturbation as evidenced by the comparing the random error of the correlation function at zero with the corresponding true quantity. Much the same observation holds for load case 4, where in addition to the random frequency bands, the occurrence and duration of the different coloured noise pockets of which the excitation signal is composed changes randomly from record to record.

Load case 5 examines the case when a narrow-band, frequency disturbance is added to the excitation. This load is modelled in exactly the same way as load case 1 except

that the  $2Hz$  harmonic is replaced by a narrow-band (0.3 Hz) coloured noise disturbance near the natural frequency of the system. The spectrum of the response is shown in figure 6.14. It is seen in table 6.6 that this disturbance causes a net increase in error in the identified natural frequency of the system and the latter is accurately captured by the perturbation method. Also the slight decrease in random error in the identified damping ratios is correctly predicted. Load case 6 consists of a superposition of two signals. The first one is a white noise signal with unit mean-square value and the second one a white noise signal modulated by randomly occurring Gaussian impulses with randomly varying duration and amplitude. This load case was chosen to simulate, in a very elementary fashion, the excitation of fundamental mode of a bridge deck by traffic. The Gaussian impulses represent the passing of a vehicle of the deck. It is well known that the arrival times generally follows a Poisson distribution (see Chen and Feng (2006), for instance), but for the present purpose, drawing the arrival times from a uniform distribution is sufficient. A typical excitation time-history together with the response of the system are shown in figure 6.14. The transients caused by the impulses are clearly visible in the response. Again, the situation is similar to the previous load cases involving non-stationary mean-square values; the random error induced to the modal parameters due to the random varying modulation

Case	Simulated Error (%)			Perturbation Method (%)		
	$\epsilon_r(f_0)$	$\epsilon_r(\xi)$	$\epsilon_r[R_x(0)]$	$\mu[\epsilon_r(f_0)]$	$\mu[\epsilon_r(\xi)]$	$\mu[\epsilon_r[R_x(0)]]$
Stationary White Signal	0.15	14.42	14.05 %	0.16 (0.02)	15.37 (1.50)	15.27 %
1	0.15	14.76	14.00 %	0.16 (0.02)	15.23 (2.00)	15.11 %
2	0.18	17.72	31.45 %	0.16 (0.02)	15.22 (2.12)	15.77 %
3	0.18	16.21	34.60 %	0.15 (0.02)	14.90 (1.57)	15.54 %
4	0.18	19.48	33.64 %	0.15 (0.02)	14.90 (1.92)	15.87 %
5	0.76	13.40	10.46 %	0.77 (0.20)	13.83 (1.81)	10.83 %
6	0.26	24.25	29.80 %	0.16 (0.02)	15.13 (2.09)	15.64 %

Tab. 6.6: Comparison of the simulated random error and the mean of the predicted random error using the perturbation method from 500 response measurements of System A in table 6.3. The values in brackets yield the sample standard deviation of the estimated errors.

functions from record to record is not picked up by the perturbation analysis and the method breaks down at the estimation of the perturbations by the plug-in method. It was checked again that if the true perturbations (i.e. as estimated from the ensemble of simulated response histories) are used in the perturbation algorithm, the true and predicted random errors in the modal parameters agree.

From the above simulations, it is to be concluded that the perturbation method does not consistently yield accurate predictions of the random error in the SSI/Cov-identified modal parameters when the response data has non-stationary characteristics. In particular, problems occur when the modulation function changes record to record, which induced an increase in random error in the modal parameters which was not reflected in the estimates predicted by the perturbation analysis. The cause of this was tracked down to the fact that the additional disturbance due to the non-stationarity was not picked up in the perturbations to the correlation function when estimated from the plug-in method. This is, however, not necessarily to be interpreted as a drawback of the combined plug-in/perturbation method: it was explained above that, when the modulation function remains the same for each record, most of the error in the correlation functions and the resulting SSI/Cov-identified modal parameters is systematic and has little effect on random error as is the case for load case 1, and in such a case the predicted and true error will be in good agreement. Therefore, to say that the perturbation method does not yield consistent estimates of the random error in the SSI/Cov-identified modal parameters from non-stationary data does not do justice to the method. However, as far as operational modal analysis is concerned, one is in general not in a situation, where the modal test can be repeated under identical non-stationary conditions and it is more likely to be in a situation as modelled in load cases 2, 3, 4 and 6, where non-stationary characteristics in a single time-history can be recorded using a short-time averaging procedure as described in Bendat and Piersol (2000). In these cases, unfortunately, as evidenced in particular by load case 6, the predicted random errors is not accurate. On a more positive note, however,

owing partly to the robustness of the SSI/Cov with respect to non-stationary data (see Basseville *et al.* (2001); Beneviste and Fuchs (1985)) and slowly varying disturbances, it is seen from table 6.6, that, considering the standard deviations from the ensemble of predicted errors for each record, the random error predictions are sensible and useful information, such as the influence of narrow-banded noise near system frequencies (load case 5) is to be gained. Nonetheless, in practice, if the data contains slowly varying trends, the estimated random errors should be treated conservatively. A remedy to the problem at hand does not seem obvious and is the subject of further research.

## 6.4 Bias Error

As explained in detail in Chapter 5, bias is introduced to the modal parameters by the SSI/Cov identification algorithm primarily due to two sources:

- truncation of singular values representing system dynamics, the truncation bias  $b_T(\chi)$
- the effect of passing noise through the nonlinear algorithm, the quadratic bias  $b_Q(\chi)$

where as before, the parameter  $\chi$  is used to denote any particular modal parameter. The bias is a systematic error and therefore if known, the estimates can be bias corrected. However, determining the bias with certainty is not a trivial task since (a) by definition, the bias involves knowledge of the parameter one is trying to estimate and (b) bias estimates are generally contaminated by random errors, taken into account in this case by the variance of the truncation bias. Therefore, in practice, bias-correcting the estimated parameters can be dangerous since the bias corrected estimates may have a larger random error than the original estimate. In this section, simulated data is used to assess the accuracy of the bias errors estimated by the perturbation method and it is investigated how to use these estimates, together with the random error studied in the previous section, to assess the uncertainty in the SSI/Cov-identified modal



parameters.

The simulations are performed on the same two SDOF systems given in table 6.3. The bias and RMS errors are investigated using the same simulated 900s ( $\Delta t = 0.05s$ ) response time-histories embedded in a 30% noise floor as for the random error for both systems. The estimation of the perturbations of the correlation functions via the plug-in method in relation to the perturbation analysis was validated in the previous section dealing with the random errors. Clearly, the latter aspect remains the same in this case. The true errors are computed from 500 simulated response time-histories and the perturbation analysis results shown are based on the first 200 response time-series of this set. The results are presented in tables 6.7 and 6.8 for system *A* and *B* respectively. It is noted that, as opposed to the previous sections, where the identified random error was normalised with respect to the mean of the identified modal parameters (i.e. a biased estimate), the results shown here are normalised with respect to the true modal parameters.

It is seen from the true errors in table 6.7 that the identified modal damping ratios are significantly biased, but this error appears to decrease as the dimension of the Hankel matrices used in the analysis is increased. A similar effect on the bias in the identified modal damping ratios as the number of correlation lags used is increased is reported by Cooper (1989). A particularly large bias is seen to occur when for the lowest dimensional ( $7 \times 4$ ) Hankel matrix. In the latter case, and for the case in which a  $13 \times 8$  Hankel matrix was used in the analysis, the RMS error defined as (Bendat and Piersol, 2000)

$$RMS(\hat{\chi}) = \sqrt{E[(\hat{\chi} - \chi)^2]} = \sqrt{Var(\hat{\chi}) + b^2(\hat{\chi})} \quad (6.16)$$

$$\text{with } b(\chi) = E[\hat{\chi}] - \chi \quad (6.17)$$

is seen to be predominantly due to bias, whereas for the  $22 \times 14$  dimensional Hankel matrix, the bias and random error carry equal weight. The identified natural fre-



**SDOF System A,  $\Delta t = 0.05s$**

	$dim(\mathcal{H}_0) = 7 \times 4$		$dim(\mathcal{H}_0) = 13 \times 8$		$dim(\mathcal{H}_0) = 22 \times 14$	
	<b>True Error</b>					
	$f_0$	$\xi$	$f_0$	$\xi$	$f_0$	$\xi$
<b><math>b</math></b>	<b>-0.044</b>	<b>0.049</b>	<b><math>-4.4 \cdot 10^{-4}</math></b>	<b>0.0058</b>	<b><math>-2.4 \cdot 10^{-4}</math></b>	<b>0.0017</b>
(%)	(-4.4%)	(489.3%)	(-0.04%)	(57.7%)	(-0.02%)	(17.4%)
<b><math>\sigma</math></b>	<b>0.0075</b>	<b>0.0092</b>	<b>0.0016</b>	<b>0.0023</b>	<b>0.0015</b>	<b>0.0017</b>
(%)	(0.75%)	(92.0%)	(0.16%)	(22.7%)	(0.15%)	(17.1%)
<b>RMS</b>	<b>0.0045</b>	<b>0.050</b>	<b>0.0017</b>	<b>0.0062</b>	<b>0.0015</b>	<b>0.0024</b>
(%)	(4.5%)	(497.9%)	(0.17%)	(62.1%)	(0.15%)	(24.3%)
	<b>Predicted by Perturbation Analysis</b>					
<b><math>\mu[b_T]</math></b>	<b>-0.023</b>	<b>0.0315</b>	<b><math>-2.1 \cdot 10^{-4}</math></b>	<b>0.0058</b>	<b><math>-1.9 \cdot 10^{-4}</math></b>	<b>0.0018</b>
(%)	(-2.3%)	(315.0%)	(-0.02%)	(57.9%)	(0.02%)	(18.0%)
<b><math>\mu[b_Q]</math></b>	<b>-0.007</b>	<b>0.0016</b>	<b><math>-7.1 \cdot 10^{-5}</math></b>	<b><math>3.4 \cdot 10^{-4}</math></b>	<b><math>-3.9 \cdot 10^{-5}</math></b>	<b><math>2.4 \cdot 10^{-4}</math></b>
(%)	(-0.7%)	(16.3%)	(0.0%)	(3.3%)	(0.0%)	(2.4%)
<b><math>\mu[\sigma(b_T)]</math></b>	<b>0.008</b>	<b>0.0068</b>	<b><math>4.8 \cdot 10^{-4}</math></b>	<b>0.0010</b>	<b><math>1.9 \cdot 10^{-4}</math></b>	<b><math>3.5 \cdot 10^{-4}</math></b>
(%)	(37.1%)	(21.6%)	(2.2%)	(17.3%)	(1.0%)	(19.4%)
<b><math>\mu[\sigma]</math></b>	<b>0.0081</b>	<b>0.0099</b>	<b>0.0017</b>	<b>0.0024</b>	<b>0.0015</b>	<b>0.0018</b>
(%)	(0.81%)	(98.6%)	(0.17%)	(23.9%)	(0.15%)	(17.7%)
<b><math>\mu[RMS]</math></b>	<b>0.025</b>	<b>0.0352</b>	<b>0.0017</b>	<b>0.0066</b>	<b>0.0015</b>	<b>0.0027</b>
(%)	(2.5%)	(352.3%)	(0.17%)	(65.8%)	(0.15%)	(26.8%)

Tab. 6.7: Comparison of the true and identified bias, random and RMS error in the SSI/Cov-identified modal damping ratio and frequency of SDOF system A. The identified errors are given as the mean of the errors computed via the perturbation analysis from 200 simulated response time histories. The corresponding true errors were computed from Monte-Carlo simulations over 500 response histories. The quantities in brackets give the corresponding normalised errors. The latter are normalised with respect to the true modal parameters (i.e.  $f_0 = 1Hz$  and  $\xi = 1\%$  of critical) with exception of the standard deviation of the truncation bias which is normalised with respect to the mean truncation bias.

quencies are much less affected by bias, with just above 5% error for the smallest dimensional Hankel matrix and less than 1% in the other two cases. As already explained, the Newmark- $\beta$  time integration method employed to compute the simulated response time histories, introduces a frequency shift whose magnitude depends on the natural frequencies of the system and the time step used in the integration. For this system, where a time step of  $\Delta t = 0.05s$  was used, it is easily calculated from equation

SDOF System B,  $\Delta t = 0.05s$

True Error						
	$f_0$	$\xi$	$f_0$	$\xi$	$f_0$	$\xi$
$b$	0.0022	0.0071	0.0046	$7.8 \cdot 10^{-4}$	0.0026	$-9.3 \cdot 10^{-4}$
(%)	(0.55%)	(47.0%)	(0.11%)	(5.2%)	(0.06%)	(-6.2%)
$\mu[\sigma]$	0.0040	0.0014	0.0037	0.0010	0.0038	0.0010
(%)	(0.10%)	(9.3%)	(0.09%)	(6.7%)	(0.10%)	(6.7%)
<i>RMS</i>	0.022	0.0072	0.0059	0.0013	0.0046	0.0014
(%)	(0.56%)	(48.1%)	(0.15%)	(8.9%)	(0.12%)	(9.2%)
Predicted by Perturbation Analysis						
$\mu[b_T]$	0.031	0.0063	0.0081	0.0022	0.0037	$7.1 \cdot 10^{-4}$
(%)	(0.78%)	(41.9%)	(0.20%)	(14.6%)	(0.09%)	(4.76%)
$\mu[b_Q]$	$6.6 \cdot 10^{-4}$	$9.3 \cdot 10^{-5}$	$1.7 \cdot 10^{-4}$	$6.3 \cdot 10^{-5}$	$1.2 \cdot 10^{-4}$	$5.2 \cdot 10^{-5}$
(%)	(0.00%)	(0.6%)	(0.00%)	(0.4%)	(0.00%)	(0.3%)
$\mu[\sigma(b_T)]$	0.0030	$5.9 \cdot 10^{-4}$	$9.3 \cdot 10^{-4}$	$2.2 \cdot 10^{-4}$	$4.7 \cdot 10^{-4}$	$1.0 \cdot 10^{-4}$
(%)	(9.5%)	(9.3%)	(11.5%)	(10.0%)	(12.9%)	(14.0%)
$\mu[\sigma]$	0.025	0.0015	0.022	0.0011	0.0023	0.0010
(%)	(0.1%)	(10.5%)	(0.09%)	(7.5%)	(0.090%)	(6.9%)
$\mu[RMS]$	0.0031	0.0066	0.0088	0.0025	0.0052	0.0013
(%)	(0.78%)	(43.3%)	(0.22%)	(16.7%)	(0.13%)	(8.3%)

Tab. 6.8: Comparison of the true and identified bias, random and RMS error in the SSI/Cov-identified modal damping ratio and frequency of SDOF system B. The identified errors are given as the mean of the errors computed via the perturbation analysis from 200 simulated response time histories. The corresponding true errors were computed from Monte-Carlo simulations over 500 response histories. The quantities in brackets give the corresponding normalised errors. The latter are normalised with respect to the true modal parameters (i.e.  $f_0 = 4Hz$  and  $\xi = 1.5\%$  of critical) with exception of the standard deviation of the truncation bias which is normalised with respect to the mean truncation bias.

3.44 that the Newmark- $\beta$  scheme introduces a frequency shift resulting in a negative bias of  $-0.81$  in the natural frequency. The true bias shown in table 6.7 was corrected for the Newmark frequency shift.

For system B, the true bias errors in the identified modal damping ratios given in table 6.8 show a similar behaviour to those of system A: the bias is largest when a low

dimensional Hankel matrix is used in the SSI/Cov identification and drops sharply with an increase of the size of the Hankel matrix. However, as the dimension of  $\mathcal{H}_0$  is further increased, the bias is seen to change sign. The bias in the identified natural frequency is small and falls below 1% error for each case shown, and decreases steadily as  $\dim(\mathcal{H}_0)$  is increased. No change in sign of the bias is observed in this case. It is noted that, as for system A, the bias shown in table 6.8 has been corrected for the frequency shift introduced by the Newmark time integration. For the case where  $\dim(\mathcal{H}_0) = 7 \times 4$ , the RMS error is strongly dominated by the bias, whereas in the two remaining cases, the contribution of the random error is significant.

It is now investigated how well the perturbation analysis predicts the bias in the SSI/Cov-identified modal parameters, and together with the random error, the RMS error. The bias in the identified modal parameters predicted by the perturbation analysis is given as the truncation bias,  $b_T$ , and the quadratic bias,  $b_Q$ . These two bias terms add linearly to yield the total bias which is to be compared with the true bias given in the tables. As described in Chapter 5, section 5.2.4, the truncation bias is affected by random errors, whose extent is expressed by the variance of the truncation bias. Tables 6.7 and 6.8 show the mean of the truncation bias identified from each of the 200 computed response time-histories, thereby obliterating the random error in the computation. However, as discussed in Chapter 5, the truncation bias itself is biased as result of the quadratic terms in equation 5.38. As discussed in the latter chapter, due to technical difficulties in determining the quadratic bias of the truncation bias, it was chosen to disregard the latter quantity. This means that the average truncation bias over 200 shown in tables 6.7 and 6.8 for both modal parameters is affected by quadratic bias of the truncation bias.

For both systems, it is seen from tables 6.7 and 6.8 that the estimated quadratic bias is small and appears to decrease as more data points are used in the identification. Also, it transpires that the bias is largely dominated by the truncation bias. The

perturbation analysis can be used to show that, in the cases studied above, the two terms which yield the quadratic bias (c.f. equation 5.10) tend to cancel each other out, a behaviour similar to that observed in the computation of the random error (see figures 6.6). However, it is noted that for shorter response histories, where the random error is more significant, we can expect a higher contribution from the quadratic bias. For system A, the bias is, on average, accurately predicted by the perturbation analysis for the two cases where the identification has been performed with the two larger dimensional Hankel matrices. In particular, the error in the damping ratios is accurately predicted. It is also noted that the sign of the bias is correctly predicted, and shows that the truncation bias is responsible for an underestimation, albeit small, of the natural frequency and an overestimation of the modal damping ratios. This supports the interpretation of the truncation bias as estimated by the perturbation analysis explained in section 5.2.3 of Chapter 5. For the case in which the identification was performed with the  $7 \times 4$  Hankel matrix, the bias in the modal damping ratio is predicted with less accuracy. However, the severity of the bias is nonetheless reflected by the perturbation analysis results and gives the user a good idea of the extent of the systematic error in the identified modal parameters. Moreover, if the modal results were to be bias corrected in this particular case, a significant improvement in the identified modal damping ratios would be gained. For system B, the agreement between the true and predicted bias is good for the case where the identification is performed using a  $7 \times 4$  Hankel matrix, but a significant discrepancy is observed for the remaining two cases; significant in the sense that if the bias computed from the perturbation analysis were used to correct the identified modal damping ratios, the bias would effectively be increased.

The random error in the estimated truncation bias is captured by the variance, or equivalently the standard deviation  $\sigma$ , of the truncation bias. The standard deviation of the truncation bias is shown in tables 6.7 and 6.8 and expressed as a percentage of the truncation bias itself. As mentioned in the introduction to this chapter, the

variance of the truncation bias should assist the user to determine whether the identified modal parameters should be bias corrected, provided that one is confident that the bias has been determined with sufficient accuracy. Firstly, it needs to be checked whether the random error in the truncation bias predicted by the perturbation analysis provides a good estimate of actual random error in this quantity. To do so, the "true" random error in the truncation bias is given in table 6.9 below. The latter is simply computed from the sample standard deviation of the truncation bias identified from each of the 200 simulated response time-histories and can be compared with the mean random error estimated for each simulated response record via the perturbation analysis shown in tables 6.7 and 6.8. A comparison between the values in table 6.9 and the truncation bias estimated via the perturbation analysis in tables 6.7 and 6.8 reveals good agreement. This also shows that the approximation made in Chapter 5 to estimate the variance of the truncation bias in order to circumvent the computation of the sensitivities of the full eigenvector matrix  $\mathbf{P}'$  is acceptable and appears not to affect the outcome significantly.

Having investigated the accuracy of the bias terms and the related random error, it needs to be determined how to make the best use of this information to assess the uncertainty in the identified modal parameters and possibly, correct the modal estimates for bias. An obvious estimate of the accuracy in the SSI/Cov-identified modal parameters, involving the bias, can be expressed by the RMS error. The latter can simply be computed from equation 6.16 by summing the squares of the standard deviation of the *biased* estimate, i.e.  $\chi(\epsilon)$ , and the total bias. It is noted that, since

		$dim(\mathcal{H}_0) = 7 \times 4$		$dim(\mathcal{H}_0) = 13 \times 8$		$dim(\mathcal{H}_0) = 22 \times 14$	
		$f_0$	$\xi$	$f_0$	$\xi$	$f_0$	$\xi$
Sys A	$\sigma[b_T]$	0.005	0.0060	$3.5 \cdot 10^{-4}$	$9.8 \cdot 10^{-4}$	$1.6 \cdot 10^{-4}$	$2.8 \cdot 10^{-4}$
	(%)	(21.2%)	(19.0%)	(1.6%)	(16.9%)	(0.84%)	(15.5%)
Sys B	$\sigma(b_T)$	0.0032	$5.5 \cdot 10^{-4}$	$8.8 \cdot 10^{-4}$	$1.9 \cdot 10^{-4}$	$4.8 \cdot 10^{-4}$	$1.0 \cdot 10^{-4}$
	(%)	(10.3%)	(8.7%)	(10.8%)	(8.6%)	(12.9%)	(13.6%)

Tab. 6.9: True random error of the truncation bias for system A and B.

the variance of the biased estimate is used, the variance of the truncation bias does not enter this RMS computation. The resulting RMS values are shown in tables 6.7 and 6.8. However, since the RMS error is dominated by the bias, or in other words, the bias error in the SSI/Cov-identified modal parameters is large compared to the random error, it would be desirable to bias correct the modal estimates rather than just having a measure of how much we can expect the estimates to differ on average from the true modal parameters. Particularly so, for applications where the identified modal damping ratios are used to fine tune a numerical or analytical model to predict the response amplitude of a structure to a certain excitation and a good estimate of the dynamic amplification factor is required. As previously mentioned, to bias correct the identified modal data, it is ideally required that (a) the bias estimate itself is unbiased and (b) has a low random error in order to avoid that the standard error of the bias corrected modal estimate becomes larger than the RMS error of the biased estimate. Denoting the bias corrected generic modal estimate by the  $\chi_{bc}(\underline{\epsilon})$ , the perturbation equations in Chapter 5 can easily be combined to express  $\chi_{bc}(\underline{\epsilon})$  as (Longman *et al.*, 1987)

$$\chi_{bc}(\underline{\epsilon}) \approx \chi(\underline{0}) - b_T[\chi(\underline{\epsilon})] + \sum_{j=1}^N \epsilon_j \delta_j (\chi - b_T(\chi)) + \sum_{k=1}^N \sum_{j=1}^N \epsilon_j \epsilon_k \delta_{jk} (\chi - b_T(\chi)) + \dots \quad (6.18)$$

Taking the above equation up to linear terms, the variance of the bias corrected modal estimate can be found to be

$$\begin{aligned} \text{Var} [\chi_{bc}(\underline{\epsilon})] &\approx \sum_{j=1}^N \text{Var} [\epsilon_j] \delta_j^2 (\chi - b_T(\chi)) & (6.19) \\ &+ 2 \sum_{\substack{j=1 \\ j \neq k}}^N \sum_{k=1}^N \text{Cov} [\epsilon_j, \epsilon_k] \delta_j (\chi - b_T(\chi)) \delta_k (\chi - b_T(\chi)) \\ &= \text{Var} [\chi(\underline{\epsilon})] + \text{Var} [b_T(\chi(\underline{\epsilon}))] & (6.20) \\ &+ 2 \sum_{\substack{j=1 \\ j \neq k}}^N \sum_{k=1}^N \text{Cov} [\epsilon_j, \epsilon_k] \delta_j (\chi - b_T(\chi)) \delta_k (\chi - b_T(\chi)) \\ &- 2 \sum_{j=1}^N \text{Var} [\epsilon_j] \delta_j (\chi) \delta_j (b_T(\chi)) \end{aligned}$$

The above equation shows the influence of both the variance of the truncation bias and biased modal estimate and the cross term is the consequence of taking the variance of the linear combination of the these two random variables. Provided the initial bias estimate is accurate, it can then be assumed that the bias corrected modal data is unbiased (or at least has negligible bias) so that the square root of  $\text{Var} [\chi_{bc}(\underline{\epsilon})]$ , i.e. the standard deviation  $\sigma [\chi_{bc}(\underline{\epsilon})]$ , yields the RMS error of  $\chi_{bc}$ . It is now obvious that if the RMS error of  $\chi_{bc}$  is larger than the RMS error of  $\chi$ , the modal parameters should not be bias corrected. The mean standard deviations of the bias corrected damping ratios over the 200 simulated response histories for system A and B are given below in table 6.10 and it can be seen that they are significantly smaller than the RMS values of the biased estimates which is again to be attributed to the fact that the bias errors are significantly large compared to the random error and the variance of the truncation bias. Provided the bias is estimated correctly, the benefit of a bias correction of the modal data is obvious. This is illustrated in figure 6.16 which shows the bias corrected SSI/Cov-identified modal damping ratios of system A with estimated random error via equation 6.19 for the first 100 simulated response time histories used in table 6.7. On the other hand, however, it is seen from the two cases for system B, in which the two larger Hankel matrices were used in the identification process, that the bias correction does more harm than good in the sense that the bias correction results in a slight increase in random error and a larger bias than in the original estimate. In practice, when the true modal parameters are not known, the engineer will not be able to assess the accuracy of the estimated bias and the two aforementioned cases for

		$\dim(\mathcal{H}_0) = 7 \times 4$	$\dim(\mathcal{H}_0) = 13 \times 8$	$\dim(\mathcal{H}_0) = 22 \times 14$
Sys A	$\mu[\sigma(b_T(\xi_{bc}))]$ (%)	0.0152 (152.4%)	0.0032 (32.5%)	0.0020 (20.4%)
Sys B	$\mu[\sigma(b_T(\xi_{bc}))]$ (%)	0.0020 (13.6%)	0.0013 (8.6%)	0.0011 (7.3%)

Tab. 6.10: Standard deviation of the bias corrected modal damping ratios  $\xi_{bc}$  for system A and B.

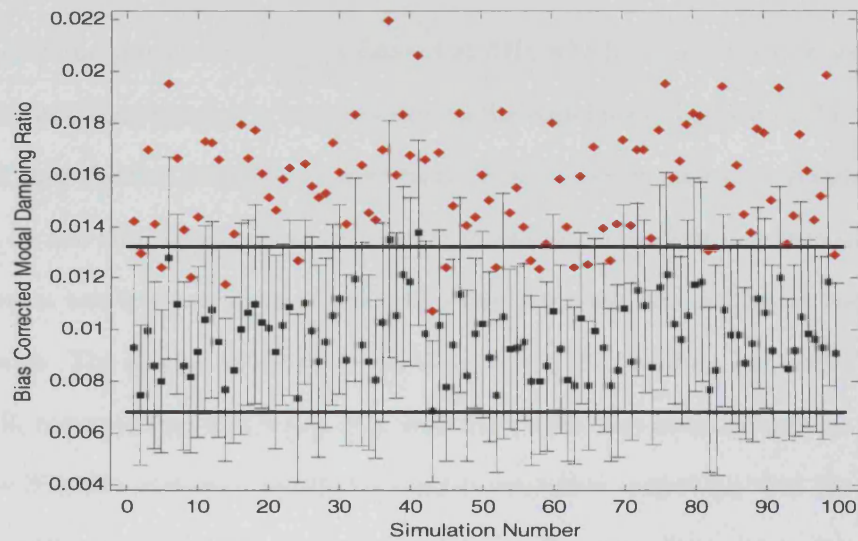


Fig. 6.16: Bias corrected modal damping ratios for system A identified with a  $13 \times 8$  Hankel matrix with error bars giving the standard deviation computed by equation 6.19. The diamonds show the actual identified modal damping ratios for each case and dashed horizontal lines the average standard deviation of the bias corrected estimates given in table 6.10.

system B, are sufficient to show that the bias estimates via the perturbation analysis cannot be taken for granted. As a result, bias corrections based on the perturbation estimated bias can be treacherous.

The question arises as to what lies at the bottom of the discrepancies observed in the estimated bias and the true bias and whether it can be rectified. Since the estimated perturbations of the correlation function (i.e. its variance and covariance) are not used in the determination of the truncation bias, it is therefore not affected by any errors in the former quantities. and the possible causes are investigated in the subsequent section.

### Errors in Bias Estimates

As explained in Chapter 5, the truncation bias arises due to truncation of small singular values that contain dynamic system information such as residual modes for instance. Truncating non-zero singular values due to noise only will have result in negligible bias. In the SDOF systems considered, the “residual mode” stems from the



fact that the signal was low-pass filtered at 6Hz which, as described in section 6.2.3, results in the addition of a *sinc* function to the correlation function of the system. To check that this disturbance introduced by the filtering operation is indeed responsible for the truncation bias in the identified modal parameters, the truncation bias of the same two systems is computed and using the same, but unfiltered response time histories. The results are shown below in table 6.11 for the damping ratio of system A and B, corrupted by 30% noise. It is seen from table 6.11 that, for system A, the bias in the SSI/Cov-identified modal damping is negligible suggesting that the correlation of the filtered noise was indeed responsible for the large bias observed earlier. The perturbation analysis confirms the marginal truncation bias. A 1.9% quadratic bias is also results from the perturbation analysis so that the total bias predicted by the algorithm overestimates the true bias. Although the latter bias estimate lacks accuracy, it nonetheless correctly predicts that the bias in the identified modal damping ratio is negligible for practical purposes. For system B, however, the bias estimates do not tie up with the true error. A total bias just below -13% was calculated in each case while the perturbation analysis predicts an insignificant bias error. Theoretically speaking, it is reasonable to expect the truncation bias to drop to a negligible level in this

Sys A	$dim(\mathcal{H}_0) = 7 \times 4$	$dim(\mathcal{H}_0) = 13 \times 8$	$dim(\mathcal{H}_0) = 22 \times 14$
True Bias			
$b(\xi)$	-0.5%	-0.3%	-0.2%
Perturbation Analysis			
$\mu[b_T(\xi)]$	-0.2%	-0.04%	-0.06%
$\mu[b_Q(\xi)]$	-1.9%	-1.9%	-1.9%
Sys B	$dim(\mathcal{H}_0) = 7 \times 4$	$dim(\mathcal{H}_0) = 13 \times 8$	$dim(\mathcal{H}_0) = 22 \times 14$
True Bias			
$b(\xi)$	-12.8%	-12.9%	-12.9%
Perturbation Analysis			
$\mu[b_T(\xi)]$	-0.05%	-0.13%	-0.23%
$\mu[b_Q(\xi)]$	0.30%	0.29%	0.28%

Tab. 6.11: Bias in the SSI/Cov-identified damping ratios from the unfiltered responses of system A and B. The values are expressed as a percentage of the true damping ratios.

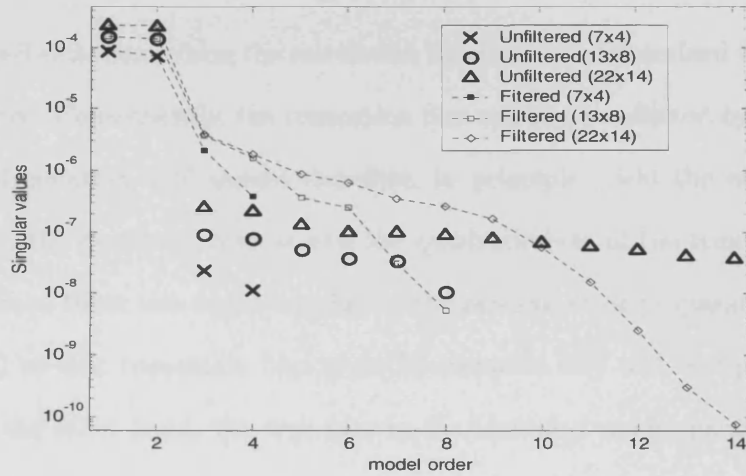


Fig. 6.17: Comparison of the singular values for system B for unfiltered and filtered response time histories. The gap separating the first two singular values from the remaining ones indicates a SODF system.

case since the noise will be uncorrelated and the only information in the data, albeit corrupted by estimation errors, is that of the system. This appears to be confirmed by the simulations for system A and the comparison of the singular values, shown in figure 6.17, indicate that this is also the case for system B. The gap separating the first two singular values from the remaining ones indicates a SODF system. What causes the bias observed for system B is unclear. In theory, the possible causes are reduced to three sources: (a) omission of the quadratic bias of the truncation bias, (b) a poor estimate of the truncation bias itself and (c) a poor estimate of the quadratic bias.

As argued above, it can be assumed that the data given in table 6.11 is not affected much by truncation bias. Since the truncated singular values are actually not identically zero, the truncation bias will affect the modal parameters to some extent. The question arises whether this could be of the order of about  $-13\%$  as in system B and is poorly predicted by the perturbation analysis. After all, the estimated quadratic bias is negligible and table 6.8 shows a trend of the true bias towards the  $-13\%$  bias as the dimension of the Hankel matrix is increased.

To assess the accuracy of the truncation bias as given by equation 5.37, we resort to

the idealised situation, where the correlation functions are determined without random disturbances. Consequently, the truncation bias will not be affected by random errors either and equation 5.37 should therefore, in principle, yield the exact truncation bias. Also, the quadratic bias as well the quadratic bias of the truncation bias will be zero (since these two terms are due to the random error propagating through the algorithm) so that truncation bias given by equation 5.37 will be equal to the total bias. On the other hand, the true bias in the identified modal parameters is easily determined since the exact modal parameters are known and can be used to gauge the accuracy of the truncation bias determined by the perturbation analysis. To do so, the auto-correlation function of a 2-DOF system is modelled according to section 3.4.3 and Appendix A, that is, by superposing the auto-correlation functions of 2 SDOF system. In other words, denoting the ac.f. of the first and second SDOF system by  $R_1(\tau)$  and  $R_2(\tau)$  respectively, the ac.f. between two simultaneously measured responses of the 2-DOF system is modelled as  $R(\tau) = R_1(\tau) + R_2(\tau)$ . The first mode with ac.f  $R_1(\tau)$ , vibrating at 1 Hz and with a decay rate of 1% of critical damping, is chosen to dominate the response by restricting the amplitude of  $R_2(\tau)$  at  $\tau = 0$  to be smaller than the amplitude of  $R_1(\tau)$  at  $\tau = 0$ . Keeping the ac.f of the first mode fixed, 16 2-DOF system are simulated as

$$R^{(k)}(\tau) = R_1(\tau) + R_2^{(k)}(\tau), \quad \text{for } k = 1, 2, \dots, 16 \quad (6.21)$$

where the amplitude of  $R_2^{(k)}(\tau)$  at  $\tau = 0$  is increased with the index  $i$  in steps of 1% from 5% to 20% of the amplitude of  $R_1(\tau)$  at  $\tau = 0$ . This can be thought of as an increasing modal participation factor of the second mode of the 2-DOF system. Similarly, the frequency of  $R_2^{(k)}(\tau)$  is increased in steps of 0.5 Hz from 0.5 Hz up to 8 Hz for each system and the corresponding modal damping ratios from 0.0025% to 0.04% of critical damping in steps of 0.0025%. Thus, the second mode of the  $k^{th}$  2-DOF system modelled according to equation 6.21 has an ac.f with an amplitude at zero lag of  $4\% + k\%$  the amplitude of the ac.f of the dominant mode, a frequency of  $k \times 0.5$  Hz and a damping ratio of  $k \times 0.0025\%$  of critical damping. The identification

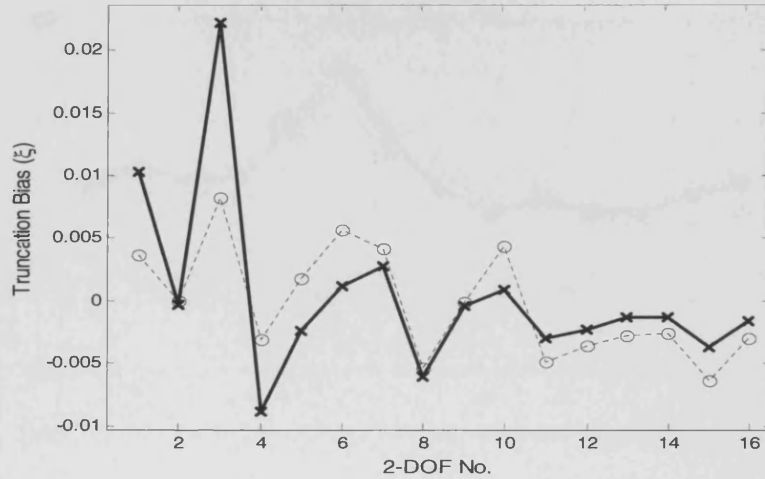


Fig. 6.18: Verification of truncation bias estimates for modal damping ratios.  $[\times]$  denotes the true truncation bias of the modal damping ratio and  $[o]$  the truncation bias estimated using the perturbation method, eq. 5.37. The abscissa indexes the 2-DOF system used according to the description above of equation 6.21.

is performed with a  $(22 \times 14)$  Hankel matrix. The bias introduced in the identified damping ratios due to truncation of the residual second mode is shown in figure 6.18. While the overall behaviour of the estimated truncation bias follows that of the true truncation bias as the frequency, damping ratio and the weight of the residual mode is varied, clear discrepancies are seen to occur. On the other hand, for some cases, notably the 2<sup>nd</sup>, 8<sup>th</sup> and 9<sup>th</sup> 2-DOF system, good agreement is observed. In particular, it transpires from figure 6.18, that the bias estimates via the perturbation method appear to be more accurate when the true truncation bias itself is small.

This behaviour of the estimated truncation bias fits the discrepancies observed for system A in table 6.7, in which case the truncation bias was accurate when the true bias (consisting mainly of truncation bias) was low but a divergence was observed for the low dimensional Hankel matrix case where the bias was large. This is however not the case for system B, where the most significant disagreement was observed for the case where the bias was lowest. As shown in figures 6.19, the discrepancy of the perturbation estimate of the truncation bias also depends significantly on the size of the Hankel matrix used: the two highlighted cases shown in figure 6.19 (top), where the identification was performed using a  $24 \times 21$  and  $28 \times 25$ , indicate that the true

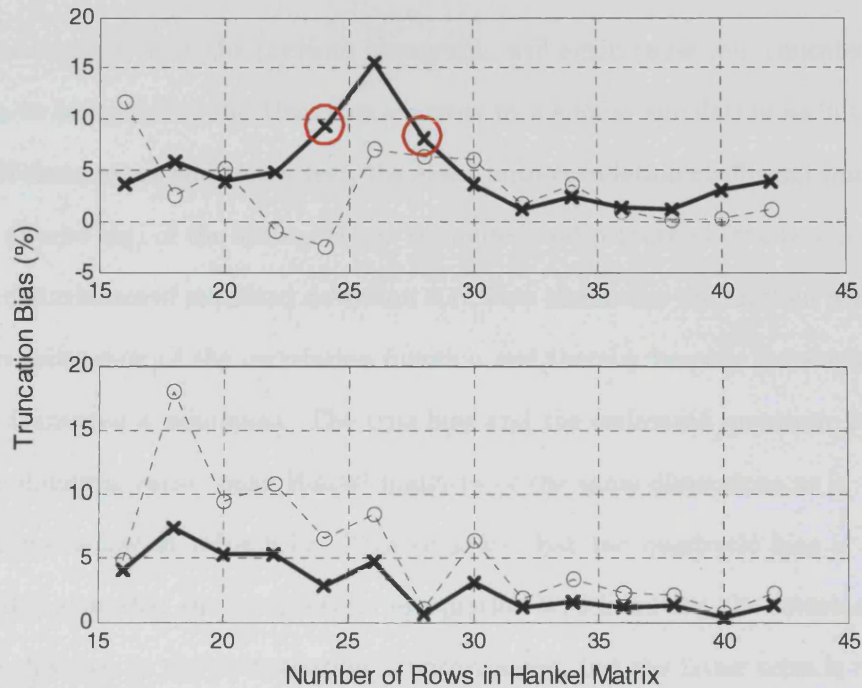


Fig. 6.19: Truncation bias of  $\xi$  as a function of the size of the Hankel matrix used for the 5<sup>th</sup> (top figure) and 10<sup>th</sup> (bottom figure) 2-DOF system described by equation 6.21. The abscissa denotes the number of rows in the Hankel matrix used, and in each case, the Hankel matrix has 3 less columns than rows. [o] denotes the perturbation estimate of the truncation bias and [x] the true truncation bias. Encircled are the cases where the identification was performed using a  $24 \times 21$  and  $28 \times 25$  dimensional Hankel matrix respectively.

truncation bias is approximately the same but the accuracy of the estimates differs significantly. Moreover, the true truncation bias in these two cases is below 10%, so that the discrepancy observed in table 6.8 may be attributed, at least partly, to this inherent fault in the truncation bias estimate. Similarly, if the true truncation bias were of the order of  $-13\%$  as the response records are not subjected to filtering (c.f. table 6.11), then the possibility exists, as can be seen from top figure in 6.19, that the low truncation bias predicted by the perturbation analysis may again be attributed to the failing of the estimate as given by equation 5.37. On the other hand, however, if the true truncation bias is near zero in the data shown in table 6.11 for system B, then the possibility must be considered that the observed bias is due to quadratic bias and that the latter is poorly predicted by the perturbation algorithm. However, assessing the accuracy of the estimated quadratic bias is more difficult since it is due to a random perturbation of the correlation function and adding this perturbation to an

idealised system as in the previous paragraph, will again cause the truncated singular values to be non-zero and therefore amounts to a similar simulation as in table 6.11. Nonetheless, as an additional test, the exact auto-correlation coefficient function (i.e. unity at zero lag) of the system B was computed and perturbed by a zero mean white noise disturbance of standard deviation 0.1. This eliminates the random perturbation due to estimation of the correlation function and thereby keeping the singular values to be truncated a minimum. The true bias and the estimated quadratic bias in the modal damping ratio, using Hankel matrices of the same dimensions as in table 6.11 are shown below in table 6.12. This suggests that the quadratic bias is estimated well. It is true that the second term in equation 5.10 involving the covariances drops out in this case as the perturbation is uncorrelated, but the latter term is unlikely to cause discrepancies in the estimates in the situation when the covariance needs to be considered. The results shown for the random error in section 6.3, support the fact that the covariance of the perturbation is adequately estimated and the expressions giving the the sensitivities involving  $\delta_{jk}(\cdot)$  are exactly the same than those involving derivatives with respect to  $\epsilon_j$  only except that the indexes change. Also, unlike the truncation bias, there is no inherent fault in the computation of the quadratic bias.

To get an idea of the magnitude of the quadratic bias of the truncation bias one may approximate the truncation bias

$$b_T[\hat{\chi}] \approx \hat{\chi} - \hat{\chi}_F \quad (6.22)$$

where  $\hat{\chi}$  denotes the modal parameters identified with small singular values set to zero

$dim(\mathcal{H}_0)$	(13 × 8)	(18 × 13)	(23 × 18)	(28 × 23)
True Bias	7.0%	1.7%	2.1%	1.4%
$b_Q(\xi)$	7.1%	3.1%	2.1%	1.5%

Tab. 6.12: The quadratic bias in the modal damping ratios using the exact auto-correlation coefficient function for system B perturbed by white noise with a standard deviation 0.1. The results are expressed as a percentage of the true damping ratio.

and  $\hat{\chi}_F$  the identified modal parameter at full model order. The approximation arises due to the fact that both modal estimates entering equation 6.22 are affected by the quadratic bias and the quadratic bias of the truncation bias so that in theory, equation 6.22 does not give an exact estimate unless the system is noise free. Equation 5.44 gives the truncation bias as

$$b_{QT}[\chi] \approx - \sum_{j=1}^N \text{Var}[\epsilon_j] [\delta_{jj\rho}(\chi) + \delta_{jj\rho\rho}(\chi)] \quad (6.23)$$

$$- \sum_{\substack{j,k \\ j \neq k}}^N \text{Cov}[\epsilon_j, \epsilon_k] [\delta_{jk\rho}(\chi) + \delta_{jk\rho\rho}(\chi)]$$

$$= - \sum_{j=1}^N \text{Var}[\epsilon_j] \delta_{jj}(b_T[\chi]) - \sum_{\substack{j,k \\ j \neq k}}^N \text{Cov}[\epsilon_j, \epsilon_k] \delta_{jk}(b_T[\chi]) \quad (6.24)$$

Replacing  $b_T[\hat{\xi}]$  by equation 6.22, the quadratic bias of the truncation bias  $b_{QT}[\chi]$  can be expressed as

$$b_{QT}[\chi] \approx - \sum_{j=1}^N \text{Var}[\epsilon_j] (\delta_{jj}(\chi) - \delta_{jj}(\chi_F)) \quad (6.25)$$

$$- \sum_{\substack{j,k \\ j \neq k}}^N \text{Cov}[\epsilon_j, \epsilon_k] (\delta_{jk}(\chi) - \delta_{jk}(\chi_F)) \quad (6.26)$$

$$= b_Q[\chi_F] - b_Q[\chi]$$

where the last equality is obtained using equation 5.10. The above equation thus shows that the quadratic bias of the truncation bias can be estimated as the difference between the quadratic bias in the modal parameters identified at full and truncated model order. For instance, the quadratic bias in the truncation bias of the modal damping ratio of system B for a  $22 \times 14$  Hankel matrix (c.f. table 6.8) was found to be  $(b_Q[\chi_F] = 5.5 \cdot 10^{-5}) - (b_Q[\chi] = 5.2 \cdot 10^{-5}) = 0.3 \cdot 10^{-6}$ . This suggests that influence of the quadratic bias on the truncation is marginal and does not affect the discrepancy observed in table 6.8. It follows from this subsection that the only source of error in the estimated bias stems from the inherent fault in the truncation bias estimate and the latter is therefore the most likely culprit for the divergence of the bias observed



in the modal damping ratios.

### **Best Practice**

Despite the lack of accuracy in estimating the bias by the perturbation method, it transpires from figures 6.18 and 6.19 that the truncation bias is better estimated when the true truncation bias is small. But on the downside, the converse does not hold i.e. a small truncation bias determined via the perturbation analysis does not necessarily imply that the true truncation bias is small as well. Since in practice, the only information available will be the one predicted by the perturbation algorithm, it follows that the bias determination can be deceitful. Nonetheless, tables 6.7 and 6.8 show that, when the true bias is large, this will be reflected in the perturbation estimates. Therefore, it seems sensible to employ the perturbation method to find the parameters (dimension of Hankel matrix and model order) that yield negligible bias, rather than performing a single identification with a chosen set of parameters and bias correcting the modal parameters. Since the RMS error appears to be dominated largely by the truncation bias, this choice will generally amount to the same as choosing the run for which the RMS error is small. Bias correction may then be omitted or if performed, is unlikely to exacerbate the error in the identified modal parameters further.

The way in which different model orders and the dimension of the Hankel matrix affect the identified modal parameters is complex and an optimisation, resulting in the most favourable parameters to use identification algorithm is not obvious and the most favourable parameters need to be found by trial and error. In other words, the identification is repeated for various sizes of Hankel matrices and model orders (and, if desired sample intervals) and the best estimate of the modal parameters are taken from the run yielding the lowest error. This is demonstrated below using, as would be the case in practice, a single response measurement from systems A and B above and the results are shown in figures 6.20 and 6.21. The labels on the abscissa of each of



the latter figures refer to the dimension of the Hankel matrix used in that particular run and are explained below in table 6.13. In each of the latter figure, the random error, the truncation bias and its random error as well as the RMS error are shown. For convenience, the quadratic bias was not included in these figures. Based on this information, the most favourable parameters to be used in the identification process can be determined.

For system A, it is seen from figure 6.20 that the truncation bias is minimal (among the cases considered) when the identification is performed at model order 4 for cases 6 and 10 i.e with Hankel matrices of dimension  $24 \times 13$  and  $30 \times 19$  respectively. Also, the associated random error is small in each of these cases indicating that the truncation can be expected to vary on average less than, say roughly 2%, if the identification were to be repeated with the same parameters for statistically equivalent response time histories. Case 2 for model order 4 marginally yields the lowest RMS error. However, the latter case has a rather large variance of the truncation bias and is therefore not considered to be represent the a good choice of parameters. It is noted again that the variance of the truncation bias does not enter the RMS computation since the variance of the biased modal damping ratios is used. The estimated bias for both of the cases is very similar, and the perturbation algorithm predicts that the bias is negligible in both cases, and being significantly smaller than the random error in the identified modal damping ratio will yield a negligible contribution to the RMS error. In fact, using equation 6.17, the RMS error can be rewritten as (Efron and Tibshirani, 1993)

$$RMS(\hat{\chi}) = \sqrt{\sigma^2(\hat{\chi}) + b^2(\hat{\chi})} \quad (6.27)$$

$$\approx \sigma^2(\hat{\chi}) \left[ 1 + \frac{1}{2} \left( \frac{b(\hat{\chi})}{\sigma(\hat{\chi})} \right)^2 \right] \quad (6.28)$$

which shows, for instance, that if the ratio of the bias to the random error is  $< 25\%$ , the bias contributes  $< 3.1\%$  to the RMS error, and as suggested in Efron and Tibshirani (1993), this can be used as a rule fo thumb to asses whether the bias can be

considered negligible. This rule is useful in the event where, for instance, two sets of modal parameters need to be compared with one set having a smaller RMS error but a higher bias than the second. Since a small identified bias does not necessarily guarantee that the true bias is equally small as discussed above, the user may decide to chose the set of parameters yielding the smaller RMS but higher bias and if the bias is still  $< 25\%$  of the random error, the bias can still be considered negligible. To check whether the identification, when performed using these parameters, truly results in more or less unbiased modal damping ratios, the SSI/Cov is applied to 200 computed response measurements and the sample random and bias error were computed. Indeed, the mean damping ratio over the 200 runs was found to be 1.0% in both cases confirming that, with these input parameters, the identification algorithm indeed yields an unbiased estimate of the modal dampig ratios. Also, the standard deviation of the SSI/Cov estimated damping ratio was in both case close to 15%. It can therefore be concluded that for system A, the perturbation analysis reliably predicted the best choice of parameters for the modal identification together with an accurate error estimates. The modal parametes identified from the single respose record, i.e. affected by random errors, were found to be  $\xi = 1.10\%$  and  $1.13\%$  of critical damping respectively for  $\dim(\mathcal{H}_0) = 30 \times 19$  and  $\dim(\mathcal{H}_0) = 24 \times 13$ , both of which fall within the standard deviation predicted by the perturbation analysis.

Label	1	2	3	4	5
$\dim(\mathcal{H}_0)$	$14 \times 11$	$18 \times 7$	$17 \times 14$	$21 \times 10$	$20 \times 17$
Label	6	7	8	9	10
$\dim(\mathcal{H}_0)$	$24 \times 13$	$23 \times 20$	$27 \times 16$	$26 \times 23$	$30 \times 19$

Tab. 6.13: Dimension of Hankel matrix  $\dim(\mathcal{H}_0)$  used with reference to figures 6.20 and 6.21

The same study is performed for system B, the results of which are represented in figure 6.21. The smallest bias is seen to occur for case 4 when the singular values were truncated to yield a system of order 6, but on the downside, it is affected by a large random error and this case is therefore discarded. Two sets of parameters among the cases considered that indicate a low bias error and variance thereof are cases 7

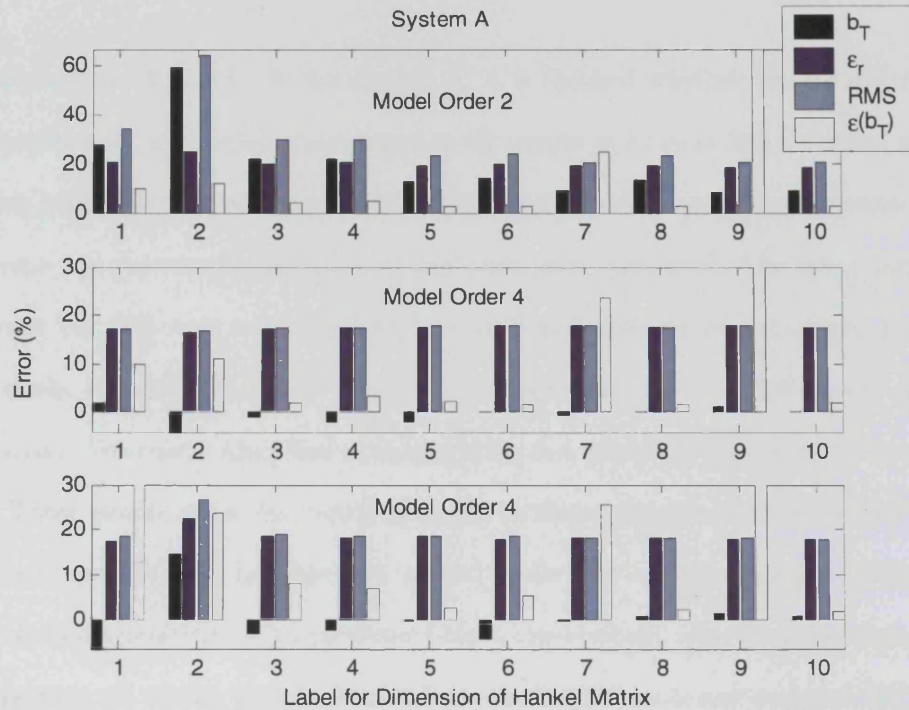


Fig. 6.20: Estimated random error  $\epsilon_r(\xi)$ ,  $RMS(\xi)$ , truncation bias  $b_T(\xi)$  and the random error in the truncation bias  $\epsilon_r(b_T(\xi))$  from a single response record for different model orders and dimensions of the Hankel matrix. The labels on the abscissa reference the dimension of Hankel matrix used as indicated in table 6.13.

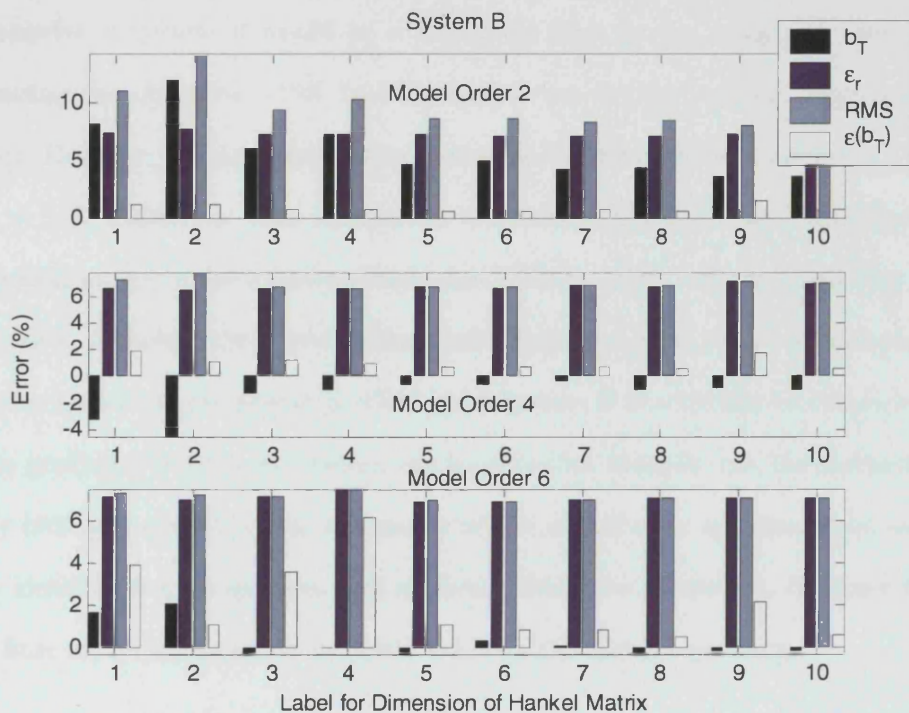


Fig. 6.21: Estimated random error  $\epsilon_r(\xi)$ ,  $RMS(\xi)$ , truncation bias  $b_T(\xi)$  and the random error in the truncation bias  $\epsilon_r(b_T(\xi))$  from a single response record for different model orders and dimensions of the Hankel matrix. The labels on the abscissa reference the dimension of Hankel matrix used as indicated in table 6.13.

for model orders 4 and 6. As for system A, it is checked whether the identification, when performed using these parameters, truly results in more or less unbiased modal damping ratios. To this end, the SSI/Cov was applied to 200 computed response measurements and the sample random and bias error were computed. The mean damping ratio over the 200 runs was found to be 1.30% and 1.32 for model orders 4 and 6 respectively, with  $\dim(\mathcal{H}_0) = 23 \times 20$  i.e. yielding a true bias of  $-12.6\%$  and  $-11.8\%$  respectively. For case 7 identified at model order 6 a quadratic bias of  $0.4\%$  was identified. These results are in fact much the same as those already obtained in table 6.11. In order to get the data in table 6.11 as well as for the two ‘best’ case considered in this case, two operations were performed that, theoretically alleviate, the truncation bias: getting rid of the “residual mode” in the former case and overspecifying the model order in the latter case. Although the perturbation algorithm does yield a near zero truncation bias, this is not observed in the true bias. What is responsible for this bias is not clear to the author. Certainly, a good explanation for the observed discrepancies in system B would be a numerical error in the computed time histories causing the observed  $-13\%$  bias, as is the case for the natural frequencies for instance. However, it is known that the Newmark- $\beta$  scheme, with parameters  $\gamma = 1/2$  and  $\beta = 1/4$ , makes the time integration unconditionally stable and introduces no numerical damping in the solution (Bathe and Wilson, 1976) and this possibility must be excluded. Although the perturbation analysis yields a much improved damping estimate for system A, the poorer prediction for system B is sufficient to conclude that the bias predicted by the perturbation can be deceitful. Nonetheless, the methods still reliably indicates excessive bias corruption of the modal data and should be used to choose identification parameters that minimise this error. However, the uncertainty in the final modal data cannot be predicted with the desired accuracy.

### 6.4.1 Influence of Non-Stationarity on Bias

In section 6.3.3, it was investigated how non-stationary characteristics in the response records affect the random error estimate in the modal damping ratios via perturbation analysis. It was shown that when the non-stationary statistics are identical for all measured response records, the random error is hardly affected. On the other hand, when the non-stationary characteristics vary from record to record, the random error estimates via the perturbation method do not tie up with the sample errors. This was explained by the fact that the correlation functions, when computed from non-stationary data do not exactly reflect the system dynamics as is the case when the data is stationary. In particular, non-stationary mean square values tend to distort the true decay of the correlation functions which biases the damping information. The error estimates via the perturbation analysis depend strongly on the estimated statistics of perturbations  $\epsilon_j$  and the study undertaken for the random error showed that the variance/ covariance as well as the system sensitivities are hardly affected by the non-stationarity in the data and as a result, the additional random error observed in the sample estimates was not picked up. This will clearly be the same for the bias estimates and only the bias introduced by the SSI/Cov itself will be reflected in the estimates.

To determine the actual bias introduced by the non-stationarity, the perturbation equations in Chapter 5 would have to be reformulated to account for this bias in the perturbations  $\epsilon_j$ , so that for instance  $E[\epsilon_j] \neq 0$  but tends to the biased correlation function. Although the response to non-stationary loading has been studied (Barnoski and Maurer, 1969; Gasparini, 1979; Sun and Kareem, 1989) and the error introduced into correlation functions from non-stationary data, by treating it as stationary, is understood (Bendat and Piersol, 2000), the difficulty is to determine the actual bias at each data point  $j$  and may be an interesting research avenue. On the other hand there is a growing tendency to employ time-frequency system identification methods which can account for the time varying statistics of the data. Such

techniques include wavelets (see for instance (Mallat, 1999)) or the Hilbert Transform (HT) combined with Empirical Mode Decomposition (EMD) methods (Huang *et al.*, 1998). Both methods enable to analyse time-series *locally* and are able to describe changes of the frequency content or in the statistics of data at a particular time of the response history, rather than yielding a *global* description where the statistics and frequency content are time-independent and apply to the whole of the response data. As a result non-stationary as well as non-linear behaviour can be described. The (EMD) method essentially empirically decomposes the measured data into its modal components through a process called shifting (Huang *et al.*, 1998), while maintaining the non-stationary and/or non-linear properties of the data. The resulting modal responses may then be treated as SODF responses and instantaneous frequencies can be obtained via the Hilbert transform from these decomposed signals. Applications for modal identification of civil engineering structures can be found for instance in (Chen *et al.*, 2004; Zhang *et al.*, 2006). A combination of the EMD method with the SSI/Data, rather than the Hilbert transform, was proposed by Yu and Ren (2005). It is noted that the latter method, like the SSI/Data on its own, cannot describe the time changing modal parameters. Similarly to the short-time Fourier transform (Bendat and Piersol, 2000), the wavelet transform localises the information of the time-histories in the time-frequency plane by using short windows at high frequencies and long windows at low frequencies thereby offering a description of non-stationary signals. Like the EMD method, it also decouples the modal components. Application to operational modal analysis have surfaced abundantly in recent years (Basu and Gupta, 1997; Bonato *et al.*, 2000; Ghanem and Romeo, 2000; Han *et al.*, 2005; Lardies and Gouttebroze, 2002; Ruzzene *et al.*, 1997). Two reviews on using this technique for structural vibration problems in civil engineering are given by Kijewski and Kareem (2003); Neild *et al.* (2003).

### 6.4.2 Efficiency of Perturbation Algorithm

The application of the perturbation analysis requires two steps: (1) the estimation of the statistics of the perturbations  $\epsilon_j$  to the computed correlation function and (2) passing the estimated correlation functions, together with the statistics of  $\epsilon_j$  through the algorithm to yield the desired error estimates.

The estimation of the statistics of via the plug-in method has been described in Chapter 3.4.3, section 3.5. In a nutshell, the efficiency of this step depends in principle on the duration of the measured time histories, which is further exacerbated by the fact that the double-sided correlation functions are required to compute variance and covariance of  $\epsilon_j$ . However, as explained in section 3.5, the use of the flat-top window dramatically improves the computational expense as it effectively picks out the portion of the double sided correlation function estimate to make the variance/covariance estimate robust.

Due to the fact that the perturbation algorithm computes the system sensitivities (a) for each data point used in the portion of the correlation function used in the analysis and (b) for each modal parameter extracted. Moreover, this involves the same steps for each of the intermediary equations (the sensitivities of the singular values and singular vectors for instance) and as a result, the computational burden is substantial. However, to compute the random error it was possible, with some effort, to implement the procedure by avoiding any loops other than iterating over the number of data points along the diagonal of the Hankel matrix which sped up the execution of the algorithm significantly. Also, the summation in the final perturbation equation 5.8 yielding the random error estimates can be executed within the loop which alleviates the storage requirement for the variables. To get the quadratic bias, however, a double loop was needed over all the mixed derivatives pairs, and also the variables needed to be stored to compute the mixed derivatives. Consequently, the computation requirement involved is significant, particularly when the response is recorded at many test points resulting in large Hankel matrices.

## 6.5 Summary and Discussion

It is shown in this chapter that the random error in the SSI/Cov-identified modal parameters is estimated very well by the perturbation method. The robustness of the method with respect to errors in the estimated statistics of the perturbations was established. Owing to the good performance of the plug-in method to estimate the variance/covariance it is seen that the addition of noise into the system is reflected in the error estimates. In fact, the virtue of the theory behind the plug-in method to estimate the statistics of the perturbations, any stationary disturbance to the data will be accounted for in the random error estimates. In all the cases used in the simulation, the perturbation method correctly accounted for the influence of the size of the Hankel matrix, of the sampling interval, the record length used and the model order selected. Non-stationarity was introduced into the response records by subjecting them to various non-stationary load cases. It was shown that in general, the perturbation method could not account for the additional random error introduced by the non-stationarity and that it tends to estimate the random error of the underlying stationary signal. However, in situations where a non-stationary frequency content is more or less repeated identically from record to record, a good estimate of the random error can still be expected.

The excellent accuracy of the random error estimates could not be reproduced for the bias. For the two systems investigated, the results were excellent for the lower frequency system but considerably less accurate for the higher frequency system. Partly responsible for the observed divergence is the artificial linearisation involved in the equations yielding the truncation bias. However even in the case, where the truncation bias is theoretically expected to be negligible, i.e. no singular values containing system information were truncated, the discrepancy between the estimated and true bias was still present, although the perturbation algorithm “correctly” predicted negligible bias. Neither the quadratic bias nor the quadratic bias of the truncation bias could account for this divergence and its cause could not be explained. However, it appears



from the simulations that when the true truncation bias is small, it is estimated more accurately by the perturbation method. Although the converse does not hold, it could nonetheless be concluded from the simulations that when the estimated bias is small, it is unlikely that the true bias is excessive. It was argued that therefore, the best practice is to apply the perturbation algorithm with different sets of identification parameters (dimension of the Hankel matrix, model order, and possibly the sampling interval) to find a set that yields a negligible truncation bias. As shown, this is possible by increasing the size of the Hankel matrix or by overspecifying the model order. This approach does not guarantee the best possible bias estimate, but severe bias appears to be reflected in the perturbation estimates so that the latter situation can be avoided.

---

## CHAPTER 7

# UNCERTAINTY IN IDENTIFIED MODAL PARAMETERS: A BOOTSTRAP APPROACH

---

### 7.1 Introduction

In this chapter, the dependent bootstrap method developed in Chapter 4 is employed to determine the error in operational modal parameters from a single set of measurements. Unlike the perturbation method in the previous chapter, which is only applicable to the correlation-driven stochastic realisations such as the SSI/Cov, the bootstrap method can, in principle, be used in conjunction with any curve-fitting algorithm. As mentioned previously, the bootstrap has been used for this purpose by Doebling and Farrar (2001*b*) to determine the error in the modal parameters from classic input/output testing. However, their bootstrapping scheme, following Hunter and Paez (1998), is different from the dependent bootstrap used in this thesis. The basis ensemble of observations in Doebling and Farrar (2001*b*); Hunter and Paez (1998) consists of a set of *independently* measured FRFs which are then bootstrapped so that Efron's original bootstrap is applicable. Applications of the bootstrap to time series in relation to modal analysis has been pioneered by Kijewski and Kareem (2000, 2002), but with the drawbacks already discussed at length in Chapter 4. The various block resampling schemes presented in Chapter 4 offer the possibility to eliminate these

drawbacks and thereby yield improved error bounds of the modal estimates. Also, the fact that it is possible to generate an ensemble of stationary time series using the stationary bootstrap, makes the method applicable for virtually any output-only identification algorithm.

## 7.2 Applicability of the Bootstrap for Operational Modal Parameters

With the dependent bootstrap of chapter 4 at hand, using it to determine the error in operational modal estimates is simple and the procedure is illustrated in figure 7.1. In a typical modal test performed on a large scale civil engineering structure, the engineer has, in general, only a single set of simultaneous responses measured at different locations along a structure at his or her disposal to determine the modal parameters of the system. If it were possible to repeat the modal test  $B$  times for  $B$  sufficiently large, a collection of  $B$  sets of estimated modal parameters can be found, from which their statistics such as the mean, standard deviation and possibly bias can be determined. This is illustrated on the right-hand-side of the diagram 7.1. However, since time constraints make it impractical to repeat a modal test a large number of times, bearing in mind that the time records need to be sufficiently long as well for a acceptable convergence of the modal estimates, the bootstrap approach can be applied to the only available set of measurements to simulate “pseudo-modal tests” and hence obtain additional response data. Once the latter is available, it is then possible to get a collection of  $B^*$  sets of *bootstrapped* modal parameters by application of a curve-fit algorithm to the bootstrapped time-series of correlation functions (depending on the algorithm used), from which the statistics of the system’s model can be determined. This is represented on the left-hand-side in figure 7.1.

While the process is straightforward, it is not necessarily obvious why the sample statistics of the ensemble of bootstrapped modal parameters yield a good approxima-

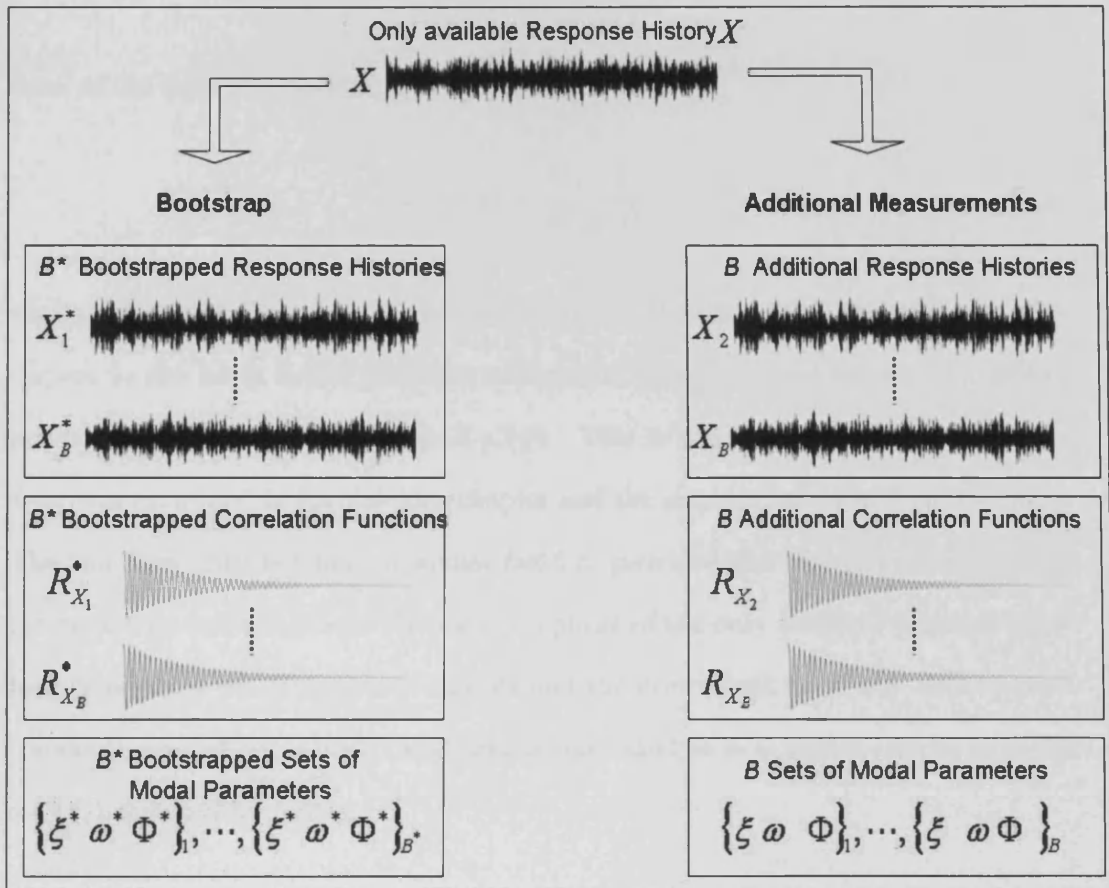


Fig. 7.1: Diagrammatic representation of bootstrap applied to operational modal analysis.

tion to the true error in the modal estimates. Suppose that the response is recorded for a total time  $T = n\Delta t$ . If the conditions of the modal test setup remain unchanged so that additionally measured responses originate from a stochastic source whose underlying distribution remains the same, then the correct error estimates on the system's modal parameters identified from response records of length  $T$  can be defined as those calculated from the  $B$  sets of identified modal parameters, when the number of repeated tests  $B \rightarrow \infty$ , and approximation to the true error is obtained with  $B$  finite. Let  $\{x_i\}$  denote the set of  $B$  measured response histories,  $\{\hat{\chi}_i\}$  the set of identified modal parameters identified from each response history  $x_i$  and  $s(\cdot)$  the estimator such that  $s(x_i) = \hat{\chi}_i$ . In other words,  $s(\cdot)$  describes the modal parameters extraction using the SSI/Cov algorithm in this case. The true, normalised random

error of the modal  $\chi$  can then be approximated as

$$\hat{\epsilon}_r(\hat{\chi}) = \frac{\hat{\sigma}(\{\hat{\chi}_i\})}{E\{\{\hat{\chi}_i\}\}} \quad (7.1)$$

where the expectation  $E[\cdot]$  is replaced by the arithmetic mean. Normalising with respect to the mean rather than the true modal parameter (not known in practice) prevents the contribution of bias in  $\hat{\epsilon}_r(\hat{\chi})$ . This is precisely how the true random error was computed in the previous chapter and the same definition will be used here. The true bias error is found in similar fashion, provided the true error is known. In the bootstrap method, the  $B^*$  bootstrap replicas of the only available response time-history replaces the  $B$  measured records and the normalised error, say the standard (random) error  $\hat{\epsilon}_r^*(\hat{\chi})$ , in the modal data is calculated as in equation 7.1 but with the set  $\{\hat{\chi}_i\}$  replaced by  $\{\hat{\chi}_i^*\}$ .

The question arises, provided the number of bootstrap replicas  $B^*$  is chosen sufficiently large, whether we can expect  $\hat{\epsilon}_r^*(\hat{\chi})$  to be a good approximation to  $\hat{\epsilon}_r(\hat{\chi})$ . It was shown in that chapter 4 that the bootstrapped covariances of the auto- and cross-correlation functions give a good approximation to the true covariances, but under the condition that the block length  $l$  is chosen appropriately. Since the optimal block length is the one that minimises the mean-square-error of the bootstrapped covariances, it follows that this gives the best possible approximation to the true quantity. Does this imply that the optimal block length to estimate the covariances is also optimal to estimate the errors in the bootstrapped modal parameters? An answer is readily obtained from the theory developed in chapter 5 where it was shown that the error in the modal parameters depends up to second order, on the covariances of the correlation functions. Therefore, if the covariances of the bootstrapped correlation functions optimally approximate the covariances of the true correlation functions, then the error in the bootstrapped modal parameters will give an optimal approximation to the true their true error. Taking into consideration the trade-off in random and bias error inherent in the bootstrapping of the time series, this justifies

the application of the bootstrap to determine the error in operational modal estimates.

### 7.3 Random Error

The study of the random errors in the SSI/Cov-identified modal parameters requires slightly less effort than was the case for the perturbation method. While the success of the latter method is dependent at the same time on (a) the perturbation algorithm itself on (b) the estimated perturbations of the correlation functions, where instabilities in either the system sensitivities or erroneous estimates of the variance and covariance (i.e. the perturbations) could result in poor error predictions, the error estimates via the bootstrap method depend entirely on the quality of the bootstrapped time series or, equivalently, correlation functions and fully benefit from the robustness of the particular identification algorithm used. The quality of the dependent bootstrap was studied in chapter 4, where it was shown that the method reliably yields reasonably accurate estimates of the variance and covariance of the correlation functions and it was argued in the previous section that this implies that we can expect the same from the error prediction in the identified modal parameters. Rather than repeating the lengthy investigation of the previous chapter, it will be sufficient to check the method on a few cases. Also, the bootstrap method will be applied in conjunction with the SSI/Data algorithm to illustrate the flexibility of the method.

#### 7.3.1 Random Errors in SSI/Cov-identified modal parameters

To allow a comparison between the performance of the bootstrap method with the perturbation analysis in predicting the random error in correlation-driven operational modal parameters, the simulations in this chapter will be performed on the same SDOF systems A and B (c.f. table 6.3) as in chapter 6. Clearly, the same input parameters to the SSI/Cov will be used for the comparison to be meaningful.

Random Error in SSI/Cov-identified Modal Parameters Predicted by the Bootstrap Method						
SYSTEM A	Estimation Error Only $T = 600s, dt = 0.05$ $dim(\mathcal{H}_0) = 13 \times 8$		Estimation Error + 30% Noise $T = 900s, dt = 0.05$ $dim(\mathcal{H}_0) = 7 \times 4$		Estimation Error + 30% Noise $T = 900s, dt = 0.05$ $dim(\mathcal{H}_0) = 22 \times 14$	
	True	Bootstrap	True	Bootstrap	True	Bootstrap
$\mu[\epsilon_r(\xi)]$ (%)	13.71	11.92 ( $\pm 1.90$ )	16.01	12.07 ( $\pm 1.74$ )	14.42	11.08 ( $\pm 1.49$ )
$\mu[\epsilon_r(f_0)]$ (%)	0.14	0.16 ( $\pm 0.03$ )	0.82	0.66 ( $\pm 0.12$ )	0.15	0.14 ( $\pm 0.02$ )
SYSTEM B	Estimation Error Only $T = 600s, dt = 0.04$ $dim(\mathcal{H}_0) = 13 \times 8$		Estimation Error + 30% Noise $T = 900s, dt = 0.04$ $dim(\mathcal{H}_0) = 7 \times 4$		Estimation Error + 30% Noise $T = 900s, dt = 0.04$ $dim(\mathcal{H}_0) = 22 \times 14$	
	True	Bootstrap	True	Bootstrap	True	Bootstrap
$\mu[\epsilon_r(\xi)]$ (%)	8.68	7.32 ( $\pm 0.86$ )	6.96	6.51 ( $\pm 0.69$ )	7.36	6.76 ( $\pm 0.70$ )
$\mu[\epsilon_r(f_0)]$ (%)	0.08	0.08 ( $\pm 0.01$ )	0.11	0.11 ( $\pm 0.01$ )	0.10	0.9 ( $\pm 0.01$ )

Tab. 7.1: Comparison of the normalised random error in the SSI/Cov-identified modal damping ratios ( $\epsilon_r(\xi)$ ) and frequencies ( $\epsilon_r(f_0)$ ) estimated via the bootstrap method and the true error estimated from 200 simulated response histories. Note that the error shown for the bootstrap is the mean of the errors estimated from 200 simulated response records and the values in parenthesis are the corresponding standard deviations. 300 bootstrapped correlation functions were computed for each response history and the optimal block length was computed using Bühlmann and Künsch's method.

As argued in the introduction to this section, not all cases investigated in chapter 6 need to be considered but a few will suffice to validate the bootstrap method.

More specifically, the cases considered are shown in table 7.1 for systems A and B together with the random errors predicted by the bootstrap method. For each case in table 7.1, 200 response histories were simulated and from each, 300 bootstrapped correlation functions were computed using the blocks of blocks method. The optimal block length was determined using Bühlmann and Künsch's method (c.f. Chapter 4). From each set of the 300 bootstrap correlation function replicas for each simulated response time history, the modal parameters were identified using the SSI/Cov algorithm and the random error estimated. Table 7.1 shows the mean of the normalised random errors computed from the 200 sets of bootstrapped normalised errors.

It is seen that the mean normalised random error predicted by the bootstrap method underestimates the true error, the more so for the lower frequency system A. Although a bias in the random error estimated via the perturbation method was observed in the previous chapter, which was attributed to bias in the estimated variances and covariances by the plug-in method, this discrepancy was small. In this case, in particular for the two cases for system A involving the 30% noise level, the difference between the true and predicted error is more pronounced. The question arises as to what lies at the bottom of this discrepancy and whether it can be rectified. The source must lie in the bootstrapped correlation functions since the error propagation through the identification algorithm is naturally accounted for since the algorithm is used on each bootstrapped correlation function. Therefore, the only points that need checking are (a) whether 300 bootstrap samples are sufficient and (b) the error in the bootstrapped correlation functions.

Invoking the equivalence between the variance and covariance of the bootstrapped correlation functions and the bootstrapped modal parameters established in section



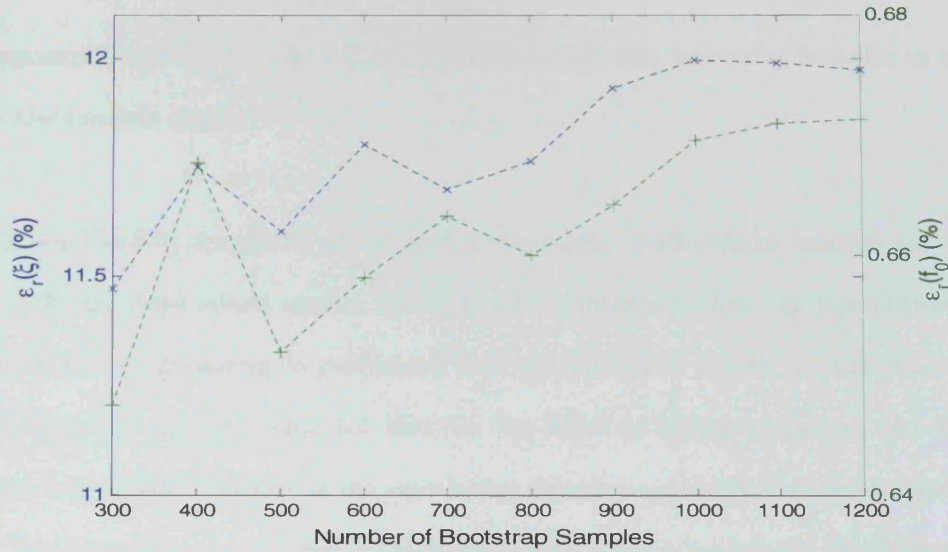


Fig. 7.2: Normalised random error in the SSI/Cov identified modal parameters as a function of the number of bootstrap replicas. The results represent the case for system  $A$  with  $T = 900s$ ,  $\Delta t = 0.05s$ ,  $\dim(\mathcal{H}_0) = 7 \times 4$  and 30% measurement noise added.  $[\times]$  represents the modal damping ratio (left hand axis) and  $[+]$  the natural frequency (right hand axis).

7.2, the answer to these questions can be found from the results in Chapter 4; it was mentioned in this chapter (c.f. page 4.4) that increasing the number of bootstrap samples beyond 300 did not yield any significant improvement in the bootstrapped variance of the correlation functions and hence, the same applies to the standard error in the bootstrapped modal parameters. As a final check, we use the case for system  $A$  with a  $7 \times 4$  Hankel matrix and 30% measurement noise added to the simulated response (middle column, first row in table 7.1). It is sufficient to use a single response measurement, since we know that on average, the normalised random error is  $12.07 \pm 1.74\%$  and the true error is 16.01%. Thus, if a number of bootstrap replicas  $> 300$  produces a random error that falls within the  $12.07 \pm 1.74\%$  interval, we can conclude that 300 replicas are sufficient. The same holds for the error in the natural frequency. The results are displayed in figure 7.2. Although an increasing trend is seen in the standard errors as the number of bootstrap samples is augmented, it appears that the errors have more or less fully converged for  $> 1000$  bootstrap samples and that they fall within the  $12.07 \pm 1.74\%$  and  $0.66 \pm 0.12$  for damping ratios and frequencies respectively predicted in table 7.1. Therefore, we can conclude that the

discrepancy observed in table 7.1 is not due to insufficient bootstrap samples to estimate the random error.

As described in chapter 4, the dependent bootstrap is affected by random and bias errors. While these errors cannot be eradicated completely, they can nonetheless be minimised if the bootstrap is performed with optimal block length. It was shown by simulation in chapter 4, table 4.2, that for the block of blocks bootstrap, the mean square error in the variance of the correlation function was lowest when the optimal block length as computed by Bühlmann and Künsch's method. However, it is also seen from the latter table that the variance in the correlation functions is underestimated in all cases and that this negative bias is maximal when the Bühlmann and Künsch block length selection method is used. For clarity, it is noted that this bias is solely due to the fact that segments of finite duration of the response history are resampled and is not to be confused with the bias that occurs at high lags in the bootstrapped correlation functions due to the collating uncorrelated segments into a new pseudo-time series. It was clearly shown in chapter 4 that the formulation of the block of blocks bootstrap technique takes care of the latter. Due to the equivalence between the error in the bootstrapped variances (and covariances) of the correlation functions and the error in the bootstrapped modal parameters established in section 7.2, this underestimation is reflected in the bootstrapped random errors in the modal parameters. This was verified by using the bootstrapped variances and covariances (as opposed to those estimated by the plug-in method) as estimates of the perturbations in the correlation function and using them in the perturbation algorithm. Indeed, the resulting random error estimates were much the same as those predicted by the direct application of the bootstrap shown in table 7.1. As mentioned, this error is inherent to the dependent bootstrap and cannot be avoided but only minimised by using the optimal block length in the computations. However, an improved estimate can be obtained by using Politis and White's method to select the block length as this (see table 4.2) yields the lowest bias but has the highest standard error. The simulations of

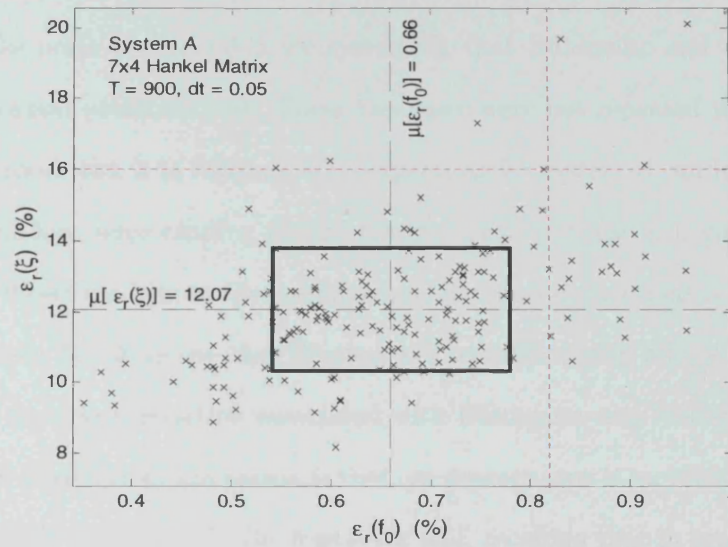
table 7.1 are repeated exactly for system *A* but using the Politis/White block length selection method and the results are tabulated in table 7.2. It is seen from table 7.2 that when Politis and White’s block length selection method is employed, the mean identified random error does indeed increase toward the true error and this is to be attributed to the smaller downward bias compared to the Bühlmann/Künsch method in the bootstrapped correlation functions (c.f. table 4.2). On the other hand however, the improved mean values come with a larger scatter as is seen from the associated standard deviations in table 7.2 which is to attributed to the larger standard error inherent in Politis and White’s block length selection method compared to Bühlmann and Künsch’s method. Nonetheless, although the random error is almost twice as large as for Bühlmann and Künsch’s method (and, indeed twice as large compared to the perturbation method, see figure 6.10(a)), the range in which we can, on average, expect the predicted error to be in, that is  $13.98(\pm 2.92)$  and  $0.72(\pm 0.16)$  for damping ratios and frequencies respectively, is satisfactory in the sense that (a) it includes the true value and (b) deviations remain on average reasonably close to the true value. When Bühlmann and Künsch’s method is used, the predicted error cluster more tightly around the biased mean random error and , on average, the true error will not be predicted but on the other hand, the occurrence of “stronger” outliers is

System A	Estimation Error Only		Estimation Error + 30% Noise		Estimation Error + 30% Noise	
	True	Bootstrap	True	Bootstrap	True	Bootstrap
	$T = 600s, dt = 0.05$ $dim(\mathcal{H}_0) = 13 \times 8$		$T = 900s, dt = 0.05$ $dim(\mathcal{H}_0) = 7 \times 4$		$T = 900s, dt = 0.05$ $dim(\mathcal{H}_0) = 22 \times 14$	
$\mu[\epsilon_r(\xi)]$ (%)	13.71	13.72 ( $\pm 3.79$ )	16.01	13.98 ( $\pm 2.92$ )	14.42	12.50 ( $\pm 2.32$ )
$\mu[\epsilon_r(f_0)]$ (%)	0.14	0.16 ( $\pm 0.04$ )	0.82	0.72 ( $\pm 0.16$ )	0.15	0.14 ( $\pm 0.02$ )

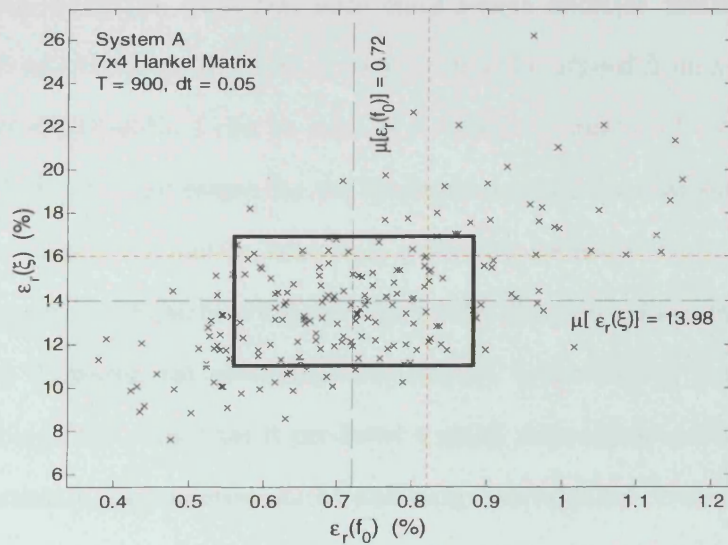
Tab. 7.2: The same simulations for system *A* as in table 7.1 but using the Politis/White block length selection method. The values in brackets are the standard deviation of the random error computed from the 200 simulated response histories in each case.



reduced. This is illustrated in the scatter graphs in figure 7.3.



(a)



(b)

Fig. 7.3: Illustration of the random error in the SSI/Cov-identified modal frequencies estimated via the blocks of blocks bootstrap method. Each cross represents the error estimated from one of the 200 simulated response histories. The two cases shown correspond to the cases in the middle column of table 7.1 for system A. Figure(a) shows the case when the block length is selected using Bühlmann/Künsch's method and figure (b) the case for Politis and White's method. The finely dotted lines (red) shows the true error.

For the two systems considered here, it appears from figures 7.3 that the block length selection of Politis and White, which comes with less bias but increased random

error in the bootstrapped correlation functions, is better suited to predict the random error in the SSI/Cov-identified modal parameters. Nonetheless, it cannot be asserted that this is always the case. For instance, it is seen from table 7.1 for the two cases including the noise perturbation for system  $B$ , that Bühlmann and Künsch's block selection method performs well. These two cases were not repeated with Politis and White's method, but it is reasonable to expect, as for system  $A$ , an increase in both the mean random error tending toward the true error but also a larger scatter about this value. When the bias in the bootstrapped correlation functions is small, as is the case for system  $B$ , where the identification was performed with a  $7 \times 4$  Hankel matrix, the smaller standard deviation associated with Bühlmann and Künsch's block selection method is preferred; the reason is that, on average, one is more likely to predict a random error that is closer to the true error and, recalling that in practice, the error has to be estimated from a single response measurement, it is clear that this is the more desirable situation. However, both block length selection methods are seen to perform well and based on the data at hand, it may be argued from a practical point of view, that either method can be used as a reliable estimator of the random error. Having tracked down the reason for the discrepancies due the bias and random error in the bootstrapped correlation functions, a possible indicator may be found in the mean-square-error that can be computed during the block selection method as detailed in chapter 4. However, the simulations in Chapter 4 also showed that this quantity was unreliable in the sense that it produced a small mean-square-error whenever the bootstrap estimate was underestimated and large mean-square-error in the case of an overestimation. For this reason, this option was not further pursued. Precisely why the bias in the bootstrapped correlation functions seems to be smaller for the higher frequency, more heavily damped system is not entirely clear but a plausible explanation is that, as mentioned in Chapter 4, the dependent bootstrap works best for time series with short range dependence.

Like the perturbation method, the bootstrap method takes into account the effects

		Model Order 2	Model Order 4	Model Order 6
System A	$\epsilon_r(\xi)$	11.08 ( $\pm 1.49$ )	11.44 ( $\pm 1.46$ )	11.71 ( $\pm 1.44$ )
	$\epsilon_r(f_0)$	0.14 ( $\pm 0.02$ )	0.14 ( $\pm 0.02$ )	0.14 ( $\pm 0.02$ )
System B	$\epsilon_r(\xi)$	6.76 ( $\pm 0.70$ )	6.93 ( $\pm 0.70$ )	7.48 ( $\pm 0.94$ )
	$\epsilon_r(f_0)$	0.9 ( $\pm 0.01$ )	0.10 ( $\pm 0.01$ )	0.12 ( $\pm 0.02$ )

Tab. 7.3: Influence of model order on bootstrap estimated random errors of SSI/Cov-identified modal parameters.

on the random error due to different parameters used in the SSI/Cov algorithm, such as the size of the Hankel matrix and the sampling interval chosen as is clearly seen in table 7.1 for system B for instance. This is to be expected since the actual algorithm is applied to each bootstrapped time history and therefore any error introduced by the algorithm itself will be reflected in the modal estimates. Similarly, the bootstrap method also takes into account different choices of model order. This is illustrated below in table 7.3. The corresponding true errors are the same as in table 6.5.

### 7.3.2 Random Errors in SSI/Data-identified modal parameters

While the bootstrap method does not match the accuracy of the perturbation method, it has the advantage over the perturbation method that it is more flexible in its usage in the sense that it is not restricted to a particular identification algorithm. Since the essence of the bootstrap is to generate additional pseudo-time series, the method is applicable to virtually any curve-fitting algorithm, whether that is in the time-domain or frequency domain. In this section, the bootstrap method is applied to the SSI/Data algorithm, briefly described in chapter 3 and its application to the enhanced frequency domain decomposition (EFFD) method is discussed.

The SSI/Data algorithm operates directly on the measured time histories, which are fed to the algorithm in the form of large data Hankel matrices (c.f. 2.3.3). As shown, in Chapter 4, to account for the efficacy of the block of blocks bootstrap method, the function that operates on the resampled time series must be symmetric

in the blocks into which the response is divided. This is, however, not the case for the SSI/Cov and nor for the SSI/Data algorithm. For the SSI/Cov, this was circumvented by reformulating the block of blocks method directly in terms of bootstrapped correlation functions (see section 4.3.2 pp. 103), where the correlation functions of individual blocks were employed to provide the required symmetry. For the SSI/Data, however, there is no obvious way around this problem and for this reason the stationary bootstrap is employed. As described in section 4.3.3, the latter yields bootstrapped replicas of the original time series and the problem of edge effects of joining independent blocks together was mitigated by choosing random block lengths from a geometric distribution, and the average length of this distribution plays the role of optimal block length. An illustration of pseudo-response records generated by the stationary bootstrap is shown in figure 7.4 below.

Having generated the bootstrap replicas of the originally measured response time-history, a set of modal parameters can be identified by applying the SSI/Data to each the bootstrapped time series and their random error can be estimated. Simulations are again performed on 900s response records of the 1Hz, 1% damped SODF system  $A$

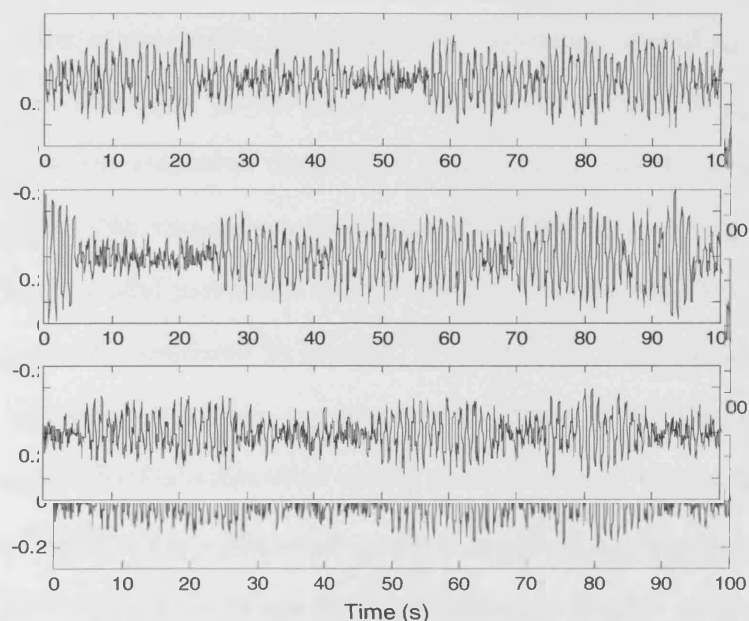


Fig. 7.4: Illustration of the response replicas by the stationary bootstrap. The top figure is the the originally measured time series. The average optimal block length is approximately 35s.

	True Error	Bootstrap
$\epsilon_r(\xi)(\%)$	15.22	14.70 $\pm$ 2.00
$\epsilon_r(\xi)(\%)$	0.18	0.19 $\pm$ 0.03

Tab. 7.4: Normalised random error estimates using the SSI/Data algorithm with the stationary bootstrap. The bootstrap error estimates are the mean of only 25 bootstrapped response records. The true error was estimated from 300 simulated response histories.

due to a white noise excitation and 30% measurement noise was added. 300 bootstrap replicas of the original time series were computed and each such record was organised in  $220 \times 17783$  data block Hankel matrix for modal parameters extraction using the SSI/Data. The results are shown in table 7.4. It is seen that, on average, the random error predicted by the SSI/Data, combined with the stationary bootstrap, predicts the random error very well. It is important to note that the random errors shown in table 7.4 are the mean of only 25 response histories and therefore, have not properly converged. However, the generally small standard deviation associated with the random errors (also shown in table 7.4) indicate that we are close to the fully converged mean values. The reason for bootstrapping only 25 simulated response histories is that the SSI/Data algorithm is much slower than its covariance-driven relative. This is due to the fact that in the former all the measured data is required leading to large Hankel matrices whose QR-decomposition is very time consuming compared to the direct SVD decomposition of the smaller Hankel matrices consisting only of a portion of the sample correlation functions. In the implementations of the SSI/Cov and SSI/Data used in this thesis, the combined duration of computing of the the auto-correlation function of a single, 900s response measurement of a SDOF system sampled at 20Hz and the subsequent modal parameter identification by the the SSI/Cov for a  $22 \times 14$  Hankel takes about 1s compared to roughly 20 seconds for the SSI/Data. Thus, if for instance 300 bootstrap replicas are generated, it takes about 1hr and 40min to obtain a set of 300 SSI/Data-identified modal parameters and estimate the random error compared to only 5min if the SSI/Cov algorithm is used. It is clear that in practice, when the response is measured at many locations along the structure, the computational effort involved increases and it transpires that the error estimation in



the modal SSI/Data-identified modal parameters becomes very time consuming. We note that the computational requirement for the block of blocks bootstrap and the stationary bootstrap are comparable. The author does not wish to claim that his implementation of the SSI/Data algorithm is optimal but the significant differences in computational efficiency are also reported in Peeters and DeRoeck (1999). Despite the computational inefficiency of the data-driven SSI/stationary bootstrap method, it is seen from table 7.4 that it is at least as accurate as for the covariance-driven SSI/block of blocks bootstrap method. Clearly, the remarks concerning the random error estimates made previously for the SSI/Cov algorithm also apply here, namely that (a) an underestimate of the random error is to be expected due the inherent bias in the stationary bootstrap and (b) all errors induced by the SSI/Data will be reflected in the random error estimates.

In principle, the bootstrap can also be applied with frequency domain identification techniques, such as the enhanced frequency domain decomposition algorithm (EFDD) commonly employed in operational modal analysis and briefly described in section 2.3.1, chapter 2. Resampled versions of the original power spectral density (PSD) matrix may be obtained either by applying Welch's method to the time-series replicas obtained via the stationary bootstrap or by direct Fourier transform of the block of blocks bootstrap auto- and cross correlation functions. However, since the modal parameters of the system are found by manual peak picking of the SVD decomposed power spectrum, the EFDD combined with the bootstrap is not practical unless the manual peak-picking procedure is automated. This is but one possible way to use the bootstrap in the frequency domain and for other methods, involving direct resampling in the frequency domain, the reader is referred to Politis (1992) for instance.

## 7.4 Non-Stationary, Non-white excitation

To conclude this section on the bootstrap random error estimates in the correlation-driven operational modal parameter estimates, the influence of non-stationary and

non-white characteristics in the loading conditions is considered. To allow a comparison with the perturbation method, the same excitation models as described in figures 6.12, 6.13 and 6.14 are considered. The additional pseudo-time series are generated using the block of blocks bootstrap method and, although Politis and White's block length selection method yielded better results than that of Bühlmann and Künsch, the latter is employed. For each case described in figures 6.12, 6.13 and 6.14, 200 responses are simulated and 300 bootstrap replica generated in each case. The results are shown below in table 7.5 and the corresponding true errors, already given in table 6.6, are repeated here for convenience.

Comparing the random error in the modal damping ratio and natural frequency for the case where the excitation consists of a pure white noise signal, a downward bias of about 3 percentage points is seen in the error estimate for the damping ratio. A small, but negligible downward bias also occurs in the estimated random error in the natural frequency. This bias was attributed earlier on in this section to the inherent downward bias in the dependent bootstrap due to the segmentation of the original time-series. While it was also shown that Politis and White's block length selection method slightly mitigated this bias error, it was nonetheless opted to use Bühlmann and Künsch's method in the simulations to follow: by keeping track of the  $\approx 3\%$  bias in the damping ratios that occurs for white noise excitation, the in-

Case	Simulated Error (%)		Perturbation Method (%)	
	$\epsilon_r(f_0)$	$\epsilon_r(\xi)$	$\mu[\epsilon_r(f_0)]$	$\mu[\epsilon_r(\xi)]$
Stationary White Signal	0.15	14.42	0.14 (0.02)	11.12 (1.48)
1	0.15	14.76	0.14 (0.02)	11.24 (1.78)
2	0.18	17.72	0.17 (0.03)	13.62 (2.89)
3	0.18	16.21	0.14 (0.03)	11.41 (2.70)
4	0.18	19.48	0.18 (0.48)	12.10 (7.12)
5	0.76	13.40	0.64 (0.16)	10.49 (2.14)
6	0.26	24.25	0.22 (0.06)	20.41 (5.73)

Tab. 7.5: Predicted random error by the block of blocks bootstrap method for system A in table 6.3. The values in brackets yield the sample standard deviation of the estimate errors.

fluence of the added non-stationary and/or non-white disturbance will be clearly seen.

For case 1, where the white noise signal is modulated by a slowly varying function that is repeated exactly for each simulated response record as described in figure 6.12, the random error in both the frequency and damping ratio changes only marginally compared to the case where the excitation consist of a pure stationary white noise signal. The same observation holds for the random errors predicted by the bootstrap method and it can be concluded that the addition of the non-stationary disturbance does not corrupt the bootstrap error estimate. It is noted that this was also the case for the perturbation method. For load case 2, where the modulation function changes randomly from record to record (see figure 6.12), a small increase in the random error of the modal parameters is observed and it was shown in section 6.3.3 that the perturbation method did, on average, not account for the extra randomness introduced by the varying modulation function. It appears from the table 7.5, however, that the bootstrap method picks up the increase in random error. Indeed, the average rise of roughly 3% error in the damping ratios as well as the slight increase in the modal damping ratios is clearly seen to occur in the errors predicted by the bootstrap. Also, the associated standard deviation of the estimated errors is reasonably low and comparable to those related to the perturbation method (c.f table 6.6) .

For load cases 3 and 4 (c.f. figure 6.13), where the influence in a non-white, non-stationary frequency content in the excitation is considered, it is seen that the bootstrap method dose not capture the increase in random error observed in both cases. This was also the case for the perturbation method, where even a slight decrease in the predicted random errors was observed. However, when the perturbation method was used, the related standard errors were small which implies that at least on average, we can expect to predict a random error representative of the estimation errors corresponding to the case where the excitation is solely due to white noise. This also appears to be the situation for load case 3 when the bootstrap method is

employed, but for load case 4, where the frequency content of the loading changes from record to record, a large standard deviation compared to the actual mean random error is observed. This means that, on average, the predicted random error will not be close to the true error and even a significant departure from the pure white noise excitation case is to be expected. This is clearly an undesirable feature and it has to be concluded that the bootstrap method is unreliable in the presence of non-stationary frequency characteristics in the ambient loading conditions. It appears as if the additional randomness introduced by the variations in the frequency content manifest themselves by a significantly higher scatter in the predicted errors, rather than an increase in the mean random error.

For load case 5 (c.f. figure 6.14), where a narrow-band frequency signal close to the natural frequency of the system was added to the underlying white noise excitation, the bootstrap method correctly predicts the slight decrease in random error also observed in the true error estimates. This change was also correctly predicted by the perturbation method. Finally, the case is considered when, in addition to a white noise floor, randomly occurring Gaussian pulses are part of the ambient excitation. This describes load case 6 (c.f. figure 6.14). Under the latter excitation, a significant increase in random error was observed in the true error and it was shown in the section 6.3.3 that the perturbation method failed to pick up this additional random disturbance and yielded random error estimates representative of the excitation due to underlying white noise floor only. The bootstrap method, on the other hand, picks up the additional disturbance by random occurrence of the pulses as is seen in table 7.5. Taking into account the downward bias inherent in the bootstrap, it is seen that the predicted error is very close to the true value. Also, relative to the actual random error, the associated standard deviation is acceptable and it transpires that, on average, we can expect a reasonable error estimate by bootstrap.

Despite the loss of accuracy observed in the bootstrap estimated random errors

due primarily to the inherent bias in the block length selection, it appears that the bootstrap method performs better when the loading conditions yield strong non-stationary/non-white characteristics, with the exception perhaps when the frequency content is non-stationary. The fact that the bootstrap method is able to pick up the the random disturbances caused by varying modulation functions such as in load cases 2 and 6 may be explained as follows. Recall that the block of blocks bootstrap consists effectively of resampling from a set whose individual members are the mean correlation functions over a succession of  $l$  overlapping segments of length  $r + 1$  of the original time series, where  $r$  is the maximum lag of interest and  $l$  is the block lengths. In other words, each member of the original set from which the bootstrapped correlation functions are formed by resampling is correlation function computed from the information of  $l + r$  successive points from the original time series. If the time series is stationary, i.e. all the points in each such block have the same distribution, then the correlation function of each block will be representative of the entire random process. This is, however, not the case when the time series is non-stationary where, for instance, some members of the set of mean correlation functions from which the final bootstrapped correlation function is resampled may be computed from a segment having a different variance or, as illustrated in figure 6.15, may have bias particular to the modulation of this particular segment. Due to resampling with replacement from this set, the effects of different weights associated each with member is more significant in the non-stationary case causing more significant changes in each bootstrapped correlation function resulting in a change in random error. It should be noted that in addition, the block length selection is also affected. For instance, when the excitation is pure white noise, the average block length (determined from Bühlmann and Küsch's method) was 17.10s compared to 18.75s for load case 6. This increase is slight but may contribute to the larger scatter observed for non-stationary response records.

Although it was not explicitly checked, similar results are to expected when Politis and White's block selection method is used, but, as described in section 7.3.2, with

a smaller bias but an increased scatter around the mean random error. One may be tempted to think that the stationary bootstrap might slightly mitigate the non-stationary characteristics due to the random block lengths involved but this is not the case. Indeed, the random errors predicted by the stationary bootstrap from the response records due to load case 6 were found to be  $20.85\% \pm 5.26$  for the modal damping ratios and  $0.26 \pm 0.06$  for the frequencies and hence its performance in the presence of non-stationarities is much the same as that for the block of blocks bootstrap.

## 7.5 Bias Error

The bootstrap method estimates the desired statistic (e.g. variance) of an estimator (the SSI/Cov-identified modal parameter  $\hat{\chi}$ ) by computing the sample statistics from the set of bootstrapped estimators  $\hat{\chi}^*$ . For example if a large number of response records were available, each yielding an estimate of the modal parameter  $\hat{\chi}$ , the bias in the modal parameter could be computed as  $E[\hat{\chi}] - \chi$ , provided the true modal parameter  $\chi$  is known. Similarly, for the bootstrap, the bias can be computed as

$$b(\hat{\chi}) = E[\hat{\chi}^*] - \chi \quad (7.2)$$

However, since the true value of the modal parameter is not known, application of the above equation is not possible. It is argued in Doebling and Farrar (2001*b*) that the bootstrap method does account for bias in the identified modal parameters induced by the curve fitting process. Also, Hunter and Paez (1998); Paez and Hunter (1998) and Kijewski and Kareem (2002) did not consider the option of estimating the bias via the bootstrap method.

The perturbation analysis in Chapter 5, provides insight into how the bias is introduced into the modal parameters by the SSI/Cov algorithm and this can be exploited to get at least an idea of the bias in the identified modal parameters. As shown, bias arises in the SSI/Cov identified modal parameters due to (a) noise propagat-

ing through the algorithm (quadratic bias and quadratic bias of the truncation bias) and (b) due to truncation of small singular values when determining the model order (truncation bias). Efron and Tibshirani (1993) provide a method to estimate the bias of a bootstrapped statistic, which simply consists in replacing the true value  $\chi$  by its estimate  $\hat{\chi}$  in equation 7.2. It is shown by Efron and Tibshirani (1993) that the latter estimate yields the bias of a statistic as a result of being estimated from a finite size sample. In the case considered here, the identified modal parameter is the random variable and the randomness is introduced via the estimated correlation functions, which are themselves random variables due the fact that they are estimated from a time-series of finite length. As shown in Chapter 5, this random error partly manifests itself as bias in the estimated modal parameters due to the fact that this random disturbance does not average to zero in the quadratic terms. Thus, Efron's method could be employed to emulate the quadratic bias but, since the random error in the modal estimate can be large, such a bias estimate can potentially be significantly affected by the random error. When the random error is small, the analysis in the previous chapter and section has shown that one can expect the quadratic bias to be negligible. Moreover, the bias tends to be dominated by the truncation bias. For these reasons, the bootstrap emulation of the quadratic bias is not further investigated.

Since the truncation bias tends to dominate the total bias, the latter needs to be evaluated if a reasonably indicative estimate of the true bias is sought. To this end, the approximation in equation 6.22 is used but with the modal estimates replaced by the bootstrapped mean to emulate the truncation bias as

$$b_{T^*}[\hat{\chi}] \approx \mu[\chi^*] - \mu[\chi_F^*] \quad (7.3)$$

where  $\mu[\chi^*]$  denotes mean of the bootstrapped modal parameters identified with small singular values set to zero and  $\mu[\chi_F^*]$  the identified modal parameter at full model order. For consistency, it is noted that the approximation arises due to the fact that the mean bootstrapped modal parameters entering equation 7.3 are affected by the

quadratic bias and the quadratic bias of the truncation bias so that a residual error due to the difference between these two quantities at the chosen and full model order affects the latter estimate. The truncation bias, estimated via equation 7.3 is given in table 7.6. It is seen that, as for the perturbation method, the bias is on average very well predicted for system A. It is noted that the zero occurs due the fact that model order 4 corresponds to the full model oder for the  $7 \times 4$  Hankel matrix. Interestingly, for system B, the bootstrap truncation bias shows again a behaviour similar to that observed for the perturbation method and the bootstrap estimates closely match the perturbation estimates. Again a similar residual bias that could not be accounted for by the perturbation method is observed. These factors allow to draw a similar conclusion as for the perturbation method. Due to the lack of accuracy, but an adequate indication of the order of magnitude of the bias, it is best practice to repeat the identification with different identification parameters until a negligible bias is reached. As evidenced from the simulation on system B, this does not necessarily yield the true bias but it appears that severe bias can be avoided by proceeding in this fashion.

It needs to be noted that the truncation bias estimated via equation 7.3 is not easily obtained. The reason being that it is not an easy task to correctly match up the same modes identified at low model and full order. Theoretically, if the modes identified at low model order are stable, they should be identified at each model order chosen. This forms the basis of the popular stabilisation diagram to distinguish between spurious and physical modes (Van der Auweraer and Peeters, 2004). However, in practice this

$dim(\mathcal{H}_0)$	$(7 \times 4)$	$(7 \times 4)$	$(22 \times 14)$	$(22 \times 14)$
Model Order	2	4	2	4
System A				
$\mu[b_{T^*}(\xi)]$	356.8 (%)	0	17.0 (%)	2.3 (%)
System B				
$\mu[b_{T^*}(\xi)]$	99.1 (%)	0	6.4 (%)	-1.6(%)

Tab. 7.6: Bias in the identified modal damping ratios estimated via the bootstrap method.



is not always the case (Van der Auweraer, 2001). However, to compute the truncation bias by equation 7.3, it is not needed to actually compute  $\chi_F$  at full model order. In much the same way as inspection of the singular value diagram can be used to assist model order selection by inspection of the largest gap in the singular values (Peeters and DeRoeck, 1999, 2001), it will reveal at which model order the singular values are of the same order of magnitude than that at full model order. Choosing a model within that range of singular values will result in only a marginal loss of accuracy but offers more flexibility. In fact, for the results in table 7.6,  $\xi_F$  was identified at modal order 8 based on figure 6.17. Moreover, to fully automate the matching process is not straightforward. In this thesis, this was done according to the succession of steps given below:

1. "Obvious" computational modes i.e. those not occurring in complex conjugate pairs or with damping ratios  $> 0.1$  are eliminated from both sets (low and full model order) of identified modal parameters.
2. The remaining modes are then paired up according to the proximity of their natural frequencies. Matching modes based on the natural frequencies was motivated by the fact that they are very stable i.e. low bias and low standard error as has been shown in many instances in this thesis.
3. Each such pair is then validated by computation of the Modal Assurance Criterion (MAC)(Allemang, 2003; Allemang and Brown, 1982) between their associated mode shapes. A good correlation between mode shapes is indicated by a  $MAC > 0.9$  (Ewins, 2000) indicating a matched pair whereas a  $MAC < 0.9$  is taken to indicate different modes. In the case where the  $MAC < 0.9$ , the mode having the second closest frequency is subjected to the test to account for the fact that closely spaced modes may cross as a result of the random error. If the  $MAC$  falls again below this threshold, the search is stopped and this mode is removed from the bootstrap sample.

This method is nonetheless not fool proof and a graphical inspection of the data is

recommended to check for outliers. As a result, a search for the best identification parameters to use can be cumbersome. Finally it is noted that the variance of the truncation bias as given by equation 7.3 cannot be estimated by the bootstrap.

## 7.6 Summary

In this chapter, the performance of the dependent bootstrap was assessed to predict the errors in in-operation identified modal parameters. Although the emphasis was on the block of blocks bootstrap in conjunction with the SSI/Cov identification algorithm, the flexibility of the method was demonstrated when applied to the SSI/Data together with the stationary bootstrap. It was shown that the bootstrap estimates the random errors reliably but that the estimates are afflicted by a downward bias error which was attributed to the inherent root-mean-square associated with the dependent bootstrap due to segmentation of the time-series. Also, it was observed that Politis and White's block length method slightly mitigates this downward bias but at the expense of the an increased scatter in the estimate random errors. Also, it appears from the simulations shown that the magnitude of this bias is smaller for short range dependent time series i.e. for systems with a higher frequency content. Furthermore, the simulations show that the bootstrap also yields very reasonable results when non-stationary and non-white characteristics are present in the data. For time-series with a non-stationary frequency content, however, the random error estimates were less good.

The bias in the SSI/Cov identified modal parameters could also be determined by emulating the truncation and quadratic bias. Simulations showed that the bootstrap bias estimates were indeed comparable to the bias estimates by the perturbation method. Consequently, the same conclusions apply here. However, the process of selecting the "best" choice of parameters to avoid the risk of excessive bias in the identified modal parameters is more involved for the bootstrap. This is due to the fact that matching up equal modes identified at different model orders will not always be straightforward and some user interaction is required.

The “blocks of blocks” bootstrap and the stationary bootstrap<sup>†</sup> are efficiently implemented and therefore, if used in conjunction with a fast curve fitting algorithm, such as the SSI/Cov, estimating the error in the parameter under consideration from a large bootstrap sample is possible without too much computational burden. On the other hand, when the identification algorithm used is slow, as is the case for the data-driven Stochastic Subspace algorithm (SSI/data), the bootstrap method becomes very inefficient.

---

<sup>†</sup>code from Kevin Sheppard’s GARCH Toolbox for Matlab

---

## CHAPTER 8

---

# CONCLUSION

---

In-operational or output-only modal testing is receiving increased attention in the civil engineering industry. Its application ranges from more sophisticated analysis procedures such as finite element updating or damage detection based on the change of observed modal parameters to more straightforward, but often vital, purposes. For example, to get more realistic information on the modal damping ratios to use in building codes to assess the floor vibration levels to satisfy serviceability concerns or simply to validate an existing finite element model. It is clear that the improvement gained by the use of experimentally determined modal parameters is entirely dependent on the truthfulness of the identified modal damping ratios. It transpired from the literature review, that, while this issue had been raised, comparatively little work appeared to have been done on the subject. In particular, the uncertainty in the identified modal parameters largely failed to be addressed in case studies dealing with output-only modal analysis. This provided the motivation for this thesis. It is aimed to develop a method to assess the uncertainty in the modal parameters of civil engineering structures identified from a *single* set of measured response records during an operational modal test.

### 8.1 Rationale

As described in the introduction to this thesis, a great variety of identification algorithms have been developed over the years to extract modal parameters from measured

data. Each of these curve-fit methods relies on different mathematical techniques and therefore differs in how the modal parameters are estimated: some being more robust to noise while others introduce less bias. As a result, determining the uncertainty in identified modal parameters is particular to the estimator used and therefore, it is not possible to treat this topic in general but it needs to be narrowed down to a particular identification algorithm. In this thesis, the focus is on the Covariance-Driven Stochastic Subspace Identification algorithm, abbreviated SSI/Cov. The latter was chosen on the basis of its generally good performance as documented in the literature and due the fact that it is widely employed in the civil engineering community and is standard in most commercially available packages.

The rationale behind the approach taken to tackle the problem at hand was (a) to develop a practical method to determine the error in the modal estimates and (b) to assess whether the error estimates made available by the method are accurate and reliable. To this end, two techniques were developed: one relying on perturbation theory and the other on the bootstrap method. To assess the performance of these methods, it was opted to proceed by simulation on simple systems since this offers the required controlled environment to validate the error estimates and, if discrepancies occur, to investigate their origin. This provides an objective assessment of the performance of the estimator and establishes a basis for practical applications. To account for adverse conditions, the performance of both methods was investigated under non-stationary and non-white loading conditions.

## 8.2 Summary of Work

Correlation-driven identification algorithms can be considered as a 2-stage procedure: in a first step, the auto- and cross- correlation functions between simultaneously measured responses histories need to be computed which are then fed to the algorithm extracting the modal parameters. Likewise, both methods developed in this thesis

to estimate the error in the identified also work in two stages. For the perturbation method, the first step consists of estimating the statistics of the perturbation to the computed correlation function. In a second step, the system sensitivities are computed and combined with the estimated statistics of the perturbations to yield the desired error. The bootstrap method starts by creating pseudo correlation functions by re-sampling from the available response record and in a second instance, a set of modal parameters are identified from each bootstrapped correlation function from which the desired error is obtained by simple sample statistics. It is clear that shortcomings in either stage, will compromise the quality of the results. Below, the work undertaken to apply the developed methods to the problem of operational modal analysis is described, the results obtained are assessed and conclusions are drawn.

### **8.2.1 The Perturbation Method**

This section summarises the work and results of chapters 3, 5 and 6. As discussed above, the first step consists in estimating the statistics of the perturbations at each data point of the computed correlations function. To be applicable in practice, this estimator needs to be robust, accurate and computationally efficient. It was shown that the desired statistics of the perturbations are given by the variance and covariance of the correlation functions, provided the latter are unbiased. Therefore, the estimation of the auto- and cross-correlation functions was reviewed and the possible bias that can arise in their computation, for instance due to windowing when computed by inverse Fourier transform of spectral densities was investigated. The variance in the estimated correlation functions was first studied analytically yielding expressions for the variance and covariance of the auto-correlation functions of SDOF systems. An approximation was undertaken. This resulted in an approximate formula giving a rule of thumb to assess at a pre-test stage the minimum record duration necessary to identify the modal parameters with a random error falling below a desired level. This formula was validated in Chapter 6. The analytical results were extended to give an approximate expression for the variance of the cross-correlation functions of MDOF

systems as a weighted sum of auto-correlation functions of the uncoupled equivalent SDOF systems, provided the system modes are sufficiently separated. Nonetheless, these analytical expressions are impractical and another method to determine the statistics of the perturbations to the correlation functions was required. To this end, the equations that yielded the analytical expressions discussed above were employed but rather than proceeding analytically, their discrete version was implemented numerically. This numerical routine has the vital attribute that it operates directly on the estimated correlation functions from the measured data. However, this technique requires the double sided, full length correlation functions as input which implies that (a) it is computationally expensive and (b) the resulting variance and covariance estimates are highly inaccurate due to the inclusion of the poorly defined tail regions. Both problems could be solved by tapering the estimated correlation functions by a flat-top window with optimal bandwidth determined by minimising the mean-square-error of the corresponding spectral density. The cut-off imposed by the flat-top window eliminates the troublesome tail regions and dramatically reduces the number of data points used in the estimation. Thus, this method yields accurate variance and covariance estimates, it is computationally efficient and fully automated. The method was validated against the theoretical values for both auto- and cross-correlation functions. Excellent agreement was observed and a comparison for the same estimate without tapering highlights the increased accuracy offered by the method. Moreover, since this method operates directly on the correlation functions computed from the measured time-histories, any stationary disturbance to the measured response records will be reflected in the estimated variance as was shown by adding noise to the simulated data. This feature is clearly very desirable in practice.

Chapter 5 presents the theory behind the computation of the system sensitivities: the second stage of the error estimation process. Since the SSI/Cov is essentially the same as the Eigensystem Realisation Algorithm (ERA) used for input-output modal analysis, the changes required to adjust the computations to operational modal analy-

sis were minor. However, it was shown that the method proposed in the original paper to calculate the variance of the truncation bias and its quadratic bias was not correct due to repeated, identically zero eigenvalues of the matrix describing the effect of reinstating the truncated non-zero singular values. As discussed in this latter chapter, an exact solution to this problem is non trivial. For the variance of the truncation bias, however, an approximation was employed and the simulations in Chapter 6 show that the latter is satisfactory. This approximation could not be carried over to the computation of the quadratic bias as simulations showed severe ill-conditioning. The reason for this behaviour is that the singular subspaces used in these computations are associated with small singular values. Such subspaces are known to be extremely sensitive. As a result, the quadratic bias in the truncation bias was not computed. The loss of accuracy due to this omission was investigated by simulation in Chapter 6, and the results obtained suggest that for practical purposes, this effect is marginal. This issue is further discussed below. The perturbation algorithm fails to yield error estimates for repeated modes. It was argued that, although it is not uncommon for civil engineering structures to have almost repeated modes due to symmetries in the geometry, it is however rare in practice to encounter the situation where system poles are identical. However, the method was extended to cover the latter case but only for the sensitivities required to estimated the random error. Importantly, however, as explained in detail in Chapter 5, the investigation into repeated singular values allowed to conclude that the original perturbation method (not accounting for degenerate eigenvalues) is able to cope with closely spaced modes.

In Chapter 6, the perturbation method is tested on simulated response data from a set of SDOF systems and the accuracy with which the random and bias errors can be estimated is investigated. In a first instance, the random error in the modal parameters due to instrumentation noise and estimation errors was investigated separately. The “exact” system sensitivities and statistics of the perturbations were used in these computations. With the latter idealisation, excellent agreement was observed between



the predicted and “true” errors and the conclusion could be drawn that a linear expansion in terms of the perturbations is sufficient to determine the random error in the SSI/Cov-identified modal parameters from output-only data. It was also shown that the random error estimate is robust with respect to errors in the estimated statistics of the perturbation with one exception; namely when the statistics of the perturbation are frequency shifted with respect to the frequencies in the computed correlation functions. However, it is expected that this is unlikely to occur when the statistics are estimated by the plug-in method. For the case where the correlation functions and their variance/covariances are estimated from simulated response records subjected to noise, it is again observed that the random error is well predicted and it is seen that the addition of the noise is clearly picked up. In all the cases used in the simulation, the perturbation method correctly accounted for the influence of the size of the Hankel matrix, of the sampling interval, the record length used and the model order selected. Finally, it was investigated how non-stationary and non-white characteristics affect the random error estimates. It can be concluded that the perturbation method can, in general, not account for the additional random error introduced by the non-stationarity and tends to estimate the random error of the underlying stationary signal. However, in situations where a non-stationary frequency content is more or less repeated identically from record to record, a good estimate of the random error can still be expected.

To investigate the predictive qualities of the algorithm to determine the bias error in the estimated modal parameters, a similar approach was taken as for the random error. However, the good agreement between the true and estimated errors observed for the random error, could not be reproduced for the bias. For the two systems investigated, the results were excellent for the lower frequency system but considerably less accurate for the higher frequency system. Partly responsible for the observed divergence is the artificial linearisation involved in the equations yielding the truncation bias. This statement was verified by simulation. However, further simulations

showed that even in the case, where the truncation bias is theoretically expected to be negligible, i.e. no singular values containing system information were truncated, the discrepancy between the estimated and true bias was still present, although the perturbation algorithm “correctly” predicted negligible bias. It was shown that the quadratic bias, whose contribution to the total bias was found to be marginal, could not account for the observed discrepancy. While the magnitude of this divergence was not dramatic, it was still significant in the sense that it was about twice as large as the standard error. Moreover, a check devised to assess whether the omission of the quadratic bias of the truncation bias could be responsible for the inaccurate estimate, showed that the quadratic bias of the truncation bias was small and its omission could not be the cause of the detected inconsistency. The question as to what lies at the bottom of the observed discrepancy therefore remains open. The possibility exists that the quadratic expansion of the perturbation equations relating to the bias is not sufficient and that the bias is dependent on higher order statistics. But on the other hand, this quadratic expansion appeared sufficient for the lower frequency system. Despite this “mysterious” discrepancy, it appears from the simulations in Chapter 6 that when the *true* truncation bias is small, it is estimated more accurately by the perturbation method. Although the converse does not hold, it does transpire from the simulations that when the *estimated* bias is small, it is unlikely that the true bias is excessive. Therefore, the best practice is to apply the perturbation algorithm with different sets of parameters (dimension of the Hankel matrix, model order, and possibly the sampling interval) to find a set that yields a negligible truncation bias. As shown in Chapter 6, this is possible by increasing the size of the Hankel matrix or by overspecifying the model order. This approach does not necessarily result in best possible bias estimate, but severe bias appears to be reflected in the perturbation estimates so that the latter situation can be avoided and a bias correction, if applied, will not exacerbate the discrepancy. Since the computation of the truncation bias is very efficient as it is independent of the statistics of the perturbation, this is readily achieved in practice.

### 8.2.2 The Bootstrap Method

This section summarises the work and results of chapters 4 and 7. The bootstrap method had previously been applied by several authors to assess the uncertainty in modal data. However, the fact that the outcome of bootstrapping time series depends on how the time-series are split up into blocks of data and then joined to yield the bootstrapped pseudo-time series was ignored by these authors and is the subject of Chapter 4. Three schemes for bootstrapping time series are investigated: the moving blocks bootstrap, the “blocks of blocks” bootstrap and the stationary bootstrap. It is shown that the moving blocks bootstrap introduces artificial damping into the system. This effect can be mitigated by the stationary bootstrap and avoided completely by using the blocks of blocks scheme. For this reason, the latter method is preferred and an efficient algorithm resulting in a set of bootstrapped auto- and cross-correlation functions was developed. Bootstrapping correlation functions rather time-series offers a significant advantage in terms of computer memory when the recorded response records are long. Not only does the resampling scheme used affect the bootstrapped statistics, but so does the size of the blocks used. The block length effectively controls the amount of bias and random error in the variance and covariance in bootstrapped correlation functions. Should the bootstrap yield a set of pseudo correlation functions that have a large bias, for example underestimate the variance and covariance, then equally the random error in the modal parameters will be underestimated. Therefore, the block length is crucial to the accuracy of the bootstrapped random errors in the modal estimates. To avoid this, two optimal block length selection methods are presented that minimise the root-mean-square error of the bootstrapped correlation functions. This ensures that the set of bootstrapped correlation functions have a variance and covariance as closely as possible within this framework to the true statistics of the correlation function. The latter methods were originally derived for univariate times-series but were extended to compute the optimal block length for cross-correlation functions. The theory was validated by simulation. This establishes the solid basis needed to assess the uncertainty in the identified modal parameters.

Simulations investigating the quality of the bootstrap method are presented in Chapter 7. The same approach was used as for the perturbation analysis as well as the same SDOF systems to allow a fair comparison between both methods. The simulations, using the blocks of blocks resampling scheme, showed that the bootstrap method yields good estimates of the random error but that they are less accurate than those obtained by the perturbation analysis. In fact, a small downward bias was observed which was attributed to the inherent, albeit optimal, root-mean-square error in the variance and covariance of the bootstrapped correlation functions. A slight improvement was observed with Politis and White's block selection method but, as argued in Chapter 7, it cannot be asserted whether this will always be the case. One of the advantages of the bootstrap method, is that it is not restricted to the SSI/Cov algorithm but can in principle be used in conjunction with any curve fitting algorithm to estimate the random error. This was demonstrated by estimating the random error in the identified modal parameters from the data-driven Stochastic Subspace Method (SSI/Data) in conjunction with the stationary bootstrap. Again good agreement was observed between the true and estimated random error. As for the perturbation method, the influence of non-stationary characteristics was investigated. It appears that the bootstrap method appears to pick up some of the additional randomness introduced by the non-stationary characteristics in the data which makes this method very attractive in practical applications. The reason for this was explained by the fact that the resampling scheme also randomises the modulation function and thereby accounting for the additional variability. In the two cases where the frequency content of the response exhibits non-stationary characteristics, the true and estimated errors agreed less well.

Finally, the problem of estimating the bias in the identified modal parameters was addressed. Based on the theory of the perturbation analysis, an bias estimate emulating the truncation bias was considered. Simulations showed that the bias thus

estimated displayed a similar behaviour to the estimates obtained by the perturbation analysis. As a result, the same conclusions apply, namely that the bootstrap bias estimates lack the accuracy aimed for but indicate severe bias in the estimates. Also, like the perturbation method, the bootstrap bias estimate does not account for the residual bias error observed in the higher frequency system. As discussed in Chapter 7, the computation of the bootstrap bias emulating the truncation bias has its drawbacks. It is difficult to automate the process and to obtain a good estimate may require some user interaction. However, the limitations cannot be adequately assessed in this case without testing the mode pairing and the accuracy of the estimate on a more complex system. Difficulties are to be expected and therefore, the perturbation method is preferred to estimate the bias.

### 8.2.3 Future Work

Although both methods allow to avoid excessive bias in the modal parameters, an improvement would be desirable, in particular for applications involving the computation of response levels which require truthful estimates of the modal damping ratios for accurate predictions. Two problems were identified in determining the bias: (a) the approximation used to estimate the truncation bias and (b) an unexplained residual bias observed in the case where the truncation bias is expected to be marginal which could not be accounted for the quadratic bias nor the quadratic bias of the truncation bias. A fair amount of effort was devoted the former problem in trying to rewrite the perturbation equation yielding the truncation bias in terms of a physically meaningful perturbation parameter but this is not trivial. To investigate the source of the unexplained residual bias, simulating the bias on a large number of systems would potentially hint into the right direction. However, if it turns out that higher order statistics are required to pin down the bias accurately, the resulting computational burden may become impractical. The above applies to the bootstrap bias estimates as well. However, the problem regarding the pairing up of the equal modes at chosen

and full model order in a robust and automated fashion is worth investigating. This problem bears similarity to sorting stable from unstable modes in a stabilisation diagram. Some innovative techniques such as fuzzy clustering may provide a solution to this problem. Another important factor that would benefit these methods in practice is the determination of the bias introduced due to non-stationarity. The problem lies in the difficulty to capture the bias introduced to the correlation functions as a result of time-averaging through the non-stationarity when the stationary correlation functions are computed and include them into the statistics of the perturbations. A possibility worth investigating is whether a comparison between the non-stationary correlation functions and the stationary correlation functions gives some clues about this bias and offer the possibility to implement this in a data driven fashion.

For either of the two methods to be applicable in practice, they have to be tested on MDOF systems. Although the theoretical basis presented in this thesis covers the MDOF scenario for both methods, a few particularities need to be considered in more detail. For the perturbation method, the critical issue is to investigate how the algorithm copes with closely spaced modes and when to switch to the repeated mode case. The bootstrap method is readily applicable to the MDOF case. However, some additional work would be valuable on some of the practical and theoretical aspects involved. These are: (a) an improved method for pairing up identical modes from different bootstrap estimates (b) guidance on which auto- or cross-correlation function(s) should be used to determine the block length and (c) to investigate in more detail, either by simulation or theoretically, that the determination of the optimal block length based on the correlation function at zero lag is also optimal or near-optimal for higher lags. Finally, to enhance the confidence that can be placed on the proposed error estimation methods, some MDOF simulations and laboratory tests on a simple rig, whose modal properties are known, would be a valuable addition.

Both methods certainly contain a few other interesting features. A point that

has captured the interest of the author is to see, whether the system sensitivities reveal themselves as reliable indicators to distinguish between structural modes and system poles introduced into the system due to the presence of harmonic forcing components. The latter modes are non physical and therefore it is not unlikely that the sensitivities associated with these poles differ significantly from those of system modes. For the bootstrap, an interesting research avenue is its application to non-stationary time series, which has received some attention in recent years. Since many real-life processes are non-stationary, such a tool would lend itself as a basis for a great variety of applications. Coupled with the attractive feature that the bootstrap method is not limited to a particular curve fitting algorithm, such a method is not likely to be superseded in the near future as the underlying data structure of response records will not change, but the curve fitting algorithms almost certainly will.





---

## APPENDIX A

# EXPRESSING THE CROSS-CORRELATION FUNCTION OF AN MDOF SYSTEM AS A SUM OF AUTO-CORRELATION FUNCTIONS OF EQUIVALENT SDOF SYSTEMS

---

It is well known that the displacement response of a viscously damped N-DOF system can be expressed as a linear combination of the undamped mode shapes weighted by the modal or normal coordinates as

$$\mathbf{x}(t) = \sum_{i=1}^N \phi_i Y_i(t) = \Phi \mathbf{Y}(t) \quad (\text{A.1})$$

where  $\phi_n$  are the undamped mode shapes of the system and it is assumed that free response mode shapes diagonalize the dissipation matrix as is the case for proportional damping (see Ewins (2000) for instance). The modal coordinates  $Y_n(t)$  can be found from the uncoupled equivalent SDOF systems corresponding to each mode using, for

instance the Duhammel integral (Clough and Penzien, 1993) i.e.

$$\ddot{Y}_n(t) + 2\xi_n\omega_n\dot{Y}_n(t) + \omega_n^2Y_n(t) = \frac{P_n(t)}{m_n} \text{ with} \quad (\text{A.2})$$

$$\text{with } Y_n = \int_0^t P_n(\tau)h_n(t-\tau)d\tau \quad n = 1, 2, \dots, N \quad (\text{A.3})$$

Here,  $P_n(t)$  denotes the modal or generalized force,  $h_n$  the impulse response function of the  $n^{\text{th}}$  mode,  $m_n$  the  $n^{\text{th}}$  modal mass and  $\omega_n$  the natural frequency of mode  $n$ . Thus, at degree-of-freedom  $l$ , the displacement is

$$x_l(t) = \sum_n^N \phi_{ln}Y_n(t) \quad \text{and} \quad (\text{A.4})$$

$$x_{ln}(t) = \phi_{ln}Y_n(t) \quad (\text{A.5})$$

where  $x_{ln}(t)$  is the output at degree-of-freedom  $l$  due to mode  $n$  only. The correlation function between any two displacements at degrees-of-freedom  $l$  and  $p$  is given by

$$R_{x_lx_p}(\tau) = E[x_l(t)x_p(t+\tau)] \quad (\text{A.6})$$

$$= \sum_m^N \sum_n^N \left( \int_0^\infty \int_0^\infty \phi_{lm}\phi_{pn}R_{P_mP_n}(\tau-u_2+u_1) \times \right. \quad (\text{A.7})$$

$$\left. \times h_m(u_1)h_n(u_2)du_1du_2 \right) \quad (\text{A.8})$$

$$= \sum_m^N \sum_n^N R_{x_{lm}x_{pn}}(\tau) \quad (\text{A.9})$$

When the damping is light and the modal frequencies are well separated, then the response process  $x_{lm}(t)$  produced by mode  $m$  is almost statistically independent of the response  $x_{pn}(t)$  produced by mode  $n$  so that the cross-terms in eq. A.9 of the form  $R_{x_{lm}x_{pn}}$  for  $n \neq m$  are small compared to those where  $n = m$  (Clough and Penzien, 1993). Thus, eq. A.9 can be approximated as

$$R_{x_lx_p}(\tau) \approx \sum_n^N R_{x_{ln}x_{pn}}(\tau) \quad (\text{A.10})$$

Now, it follows from equations A.8 that

$$R_{x_l x_p} = \frac{\phi_{ln} \phi_{pn}}{\phi_{qn} \phi_{qn}} R_{x_{qn} x_{qn}} \quad \text{any } q \quad (\text{A.11})$$

Thus,

$$R_{x_l x_p} \approx \sum_n \frac{\phi_{ln} \phi_{pn}}{\phi_{qn} \phi_{qn}} R_{x_{qn} x_{qn}} \quad (\text{A.12})$$

Assuming that the excitation consists of uncorrelated white noise inputs  $p_i$  at degrees-of-freedom  $i$ , we can write

$$R_{P_n P_m}(\tau) = \sum_l^N \sum_r^N \phi_{ln} \phi_{rm} R_{p_l p_r}(\tau) = \sum_l^N \phi_{ln} \phi_{lm} R_{p_l p_l}(\tau) \quad (\text{A.13})$$

$$= \sum_l^N \phi_{ln} \phi_{lm} S_l \delta\tau = S_0 \delta\tau \quad (\text{A.14})$$

with  $S_0 = \sum_l^N \phi_{ln} \phi_{lm} S_l$  and  $P_m$  denotes the  $m^{\text{th}}$  modal force. It follows therefore from equations A.12 and A.13 that the correlation functions  $R_{x_l x_p}$  between outputs measured at different degrees-of-freedom  $l$  and  $p$  along a structure excited by uncorrelated white noise can be approximated as a linear combination of the auto-correlation functions of SDOF systems with modal frequencies and damping ratios of the structure excited by white noise.

Using equation 3.3, the variance of the unbiased correlation functions  $R_{x_l x_p}$  can therefore be written as

$$\text{Var}(R_{x_l x_p}(\tau)) = \frac{1}{T - \tau} \int_{-T+\tau}^{T-\tau} \left(1 - \frac{|\tau|}{T}\right) [R_{x_l x_l}(\tau) R_{x_p x_p}(\tau) + R_{x_l x_p}(t + \tau) R_{x_p x_l}(t - \tau)] d\tau \quad (\text{A.15})$$

Substituting the approximation made in equation A.10 in the above equation, one

obtains

$$\begin{aligned} \text{Var}(R_{x_l x_p}(\tau)) \approx & \frac{1}{T-\tau} \int_{-T+\tau}^{T-\tau} \left(1 - \frac{|\tau|}{T}\right) \left[ \left( \sum_n R_{x_{ln} x_{ln}}(\tau) \right) \left( \sum_m R_{x_{pm} x_{pm}}(\tau) \right) \right. \\ & \left. + \left( \sum_n R_{x_{ln} x_{pn}}(t+\tau) \right) \left( \sum_m R_{x_{pm} x_{lm}}(t-\tau) \right) \right] d\tau \end{aligned} \quad (\text{A.16})$$

Expanding the sums then yields

$$\begin{aligned} \text{Var}(R_{x_l x_p}(\tau)) \approx & \sum_n \left\{ \frac{1}{T-\tau} \int_{-T+\tau}^{T-\tau} \left(1 - \frac{|\tau|}{T}\right) [R_{x_{ln} x_{ln}}(\tau) R_{x_{pn} x_{pn}}(\tau) + \right. \\ & \left. + R_{x_{ln} x_{pn}}(t+\tau) R_{x_{pn} x_{ln}}(t-\tau)] d\tau \right\} \end{aligned} \quad (\text{A.17})$$

$$+ \frac{1}{T-\tau} \int_{-T+\tau}^{T-\tau} \left(1 - \frac{|\tau|}{T}\right) \sum_n \sum_{\substack{m \\ m \neq n}} \times \quad (\text{A.18})$$

$$\times [R_{x_{ln} x_{ln}}(\tau) R_{x_{pm} x_{pm}}(\tau) + \quad (\text{A.19})$$

$$+ R_{x_{ln} x_{pn}}(t+\tau) R_{x_{pm} x_{lm}}(t-\tau)] d\tau \quad (\text{A.20})$$

Since it was assumed that the modal frequencies are well-separated, it follows that the second term in equation A.17 is much smaller than the first term since the integral of the product of two correlation functions almost cancels due to the oscillation about the abscissa. This is much the same situation than before (eq. A.8) since the auto-correlation functions are proportional to the impulse response functions for white noise excitation. Proceeding as in equation A.12, we can write

$$R_{x_{pn} x_{pn}} = \frac{\phi_{pn} \phi_{pn}}{\phi_{ln} \phi_{ln}} R_{x_{ln} x_{ln}}, \quad R_{x_{ln} x_{pn}} = \frac{\phi_{ln} \phi_{pn}}{\phi_{ln} \phi_{ln}} R_{x_{ln} x_{ln}}, \quad R_{x_{pn} x_{ln}} = \frac{\phi_{pn} \phi_{ln}}{\phi_{ln} \phi_{ln}} R_{x_{ln} x_{ln}} \quad (\text{A.22})$$

Using the notation above and neglecting the second term in equation A.17 the variance may be written

$$\text{Var}(R_{x_l x_p}(\tau)) \approx \sum_n \frac{\phi_{pn} \phi_{pn}}{\phi_{ln} \phi_{ln}} \text{Var}(R_{x_{ln} x_{ln}}(\tau)) \quad (\text{A.23})$$

Thus, the variance of the correlation functions  $R_{x_l x_p}$  between outputs measured at different degrees-of-freedom  $l$  and  $p$  along a structure excited by uncorrelated white noise can be approximated as a linear combination of the variance of the auto-correlation

functions of SDOF systems with modal frequencies and damping ratios of the structure excited by white noise.

---

## APPENDIX B

# ADDITIONAL EXPRESSIONS FOR THE DERIVATIVES OF THE MODAL FREQUENCIES AND DAMPING RATIOS

---

This Appendix gives the remaining derivatives needed for the calculation of the derivatives of the modal frequencies and damping ratios. Because these expressions are lengthy, they were omitted in 5.3 in Chapter 5.

### B.1 Expression for $\delta_{jk\rho}(\omega_i)$

$$\begin{aligned} \delta_{jk\rho}(\omega_i) = & \frac{\Re[\lambda_{c_i}(\mathbf{Q})] \Re[\delta_{jk\rho}(\lambda_{c_i})] + \Im[\lambda_{c_i}(\mathbf{Q})] \Im[\delta_{jk\rho}(\lambda_{c_i})]}{|\lambda_{c_i}(\mathbf{Q})|} & (\text{B.1}) \\ & + \frac{\Re[\delta_{jk}(\lambda_{c_i})] \Re[\delta_{\rho}(\lambda_{c_i})] + \Im[\delta_{jk}(\lambda_{c_i})] \Im[\delta_{\rho}(\lambda_{c_i})]}{|\lambda_{c_i}(\mathbf{Q})|} \\ & + \frac{1}{2} \frac{\Re[\delta_k(\lambda_{c_i})] \Re[\delta_{j\rho}(\lambda_{c_i})] + \Im[\delta_k(\lambda_{c_i})] \Im[\delta_{j\rho}(\lambda_{c_i})]}{|\lambda_{c_i}(\mathbf{Q})|} \\ & + \frac{1}{2} \frac{\Re[\delta_j(\lambda_{c_i})] \Re[\delta_{k\rho}(\lambda_{c_i})] + \Im[\delta_j(\lambda_{c_i})] \Im[\delta_{k\rho}(\lambda_{c_i})]}{|\lambda_{c_i}(\mathbf{Q})|} \\ & - \frac{1}{2} \frac{\delta_j(\omega_i) \delta_{k\rho}(\omega_i) + 2\delta_{jk}(\omega_i) \delta_{\rho}(\omega_i) + \delta_k(\omega_i) \delta_{j\rho}(\omega_i)}{|\lambda_{c_i}(\mathbf{Q})|} \end{aligned}$$

## B.2 Expression for $\delta_{jk\rho}(\xi_i)$

$$\begin{aligned}
\delta_{jk\rho}(\xi_i) &= \frac{\Re[\lambda_{c_i}(\mathbf{0})] \delta_{jk\rho}(\omega_i)}{\omega_i^2(\mathbf{0})} - \frac{\Re[\delta_{jk\rho}(\lambda_{c_i})]}{\omega_i(\mathbf{0})} & (B.2) \\
&+ \frac{1}{2} \frac{\Re[\delta_j(\lambda_{c_i})] \delta_{k\rho}(\omega_i) + \Re[\delta_{k\rho}(\lambda_{c_i})] \delta_j(\omega_i)}{\omega_i^2(\mathbf{0})} \\
&+ \frac{1}{2} \frac{\Re[\delta_k(\lambda_{c_i})] \delta_{j\rho}(\omega_i) + \Re[\delta_{j\rho}(\lambda_{c_i})] \delta_k(\omega_i)}{\omega_i^2(\mathbf{0})} \\
&+ \frac{\Re[\delta_{jk}(\lambda_{c_i})] \delta_\rho(\omega_i) + \Re[\delta_\rho(\lambda_{c_i})] \delta_{jk}(\omega_i)}{\omega_i^2(\mathbf{0})} \\
&- \frac{\Re[\lambda_{c_i}(\mathbf{0})] \delta_{k\rho}(\omega_i) \delta_j(\omega_i)}{\omega_i^3(\mathbf{0})} \\
&- \frac{(\Re[\delta_k(\lambda_{c_i})] \delta_\rho(\omega_i) + \Re[\delta_\rho(\lambda_{c_i})] \delta_k(\omega_i)) \delta_j(\omega_i)}{\omega_i^3(\mathbf{0})} \\
&- \frac{\Re[\delta_j(\lambda_{c_i})] \delta_\rho(\omega_i) \delta_k(\omega_i) + \Re[\lambda_{c_i}(\mathbf{0})] \delta_j(\delta_k(\omega_i) + \delta_j(\omega_i))}{\omega_i^3(\mathbf{0})} \\
&- \frac{3 \Re[\lambda_{c_i}(\mathbf{0})] \delta_j(\omega_i) \delta_k(\omega_i) \delta_\rho(\omega_i)}{\omega_i^4(\mathbf{0})}
\end{aligned}$$

### B.3 Expression for $\delta_{jk}(\mathbf{A})$

$$\begin{aligned}
2\delta_{jk}(\mathbf{A}) &= 2\boldsymbol{\Sigma}_1^{-1/2}\mathbf{U}_1^T \left[ \mathcal{H}_1\mathbf{V}_1\delta_{jk}(\boldsymbol{\Sigma}_1^{-1/2}) + \mathcal{H}_1\delta_{jk}(\mathbf{V}_1)\boldsymbol{\Sigma}_1^{-1/2} \right] \\
&+ 2 \left[ \boldsymbol{\Sigma}_1^{-1/2}\delta_{jk}(\mathbf{U}_1^T) + \delta_{jk}(\boldsymbol{\Sigma}_1^{-1/2})\mathbf{U}_1^T \right] \mathcal{H}_1\mathbf{V}_1\boldsymbol{\Sigma}_1^{-1/2} \\
&+ \delta_j(\boldsymbol{\Sigma}_1^{-1/2}) \left[ \delta_k(\mathbf{U}_1^T)\mathcal{H}_1\mathbf{V}_1\boldsymbol{\Sigma}_1^{-1/2} + \mathbf{U}_1^T\delta_k(\mathcal{H}_1)\mathbf{V}_1\boldsymbol{\Sigma}_1^{-1/2} \right. \\
&+ \mathbf{U}_1^T\mathcal{H}_1\delta_k(\mathbf{V}_1)\boldsymbol{\Sigma}_1^{-1/2} + \mathbf{U}_1^T\mathcal{H}_1\mathbf{V}_1\delta_k(\boldsymbol{\Sigma}_1^{-1/2}) \left. \right] \\
&+ \delta_k(\boldsymbol{\Sigma}_1^{-1/2}) \left[ \delta_j(\mathbf{U}_1^T)\mathcal{H}_1\mathbf{V}_1\boldsymbol{\Sigma}_1^{-1/2} + \mathbf{U}_1^T\delta_j(\mathcal{H}_1)\mathbf{V}_1\boldsymbol{\Sigma}_1^{-1/2} \right. \\
&+ \mathbf{U}_1^T\mathcal{H}_1\delta_j(\mathbf{V}_1)\boldsymbol{\Sigma}_1^{-1/2} + \mathbf{U}_1^T\mathcal{H}_1\mathbf{V}_1\delta_j(\boldsymbol{\Sigma}_1^{-1/2}) \left. \right] \\
&+ \boldsymbol{\Sigma}_1^{-1/2}\delta_j(\mathbf{U}_1^T) \left[ \delta_k(\mathcal{H}_1)\mathbf{V}_1\boldsymbol{\Sigma}_1^{-1/2} + \mathcal{H}_1\delta_k(\mathbf{V}_1)\boldsymbol{\Sigma}_1^{-1/2} + \mathcal{H}_1\mathbf{V}_1\delta_k(\boldsymbol{\Sigma}_1^{-1/2}) \right] \\
&+ \boldsymbol{\Sigma}_1^{-1/2}\delta_k(\mathbf{U}_1^T) \left[ \delta_j(\mathcal{H}_1)\mathbf{V}_1\boldsymbol{\Sigma}_1^{-1/2} + \mathcal{H}_1\delta_j(\mathbf{V}_1)\boldsymbol{\Sigma}_1^{-1/2} + \mathcal{H}_1\mathbf{V}_1\delta_j(\boldsymbol{\Sigma}_1^{-1/2}) \right] \\
&+ \boldsymbol{\Sigma}_1^{-1/2}\mathbf{U}_1^T\delta_j(\mathcal{H}_1) \left[ \delta_k(\mathbf{V}_1)\boldsymbol{\Sigma}_1^{-1/2} + \mathbf{V}_1\delta_k(\boldsymbol{\Sigma}_1^{-1/2}) \right] \\
&+ \boldsymbol{\Sigma}_1^{-1/2}\mathbf{U}_1^T\delta_k(\mathcal{H}_1) \left[ \delta_j(\mathbf{V}_1)\boldsymbol{\Sigma}_1^{-1/2} + \mathbf{V}_1\delta_j(\boldsymbol{\Sigma}_1^{-1/2}) \right] \\
&+ \boldsymbol{\Sigma}_1^{-1/2}\mathbf{U}_1^T\mathcal{H}_1\delta_j(\mathbf{V}_1)\delta_k(\boldsymbol{\Sigma}_1^{-1/2}) + \boldsymbol{\Sigma}_1^{-1/2}\mathbf{U}_1^T\mathcal{H}_1\delta_k(\mathbf{V}_1)\delta_j(\boldsymbol{\Sigma}_1^{-1/2})
\end{aligned} \tag{B.3}$$

### B.4 Expression for $\delta_{jk}(\mathbf{U}_1)$

$$\begin{aligned}
\delta_{jk}(\mathbf{U}_1) &= \mathcal{H}_0\delta_{jk}(\mathbf{V}_1)\boldsymbol{\Sigma}_1^{-1} + \mathcal{H}_0\mathbf{V}_1\delta_{jk}(\boldsymbol{\Sigma}_1^{-1}) \\
&+ \frac{1}{2} \left[ \mathcal{H}_0\delta_j(\mathbf{V}_1)\delta_k(\boldsymbol{\Sigma}_1^{-1}) + \mathcal{H}_0\delta_k(\mathbf{V}_1)\delta_j(\boldsymbol{\Sigma}_1^{-1}) \right. \\
&+ \delta_j(\mathcal{H}_0)\mathbf{V}_1\delta_k(\boldsymbol{\Sigma}_1^{-1}) + \delta_k(\mathcal{H}_0)\mathbf{V}_1\delta_j(\boldsymbol{\Sigma}_1^{-1}) \\
&+ \left. \delta_j(\mathcal{H}_0)\delta_k(\mathbf{V}_1)\boldsymbol{\Sigma}_1^{-1} + \delta_k(\mathcal{H}_0)\delta_j(\mathbf{V}_1)\boldsymbol{\Sigma}_1^{-1} \right]
\end{aligned} \tag{B.4}$$



## B.5 Expression for $\delta_j(\Delta\Lambda')$ and $\delta_{jk}(\Delta\Lambda')$

$$\begin{aligned}\delta_j(\Delta\Lambda') &= \delta_j(\mathbf{P}'^{-1}) \mathcal{H}_1 \mathbf{V}_2 \Sigma_2^{-1} \mathbf{U}_{21}^T \mathbf{P}' + \mathbf{P}'^{-1} \delta_j(\mathcal{H}_1) \mathbf{V}_2 \Sigma_2^{-1} \mathbf{U}_{21}^T \mathbf{P}' \quad (\text{B.5}) \\ &+ \mathbf{P}'^{-1} \mathcal{H}_1 \delta_j(\mathbf{V}_2) \Sigma_2^{-1} \mathbf{U}_{21}^T \mathbf{P}' + \mathbf{P}'^{-1} \mathcal{H}_1 \mathbf{V}_2 \delta_j(\Sigma_2^{-1}) \mathbf{U}_{21}^T \mathbf{P}' \\ &+ \mathbf{P}'^{-1} \mathcal{H}_1 \mathbf{V}_2 \Sigma_2^{-1} \delta_j(\mathbf{U}_{21}^T) \mathbf{P}' + \mathbf{P}'^{-1} \mathcal{H}_1 \mathbf{V}_2 \Sigma_2^{-1} \mathbf{U}_{21}^T \delta_j(\mathbf{P}')\end{aligned}$$

$$\begin{aligned}\delta_j(\Delta\Lambda') &= \mathbf{P}'^{-1} \mathcal{H}_1 \mathbf{V}_2 \left[ \Sigma_2^{-1} \mathbf{U}_{21}^T \delta_{jk}(\mathbf{P}') + \Sigma_2^{-1} \delta_{jk}(\mathbf{U}_{21}^T) \mathbf{P}' + \delta_{jk}(\Sigma_2^{-1}) \mathbf{U}_{21}^T \mathbf{P}' \right] \quad (\text{B.6}) \\ &+ \left[ \delta_{jk}(\mathbf{P}'^{-1}) \mathcal{H}_1 \mathbf{V}_2 + \mathbf{P}'^{-1} \mathcal{H}_1 \delta_{jk}(\mathbf{V}_2) \right] \Sigma_2^{-1} \mathbf{U}_{21}^T \mathbf{P}' \\ &+ \frac{1}{2} \left[ \delta_j(\mathbf{P}'^{-1}) \delta_k(\mathcal{H}_1) \mathbf{V}_2 \Sigma_2^{-1} + \delta_j(\mathbf{P}'^{-1}) \mathcal{H}_1 \delta_k(\mathbf{V}_2) \Sigma_2^{-1} + \delta_j(\mathbf{P}'^{-1}) \mathcal{H}_1 \mathbf{V}_2 \delta_k(\Sigma_2^{-1}) \right. \\ &+ \delta_k(\mathbf{P}'^{-1}) \delta_j(\mathcal{H}_1) \mathbf{V}_2 \Sigma_2^{-1} + \delta_k(\mathbf{P}'^{-1}) \mathcal{H}_1 \delta_j(\mathbf{V}_2) \Sigma_2^{-1} \\ &+ \delta_k(\mathbf{P}'^{-1}) \mathcal{H}_1 \mathbf{V}_2 \delta_j(\Sigma_2^{-1}) \left. \right] \mathbf{U}_{21}^T \mathbf{P}' \\ &+ \frac{1}{2} \delta_j(\mathbf{P}'^{-1}) \mathcal{H}_1 \mathbf{V}_2 \Sigma_2^{-1} \left[ \delta_k(\mathbf{U}_{21}^T) \mathbf{P}' + \mathbf{U}_{21}^T \delta_k(\mathbf{P}') \right] \\ &+ \frac{1}{2} \delta_k(\mathbf{P}'^{-1}) \mathcal{H}_1 \mathbf{V}_2 \Sigma_2^{-1} \left[ \delta_j(\mathbf{U}_{21}^T) \mathbf{P}' + \mathbf{U}_{21}^T \delta_j(\mathbf{P}') \right] \\ &+ \frac{1}{2} \left[ \mathbf{P}'^{-1} \delta_j(\mathcal{H}_1) \delta_k(\mathbf{V}_2) \Sigma_2^{-1} + \mathbf{P}'^{-1} \delta_j(\mathcal{H}_1) \mathbf{V}_2 \delta_k(\Sigma_2^{-1}) + \mathbf{P}'^{-1} \mathcal{H}_1 \delta_j(\mathbf{V}_2) \delta_k(\Sigma_2^{-1}) \right. \\ &+ \mathbf{P}'^{-1} \delta_k(\mathcal{H}_1) \delta_j(\mathbf{V}_2) \Sigma_2^{-1} + \mathbf{P}'^{-1} \delta_k(\mathcal{H}_1) \mathbf{V}_2 \delta_j(\Sigma_2^{-1}) \\ &+ \mathbf{P}'^{-1} \mathcal{H}_1 \delta_k(\mathbf{V}_2) \delta_j(\Sigma_2^{-1}) \left. \right] \mathbf{U}_{21}^T \mathbf{P}' \\ &+ \frac{1}{2} \mathbf{P}'^{-1} \left[ \delta_j(\mathcal{H}_1) \mathbf{V}_2 \Sigma_2^{-1} \delta_k(\mathbf{U}_{21}^T) + \mathcal{H}_1 \mathbf{V}_2 \delta_j(\Sigma_2^{-1}) \delta_k(\mathbf{U}_{21}^T) \right. \\ &+ \delta_k(\mathcal{H}_1) \mathbf{V}_2 \Sigma_2^{-1} \delta_j(\mathbf{U}_{21}^T) + \mathcal{H}_1 \mathbf{V}_2 \delta_k(\Sigma_2^{-1}) \delta_j(\mathbf{U}_{21}^T) \left. \right] \mathbf{P}' \\ &+ \frac{1}{2} \mathbf{P}'^{-1} \left[ \delta_j(\mathcal{H}_1) \mathbf{V}_2 \Sigma_2^{-1} \mathbf{U}_{21}^T \delta_k(\mathbf{P}') + \mathcal{H}_1 \delta_j(\mathbf{V}_2) \Sigma_2^{-1} \mathbf{U}_{21}^T \delta_k(\mathbf{P}') \right] \quad (\text{B.7}) \\ &+ \mathcal{H}_1 \mathbf{V}_2 \delta_j(\Sigma_2^{-1}) \mathbf{U}_{21}^T \delta_k(\mathbf{P}') \\ &+ \delta_k(\mathcal{H}_1) \mathbf{V}_2 \Sigma_2^{-1} \mathbf{U}_{21}^T \delta_j(\mathbf{P}') + \mathcal{H}_1 \delta_k(\mathbf{V}_2) \Sigma_2^{-1} \mathbf{U}_{21}^T \delta_j(\mathbf{P}') \\ &+ \mathcal{H}_1 \mathbf{V}_2 \delta_k(\Sigma_2^{-1}) \mathbf{U}_{21}^T \delta_j(\mathbf{P}') \\ &+ \mathbf{P}'^{-1} \mathbf{V}_2 \Sigma_2^{-1} \left[ \delta_j(\mathbf{U}_{21}^T) \delta_k(\mathbf{P}') + \delta_k(\mathbf{U}_{21}^T) \delta_j(\mathbf{P}') \right]\end{aligned}$$

---

## REFERENCES

---

- Abdel-Ghaffar, A. M. (1978). Vibration studies and tests for a suspension bridge. *Earthquake Engineering and Structural Dynamics* **6**, 473–496.
- Abdelghani, M., M. Verhaegen, P. VanOverschee and B. DeMoor (1998). Comparison study of subspace identification methods applied to flexible structures. *Mechanical Systems and Signal Processing* **12**(5), 679–692.
- Adelman, H. M. and R. T. Haftka (1986). Sensitivity analysis of discrete structural systems. *AIAA Journal* **24**(5), 823–832.
- Adhikari, S. and J. Woodhouse (2001a). Identification of damping: Part 1, viscous damping. *Journal of Sound and Vibration* **243**(1), 43–61.
- Adhikari, S. and J. Woodhouse (2001b). Identification of damping: Part 2, non-viscous damping. *Journal of Sound and Vibration* **243**(1), 63–88.
- Aenelle, M. L., R. Brincker and A. F. Canteli (2005). Some methods to determine scaled mode shapes in natural input modal analysis. *Proceedings of the 23rd IMAC*. Orlando, Florida, USA.
- Akaike, H. (1974). Stochastic theory of minimal realization. *IEEE Transactions on Automatic Control*. No.6, Vol. Ac-19.
- Allemang, R. J. (2003). The modal assurance criterion: Twenty years of use and abuse. *Journal of Sound and Vibration* **37**(8), 14–23.
- Allemang, R. J. and D. L. Brown (1982). A correlation coefficient for modal vector analysis. *1st International Modal Analysis Conference*. pp. 110–116.

- Andersen, P. (1997). Identification of Civil Engineering Structures using Vector ARMA Models. Thesis. Aalborg University. Denmark.
- Andersen, P. and R. Brincker (1999). Estimation of modal parameters and their uncertainties. *Proceedings of the 17th IMAC*. Kissimmee, Florida. Kissimmee, Florida. pp. 323–329.
- Andersen, P., R. Brincker and P. H. Kirkegaard (1995). On the uncertainty of identification of civil engineering structures using ARMA models. *Proceedings of the 13th IMAC*. Nashville, Tennessee. pp. 1115–1121.
- Andersen, P., R. Brincker and P. H. Kirkegaard (1996). Theory of covariant equivalent ARMAV models of civil engineering structures. *Proceedings of the 14th IMAC*. Kissimmee, Florida, USA.
- Arun, K. S. and S. Y. Kung (1990). Balanced approximation of stochastic systems. *Journal of Matrix Analysis*. 11(1)
- Asmussen, J. C. (1997). Modal analysis based on the Random Decrement Technique. Thesis. University of Aalborg, Denmark.
- Asmussen, J. C., S. R. Ibrahim and R. Brincker (1998). Random decrement: Identification of structures subjected to ambient excitation. *Proceedings of the 16th International Modal Analysis Conference (IMAC)*. Santa Barbara, California. pp. 914–921.
- Barnoski, R. L. and J. R. Maurer (1969). Mean-square response of simple mechanical systems to nonstationary random excitation. *Journal of Applied Mechanics*, 221–227.
- Bartlett, M. S. (1946). On the theoretical specification of sampling properties of autocorrelated time series. *Journal of the Royal Statistical Society* 8(1), 27–41.
- Basseville, M., A. Beneviste, M. Goursat, L. Hermans, L. Mevel and H. Van der Auweraer (2001). Output-only subspace-based structural identification: From theory to industrial applications. *Journal of Dynamic Systems, Measurement and Control* 123, 668–676.

- Basu, B and V. K. Gupta (1997). Non-stationary seismic response of MDOF systems by wavelet transform. *Earthquake Engineering and Structural Dynamics* **26**, 1243–1258.
- Bathe, K.-J. and E. L. Wilson (1976). *Numerical Methods in Finite Element Analysis*. Prentice-Hall, Inc.
- Bazan, F. S. V. (2004). Eigensystem realization algorithm (ERA): reformulation and system pole perturbation analysis. *Journal of Sound and Vibration* **274**(1-2), 433–444.
- Bendat, J. S. and A. G. Piersol (2000). *Random Data: Analysis and Measurement Procedures*. third edition ed. John Wiley and Sons, Inc.
- Beneviste, A. and J. J. Fuchs (1985). Single sample modal identification of a nonstationary stochastic process. *IEEE Transactions on Automatic Control*. Vol. **AC-30**
- Bergman, M, R. W. Longman and J-N. Juang (1989). Variance and bias computation for enhanced system identification. *Proceedings of the 28th Conference on Decision and Control*.
- Bonato, P., R. Ceravolo, A. De Stefano and F. Molinari (2000). Use of cross-time-frequency estimators for structural identification in non-stationary conditions and under unknown excitation. *Journal of Sound and Vibration* **237**(5), 775–791.
- Brillinger, D. R. (1975). *Time Series: Data Analysis and Theory*. Holt, Rinehart and Winston. New York.
- Brincker, R. and P. Andersen (2005). Ambient response analysis of the heritage court tower building structure. *Proceedings of the 18th IMAC*. San Antonio, Texas, USA.
- Brincker, R., J. B. Frandsen and P. Andersen (2005a). Ambient response analysis of the great belt bridge. *Proceedings of the 18th IMAC*. San Antonio, Texas, USA.
- Brincker, R., L. M. Zhang and P. Andersen (2000). Modal identification of output-

- only systems using frequency domain decomposition. In: *Proceedings of the 18th IOMAC*. San Antonio, Texas, USA. San Antonio, Texas, USA.
- Brincker, R., L. Zhang and P. Andersen (2001). Damping identification by frequency domain decomposition. *Proceedings of the 19th International Modal Analysis Conference (IMAC XIX)*. Kissimmee, Florida, USA.
- Brincker, R., P. Andersen and N. Moller (2005*b*). An indicator for separation of structural and harmonic modes in output-only modal testing. *Proceedings of the 18th IMAC.*, San Antonio, Texas
- Brincker, R., S. Krenk and J L. Jensen (1991). Estimation of correlation functions by the random decrement technique. *Proceedings of the 9th IMAC and Exhibit.*, Firenze, Italy
- Brown, D. L. (1979). Parameter estimation techniques for modal analysis. *SAE Paper*. Vol. 790221
- Brownjohn, J. M. W. (2005). Long-term monitoring of dynamic response of a tall building for performance evaluation and loading characterisation. *Proceedings of the 1st IOMAC*, Copenhagen, Denmark
- Brownjohn, J. M. W., A. A. Dumanoglu, R. T. Severn and A. Bakeborough (1989). Ambient vibration survey of the bosphorus suspension bridge. *Earthquake Engineering and Structural Dynamics*. **18**
- Brownjohn, J. M. W., A. A. Dumanoglu, R. T. Severn and C. A. Taylor (1987). Ambient vibration measurements of the Humber suspension bridge and comparison with calculated characteristics. *Proceedings of the Institution of Civil Engineers* **83**(Part 2), 561–600.
- Bühlmann and H. R. Künsch (1995). The blockwise bootstrap for general parameters of a stationary time series. *Scandinavian Journal of Statistics* **22**, 35–54.
- Bühlmann, P. (1996). Locally adaptive lag-window spectral estimation. *Journal of Time Series Analysis* **17**(3), 247–270.

- Bühlmann, P. (2002). Bootstrap for time series. *Statistical Science* **17**(1), 52–72.
- Bühlmann, P. and H. R. Künsch (1999). Block length selection in the bootstrap for time series. *Computational Statistics and Data Analysis* **31**, 295–310.
- Caicedo, J. M., J. Marulanda, P. Thomson and S. J. Dyke (2001). Monitoring of bridges to detect changes in structural health. *Proceedings of the 2001 American Control Conference*. Arlington, Virginia.
- Calcada, R, A. Cunha and R Delgado (2005a). Analysis of traffic-induced vibrations in a cable-stayed bridge. part i: Experimental assessment. *Journal of Bridge Engineering* **10**(4), 370–385.
- Calcada, R, A. Cunha and R Delgado (2005b). Analysis of traffic-induced vibrations in a cable-stayed bridge. part ii: Numerical modeling and stochastic simulation. *Journal of Bridge Engineering* **10**(4), 386–397.
- Campbell, N. A. (1978). The influence function as an aid in outlier detection in discriminant analysis. *Applied Statistics* **27**(3), 251–258.
- Cantieni, R. (2001). Assessing a dam's structural properties using forced vibration testing. *Proceedings of the IABSE, International conference on Safety, Risk and Reliability -Trends in Engineering*. Malta.
- Cantieni, R. (2005). Experimental Methods used in System Identification of Civil Engineering Structures. *Proceedings of the 1st IOMAC*. Copenhagen, Denmark
- Carlstein, E. (1986). The use of subseries values for estimating the variance of general statistic from stationary sequence. *The Annals of Statistics* **14**(3), 1171–1179.
- Cauberghe, B., Guillaume P, P. Verboven, S. Vanlanduit and E. Parloo (2004). Frequency response function-based parameter identification from short data sequences. *Mechanical Systems and Signal Processing* **18**, 1097–1116.
- Caughey, T. K. and J. H. Stumpf (1961). Transient response of a dynamic system under random excitation. *Journal of Applied Mechanics* **28**(4), 563–566.

- Chen, J., Y. L. Xu and R. C. Zhang (2004). Modal parameter identification of the tse-ma suspension bridge under typhoon victor: EMD-HT method. *Journal of Wind Engineering and Industrial Aerodynamics* **92**, 805–827.
- Chen, Y. and M. Q. Feng (2006). Modeling of traffic excitation for system identification of bridges. *Computer-Aided Civil and Infrastructure Engineering* **21**, 57–66.
- Cherng, A. (2003). Optimal sensor placement for modal parameter identification using signal subspace correlation techniques. *Mechanical Systems and Signal Processing* **17**(2), 361–378.
- Clarkson, B. L. and C. A. Mercer (1965). Use of cross-correlation in studying the response of lightly damped structures to random forces. *AIAA Journal* **3**(12), 2287–2291.
- Clough, R. W. (1960). The finite element in plane stress analysis. *Proceedings of the 2nd ASCE Conference on Electronic Computation*.
- Clough, R. W. and J Penzien (1993). *Dynamics of Structures*. 2nd edition, MacGraw-Hill.
- Cole, H. A. (1973). On-line failure detection and damping measurement of aerospace structures by random decrement signatures. *NASA CR-2205*.
- Cooley, J. W. and J. W. Tuckey (1965). An algorithm for machine calculation of complex fourier series. *Mathematics of Computation* **19**(90), 297–301.
- Cooper, J. E. (1989). Comparison of some time domain system identification techniques using approximate data correlations. *International Journal of Analytical and Experimental Modal Analysis* **4**, 51–57.
- Cooper, J. E. and J. R. Wright (1992). Spacecraft in-orbit identification using eigensystem realisation methods. *Journal of Guidance, Control and Dynamics* **16**(2), 352–359.

- Crawford, R. W. H. S. (1964). Determination of the natural period of buildings. *Bulletin of the Seismological Society of America* **54**(6), 1743–1756.
- Cunha, A. and E. Caetano (2005). From input-output to output-only modal identification of civil engineering structures. *Proceeding of the 1st IOAMC conference*. Copenhagen, Denmark.
- Cunha, A., E. Caetano and R Delgado (2001). Dynamic test on a large cable-stayed bridge: An efficient approach. *Journal of Bridge Engineering* **6**(1), 54–62.
- Cunha, A., E. Caetano, R. Brincker and P. Andersen (2004). Identification from the natural reponse of vasco da gamma bridge. *Proceedings of the 23rd IMAC*. Detroit, Michigan.
- Dailey, R. L. (1989). Eigenvector derivatives with repeated eigenvalues. *AIAA Journal* **27**(19), 1386–1390.
- Desforges, M. J. and J. E. Cooper (1997). Detecting changes in modal parameters using ambient response data. *Proceedings of DAMAS Conference*. Sheffield. pp. 409–418.
- Desforges, M. J., J. E. Cooper and J. R. Wright (1995). Spectral and modal parameter estimation from output-only measurements. *Mechanical Systems and Signal Processing* **9**(2), 169–186.
- DeSmet, C. A. M., A. J. Felber and R Cantieni (1996). Ambient vibration study of the new Rheinbridge for highway N4. *Proceedings of the 14th International Modal Analysis Conference (IMAC XIV)*. Dearborn, Michigan, USA. pp. 63–69.
- Doebbling, S. W. and C. R. Farrar (1996). Computation of structural flexibility for bridge health monitoring using ambient modal data. *Proceedings of the 11th ASCE Engineering Mechanics Conference*. pp. 1114–1117.
- Doebbling, S. W. and C. R. Farrar (2001a). Estimation of statistical distributions for modal parameters identified from averaged frequency response functions. *Journal of Vibration and Control* **7**(4), 603–624.



- Doebbling, S. W. and C. R. Farrar (2001b). Estimation of statistical distributions for modal parameters identified from averaged frequency response function data. *Journal of Vibration and Control* **7**(4), 603–624.
- Efron, B. (1979). Bootstrap methods: Another look at the jackknife. *Annals of Statistics* Vol. **7**, 1–26.
- Efron, B. and R. Tibshirani (1993). *An Introduction to the Bootstrap*. Vol. Volume 57 of Applied Monographs on Statistics and Applied Probability. McGraw-Hill. New York.
- Ewins, D. J. (2000). *Modal Testing: Theory , Practice and Applications*. Research Studies Press Ltd. Great Britain.
- Farrar, C. R. and III. G. H. James (1997). System identification from ambient vibration measurements on a bridge. *Journal of Sound and Vibration* **205**(1), 1–18.
- Farrar, C. R., T. A. Duffey, P. J. Cornwell and S. W. Doebling (1999). Excitation methods for bridge structures. *Proceedings of the 17th IMAC*. Kissimmee, Florida, USA.
- Felber, A. J. (1993). Development of a Hybrid Bridge Evaluation System. Thesis. Department of Civil Engineering, University of British Columbia.
- Felber, A. J. and C. Ventura (1996). Frequency domain analysis of the ambient vibration data of the queensborough bridge main span. *Proceedings of the 14th Modal Analysis Conference (IMAC XIV)*.
- Felber, A. J., R Cantieni and R Cantieni (1996). Ambient vibration study of the ganterbridge. *Proceedings of the 14th International Modal Analysis Conference (IMAC XIV)*. Dearborn, Michigan, USA.
- Fox, R. L. and M. P. Kapoor (1968). Rate of change of eigenvalues an eigenvectors. *AIAA Journal* **6**(12), 2426–2429.

- Friswell, M. I. (1996). The derivatives of repeated eigenvalues and their associated eigenvectors. *Journal of Vibration and Acoustics, Transactions of the ASME* **118**, 390–397.
- Fukuzono, K (1986). Investigation of Multiple Reference Ibrahim Time Domain Modal Parameter Estimation Technique. Thesis. Department of Mechanical and Industrial Engineering. University of Cincinnati.
- Gade, S., N. B. Moller, H. Herlufsen and H. Konstantin-Hansen (2005). Frequency domain techniques for operational modal analysis. 1st International Operational Modal Analysis Conference. Denmark, Copenhagen. Denmark, Copenhagen.
- Gasparini, M (1979). Response of MDOF systems to nonstationary random excitation. *Journal of the Engineering Mechanics division* (13), 27.
- Ghanem, R. and F. Romeo (2000). A wavelet-based approach for the identification of linear time-varying dynamical systems. *Journal of Sound and Vibration* **234**(4), 555–576.
- Giampellegrini, L. and P. D. Greening (2005). Estimation errors in operational modal analysis. *Proceeding of the 1st IOMAC*. Copenhagen, Denmark
- Giuffre, A. and P. E. Pinto (1974). Expected fatigue life of bridges under traffic load. *MECCANICA: An international Journal of Theoretical and Applied Mechanics* (9),1, p.24–29.
- Golub, G. H. and C. F. Van Loan (1996). *Matrix Computations*. The John Hopkins University Press.
- Guillaume, P., P. Verboven and S. Vanlanduit (1998). Frequency-domain maximum likelihood approach for the extraction of modal parameters with confidence intervals. *Proceedings of ISMA 23*. Leuven, Belgium.
- Guillaume, P., P. Verboven, S. Vanlanduit, H. Van der Auweraer and B. Peeters (2003). A polyreference implementation of the least-squares complex frequency-domain estimator. *Proceedings of the 21st IMAC*. Kissimmee, Florida , USA.

- Hall, P. (1985). Resampling a coverage pattern. *Stochastic Processes and their Applications* **20**, p.231–246.
- Hall, P., J. Horowitz and B-Y. Jing (1995). On blocking rules for the bootstrap with dependent data. *Biometrika* **82**(3), 561–74.
- Hampel, F, E. M. Ronchetti, P. J. Rousseeuw and W. A. Stahel (1986). *Robust Statistics: The Approach Based on Influence Functions*. Wiley. New York.
- Han, J-G., W-X. Ren and X-X Xu (2005). Wavelet-based modal parameter identification through operational measurements. *Proceedings of the 1st IOMAC*. Denmark, Copenhagen.
- Herlufsen, H., P. Andersen, S. Gade and R. Brincker (2005). Identification techniques for operational modal analysis-an overview and practical experiences. *IOMAC, 1st International Modal Analysis Conference*. Copenhagen, Denmark. pp. 273–285.
- Hermans, L. and H Van der Auweraer (1999). Modal testing and analysis of structures under operational conditions: Industrial applications. *Mechanical Systems and Signal Processing* **13**(2), 193–216.
- Hermans, L., H. Van der Auweraer and P. Guillaume (1998). A frequency-domain maximum likelihood approach for the extraction of modal parameters from output-only data. *Proceedings of ISMA 23*. Leuven, Belgium. pp. 367–376.
- Heyde, C. C. and Y. Yang (1997). On defining long range dependence. *Journal of Applied Probability* **34**(939), 944.
- Ho, B. and R. E. Kalman (1966). Efficient construction of linear state variable models from input/output functions. *Regelungstechnik*.
- Holmes, J. D. (1998). Wind loading of structures. *Progress in Structural Engineering* **1**(2), 193–199.
- Horta, L. G. and J-N. Juang (1986). Identifying approximate linear models for simple nonlinear systems. *Journal of Guidance, Control and Dynamics* **9**(4), 385–390.

- Huang, N. E., Z. Shen, S. R. Long, M. C. Wu, H. H. Shih, Q. Zheng, N-C. Yen, C. C. Tung and H. H. Liu (1998). The empirical mode decomposition and hilbert spectrum for non-linear and non-stationary time series analysis. *Proceedings of the Royal Society of London* **454(A)**, 903–995.
- Hunter, N. F. and T. L. Paez (1998). Applications of the bootstrap to mechanical system analysis. *Experimental Techniques : Statistical Series (Part 6)*, 34–37.
- Ibrahim, S. R. (1977). Random decrement technique for modal identification fo structures. *Journal of Spacecrafts and Rockets* **14**, 696–700.
- Ibrahim, S. R. and E. C. Mikulcik (1977). A method for the direct identification of vibration parameters form the free response. *The Shock and Vibration Bulletin* **47(4)**, 183–198.
- James, III. G. H., T. G. Carne and J. P. Lauffer (1993). The natural excitation technique (NExT) for modal parameter extraction from operating wind turbines. Report.
- James, III. G. H., T. G. Carne and J. P. Lauffer (1995). The natural excitation technique (NExT) for modal parameter excitation form operating structures. *Modal Analysis: The International Journal of Analytical and Experimental Modal Analysis* **10(4)**, 260–277.
- James, III. G. H., T. G. Carne and R. L. Mayes (1996). Modal parameter extraction from large operating structures using ambient excitation. Kissimmee, Florida, USA. Proceedings of the 14th IMAC. Kissimmee, Florida, USA.
- Jeary, A. P. (1992). Establishing non-linear damping characteristucs od structures from non-stationary response time-histories. *The Structural Engineer* **70(4)**, 61–66.
- Jeary, A. P. (1996). The description and measurement of nonlinear damping in structures. *Journal of Wind Engineering and Industrial Aerodynamics* **59**, 103–114.
- Jenkins, G. M. and D. G. Watts (1968). *Spectral Analysis and its Applications*. Holden-Day.

- Juang, J-N. (1994). (1994) *Applied System Identification*. Prentice-Hall
- Juang, J-N. and H. Suzuki (1998). An eigensystem realisation in the frequency domain for modal parameter identification. *Journal of Acoustics, Stress and Reliability in Design* 110(1), 24–29.
- Juang, J-N. and R. S. Pappa (1984). An eigensystem realization algorithm for modal parameter identification and model reduction. *Journal of Guidance, Control and Dynamics* 8(5), 620–627.
- Juang, J-N. and R. S. Pappa (1986). Effects of noise on modal parameters identified by the eigensystem realisation algorithm. *Journal of Guidance, Control and Dynamics* 9, 294–303.
- Juang, J-N., J. E. Cooper and J. R. Wright (1988). An eigensystem realisation algorithm using data correlations (ERA/DC) for modal parameter identification. *Control Theory and Advanced Technology* 4(1), 5–14.
- Juang, J-N., P. Ghaemmaghami and B. L. Kyong (1989). Eigenvalue and eigenvector derivatives of a nondefective matrix. *Journal of Guidance, Control and Dynamics* 12(4), 480–486.
- Kantz, H. and T. Schreiber (1997). *Nonlinear Time Series Analysis*. Cambridge University Press.
- Kareem, A (1987). Wind effects on structures: A probabilistic approach. *Probabilistic Engineering Mechanics* 2(4), 166–200.
- Kijewski, T. and A Kareem (2000). Reliability of random decrement technique for estimates of structural damping. *Proceedings of the 8th ASCE Specialty Conference on Probabilistic Mechanics and Structural Reliability*.
- Kijewski, T. and A Kareem (2002). On the reliability of system identification: Applications of bootstrap theory. *Structural Safety* 24, 261–280.

- Kijewski, T. and A. Kareem (2003). Wavelet-transforms for system identification in civil engineering. *Computer-Aided Civil and Infrastructure Engineering* **18**, 339–355.
- Künsch, H. R. (1989). The jackknife and the bootstrap for general stationary observations. *Annals of Statistics* **17**(3), 1217–1241.
- Lahiri, S. N. (1999). Theoretical comparison of block bootstrap methods. *The Annals of Statistics* **27**(1), 386–404.
- Lardies, J and S. Gouttebroze (2002). Identification of modal parameters using the wavelet transform. *International Journal of Mechanical Sciences* **44**, 2263–2283.
- Leurs, W., F. Deblauwe and F. Lembregts (1993). Modal parameter estimation based on complex mode indicator functions. *The 11th International Modal Analysis Conference (IMAC)*. Kissimmee, Florida. pp. 1035–1041.
- Lew, J.-S., J.-N. Juang and R. W. Longman (1993). Comparison of several system identification methods for flexible structures. *Journal of Sound and Vibration* **167**(3), 461–480.
- Lim, K. B. and J.-N. Juang (1989). Eigenvector derivatives of repeated eigenvalues using singular value decomposition. *Journal of Guidance, Control and Dynamics* **12**(2), 282–283.
- Liu, K. (1995). Application of svd in optimization of structural modal test. *Computers and Structures* **63**(1), 51–59.
- Liu, R. Y. and K. Singh (1992). Moving blocks jackknife and bootstrap capture weak dependence. In *Exploring the Limits of Bootstrap*, (R. Lepage and L. Billard, eds.), p.225-248, Wiley, New York.
- Ljung, L. (1987). *System Identification: Theory for the User*. Prentice-Hall, Inc.
- Longman, R. W. and J.-N. Juang (1987). A variance based confidence criterion for era identified modal parameters. *Advances in the Astronautical Sciences, Proceeding of the 1987 AAS/AIAA*.

- Longman, R. W., M Bergman and J-N. Juang (1987). Variance and bias confidence criteria for era modal parameter identification. *Proceedings of the 1988 AAS/AIAA*.
- Luongo, A. (1993). Eigensolutions sensitivity for nonsymmetric matrices with repeated eigenvalues. *AIAA Journal* **31**(7), 1321–1328.
- Luongo, A. (2006). Free vibrations and sensitivity analysis of a defective two degree-of-freedom system. *AIAA Journal* **33**(1), 120–127.
- Ma, F. and C. H. Ng (2004). On the orthogonality of natural modes of vibration. *Mechanics Research Communications* **31**, 295–299.
- Maia, N. M. M., J. M. M. Silva, J. He, N. Lieven, J. Skingle, W. To and A. Urgueira (1997). *Theoretical and Experimental Modal Analysis*. Research Studies Press Ltd.
- Mallat, S. G. (1999). *A Wavelet Tour of Signal Processing*. 2nd ed. Academic Press.
- MATLAB. *The MathWorks, Inc.*
- McLamore, V. R., G. Hart and T. R. Stubbs (1971). Ambient vibration of two suspension bridges. *Journal of the Structural Division, ASME* **97**(N.ST10), 2567–2582.
- Mevel, L, A. Beneviste, M. Basseville and M. Goursat (2002a). Blind subspace-based eigenstructure identification under non-stationary excitation using moving sensors. *IEEE Transactions on Signal Processing* **SP-50**(1), 41–48.
- Mevel, L, M. Basseville, A. Beneviste and M. Goursat (2002b). Merging sensor data from multiple measurement set-ups for non-stationary subspace-based modal analysis. *Journal of Sound and Vibration* **249**(4), 719–741.
- Mohanty, P. (2005). Operational Modal Analysis in the Presence of Harmonic Excitations. Thesis. Delft.
- Neild, S. A., P. D. McFadden and M. S. Williams (2003). A review of time-frequency methods for structural vibration analysis. *Engineering Structures* **25**(6), 713–728.
- Nelson, R. B. (1976). Simplified calculations of eigenvector derivatives. *AIAA Journal* **14**, 1201–1205.

- Oppenheim, A. V. and R. W. Schaffer (1988). *Digital Signal Processing*. Prentice Hall.
- Paez, T. L. and N. F. Hunter (1998). Statistical series: Part-5: Fundamental concepts of the bootstrap for statistical analysis of mechanical systems. *Experimental Techniques* **22**(3), 35–38.
- Pandit, S. M. and S. M. Wu (1983). *Time Series and System Analysis*. John Wiley.
- Pang, T. (1997). *An Introduction to Computational Physics*. Cambridge University Press.
- Parloo, E., B. Cauberghe, F. Benedettini, R. Alaggio and P. Guillaume (2005). Sensitivity-based operational mode shape normalisation: Application to a bridge. *Mechanical Systems and Signal Processing* **19**, 43–55.
- Paultre, P., J. Proulx and M Talbot (1995). Dynamic testing procedures for highway bridges using traffic loads. *Journal of Structural Engineering* **121**(2), 362–376.
- Peeters, B. (2004). Polymax modal parameter estimation from operational data. *Proceedings of ISMA 2004*. Belgium, Leuven.
- Peeters, B. and G. DeRoeck (1999). Reference-based stochastic subspace identification for output-only modal analysis. *Mechanical Systems and Signal Processing* **13**(6), 855–878.
- Peeters, B. and G. DeRoeck (2001). Stochastic system identification for operational modal analysis: A review. *Journal of Dynamic Systems, Measurement and Control* **123**, 659–667.
- Penrose, R. (1956). On the best approximate solution of linear matrix equations. *Proceedings of the Cambridge Philosophical Society* **52**, 17–19.
- Penzien, J. and R. W. Clough (1993). *Dynamics of Structures*. 2nd edition ed. McGraw-Hill.
- Peterson, L. D., S. J. Bullock and S. W. Doebling (1996). The statistical sensitivity of experimental modal frequencies and damping ratios to measurement noise. *Modal*



- Analysis: The International Journal of Analytical and Experimental Modal Analysis* **11**(1), 63–75.
- Pietrzko, S., R Cantieni and Y. Deger (1996). Modal testing of steell/concrete composite bridge with servo-hydraulic shaker. *Proceedings of the 14th International Modal Analysis Conference (IMAC XIV)*. Dearborn, Michigan, USA.
- Pires, A. and J. A. Branco (2002). Partial influence functions. *Journal of Multivariate Analysis* **83**, 451–468.
- Plaut, R. H. and K. Huseyin (1973). Derivatives of eigenvalues and eigenvectors in non-self-adjoint systems. *AIAA Journal* **11**(2), 250–251.
- Politis, D. N. (1992). Bootstrap confidence bands for spectra and cross-spectra. *IEEE Transactions on Signal Processing* **40**(5), 1206–1214.
- Politis, D. N. (1994). The stationary bootstrap. *Journal of the American Statistical Association* **89**(428), 1303–1313.
- Politis, D. N. (2003a). Adaptive bandwidth choice. *Journal of Nonparametric Statistics* **15**(4-5), 517–533.
- Politis, D. N. (2003b). The impact of bootstrap methods on time series analysis. *Statistical Science* **18**(2), 219–230.
- Politis, D. N. and H. White (2004). Automatic block-length selection for the dependent bootstrap. *Econometric Reviews* **23**(1), 53–70.
- Politis, D. N. and J. P. Romano (1992). A general resampling scheme for triangular arrays of  $\#$ -mixing random variables with application to the problem of spectral density application. *The Annals of Statistics* **20**(4), 1985–2007.
- Prevosto, M. (1982). Algorithmes d'Identification de Caracteristiques Vibratoires de Structures Mechaniques Complexes. Thesis. Univ. de Rennes I, France.

- Pridham, B. A. and J. C. Wilson (2003). A study of damping errors in correlation-driven stochastic realizations using short data sets. *Probabilistic Engineering Mechanics* **18**(2), 61–77.
- Priestley, M. B. (2004). *Spectral Analysis and Time Series*. Academic Press. Suffolk.
- Qin, Q. and L. Z. Qian (2001). Modal identification of the tsing ma bridge using improved eigensystem realization algorithm. *Journal of Sound and Vibration* **247**(2), 325–341.
- Ren, W-X. and Z-H. Zong (2004). Output-only modal parameter identification of civil engineering structures. *Structural Engineering and Mechanics*.
- Reynolds, P., A Pavic and M. Willford (2005). Prediction and measurement of stadia dynamics properties. *Proceedings of the 23rd IMAC*. Orlando, Florida, USA. Orlando, Florida, USA.
- Ristinmaa, Matti, Göran Sandberg and Karl-Gunnar Olsson (1999). Calfem: A finite element toolbox to Matlab.
- Rodrigues, J., R. Brincker and P. Andersen (2004). Improvement of frequency domain output-only modal identification from the application of the random decrement technique. *Proceedings of the International Modal Analysis Conference (IMAC)*. Dearborn, Michigan, USA.
- Rose, C. and M. D. Smith (2002). *Mathematical Statistics with Mathematica*. Springer-Verlag. New York.
- Ruiz-Sandoval, M. E. (2004). “Smart” Sensors for Civil Infrastructures Systems. Thesis. University of Notre Dame. Indiana, Notre Dame.
- Ruzzene, M., A. Fasana, L. Garibaldi and B. Piombo (1997). Natural frequencies and damping identification using wavelet transform: Application to real data. *Mechanical Systems and Signal Processing* **11**(2), 207–218.

- Schmidt, H (1985a). Resolution bias errors in spectral density, frequency response and coherence function measurements, i: General theory. *Journal of Sound and Vibration* **101**(3), 347–362.
- Schmidt, H (1985b). Resolution bias errors in spectral density, frequency response and coherence function measurements, iii: Application to second order systems (white noise excitation). *Journal of Sound and Vibration* **101**(3), 377–404.
- Shih, C. Y., Y. G. Tsuei, R. J. Allemang and D. L. Brown (1988). Complex mode identification function and its applications to spatial domain parameter estimation. *Mechanical Systems and Signal Processing* **4**(2), 367–377.
- Staszewski, W. J. (1998). Identification of non-linear systems using multi-scale ridges and skeletons of the wavelet transform. *Journal of Sound and Vibration* **214**(4), 639–658.
- Stewart, G. W. (1990). Perturbation theory for the singular value decomposition. *Computer Science Technical Report Series*, CS-TR-2539
- Stewart, M. (2006). Perturbation theory for singular subspaces and singular values in the presence of small singular values. *Linear Algebra and its Applications* **419**(1), 53–77.
- Strang, Gilbert (1998). *Linear Algebra and Its Applications*. 3 ed. Harcourt. San Diego.
- Straser, E. G., A. S. Kiremidjian, T. H. Meng and L. Redlefsen (1998). A modular wireless network platform for monitoring structures. Vol. 3243 of *Proceedings - SPIE The international Society For Optical Engineering*. pp. 450–456.
- Sun, Wei-Joe and A Kareem (1989). Response of MDOF systems to nonstationary random excitation. *Engineering Structures* **11**, 83–91.
- Turner, J. D. and A. J. Pretlove (1988). A study of the spectrum of traffic induced bridge vibration. *Journal of Sound and Vibration* (122), 31–42.

- Van der Auweraer, H. (2001). Structural dynamics modeling using modal analysis: Applications, trend and challenges. *Proceedings of IMTC, 18th IEEE Instrumentation and Measurement Technology Conference*. pp. 1502–1509.
- Van der Auweraer, H. and B. Peeters (2004). Discriminating physical poles from mathematical poles in high order systems: Use and automatation of the stabilization diagram. *Proceedings of the IMCT, the 21st IEEE Instrumentation and Measurement Technology Conference*. Como, Italy. pp. 2193–2198.
- Vandiver, J. K., A. B. Dunwoody, R. B. Campbell and M. F. Cook (1982). A mathematical basis for the random decrement signature analysis technique. *Journal of Mechanical Design* **104**, 307–313.
- VanOverschee, P. and B. DeMoor (1993). Subspace algorithm for the stochastic identification problem. *Automatica* **29**(3), 649–660.
- VanOverschee, P. and B. DeMoor (1996). *Subspace Identification for Linear Systems: Theory-Implementation-Applications*. Kluwer Academic Publishers.
- Vold, H, J. Kundrat, G. T. Rocklin and R. Russel (1982). A multi-input modal parameter estimation algorithm for mini-computers. *SAE Technical Paper*.
- Welch, P. D. (1967). The use of Fast Fourier Transform for the estimation of power spectra: A method based on time averaging over short, modified periodograms. *IEEE Trans. Audio Electroacoustics* **AU-15**, 70–73.
- Williams, A. B. and F. J. Taylor (1995). *Electronic Filter Design Handbook*. McGraw-Hill.
- Woodhouse, J. (1998). Linear damping models for structural vibration. *Journal of Sound and Vibration* **215**(3), 547–569.
- Yu, Dan-Jiang and W Ren (2005). EMD-based stochastic subspace identification of structures from operational vibration measurements. *Engineering Structures* **27**, 1741–1751.

- Zhang, L., R. Brincker and P. Andersen (2005a). An overview of operational modal analysis: Major developments and issues. Proceedings of the 1st IOMAC. Copenhagen, Denmark. Copenhagen, Denmark.
- Zhang, L., T. Wang and Y. Tamura (2005b). Frequency-spatial domain decomposition technique with application to operational modal analysis of civil engineering structures. *Proceedings of the 1st IOMAC*. Copenhagen, Denmark.
- Zhang, Xin, Brownjohn and Yi P. T.-C. Wang (2006). Direct observations of non-stationary bridge deck aeroelastic vibration in wind tunnel. *Journal of Sound and Vibration* **291**, 202–214.
- Zhang, Zhen-Yu and Hui-Sheng Zhang (2001). Eigensensitivity analysis of a defective matrix. *AIAA Journal* **39**(3), 473–479.